ROLE OF GLOBAL FUEL-AIR EQUIVALENCE RATIO AND INTAKE CHARGE PREHEATING IN DUAL FUEL DIESEL ENGINES RUN ON BIOGAS AND BLENDED OXYGENATED PILOT FUELS

A Thesis

Submitted in Partial Fulfillment of the Requirements for

the Award of the Degree of

DOCTOR OF PHILOSOPHY

By

Achinta Sarkar

Department of Mechanical Engineering
Indian Institute of Technology Guwahati
Guwahati – 781039, India

October 2018

Dedicated to my Parents.....

Mrs. Shefali Sarkar

and

Mr. Amal Krishna Sarkar

Declaration

I hereby certify that the work presented in this dissertation entitled "**ROLE OF GLOBAL FUEL-AIR EQUIVALENCE RATIO AND INTAKE CHARGE PREHEATING IN DUAL FUEL DIESEL ENGINES RUN ON BIOGAS AND BLENDED OXYGENATED PILOT FUELS,"** is utterly performed by myself, else stated, under the supervision of Professor Ujjwal K. Saha. Any part of this work has not earlier been submitted for the award of any degree, diploma, associate-ship, fellowship or its equivalent to any University or Institution.

Date:

Achinta Sarkar
Registration No. 126103042
Department of Mechanical Engineering
Indian Institute of Technology Guwahati
Guwahati-781039

Department of Mechanical Engineering
Indian Institute of Technology Guwahati
Guwahati – 781039
India

Certificate

It is certified that the work delineated in the thesis entitled 'Role of Global Fuel-Air Equivalence Ratio and Intake Charge Preheating in Dual Fuel Diesel Engines Run on Biogas and Blended Oxygenated Pilot Fuels,' submitted by **Mr. Achinta Sarkar**, a student in the Department of Mechanical Engineering, Indian Institute of Technology Guwahati, India, for the Award of the Degree of Doctor of Philosophy has been carried out under my supervision. This research work has not been submitted previously elsewhere for the award of any other degree or diploma.

Date:

Ujjwal K. Saha
Professor
Department of Mechanical Engineering
Indian Institute of Technology Guwahati
Guwahati-781039

Abstract

Diesel engines have been serving dedicatedly from long before to sustain the progress and prosperity of the modern civilization around the globe. However, due to some alarming concerns like acceleration of hiking of diesel oil prices, scarcity of the reserves of this fossil oil and carcinogen greenhouse gas (GHG) emission, the community of engine research is searching an alternative way to generate the environmentally friendly power with the use of renewable fuels. The diesel engines mainly generate a tremendous quantity of carcinogenic oxides of nitrogen (NO_x) and soot. The recently reported works reveal that the conversion of pure diesel mode (PDM) to dual fuel mode (DFM) of engine operation has a great ability to curtail the NO_x and soot. Moreover, in DFM both renewable liquid and gaseous fuels can simultaneously be used. In DFM, the liquid fuel (pilot) is injected into the engine cylinder to initiate the combustion of the premixed gaseous fuel and air mixture. In this context, during the last two decades, biodiesels, alcohols, and ethers in various forms as pilot and biogas as the attractive inducted gaseous renewable fuels are found. However, owing to the different fuel characteristics of this two higher-cetane (liquid) and higher-octane (gaseous) fuels, there is a performance penalty in DFM as compared to PDM. Besides biogas has inferior lower heating value (LHV) and very high self-ignition temperature. Thus, the researchers have observed comparatively more deterioration in DFM engine performance at engine standard compression ratio (CR) and injection timing (IT). Nevertheless, the major benefits to run the DFM engine at standard CR and IT are easy to fall back in PDM in any case of the shortage of gaseous fuel. Hence, keeping this vista in mind, the present study aims to improve the biogas run DFM engine performance (at standard IT =23 CAD bTDC and CR = 17.5) that is competitive to PDM using various liquid oxygenated fuels blended with diesel fuel. This idea is mainly to generate the power in the rural areas of the developing countries like India.

Due to the use of a higher quantity of biogas in DFM, the researchers never achieved an efficient engine performance at standard CR and IT as compared to PDM. In addition, there is no contemporary study on the effects of the crucial parameter global fuel-air equivalence ratio (Φ_{global}) on DFM engine overall performance. Besides, owing to the higher heat capacity of biogas, there will be the cooling effects at the time of combustion with the consequence of slower reaction rate of the gas mixture and extinction of the flame front. Hence, there can be the significant improvement in the overall performance of the DFM engine with the technique of intake charge preheating. In this research work, a series of investigations have been carried out with numerous Φ_{global} from part to higher loads with the intake charge (biogas-air mixture)

preheating at the standard IT = 23 CAD bTDC and CR = 17.5 using various oxygenated liquid fuels as the pilot fuel. It is noticed that from the part to higher loads, there is a significant improvement in engine performance with preheating as compared to the ones without preheating. The preheating is done with a cross-flow heat exchanger (CFHE) using engine exhaust. The optimum ranges of Φ_{global}/loads (bar) are found as 0.29–0.31/0.83, 0.35–0.36/1.65, 0.40–0.43/2.48, 0.47–0.50/3.31, and 0.53–0.60/4.14.

The pilot fuels that are considered in the present investigation are: (a) diesel, (b) binary blends of 5% ethanol blended with 95% diesel (E-5), (c) five ternary blends (TB) of diesel-biodiesel-ethanol (D-B-E), (d) ternary blend of D-B-butanol (TB-BT) and (e) ternary blend of D-B-diethyl ether (TB-DEE). As there is the improvement of engine performance with preheating, all the experiments with the blended fuels are carried out with the preheating of the intake charge. The preheating temperature is controlled at 55 ± 2° C depending upon the appearance of knocking sound, controlling of Φ_{global} and depending upon the engine volumetric efficiency. In the performance analysis, the parameters such as brake specific energy consumption (BSEC), brake thermal efficiency (BTE), volumetric efficiency (VE), liquid fuel replacements (LFR), actual diesel replacements (ADR), fuels energy shares, Φ_{global}, premixed fuel-air equivalence ratio ($\Phi_{premixed}$) have been considered. In the combustion analysis, the cylinder pressure history, net heat release rate (NHRR), ignition delay (ID), combustion duration (CD), cylinder mean gas temperature (CMGT), and cycle-by-cycle variations of the cylinder peak pressure (CPP) are considered. Further, for the emission analysis, carbon dioxide (CO_2), carbon monoxide (CO), hydrocarbon (HC), and oxides of nitrogen (NO_x) are chosen. In order to accomplish this benchmark research work, a thermodynamic study is also carried out. The thermodynamic analysis includes energetic and exergetic study based on the first and second law of thermodynamics, respectively.

Keywords: Diesel engine, Dual fuel diesel engine, Fuel-air Equivalence Ratio, Preheating, Renewable Fuel, Oxygenated fuels, Blends, Performance, Combustion, Emissions, Energy, Exergy.

Acknowledgements

PhD program is a dream work to the people who are born for the research to keep a trace to the inheritor and to make the world as a better place for all living elements in the green ecosystem. It is a magnificent training and prodigious learning program. PhD also teaches one, how to transfer and acquiring of knowledge being a member in the scientific fraternity, to work in a group, to know people and to make one understandable to other. In this regards, I have interacted with many of personalities and got their trustworthy support, which is a must requirement to accomplish this mission.

In the beginning, I am taking it as an opportunity to express my heartfelt gratitude to my esteemed supervisor, Prof. Ujjwal K. Saha, Department of Mechanical Engineering, Indian Institute of Technology Guwahati, India, for accepting me as his PhD student. He has given me a complete freedom in my research work that helped me to come at a remarkable level of my research work. He always has listened to my ideas with patience and constantly motivated to accomplish my goal. As I most of the times have suffered from my bad health conditions, hence, he always has encouraged me to take care of my health and at the same time showed me a way to pursue my research work. I have learned from him, how to work with enthusiasm and energy even in the worst situation. It is hard to express my gratitude with only a few words to my honorific Professor. The best way to express my thanks to him will probably be to follow the lessons I have learned from him in my entire life.

My sincere acknowledgment goes to Prof. P. Mahanta, Prof. Anoop K. Dass the former HODs and Prof. Santosha K. Dwivedy the present HOD of Mechanical Engineering Department for their encouragement, guidance, and support in all stage of my PhD work. I also wish to express my heartfelt gratitude to the members of my Doctoral Committee Prof. Niranjan Sahoo, Dr. Vinayak Kulkarni, and Prof. G. Pugazhenthi for their immense support and precious suggestions about the critical issues related to my research work. I am also very much thankful to Prof. S. Kanagaraj, to allow me to work in the Material Science Laboratory of the Mechanical Engineering Department. It is my great pleasure to thank Prof. P. Mahanta, Dr. Amaresh Dalal, Dr. Ganesh Natarajan, and Dr. Chandramohan Somayaji for their excellent teaching during the coursework.

I would like to thank Scientific Officers, Mr. R. Saikia, Mr. N. Borah, and Monuranjan Dowarah, Department of Mechanical Engineering, for their fanatical support to purchase

various apparatus and laboratory necessitates. I am also thankful to the technician and technical support staffs of the Mechanical Engineering Department specifically Mr. Dillip Chetri, Mr. Mrinal Sharma, Mr. Jaikrishna Saikia, and Mr. Saiffuddin Ahmed. I am grateful to Mr. Lalan Sahani who has helped me to overhaul the engine in my crucial time of research work.

I am highly obliged to my seniors and my colleagues Dr. Biplab K. Debnath, Dr. Bhaskor J. Bora, Mr. Maryom Dabi, Mr. Parag Kamal Talukdar, Mr. Wittison Kamei, Mr. Milan Krishna Singha Sarkar, Mr. Siddesh Desai, and Mr. Santosh Hotta and many individuals those who are enriched not only my PhD tenure but also made my life pleasant. Their motivation, encouragement, and support are acknowledged gratefully.

In my opinion parents is the real god. Without their blessing, completion of PhD could be a dream work for me. Although, my family has been pursuing in the worst financial situation, however, my father who is a serious patient of the heart attack never forced me to leave my PhD work. I owe to both of them, whatever I achieved in my life. I also want to acknowledge gratefully to my elder brother Mr. Pradip Mallick, younger brother Mr. Apurba Sarkar, and my maternal uncles Mr. Sanjoy Mandal and Shubal Mandal for their continuous support from initial to the final stage of my PhD work.

April 30, 2019 **Achinta Sarkar**
Guwahati, India

Contents

Nomenclature

Abbreviations			
ADR	Actual Diesel Replacements (%)	DLU	Dynamometer Loading Unit
AL	Applied Load	DR	Diesel Replacements (%)
ALPING	Advanced Low-Pilot-Ignited Natural Gas	E	Ethanol
AFR	Air-fuel Ratio	E5	5% Ethanol Blended with Diesel
aTDC	After Top Dead Center	EGA	Exhaust Gas Analyzer
bTDC	Before Top Dead Center	EGR	Exhaust Gas Recirculation
B	Biodiesel	EIA	Energy Information Administration
BAU	Business-as-Usual	EOC	End of Combustion (CAD)
BES	Biogas Energy Share (%)	EPA	Environmental Protection Agency
BFCV	Biogas Flow Control Valve	FFM	Fuel Flow Meter
BFES	Blended Fuel Energy Share (%)	GC	Gas Chromatography
BFR	Biogas Flow Rate (kg/h)	EVO	Exhaust Valve Opening
BMEP	Brake Mean Effective Pressure (bar)	FCE	Fuel Conversion Efficiency (%)
BMF	Burned Mass Fraction (%)	FCI	Fuel Conversion Irreversibility (%)
BSFC	Brake Specific Fuel Consumption (kg/kWh)	GDP	Gross Domestic Product
BSEC	Brake Specific Energy Consumption (kJ/s)fuel/kW	GHG	Greenhouse Gas
BTE	Brake Thermal Efficiency (%)	ID	Ignition Delay (CAD)
BT	Butanol	IEA	International Energy Outlook
BTL	Biomass-to-Liquid	ICT	Intake charge temperature
BP	Brake Power (kW)	IMEP	Indicated Mean Effective Pressure (bar)
CAD	Crank Angle Degree	IT	Injection Timing (CAD)
CAGR	Compound Annual Growth Rate	JOME	Jatropha Oil Methyl Ester
CD	Combustion Duration (CAD)	LAIMEP	Lost Available IMEP
CFHE	Cross Flow Heat Exchanger	LFF	Liquid Fuel Flow
CI	Compression Ignition	LFR	Liquid Fuel Replacement (%)
CMGT	Cylinder Mean Gas Temperature (K)	LHR	Low Heat Rejection
CNG	Compressed Natural Gas	LPG	Liquefied Petroleum Gas
COV	Coefficient of Cyclic Variation (%)	LHV	Lower Heating Value (kJ/kg)
CPP	Cylinder Peak Pressure (bar)	LTC	Low Temperature Combustion
CR	Compression Ratio	M	Manometer
DAS	Data Acquisition System	Me	Methanol
D-B-E	Diesel-Biodiesel-Ethanol	NAPCC	National Action Plan on Climate Change
D-B-BT	Diesel-Biodiesel-Butanol	NG	Natural Gas
D-B-DEE	Diesel-Biodiesel-Diethyl Ether	NHRR	Net Heat Release Rate (J/CAD)
DEE	Diethyl Ether	NMHC	Non-Methane Hydrocarbons
DFM	Dual Fuel Mode	*nr*-DFM (WOP)	DFM Run with Diesel + without Preheated Biogas-Air Mixture

nr-DFM (WP)	DFM Run with Diesel + with Preheated Biogas-Air Mixture	SOC	Start of Combustion (CAD)
OECD	Organization for Economic Co-Operation and Development	SOME	Soybean Oil Methyl Ester
PCA	Paris Climate Agreement	STD	Standard Diesel
PCMGT	Peak Cylinder Mean Gas Temperature	TB	Ternary Blend
PDM	Pure Diesel Mode	TDC	Top Dead Center
PME	Pongamia Oil Methyl Ester	THC	Total Hydrocarbons
P-NHRR	Peak Net Heat Release Rate (J/CAD)	UNFCCC	United Nations Framework Convention on Climate Change
POI	Point of Ignition	VCR	Variable Compression Ratio
RME	Rapeseed Methyl Ester	VE	Volumetric Efficiency (%)
PZ	Pressure Transducer	WCOME	Waste Cooking Oil Methyl Ester
ROR	Rate of Reaction	WOP	Without Preheating
SI	Spark Ignition	WP	With Preheating
SIT	Static Injection Timing	WRI	World Resources Institute
Notations			
C_d	Coefficient of Discharge	K	Number of Cylinders
CH_4	Methane	L	Engine Stroke Length (m)
C_2H_5OH	Ethanol	$\dot{m}$	Mass Flow Rate (kg/s)
C_4H_9OH	Butanol	N	Engine Speed (rpm)
$C_2H_5OC_2H_5$	Diethyl ether	n	Number of Revolutions Per Cycle
$C_{12}H_{26}$	Diesel	P	Instantaneous Pressure/Boost Pressure (bar)
CO_2	Carbon Dioxide	Q	Energy Per Unit Time (kW)
C_P	Specific Heat (kJ/kg.K)	r	Dynamometer Arm Radius (m)
d	Orifice Diameter (m)	S_g	Entropy Generation (kW/K)
D	Engine Cylinder Diameter (m)	T	Temperature (K)
E	Exergy (kW)	V	Instantaneous Volume (m^3)
E_A	Activation Energy (kJ/kg)	x	Mole Fraction of Methane
F	Load ($kg.m/s^2$)	y	Mole Fraction of Carbon Dioxide
g	Acceleration due to Gravity (m/s^2)	$z1, z2, z2$	Constants
Subscripts			
a	air	eg	exhaust gas
bg	biogas	in	input/intake
cw	cooling water	pa	preheated air
cmw	calorimeter water	pd	pilot diesel
d	diesel	0	dead state
des	destracted	s	shaft
Superscripts			
cw	cooling water	eg	exhaust gas
e	exit	i	inlet
Greek Symbols			
Φ_g	Global fuel-air equivalence ratio	ρ	Density (kg/m^3)
θ	Instantaneous crank angle (CAD)	γ	Specific Heat Ratio

List of Figures

List of Tables

Chapter-1

Introduction

Chapter

Highlights:

- *Energy demand and GHG emission increase simultaneously and are found higher in the developing countries*
- *Renewable energy sources have the great prospects*
- *Dual fuel concept of diesel engines can be the alternative method to use cheaper gaseous fuels like biogas and to produce energy efficiently.*
- *Huge possibility to improve the dual fuel engine performance at standard operating operating parameters*

Overview: *To sustain the progress and comfort lifestyle in the modern society, the fossil fuels have been used rapidly. Therefore, the green ecosystems in the world have been shoved into a completely devastating state due to the unbridled pollutant emission on combustion of these fossil fuels. Consequently, the control of global warming and greenhouse gas (GHG) emission have become a major challenge to the research communities around the globe. Besides, the developing realms like India in the world are heavily dependent on imported fossil fuels to meet the ever-increasing energy demand to sustain the progress and prosperity. The fossil energy in India is primarily used in transport and stationary power production sectors. However, the reserves of the fossil fuels are depleting with acceleration and making a relic of serious concern to the developing nations. Hence, it has become necessary to harness and utilize effectively of the renewable fuels either as pure or as supplementing with fossil fuels. Among different alternative renewable energy sources, alcohols, ether, biodiesel, and biogas are found to be promising. This chapter briefly discusses the energy and climate scenario in the world and in India. In addition, various renewable alternative energy sources, dual fuel concept, and emission standards are also elaborated. At the end, the objective of the present research work has been elaborated. Finally, the organization of the thesis and the roadmap are explained.*

Chapter Layout:

1.1 The World Energy and Climate Scenario

Modern lifestyles are extremely dependent on the use of energy to sustain comfort and luxury. The non-renewable fossil petroleum and coal are the major sources of energy to meet the demand of the energy that has the immense adverse impact on the environment. However, the reserves of fossil fuels around the globe are limited concerning the faster rate of depletion. Fossil oil being the product of the burial and transformation of biomass over the last 200 million years, the amount of underground oil is finite. According to an estimate, the reserves will last another 218 years for coal, 41 years for oil, and 63 years for natural gas, under a business-as-usual scenario (Agarwal, 2007). Oil has no equal as an energy source because of its intrinsic qualities such as extractability, transportability, versatility, and cost. Consequently, it has become essential to search for an alternative source of energy to transmit the use of fossil based fuel into the sustainable energy sources. To reduce the detrimental effects of GHG, produced from combustion of fossil fuel, the various agreements are signed among the nations in the world that discussed later. Figs 1.1 and 1.2 show the use of different primary fuels and the corresponding emission of CO_2.

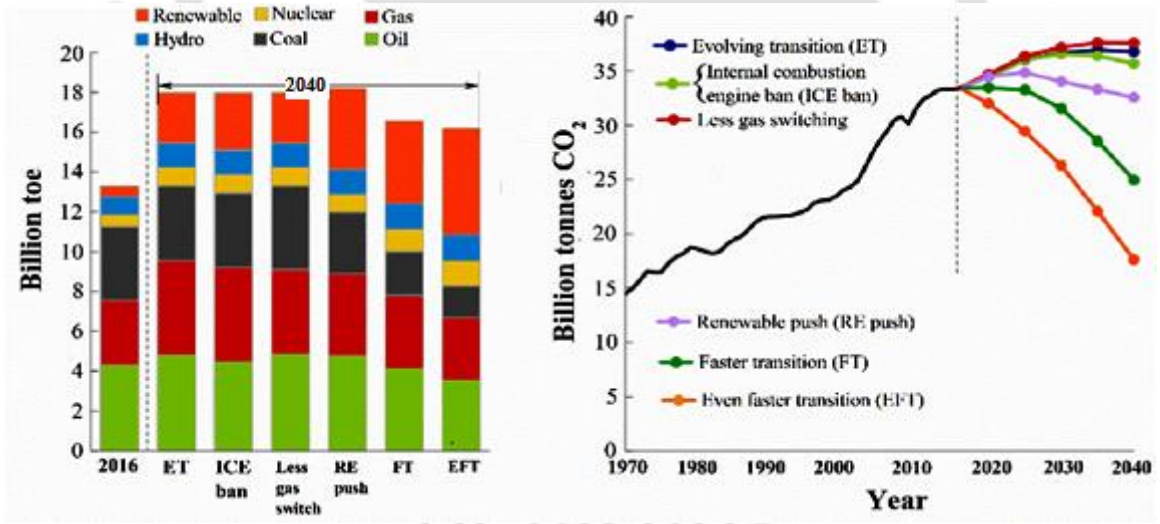

Fig. 1.1 Use of different fuels and the corresponding emission of CO_2 (***Source*:** BP Outlook, 2018)

1.2 Energy Scenario in India

Production, conversion, reservation, and efficient utilization of fossil and renewable energy sources are the key challenges to the researchers throughout the globe to keep a balance between the supply and demand in transport and power production sectors. The fuel energies are being supplied to meet the demand in these sectors are mainly from the limited fossil reservoirs. The British Petroleum (BP) Energy Outlook 2035 (BP Energy Outlook, 2017)

reported that the fossil fuels (oil, coal, and gas) will remain the dominant sources of energy and will supply almost 75% of total energy until 2035. Consequently, the depletion of inadequate reserves of fossil fuels has become faster which is challenging the country's energy security. Besides, the burning of these fossil fuels brings the globe at the carbon age with the consequence of global warming and dangerous threat to the green ecosystem. India among the realms of the world is the fastest growing economy and has the second largest population in the world. Therefore, it has become the largest energy consumer in the world. India, China, and the USA have the world population of 18, 19, and 4%, respectively. According to International Energy Outlook (IEA) report (India Energy Outlook: IEA Special Report, 2015), India consumed 6% of the world energy, while, China and the USA consumed 22, and 16% respectively. However, according to this report, in 2040, India will be the largest populous nation in the world concerning the energy consumption and will be the major driving force in global trends in all aspects. Nevertheless, to sustain the progress of the nation, the crucial challenge is to ensure the balance of demand and supply of energy. The country has been meeting its commercial energy demand largely by imported fossil fuels such as coal, petroleum oil, and natural gas. The scenario of these fuels has been described briefly as below.

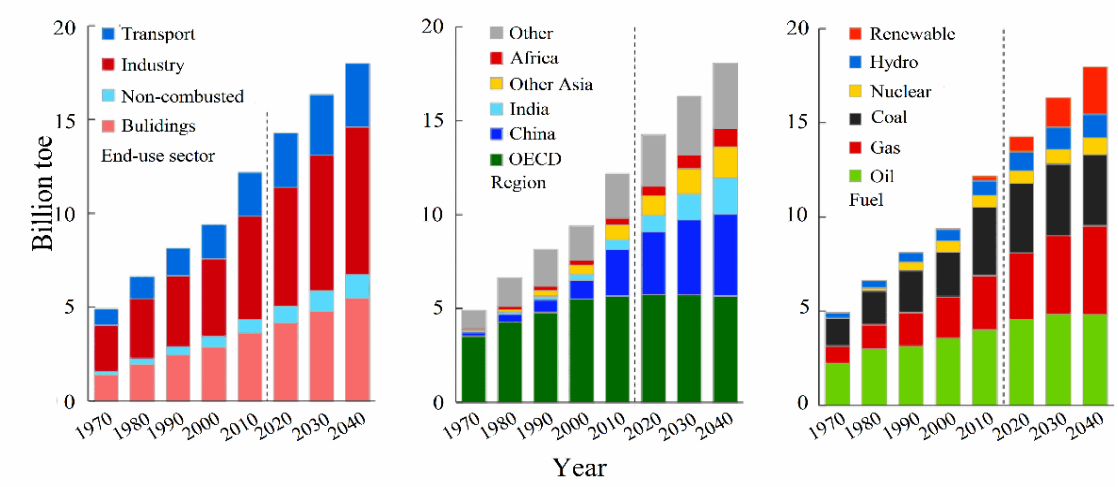

Fig. 1.2 Forecasting of worldwide energy use by end-use sector and region and corresponding demand for the use of different fuels (***Source*:** BP Outlook, 2018)

1.2.1 Petroleum Oil

Fossil oils are highly traded commodity in the world. In India, oil is considered as the second largest primary source of energy for the commercial power production sectors. However, the country has relatively poor resources of fossil oil reserves. Currently, India has a total petroleum oil reserve of 5.7 billion barrels in offshore and onshore which is only 0.5% of the

world reserves (India Energy Outlook: IEA Special Report, 2015). However, the resources are insufficient to meet the rigorous budding demand of the country. Figures 1.3 and 1.4 show the production, import, and import dependency of fossil oil in India (National Energy Map for India: Technology Vision 2030; World Energy Outlook, 2009). They clearly indicate that the import and import dependency of petroleum oil increase with times and the increment is projected to be very high beyond the year of 2030. Therefore, according to various data published in the open literature, India needs to proceed with concrete and meaningful policies to implement more renewable fuels to ensure the energy security of the country. Presently, the country is importing the crude oil from the most politically unstable Persian Gulf countries accounting for 65% of total import. However, under the new policy, India is seeking new sources like Sudan, Nigeria, Syria, Vietnam, Russia, North America, etc. According to the energy information agency (EIA), India will be the fourth largest oil importer in the world by 2025 after USA, China, and Japan (http://www.eia.doe.gov/emeu/cabs/India/Oil.html).

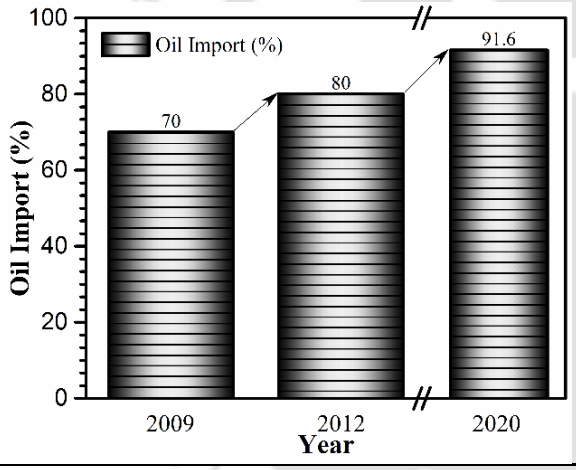

Fig. 1.3 India's oil dependency on imported crude petroleum oil (***Source*:** IEA, World Energy Outlook, 2009)

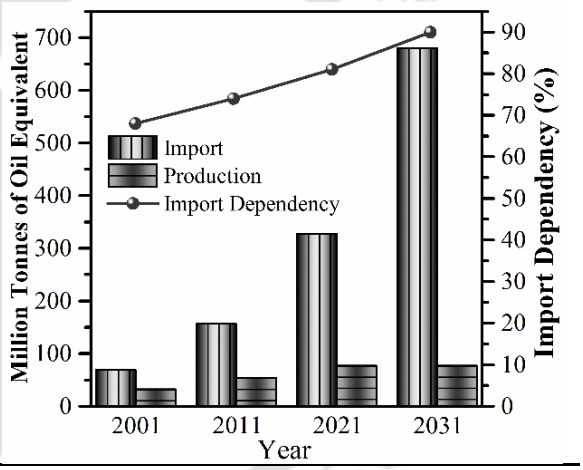

Fig. 1.4 Production, import and import dependency of fossil oil in the BAU scenario (***Source*:** National Energy Map for India: Technology Vision, 2035)

1.2.2 Natural Gas

As the reserves of natural gas are abundant and combustion of this low carbon fuel produces less pollutants in comparison to higher carbon gaseous fuels, hence it is considered as a "bridge" fuel to "low-carbon future" (Ahuja and Tatsutani, 2009; Kirkland, 2010). In recent times, the Government of India has targeted natural gas as the fuel for future for domestic and commercial purposes. However, the country is not endowed with adequate sources of natural gas and has only 0.7% of the world reserves (British Petroleum, 2013). However, the use of gas was increased by twofold during 2002–2012 (British Petroleum, 2013). It was estimated

by the World Energy Outlook, 2013 that, in India, natural gas had the fastest growing demands as compared to coal and oil. During 1990–2011, the compound annual growth rates (CAGR) of coal, oil, and natural gas were 4.9, 5.6, and 7.5%, respectively (IEA, 2013). The CAGR of coal, oil, and natural gas during the fiscal of 2011–2035 will be 3.1, 3.5, and 4.4%, whereas the average CAGR of the world is estimated at only 1.6% (IEA, 2013). Hence, due to the limited reserves of natural gas and its increasing demand, the dependency on imported natural gas is increasing. According to business-as-usual (BAU) scenario (Fig.1.5), the import dependency of natural gas from 2001 to 2021 will increase from almost 0 to 66%. Whereas in 2031, the dependence will hover between 66 and 67% (Fig. 1.5) due to the development of infrastructures like making network of pipeline to ensure the supply of gas at proper station and the bilateral agreement between India and the gas exporting countries (National Energy Map for India: Technology Vision, 2030).

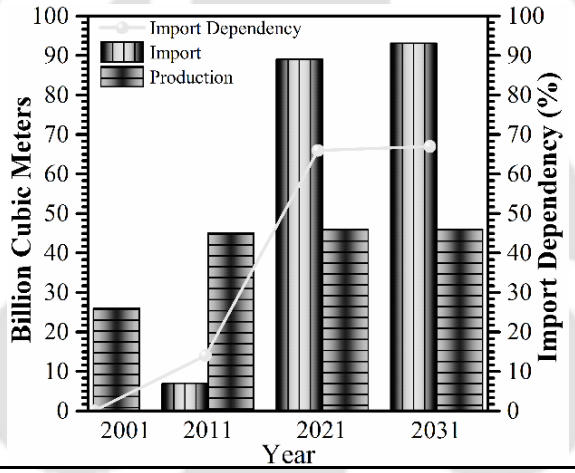

Fig. 1.5 Production, import and import dependency of natural gas in the business as usual scenario (***Source*:** National Energy Map for India: Technology Vision, 2035)

1.2.3 GDP and Climate in India

The relation of the growth of gross domestic product (GDP) to energy usage in India is shown in Fig. 1.6. It is seen that with the increase of GDP, energy demand increases at a faster rate. On the other hand, meeting this energy demand has been fulfilled and is being targeted by importing the fossil fuels such as coal, petroleum oil, and natural gas. The above discussion on the production, import, and import dependency of fossil fuels (coal, oil, and natural gas) implies that India has no other significant options to meet the energy demand and to sustain the growth of the GDP. However, as all these fuels are carbonaceous, the country has become one of the most abundant greenhouse gas (GHG) emitters in the world with the global share of 6.5% (Olivier *et al*., 2015). As stated in World Resources Institute (WRI) data, the top 10 GHG gas

emitters in the world are China, USA, European Union, India, Russian Federation, Indonesia, Brazil, Japan, Canada, and Mexico and they are responsible for the emission of 70% of the total global GHG (http://www.wri.org/blog/). Among them, India is the fourth largest emitter of the GHG. According to the Biennial Update Report (BUR) 2010, India released approximately 2136.84 million tonnes of CO_2 equivalent to GHG and, in 2030, the emission will climb up to 90% in contrast to present emission status (PARIS SUMMIT, 2015). However, by increasing the GHG emission, the whole world would keep in an entirely devastating states, which would destroy the green ecosystem, and for that reason, the historical Paris Climate Agreement (PCA) under the United Nations Framework Convention on Climate Change (UNFCCC) has been signed among 191 nations in the world. The countries except the USA have committed to hover "the increase in the global average temperature to well below 2 °C above pre-industrial levels and pursue efforts to limit the temperature increase to 1.5 °C above pre-industrial levels" (UNFCCC 2015). In this aspect, the agreement makes its own constitution for the developed and developing countries and binds them in a common platform to achieve the goals of the agreement. India is also very keen and conscious of her responsibility about the PCA. In this noble aspect, the Government of India has implemented eight national policies on a long-term basis in the context of climate change in the report of National Action Plan on Climate Change (NAPCC) to reduce the GHG (http://www.moef.nic.in/ccdnapcc).

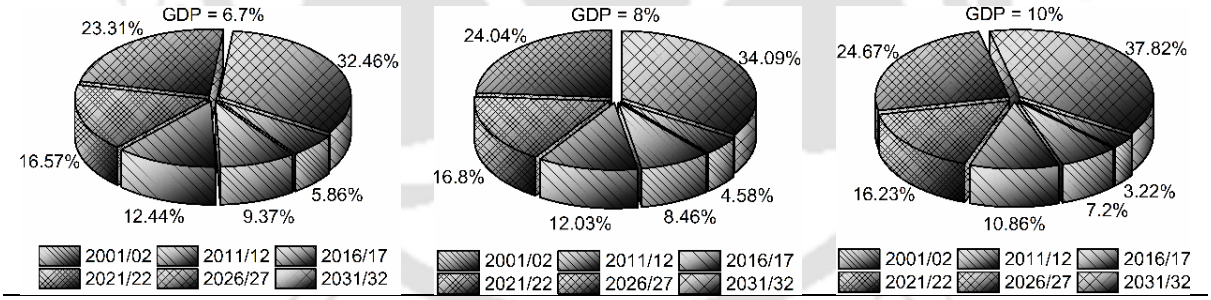

Fig. 1.6 The relation of the growth of GDP and the energy dependency in India (***Source*:** National Energy Map of India, Technology Vision, 2030)

1.2.4 Energy Use in Transport Sector

According to BAU scenario, the energy use in the transport sector in 2031 will be increased by 186.34% for the consumption in 2016 as shown in Fig. 1.7 (National Energy Map for India: Technology Vision, 2030). Figure 1.8 shows the net import, net production, net supply, and consumption by the different industrial and transport sectors and the total consumptions by all the sectors which are consuming petroleum oil (National Energy Map for India: Technology Vision, 2030). As observed in Fig. 1.8, the oil used in transport sector is increasing with time,

and in the year of 2031/32, the consumption of oil according to BAU scenario will be enhanced approximately by 188.24% with respect to the present time (2016/17), and this will be the maximum consumption as compared to the consumption by the others power production sectors (National Energy Map for India: Technology Vision, 2030).

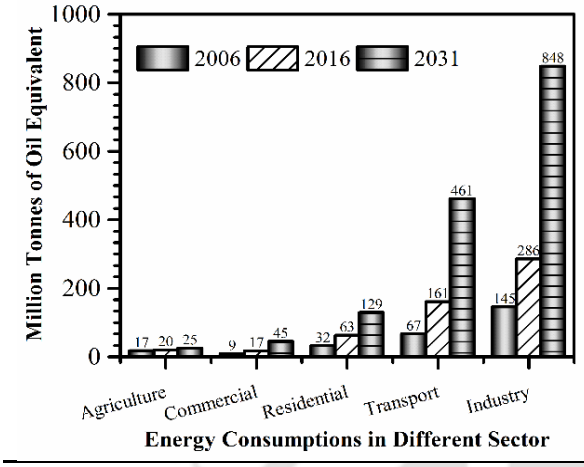

Fig. 1.7 Sector-wise energy consumption in the BAU Scenario. (***Source*:** National Energy Map of India, Technology Vision, 2030)

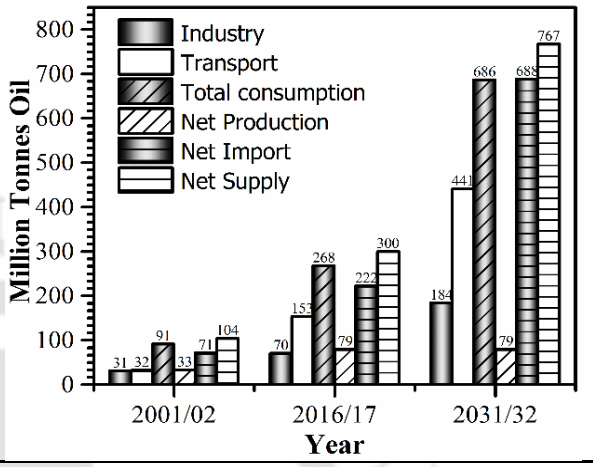

Fig. 1.8 Petroleum oil import, production, supply, and use in the transport sector. (***Source*:** National Energy Map of India, Technology Vision, 2030)

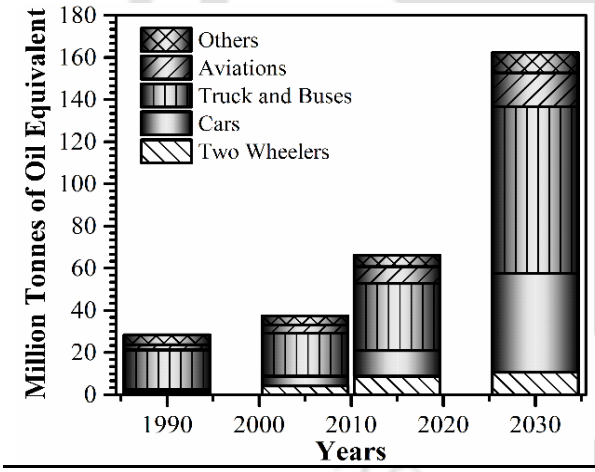

Fig. 1.9 Energy consumption in the transport sector by mode in India. (***Source*:** IEA, 2007) (Mtoe = Million tonnes of oil equivalent)

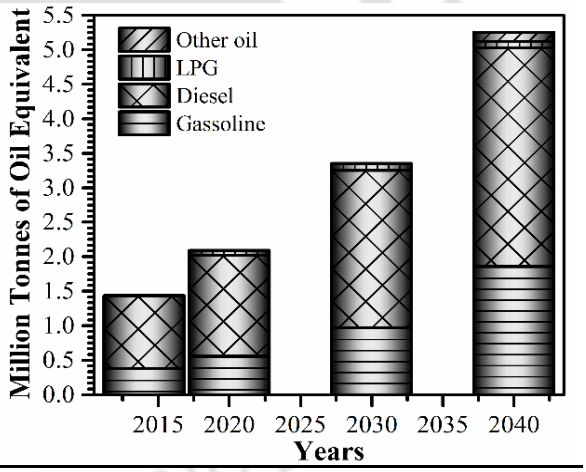

Fig. 1.10 Category-wise fuel demand in the transport sector in India (***Source*:** World Energy Outlook, IEA-2015)

Figure 1.9 shows the energy consumption in transport sectors by various modes in India (International Energy Agency, World Energy Outlook, 2007). The use of energy (oil) in trucks and buses is found to be very high in comparison to the consumption by the other light vehicles. On the other hand, the engines in trucks and buses are generally run with diesel. Therefore, diesel consumption will be expected to be high. Figure 1.10 shows the diesel consumption from 2014 to 2040. The consumption of diesel in the transport sector is found to be dominant. In

2013, the diesel consumption in the transportation sector was 1 mb/d (million barrel/day) which was 70% of the total oil consumption. This is because of a large number of freight vehicles (approximately, 60% run with diesel) and buses (around 35%) have been working in the transport sector. As a result, the use of total oil and at the same time the use of diesel will be enhanced extensively by 2040 (World Energy Outlook, 2009). The discussions in the previous sections revealed that with the enhancement of GDP, energy use in India increases. On the other hand, India is heavily dependent on imported fossil fuels. Consequently, GHG emission in India is increasing excessively. Figure 1.11 shows the GHG emission in different sectors (Busby and Shidore 2017). Figure 1.12 shows the GHG emissions in transport sectors by various modes (India: Greenhouse Gas Emissions, 2007).

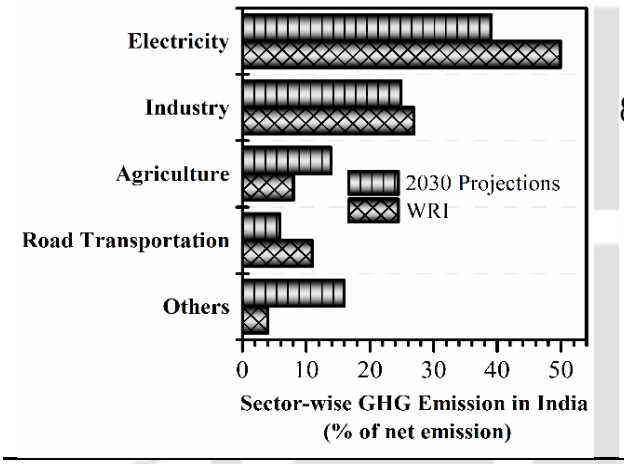

Fig. 1.11 Sector-wise greenhouse gas emission in India. (***Source*:** Busby and Shidore, 2017)

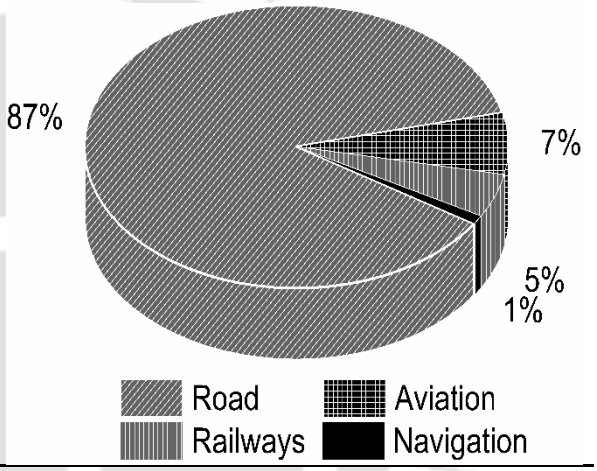

Fig. 1.12 Greenhouse gas emission in transport sectors by mode of transport in India in 2007. (***Source*:** INCCA-2007)

The previous discussion on GHG emissions in the road transport sector, it is evident that the GHG increases due to predominant use of fossil diesel fuel. However, it can be reduced by the use of the liquid and gaseous biofuels fuels. Figure 1.13 shows the scenario of increasing use of biofuels all over the world (OECD/IEA 2011). The use of biofuels from the present to the projected future is increasing, and the increment is found to be higher in the OECD countries than in the developing countries. It may be due to the development of new technologies and the transfer of technologies between the OECD countries. However, in India, the use of biofuels is also increasing (Fig. 1.13). Figure 1.14 shows the promising sources of biofuel in different strategic states (National Policy on Biofuels, 2009). Some of the biofuels are in the commercial stage, and some of them are in the research and development stage. In Table 1.1, the different biofuels are presented, and the safe use of biofuels blended with the conventional petroleum fuels is described (OECD/IEA 2011).

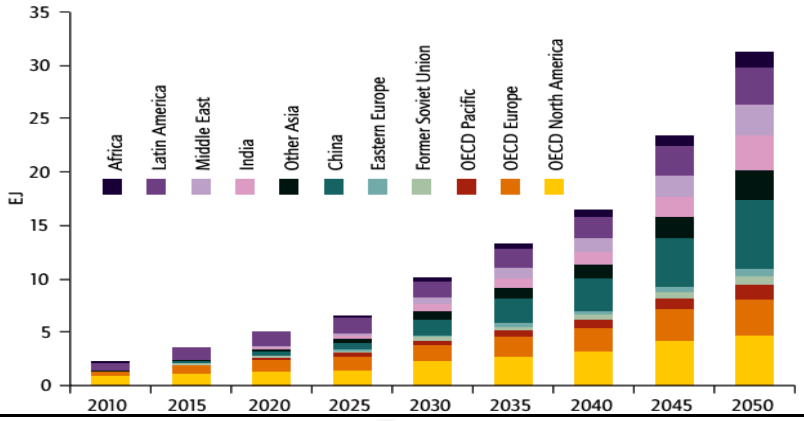

Fig. 1.13 Biofuel energy demand in the transport sector in different regions of the world (***Source*: IEA, Technology Road Map, Biofuels fuels for Transport**) (**EJ** = exajouls)

1.3 Prospects of Biofuels in India

The practice on the use of biofuels in India is lagging behind the other nations around the globe. To accelerate the implementation of biofuels and to concern the susceptibility of energy security, the Government of India under the Ministry of New and Renewable Energy announced "National Policy on Biofuels" in 2009. A minimum volume percentage of 20% of biodiesel and ethanol has been proposed by 2017 to use as the blended fuel with the petroleum fuels. In the policy, 400 species of trees having non-edible oilseeds were targeted to investigate the usability as a fuel depending upon the techno-economic sustainability (National Policy on Biofuels 2009). In the recent times, ethers, various alcohols, and biogas are observed to be the promising fuel particularly in the field of internal combustion engines.

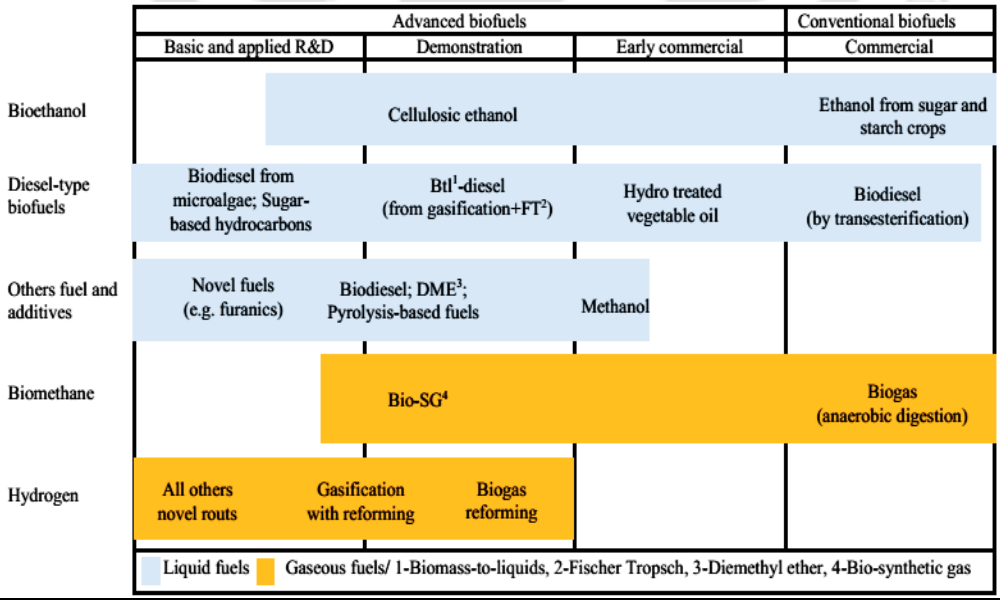

Fig. 1.14 Commercial status of primary biofuel technology in the world (***Source*: IEA, Technology Road Map, Biofuel fuels for Transport**)

1.4 Alternative Renewable Fuels

Stringent emission regulations and concerns over energy security have recently amplified research interest on alternative renewable fuels. Renewable fuels have their own lifecycle. The combustion of biofuels produces CO_2. However, CO_2 is consumed by the biofuel plants as they grow. This is why they are termed as carbon-neutral fuels. Consequently, they emit very low GHG in comparison to fossil fuels. Hence, the alternative green renewable fuels have great prospects and are competitive to fossil petroleum fuels. It can therefore be predominantly used as the alternative source of energy in the stationary and transport sectors.

Table 1.1 Overview of biofuel blending characteristics **(OECD/IEA2011)**

Biofuels	**Blending characteristics**
Sugar-based ethanol	E10 (Ethanol)-E15 (E25 in Brazil) in conventional vehicles; E85-E100 in ethanol vehicles
Starch-based ethanol	Same as above
Conventional biodiesel (fatty acid methyl ester)	Upto B-20 (biodiesel 20%) in conventional diesel engines
Hydrotreated vegetable oil (HVO)	Fully compatible with existing vehicles and distribution infrastructures
BtL (biomass-to-liquid)-diesel	Same as above
Algae oil based biodiesel/bio-jet fuel	After hydrotreating: fully compatible with existing vehicles and distribution infrastructures
Biogas	After upgrading: fully compatible with natural gas vehicles and fueling infrastructures
Bio-SG	Same as above
Bio-butanol	Use in gasoline vehicles in blends up to 85%
Dimethyl ether	Compatible with LPG infrastructure
Methanol	10-20% in gasoline engine, blends up to 85% in FFVs (Flexible-fuel vehicles)
Sugar-based diesel/jet-fuel	Fully compatible with existing vehicles and distribution infrastructures

***Source*:** IEA, Technology Road Map, Biofuels for Transport

1.4.1 Biodiesels

Biodiesel is a clean-burning alternative renewable fuel. It is mainly produced by transesterification of vegetable oils (edible or non-edible) and animal fats (triglycerides) with an alcohol (methanol or ethanol) (Ma and Hanna, 1999; Li *et al*., 2013; Virginio e Silva *et al*., 2018). Biodiesel as a fuel has the inherent physical and chemical properties over the petro-diesel such as (i) almost negligible sulfur and aromatic content, (ii) higher flash point, lubricity and almost diesel-like cetane number, (iii) biodegradable, and (iv) non-toxic. It also has the ability to reduce the emission of CO, SO_2, HC, particulate matters, polyaromatics, and smokes than fossil diesel. However, there are some limitations to use pure biodiesel as fuel due to

higher viscosity, higher pour point, lower calorific value, low volatile and oxidation ability, and a good solvent of some elastomeric sealants that can cause the erosion problems in engine fuel lines (Cetinkaya *et al*., 2005; Bhale *et al*., 2009) in comparison to fossil diesel. It is reported that up to 20 vol.% of biodiesel blended with diesel is almost similar to petrodiesel (OECD/IEA, 2011). While higher volume contents of biodiesel in blend adversely deteriorates the engine performance (Cetinkaya *et al*., 2005; Bhale *et al*., 2009).

1.4.2 Ethanol

Ethanol has been known as a fuel for a long time. It was the thought of Sir Henry Ford that ethanol would be the future fuel for the internal combustion engines mainly for the spark-ignition engines. However, due to the sudden flashing of the popularity of gasoline, ethanol is unable to compete with petroleum fuels. As a fuel, the major advantages of ethanol are (i) purely renewable and easy to produce from any biological feedstock's by fermentation, (ii) oxygenated fuel, (iii) generated lesser GHG, (iv) negligible sulfur and particulate matter emission, and (v) 100% biodegradable. Recently, the practice of using of ethanol in diesel engines in different modes of engine operations has become popular among the researchers all over the world. However, to achieve an efficient engine operation in diesel engines, the quantity of ethanol in the blend must be optimized (Paul *et al*., 2017; Alptekin, 2017). The practice of ethanol production and usability in energy sectors are increasing significantly (Sakthivel *et al*., 2018).

1.4.3 Butanol

Butanol can be produced from fossil fuels as well as from biological feedstocks by fermentation. Hence, it can be considered as a purely renewable fuel. It has some attractive advantages as fuel over the low carbon alcohols (ethanol and methanol) such as higher energy density, miscibility with petroleum oil, lower heat of vaporization, higher Cetane number (Doğan, 2011). Further, it emits lower GHG and is noncorrosive (Cheng, 2010), and can be used in engines without modification. Butanol, having higher viscosity than diesel, can also be blended with diesel for its use in diesel engines.

1.4.4 Diethyl Ether

Diethyl ether (DEE) has been in use since long to reduce the problem of cold starting. DEE, a renewable fuel, is produced from ethanol by the process of dehydration using an acid catalyst (Sezer, 2011). It has the same oxygen quantity as that of butanol. Its superior fuel properties

make it suitable for diesel engines. In recent times, DEE, as a very high cetane number (higher than 125) fuel (Rakopoulos et al., 2012), has become popular as the ignition improver in dual fuel diesel engine that run on less reactive gaseous fuels (e.g., biogas, methane, producer gas, and other gaseous fuels). As a fuel, the other eye-catching properties of DEE are reasonable energy density, high oxygen content, low self-ignition temperature, wide flammability limits, and high miscibility with the diesel fuel. However, it is highly volatile and has a tendency to form peroxide due to faster oxidation and causes anesthetic effects on human healths (Bailey et al., 1997).

1.4.5 Biogas

Biogas, the cheapest renewable fuel in the world, can be produced by the natural anaerobic digestion process. Biogas was first produced in France in 1860 (Cheng 2010), and is currently being produced all over the world. In recent times, biogas has become one of the popular fuels in the field of power production by diesel engines. In diesel engines, biogas is considered as a less reactive gaseous fuel. It is inducted into the intake manifold of the engine in dual fuel mode (DFM), which is then ignited by a higher cetane fuel sprayed over the gas-air mixture. The worldwide biogas production has increased remarkably, and this can play a strategic role in the developing market for renewable energy. It is estimated that the production of biogas from 2012 to 2022 will be doubled (from 14.5 to 29.5 gigawatts) (Maroneze *et al*., 2014, Kárászová *et al*., 2015). The production of biogas by anaerobic digestion is also referred as the waste management of organic material (Borjesson and Berglund, 2006). However, biogas as a fuel has some disadvantages notable among which are its lower calorific value, higher auto-ignition temperature, presence of CO_2 as flame inhibitor, and generation of corrosive H_2S as trace components.

1.5 Dual Fuel Concept

Dual fuel concept is old, but the technology has been developing (Karim, 1980). The benefit of this technique is that it allows the simultaneous use of both the liquid and gaseous fuels. Therefore, both lucrative liquid and gaseous renewable fuels at a time can be utilized in DFM of diesel engine. The major advantage in DFM lies with the reduction of NO_x and smoke over PDM (Mustafi and Raine, 2008, Yoon and Lee, 2011). However, in DFM, a very careful control of fuels (both the liquid and gaseous) in terms of equivalence ratio is essential. This is because the liquid fuel (such as diesel) has the substantial lower auto-ignition temperature as compared to gaseous fuel. Since in DFM the liquid fuel is sprayed over the compressed and

inducted gaseous fuel-air mixture to originate the flame fronts from each of the ignited points of the atomized liquid fuel, the induction of a higher amount of gaseous fuel can cool down the initial cylinder mean gas temperature (CMGT). Consequently, the extinction of the flame front can cause the phenomena of misfire. In this context, to improve the quality of DFM engine performance, preheating can be an efficient technique (Feroskhan et al., 2018).

Table 1.2 Emission Standards for Diesel and Gas Engines (g/kWh)

Type and Time		CO	NMHC	CH_4 (x1)	NOx	PM(x2)
Euro-3	Oct. 1999	3.00	0.40	0.65	2.0	0.02
Euro-3	Oct. 2000	5.45	0.78	1.6	5.0	0.16
Euro-4	Oct. 2005	4.00	0.55	1.1	3.5	0.03
Euro-5	Oct. 2008	4.00	0.55	1.1	2.0	0.03
Euro-6	Jan. 2013	4.00	0.16(x3)	0.5	0.4	0.01(x4)

NMHC-non-methane hydrocarbons; (x1)For Natural gas engine only; (x2) Not applicable for gas fueled engines; (x3)THC (total hydrocarbons) limits apply for diesel; (x4)It may apply to prevent ultra-fine particles from flow through filters

1.6 Emission Regulation Norms

Concerning the deadly impact of the pollutant on the environment due to increase use of stationary and automotive diesel engines, the emission regulations throughout the world have become more and more stringent. The vehicular air pollution first attempted to measure in the USA in 1965. In Europe, emission norms were implemented from the year 1970 (Pundir, 2010). India is following the European emission regulation acts with minor modification. The European emission norms for diesel and gas engines are represented in Table 1.2; whereas the Indian emissions norms for the dual fuel diesel engine is portrayed in Table 1.3.

Table 1.3 Dual Fuel Diesel (Genset) Engine Emission Norms (Central Pollution Control Board, Ministry of Environment, Forest, and Climate Change)

Power Limit	Emission Limits (g/kWh)			Smoke Limit (Light absorption coefficient, m^{-1})
	NO_x + THC or NO_x +NMHC	CO	PM	
Up to 19 kW	≤ 7.5	≤ 3.5	≤ 0.3	≤ 0.7
19 ≤ kW≤ 75	≤ 4.7	≤ 3.5	≤ 0.3	≤ 0.7
75 ≤ kW≤ 800	≤ 4.0	≤ 3.5	≤ 0.2	≤ 0.7

1.7 Objectives of the Present Investigation

In the open literature, it is noticed that most of the researchers carried out investigations at very high biogas flow rate at which the sign of misfire appears. Consequently, at the standard setting

of operating parameters (IT = 23 CAD bTDC and CR = 17.5), the investigators noticed a substantial deterioration of DFM engine performance as compared to PDM of engine operation. The higher consumption of biogas may lead to higher engine speed fluctuation, unstable engine operation, higher cycle-by-cycle variations, overheating of the nozzle tip, vibration due to the rate of change of acceleration. Hence, in DFM, the proportion of total (gaseous + liquid) fuel and air is very crucial in terms of global fuel-air equivalence ratio (Φ_{global}). Besides, due to very high self-ignition temperature of biogas, the combustion wall temperature and the gas mixture temperature reduce thereby slowing down the reaction rate. On the other hand, CO_2 present in biogas retards the flame propagation. The biogas DFM engine's overall performance (performance, combustion, and emission) can therefore be improved by preheating the intake charge. In addition, due to supplementation of biogas in the air stream, a considerable amount of air is replaced by biogas. This reduces the oxygen quantity in the fresh intake charge or in other words the reduction in volumetric efficiency (VE). An addition of oxygenated fuel in a scientific way can improve the biogas run DFM engine performance. The present investigation is thus aimed towards a clean and an efficient power production from a diesel engine under dual fuel mode, and in view of this, the following objectives are set:

- ✓ To find the optimum ranges of Φ_{global} at each of the applied loads based on engine overall performance (performance, combustion, and emission).
- ✓ To experiment at the optimum ranges of Φ_{global} with intake charge preheating (using a cross-flow heat exchanger) and to find the engine overall performance.
- ✓ To use binary blend (5% ethanol and 95% diesel) as the pilot fuel to find the effect of oxygenated fuel on the DFM engine behaviour.
- ✓ To use various ternary blends (TB) of diesel-biodiesel-ethanol and to arrive at the optimum blend based on engine overall performance.
- ✓ To use the TBs of diesel-biodiesel-butanol (abbreviated as TB-BT) and diesel-biodiesel-diethyl ether (abbreviated as TB-DEE) in DFM and to find the engine overall performance.
- ✓ Energetic and exergetic analysis of the biogas run DFM engine using ternary blends and with preheating.

1.8 Organization of the Thesis and the Road Map

The thesis consists of nine chapters. **Chapter 1** introduces the global energy scenarios, worldwide climate status, and prospects of using green renewable fuels in diesel engines in DFM. This is followed by the objective of the investigation. **Chapter 2** presents the state-of-

the-art literature survey on usability of various liquid oxygenated fuels in biogas run DFM engines, a contemporary analysis of energy and exergy of DFM engines and highlights the scopes of the present work. **Chapter 3** outlines the test setup and the associated instruments. **Chapter 4** elaborates the method of optimizing Φ_{global} based on engines overall performance, and defines the optimum ranges of Φ_{global}. **Chapter 5** discusses the results of E5 blends (consists of 5% ethanol and 95% diesel by volume) in the biogas run DFM engine. **Chapter 6** gives the results on the use of various ternary blends (TBs) of diesel-biodiesel-ethanol. **Chapter 7** analyses the results of ternary blends of diesel-biodiesel-ethanol, ternary blends diesel-biodiesel-butanol and ternary blends diesel-biodiesel-diethyl ether. **Chapter 8** gives the energetic and exergetic analysis of the DFM engine. **Chapter 9** recaps the key findings of the investigation and proposes the future scopes.

Road Map

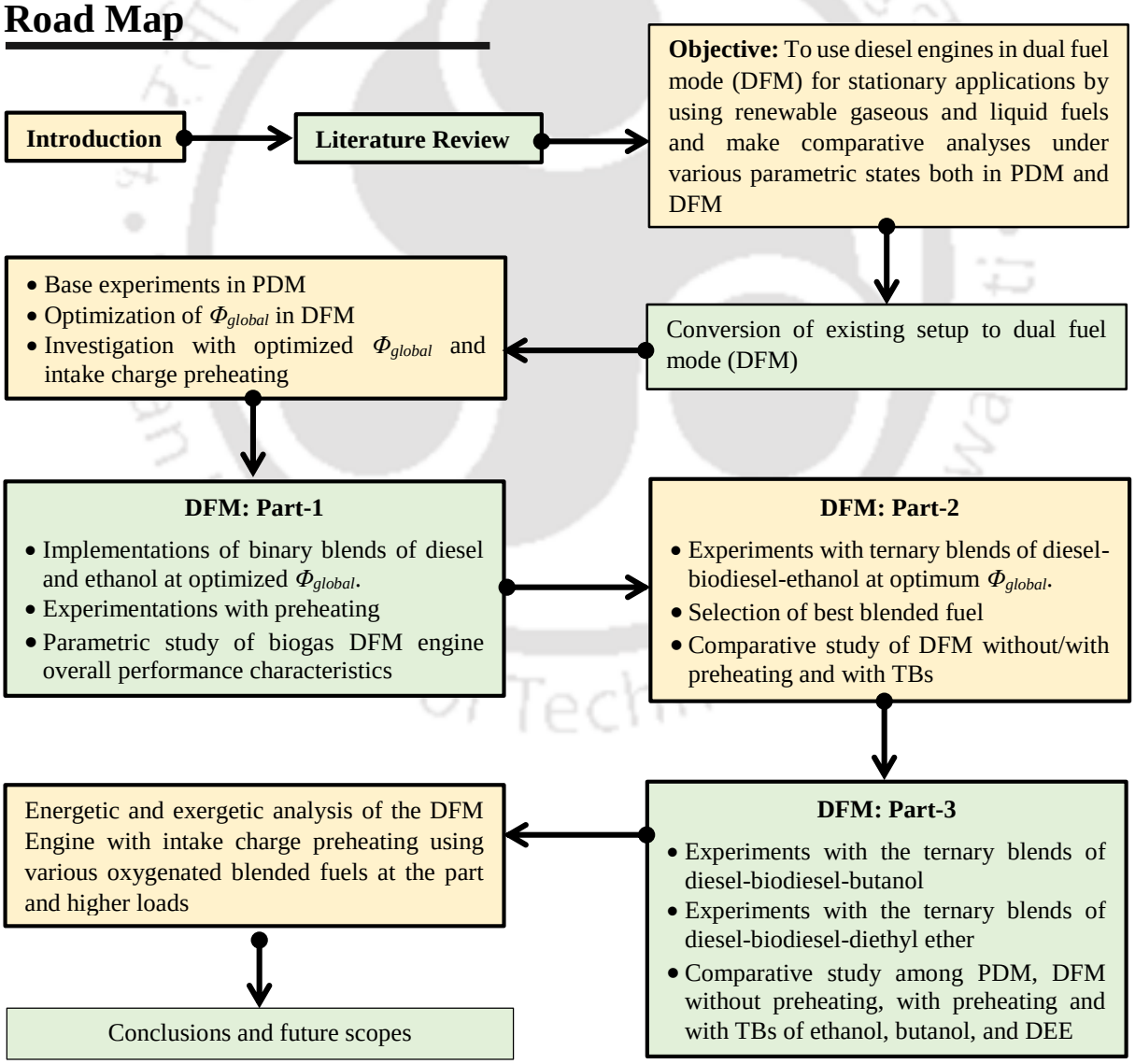

Chapter-2

Literature Review

Chapter

Highlights:

- *The DFM technology is robust in terms of usability of various kind of fuels*
- *Preheating, inducted fuel flow rates, equivalence ratio, injection timing and compression ratio are found to be the significant parameters in DFM*
- *The CA50 and CD are revealed as the most crucial parameters in DFM*
- *Oxygenated renewable liquid fuels are observed to be promising in DFM*
- *Control of both liquid and gaseous fuels are essential to achieve an efficient DFM engine performance*
- *Quality of energy utilization in DFM improves with intake charge preheating and by the use of renewable liquid oxygenated fuels*

Overview: *The dual fuel engine technology can be viable to enhance the use of both renewable liquid (biodiesel, alcohols, DEE) and gaseous fuels (such as biogas, producer gas). The dual fuel mode (DFM) not only reduces the consumption of diesel or substitute the diesel, but there is an advantage of operating the engine in pure diesel mode in case there is a shortage of primary gaseous fuel. This chapter makes an in-depth analysis to unveil the physical characteristics of the most influential parameters of DFM engines with specific reference to the use of biogas with ternary blends of 'diesel-biodiesel-ethanol,' 'diesel-biodiesel-butanol,' and 'diesel-biodiesel-DEE'. The chapter also addresses the issues on how the gaseous fuel flow rate, preheating of the intake charge, compression ratio, injection timing and the type of oxygenated fuels dominate the performance, combustion and emission characteristics. In order to understand the quality of the output energy and the energy being used to run the DFM engine, a review on the energy and exergy analysis has also been incorporated. At the end, the key scopes of the present state-of-the-art review study are also illuminated to relate with the objectives of the present investigation.*

Chapter Layout:

2.1 Prospects of DFM Engine

In the evolution of internal combustion engine technology, J. J. E. Lenoir (1822-1900) developed the first commercial engine with the only thermal efficiency of 5% (Heywood, 1988). It was the gas (coal gas-air mixture) inducted two-stroke engine. During the same time interval (1867), N. A. Otto (1832-1991) and E. Langen (1833-1995) developed an engine running with gas and working with a free piston and rack mechanism having the efficiency of more than doubled (11%) to that of the Lenoir engine (Pundir, 2010). The first prototype engine (four-stroke) built and proposed by Otto in 1876 is considered as the foundation of the modern automotive engine (Stone, 1999). This engine is known as the spark-ignition (SI) engine. Sir Rudolf Diesel in 1892 developed the historical engine, which today is known as compression ignition (CI) engine (Pulkrabek, 2003) having efficiency more than that of SI engine. This heat engine was developed based on the reversible cycles that were proposed by French Engineer Sadi Carnot in 1824 (Sonntag and van Wylen, 1991).

In the generation of power from the patented CI engine, coal dust and later on coal gas were used using the principle of dual fuel engine technology (Sahu, 2010). The earliest investigation on DFM with hydrogen as the secondary fuel in a diesel engine was carried out by Cave in 1929, and Helmore and Sokes in 1930. In 1939, the National Gas and Oil Engine Co. developed the first commercial DFM engine in Great Britain (Sahu, 2010). The production of DFM engines was accelerated during the Second World War in Great Britain, Italy, and Germany due to the lack of fossil oil. Concerning the detrimental impacts on the green environment on the use of fossil oil and faster depletion and unbearable hiking of the prices of the fossil oils, the implementation and evolution of the DFM engine after the Second World War were hastened. In the recent times, the researchers throughout the globe have been trying to implement the various renewable gaseous fuels such as biogas (Debnath, 2013; Bora, 2015), hydrogen (Patro, 1994; Liu, 1995; Korakianitis et al., 2010; Kumar *et al*., 2018), and producer gas (Dhole *et al*., 2014; Carlucci *et al*., 2017; Ramadhas *et al*., 2008). The others popular fuels have been successfully implemented in DFM are natural gas (Corrêa and Arbilla, 2005; Korakianitis *et al*., 2011; Fu *et al*., 2018) and liquefied petroleum gas (LPG) (Selim, 2005; Guan *et al*., 2017). In the DFM, the practices of using various renewable oxygenated liquid fuels have also become popular to initiate the combustion as pure or blended with the fossil diesel fuel. The promising liquid oxygenated fuels noticed to implement in DFM are biodiesel (Barik and Sivalingam, 2014; Kalsi and Subramanian, 2017), alcohols (Kumar and Raj, 2013; Pan *et al*., 2015; Senthilraja *et al*., 2016) and ether (Park *et al*., 2014; Wang *et al*., 2016; Barik and Murugan, 2016).

2.2 DFM Engine Working Principle and Modifications

In DFM, two different fuels having different phases (gas and liquid) and octane/cetane are used. The gaseous fuels used generally have very high octane number and are called as the less reactive fuels in terms of very high auto-ignition temperature in comparison to liquid fuels having higher cetane number (Hwang *et al*., 2017). The gaseous fuel in DFM is inducted through the intake port using a mixing chamber. The liquid fuel is injected over the inducted compressed gas-air mixture. The temperature of the compressed gas-air mixture at top dead center (TDC) reaches beyond the auto-ignition temperature of the liquid fuel. Again, this sprayed liquid fuel is atomized and are floated over the entire mixture. Therefore, the atomized droplets of liquid fuel instantly come at the gaseous state after immediate evaporation and then burn rapidly. The flames originate from these individual atomized droplets and propagate through the ignitable gas-air mixture. The power is thereby generated during the expansion stroke. Consequently, the DFM engine behaves like an SI engine during the induction of gaseous fuel and due to the phenomena of flame propagation. Whereas, the injection of pilot fuel and the start of combustion (SOC) of the pilot fuel in DFM is similar to the diesel engine. The interchangeable operating mode of the engine from DFM to PDM is one of the stands out feature of the DFM engine (Badr *et al*., 1999). The concept can substantially reduce the smoke and NO_x emission (Turner and Weaver, 1994). However, there is a performance penalty at part loads as compared to higher one. It is associated with the lower liquid fuel consumption, revealed by the higher specific energy consumption of gaseous fuel and appearance of higher cycle-by-cycle variations. It arises due to the extinction of flame propagation through the gas-air mixture (Elliot and Davis, 1951; Ding and Hill, 1986; Karim, 1987). These limitations can be settled by controlling the fuel-air equivalence ratio, the preheating of the intake charge and by reducing the engine speed (Karim, 1991).

2.3 Combustion Characteristics of the DFM Engine

Combustion is a crucial parameter for any heat engine that defines an efficient conversion of chemical energy into thermal energy and corresponding high-grade (shaft) energy. The combustion in PDM of diesel engine consists of four phases such as (i) ignition delay (ID), (ii) premixed combustion phase, (iii) controlled (or normal) combustion phase, and (iv) diffusion or late combustion (Fig. 2.1). The points of the start of injection (SOI), start of combustion (SOC) and end of combustion (EOC) are denoted in Fig. 2.1.

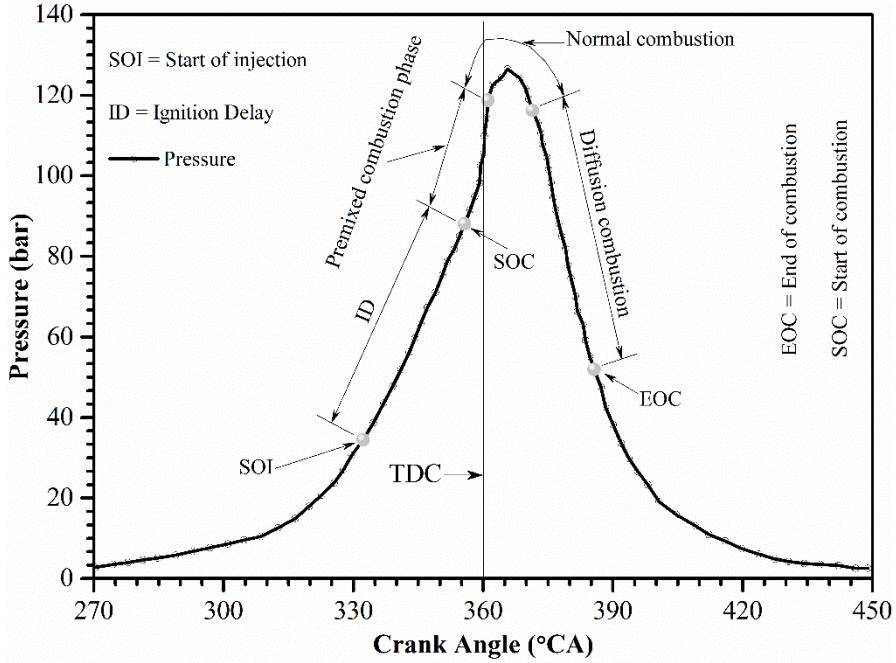

Fig. 2.1 Combustion phases in a PDM (Nwafor, 2003)

As illustrated in Fig. 2.2, the combustion in DFM consists of five phases, viz., (i) injected liquid (pilot) fuel ignition delay (ID_L), (ii) liquid fuel premixed combustion phase, (iii) inducted gaseous fuel ignition delay (ID_g), (iv) gaseous fuel rapid combustion phase, and (v) diffusion combustion phase. In DFM, two ignition delays and two start of combustion can be noticed (Fig. 2.2). Consequently, the combustion in DFM is more parametric dependent than PDM. Hence, the combustion in DFM is more complicated than the PDM.

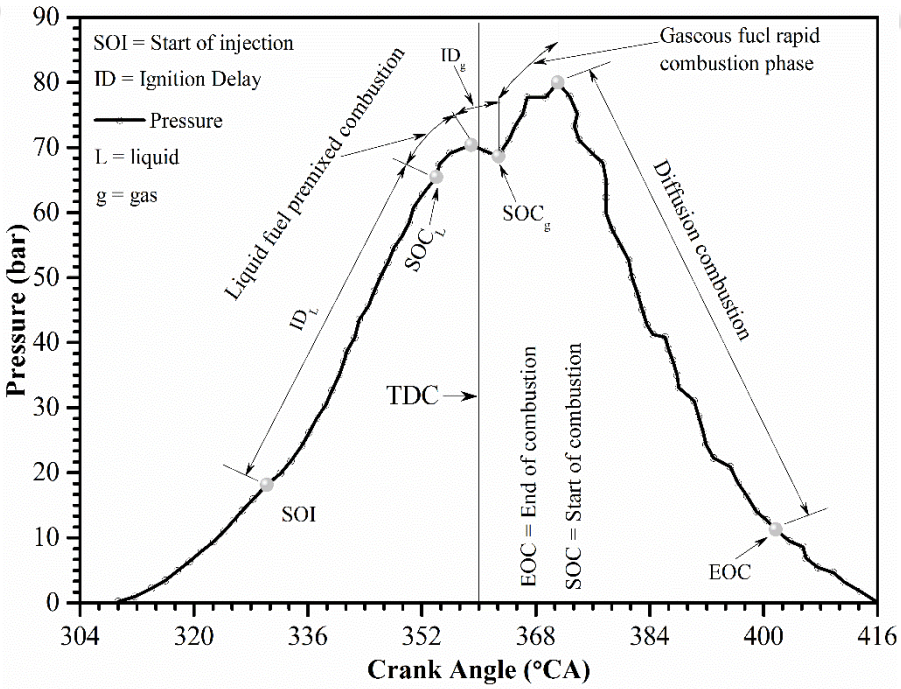

Fig. 2.2 Combustion phases in DFM engine (Nwafor, 2003)

2.4 Prospects of Bio-liquid Fuels in DFM

It is a well-known fact that ethanol, butanol, and biodiesel are the clean, eco-friendly, non-toxic, biodegradable, and oxygenated fuels. They have the ability to curtail the GHG emission and can reduce dependency on the imported fossil diesel fuel (Yoon *et al.*, 2009; Seung *et al.*, 2010; Tüccar *et al.*, 2014; Roy *et al.*, 2016). On the other hand, diethyl ether (DEE), despite of its adverse effects on human health (Bailey *et al.*, 1997), seems to be the most promising renewable fuel to generate power from diesel engines (Rakopoulos *et al.*, 2012). Thus, it is essential to discuss the benefits of these renewable fuels and their scope in DFM.

As a fuel for diesel engines, biodiesel, ethanol, butanol, and DEE have some advantages and disadvantages (Seung *et al.*, 2010; Pidol *et al.*, 2012; Zhu *et al.*, 2013; Srihari, 2017). However, the ternary blends of diesel-biodiesel-ethanol, diesel-biodiesel-butanol and diesel-biodiesel-DEE exhibit some advantages over the individual fuels such as diesel, biodiesel, and ethanol (Zhu *et al.*, 2013; Hulwan *et al.*, 2011; Pidol *et al.*, 2012; Srihari, 2017). In this section, the review study is confined solely to the use of ternary blends of diesel-biodiesel-ethanol/butanol/DEE.

The comparative analysis of the usage and effects of various ternary blends in DFM engines is presented in Table 2.1 (Hulwan *et al.*, 2011; Park *et al.*, 2012; Pidol *et al.*, 2012; Lee *et al.*, 2012; Fang *et al.*, 2013; Tüccar *et al.*, 2014; De Oliveira *et al.*, 2015; Ibrahim, 2016; Roy, 2016; Srihari, 2017; Venu and Madhavan, 2017; Emiroğlua and Şen, 2018). The parameters considered are ignition delay (ID), combustion duration (CD), cylinder peak pressure (CPP), peak net heat release rate (P-NHRR), carbon monoxide, unburnt hydrocarbon (HC) and NO_x. It is observed that ID increases with the increase of ethanol percentage in the ternary blends and reduces with the advancement of injection timing (IT). Both premixed CD and total CD reduce with the addition of ethanol in the blends and with the advancement of IT. Mostly, the CPP is found to increase with the increase of ethanol percentage in the blend and with the advancement of IT, however, in some cases, the reverse trend is also observed. The P-NHRR is found to increase with the increase of ethanol volume percentage in the blend, with load and with the advancement of IT. In presence of ethanol in the blends, both CO and HC decrease at higher loads and with the advancement of IT. In most cases, the NO_x is found to decrease with the addition of ethanol in the ternary blend, while it increases with the advancement of IT.

Table 2.1 Combustion and emission characteristics of diesel engines with various ternary blends of diesel, biodiesel, and ethanol

Investigators	Blend (D:B:E)	Operating parameters	ID	CD	CPP	P-NHRR	Emissions		
							CO	HC	NOx

Hulwan and Joshi (2011)	70:10:20
	50:20:30
	50:10:40
	Biodiesel: JOME
		rpm =1200 and 1600;
		load = 0.1-0.6 MPa;
		IT = 13, 18, 21 CAD bTDC
			↑with ↑ethanol% and ↑rpm	Total CD ↓with ↑E% and ↑IT	↓with ↑E% and ↑rpm; ↑with ↑IT; CPP advanced and retarded with ↑E% and ↑IT relative to diesel fuel, respectively	↑with ↑E% with ↑load; it is advanced and retarded upon ↑IT even at ↑ethanol% relative to base diesel	↓with ↑load and cylinder temperature; ↓at high load with ↑E%	-	↓with ↑ E%; ↑ with ↑IT

Park *et al.* (2012)	75:5:20
	70:10:20
	60:20:20
	Biodiesel: SOME
		rpm = 1200;
		injection pressure = 120 MPa;
		IT = 30 CAD bTDC-TDC
			↑with ↑ethanol% and advancing of IT	Premixed-CD reduces with the addition of biodiesel	↑ with ↑E% and ↑IT	Not show clear trends, however, NHRR with blended fuels are found to similar or higher than diesel	↓with ↑biodiesel volume and at slight ↑IT	↓ with ↑biodiesel and with CA-50 that were lie in between the ITs 25-30° bTDC	↓with the retardation of CA50 and due to prolonged ID

Pidol *et al.* (2012)	40(FT):40:20 40:40:20 40(FT):40:20 + iso-pentane Biodiesel: RME	rpm/load (bar) = 1500/3, 2500/6, 4000/full load	40:40:20 and 40(FT):40:20 + iso-pentane have the maximum ID	-	↓for ethanol blended fuels (due to lower cetane); ↑with cetane enhancer (iso-pentane)	40:40:20 and 40(FT):40:20 + iso-pentane display same behaviors	↑with all blended fuels (more than 100%)	↑with all blended fuels (more than 100%)	↓with EGR%

Lee *et al.* (2012)	85:5:10
	70:10:20
	55:15:30
		rpm = 1500;
		load = 90 N.m;
		IT = 0-12 CAD bTDC
		IT=18-33 CAD bTDC (pilot injection)
			↑with ↑E% and ↑rpm; ↓for pilot injection	Total-CD ↓with ↑ethanol%	↑ with ↑ethanol% for single injection but higher is noticed with pilot injection	↑with ↑ethanol% and found higher than pure diesel	Noticed similar trends to that of pure diesel	Found similar trends to that of pure diesel	↑with ↑ El%

Fang *et al.* (2013)	90:10:0
	80:10:10
	70:10:20
	Biodiesel: WCOME
		rpm=1450;
		load = 0.3-0.9 MPa;
		IT (CAD, aTDC) = -7.5-5;
		EGR=30%
			↑with ↑ethanol%	Total-CD ↓with ↑ethanol%	↓with ethanol%; shifted to the right side from the TDC	↑with ↑ethanol%; shifted to the right side from the TDC	↑with ↑load, due to ↑local Φ; ↓with ↑IT/ ↓E%	↓with ↑load, ↑IT, ↓E%; ↑due to lower cylinder temperature	↓with ↓IT and ↑E%

↑ indicates the increasing and advancement trends; ↓ indicates the decreasing and retardation trends; E% = ethanol percentage, Φ = equivalence ratio

Table 2.1 Combustion and emission characteristics of diesel engines with various ternary blends of diesel, biodiesel, and ethanol (contd.)

Investigators	Blends	Operating parameters	ID	CD	CPP	P-NHRR	Emissions		
							CO	HC	NO_x
Tüccar *et al.* (2014)	D80:B20 D70:B20:BT:10 D60:B20:BT:20	rpm varying from 1200 to 2800 rpm	-	-	-	-	↑with rpm, ↓due to "BT" and "B"	-	Found higher with D80:B20 and lower with BT20
De Oliveira et al. (2015)	D93:B7:E0 D88:B7:E5 D83:B7:E10	rpm = 1800; load varying 0-37 kW	↑with ↑E%	Total-CD ↓with ↑E%	↑ with ↑loads and ↑E%	↑ with ↑loads and ↑E%	↑low-load; ↓higher-load (10% -ethanol)	↑low-load; ↓higher-load	↓with ↑E%
Ibrahim (2016)	D50:B50 D45:B45:BT10 D40:B40:BT20	rpm = 1500, torque varying	-	↑ with ↑loads	-	Maximum found with BT10 and B100	-	-	Slightly ↑ due to "B" and "BT"
Roy (2016)	D80:B20, D50:B50, B100; Added 5 and 10 vol.% of E and DEE to each blends prepare the new blends	rpm varying from 800 to 1200 rpm	-	-	-	-	Noticed lower CO with ethanol except E15 than DEE	Found lower emission with ethanol than DEE (highly volatile)	Lower emission is observed
Srihari (2017)	D75:B20:DEE5 D70:B20:DEE10 D70:B20:DEE15	rpm = 2000; load varying from 0-14 N.m	↓ due to DEE	-	Found maximum with DEE15	-	At higher load lower emission noticed with DEE than PDM	Lower emission achieved with DEE10 and 15	↓with ↑ DEE vol.%
Venu and Madhavan (2017)	D40:B40:E20 D40:B40:M20 Make new blends by adding DEE5 and 10 with each of the blends	rpm = 1500, load varying from 0%, 25% to 100%	The lower ID found with DEE5 with ethanol	↑ with ↑loads, ↓with ↑ of DEE vol.% due to improve combustion	At all load found higher with DEE5 and at 100% load the variations noticed lower with DEE	Similar trends as CPP were also observed with peak NHRR	At 80% load minimum CO emission was found for all fuels, Ethanol blend and DEE5 produced lower emission	Lower emission observed with diesel fuel and DEE5 with methanol at all loads	Lower emission found with methanol-DEE5 and higher with ethanol-DEE5
Emiroğlua and Şen (2018)	D80:B20:BT10 D80:B20:E10 D80:B20:M10	rpm = 1500; load varying 0.09-0.36 MPa	↓with increasing loads and found lower with E10	↑ with ↑loads, noticed lower with BT10	↑ with ↑loads, E10< BT10	↑ with ↑loads, peaks are more or less similar	Found higher at maximum load, E10< BT10	Slightly ↑ with ↑ load, E10> BT10	↑ with ↑loads, E10> BT10

↑ and ↓ indicate increasing and decreasing trends respectively; E = ethanol; DEE = diethyl ether, B = biodiesel; M = methanol

The higher ID in presence of ethanol in the blend may allow to occurr the proper mixing of fuel and air with the increased negative work (Caton *et al*., 2011; Park *et al*., 2012). The most interesting matter with the use of ethanol is that it reduces the total CD with respect to PDM as discussed above. The shorter total CD means, the higher utilization of the mean effective pressure developed inside the combustion chamber and lower probability to waste the energy into the dead state (Hagen *et al*., 2013). Besides, CO and HC are found to reduce with the diesel-biodiesel-ethanol (D-B-E) blends with the penalty of a little higher NO_x emission. In addition, many investigations demonstrate a reduction of smoke emission with the use of ethanol and biodiesel (Yoon *et al*., 2009; Khoobbakht *et al*., 2016; Zaharin *et al*., 2017; Geo *et al*., 2017).

Butanol (BT) has the higher calorific value, higher viscosity, and lower heat of vaporization than ethanol. It has also some attractive fuel characteristics like higher energy density than any alcohols. Butanol is biological, miscible with the petroleum oil, and can be used in engines without modification. Besides, DEE as the fuel additives has become attractive to the researchers working on a diesel engine, having a very high cetane number (>125). Therefore, it can be used as the ignition improver. Consequently, the DEE has the promising prospects for its use with less reactive gaseous fuel in DFM. It also has the reasonable energy density, high oxygen content, low self-ignition temperature, wide flammability limits, and high miscibility with diesel fuel. Most of the researchers observed competitive engine performance (Rakopoulos, 2013; Tüccar *et al*., 2014; Roy, 2016; Venu and Madhavan, 2017), combustion (Rakopoulos, 2013; Venu and Madhavan, 2017) and emission (Rakopoulos, 2013; Tüccar *et al*., 2014; Roy, 2016; Venu and Madhavan, 2017) with the use of these fuels blended with diesel and biodiesel in comparison to PDM. As evident from the above discussion, the ternary blends (Diesel-Biodiesel – Ethanol/Butanol/DEE) can be efficiently used in the dual fuel diesel engines. Hence, there is a great possibility to use the maximum amount of renewable fuels and to replace a higher quantity of petrodiesel fuel.

2.5 Biogas as Fuel in DFM

Biogas, the cheapest renewable fuel, can be produced from almost all types of biological feedstocks by anaerobic digestion. Therefore, the availability of ample raw materials, lower cost of production, biogas has become the promising fuel over the gaseous fuels available in the open market. The most promising features of biogas are that it is carbon neutral in nature and easy to transport. However, the compositions of biogas are varied depending upon the anaerobic reaction.

Table 2.2 Composition of biogas with trace elements

Researchers	**Major composition (%vol.)**		**Trace composition (%vol.)**
	CH_4	CO_2	
Huang and Crookes (1998)	50-70	25-50	N_2 (0.3-3), H_2 (1-5), identified H_2S as remain trace element
Hagen *et al.* (2001), Krich *et al.* (2005), Persson and Wellinger (2006), Wellinger and Lindberg (2010),	40-75	15-60	N_2 (0-2), H_2S (0.005-0.2), H_2O (5-10), siloxane (0-0.02) NH_3 (<1), CO (0-1) O_2 (0-2).
Rahmouni *et al.* (2002), Bahman *et al.* (2007), Duc and Wattanavichien (2007), Maji *et al.* (2008)	30-73	19-40	N_2 (5-40), H_2 (1-3), O_2 (0-5), H_2S (20 ppm)
Balat and Balat (2009)	55-65	35-45	N_2 (0-3), H_2 (0-1), O_2 (0-2), H_2S (0-1), NH_3 (0-1)
Papadias and Ahmed (2012)	Siloxanes-D4, Siloxanes-D5, Siloxanes-L2		

2.5.1 Biogas Major Compositions and Trace Elements

Anaerobic micro-bacterial biological digestion of the raw materials has responsible to engender of different composition of biogas. Methane (CH_4) and carbon dioxide (CO_2) are the major components and some other trace components present in biogas are portrayed in Table 2.2. The adverse effects of some trace elements present in biogas are presented in Table 2.3.

Table 2.3 Biogas impurities and their consequences (Ryckebosch *et al.* 2010)

Impurity	**Possible impact**
Water	Corrosion in compressors, gas storage tanks and engines due to reaction with H_2S, NH_3, and CO_2 to form acids
Dust	Clogging due to deposition in compressors, gas storage tanks
H_2S	Corrosion in compressors, gas storage tanks, and engines, the toxic (H_2S) concentrations (> 5 cm^3m^{-3}) remain in the biogas, SO_2 and SO_3 are formed due to combustion, which are more toxic than H2S and causes corrosion with water
CO_2	Low calorific value behave as an ignition inhibitor
Siloxanes	Formation of SiO_2 and microcrystalline quartz due to combustion; deposition on spark plugs, valves and cylinder heads abrading the surface

2.5.2 Biogas Physical Properties

The physical and chemical properties of any fuel define its usability. The physical properties of biogas such as auto-ignition temperature, octane number, and significant magnitude of heating value reveal that the fuel is appropriate for both SI and CI engines in DFM (Table 2.4). However, it has some disadvantages as a fuel for DFM engine (Table 2.3). Nevertheless, the quality of biogas composition can be improved with the improvement of anaerobic reactions of the raw material from which biogas are usually generated.

2.6 Biogas Run DFM Engine: Analysis of Parameters

In this section, the performance of biogas run DFM engines is analyzed in the light of reported parametric studies. The discussion of biogas as a fuel for DFM engine has also been made. Further, the possibility of using liquid ternary blends (Diesel-Biodiesel-Ethanol/Butanol/DEE) in DFM engines is also addressed. Ternary blends are considered in the present literature survey to apprehend the maximum usability of the renewable fuels in DFM.

2.6.1 Performance Analysis

The parameters considered are the biogas flow rate (BFR), liquid fuel replacement (LFR), brake thermal efficiency (BTE) and fuel energy share.

2.6.2 Variations of BFR and LFR

The BFR and LFR characteristics of the DFM engine as a function of load, IT, and CR are represented in Fig. 2.3. Bora and Saha (2016a) have observed that at a certain load, the BFR decreases with the increase of CR and with the advancement of IT. The overall reduction of 24.81% of BFR upon increase of CR from 16 to 18 was noticed. Although, in this reduction of BFR, the IT was not addressed. Similarly, upon advancement of IT from 26 to 32 CAD bTDC, there was a reduction of BFR by 8.84%, 6.21%, 2.9%, and 4.25% at the CR of 18, 17.5, 17, and 16, respectively. The trend of LFR was noticed to be similar to that of BFR. At the CR = 18, load = 100% (= 4.24 bar), the investigators found the maximum LFR of 83.17%, 82.67% and 79.32% at the ITs of 26, 29 and 32 CAD bTDC, respectively. The experiments were performed at the BFR in which misfire sound appeared. As a result, the engine consumed a higher amount of biogas (approximately, 1.8 kg/h<BFR<3 kg/h). Almost similar results were reported by other investigators (Bora *et al*., 2014; Debnath *et al*., 2014a; Verma *et al*., 2014; Bora and Saha, 2015a; Bora and Saha, 2015b; Bora and Saha, 2016b; Bora and Saha, 2017) where different biodiesels (Bora and Saha, 2015b) and emulsified biodiesel (Debnath *et al*., 2014a; Bora and Saha, 2015a) as the pilot fuels had been used.

Verma *et al*. (2017a) conducted DFM experiments with varying composition of biogas (comprising 93%, 84%, and 75% of CH_4 by volume respectively). The consumptions of biogas (approximately, 0.54 kg/h<BFR<1.69 kg/h) were confined at a point where misfire was noticed to achieve maximum substitution (approximately, at zero load = 88% >substitution> at maximum load = 65%) of diesel fuel as portrayed in Fig. 2.3(d). They achieved the reverse trends of diesel substitution (Fig. 2.5c). Barik and Murugan (2014) conducted a series of experiments using raw biogas for different BFR (0.3-1.2 kg/h) and loads and optimized the BFR at 0.9 kg/h.

Table 2.4 Physical Properties of Biogas Found in Recent Study

Investigators	Properties of biogas used in the study										
	Composition vol.%		Lower heating value (MJ/kg)	A/F ratio (Stoichiometric)	Flame speed (m/s)	Flammability limit (vol.% in air)	Density (kg/m^3) (1 atm)	Methane number	Octane number	Auto-ignition temperature (˚C)	Lower Wobbe index (kW h/m^{3}N)
	CH_4 (%)	CO_2 (%)									
Sita (2001), Bedoya *et al.* (2009),	30	70	6.70	2.30	-	-	-	-	-	-	-
	40	60	9.80	3.30	-	-	-	-	-	-	-
Nathan *et al.* (2010),	50-57	41-50	13.30-17.22	4.60-5.70	0.25	7.50 (Leaner), 14 (Richer)	1.2 (15˚C)	-	130	650	-
Bedoya *et al.*(2012),	60	40	17-23.73	5.70-6.08	0.25	7.50-14	1.2 (15˚C)	130-160	130-160	650	6.16
Bedoya *et al.* (2013),	70	30	23	7.90	-	-	-	-	-	-	-
Maizonnasse *et al.* (2013)	73	27	25.14	8.54	-	-	-	-	-	-	-
	80	20	29.60	10.10	-	-	-	-	-	-	-
Duc and Wattanavichien (2007)	73	19	26.17	17.23	-	-	0.9145 (0 ˚C)	-	-	-	-
Rahmouni *et al.* (2002), Bahman *et al.* (2007), Maji *et al.* (2008),	30-73	20-40	26.17	17.20	-	-	0.65-0.91	-	130	632-813	-

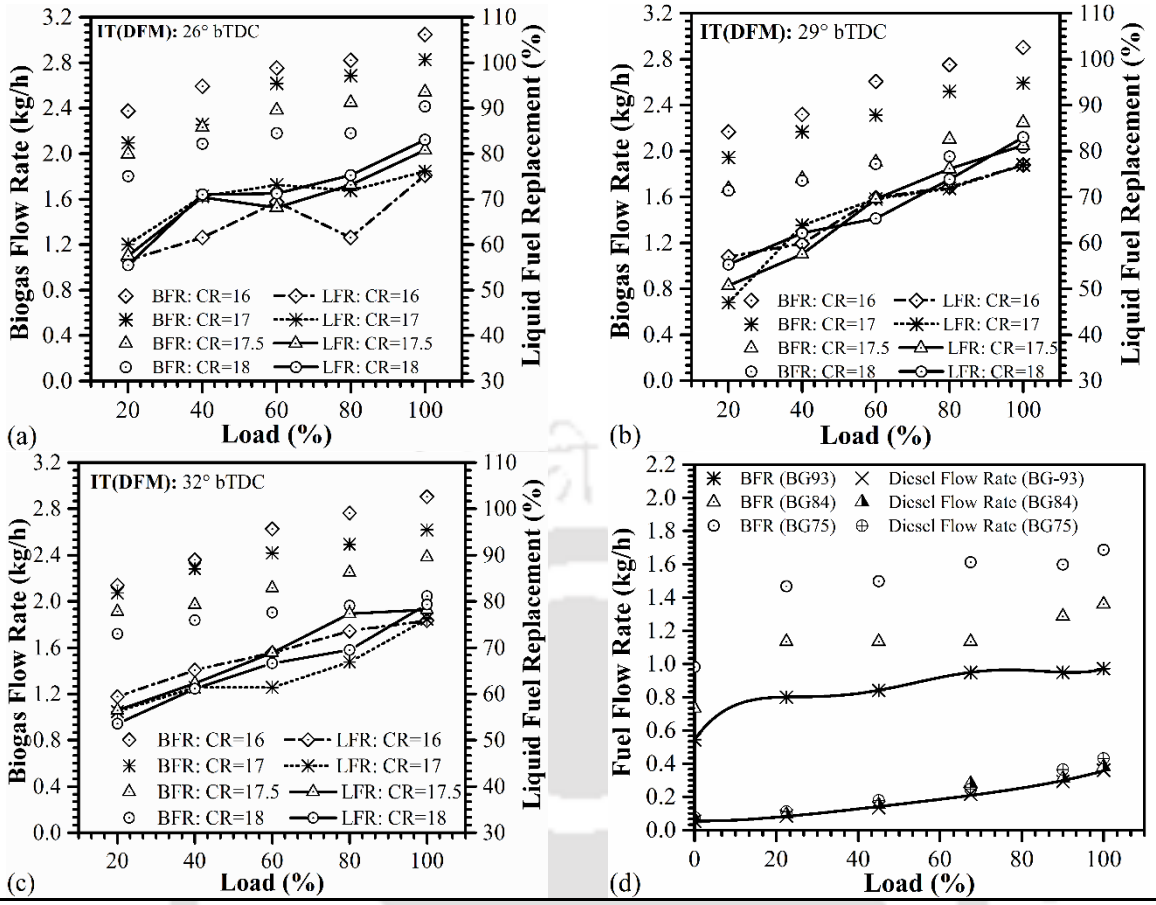

Fig. 2.3 Variation of fuel flow rates with engine load:
(a)-(c) Bora and Saha (2016a), (d) Verma *et al*. (2017a)

2.6.3 Characteristics of BTE

The BTE (instead of BSFC and BSEC) is considered in the following discussion, as in physical sense and by definition, the parameters BSFC and BSEC both are similar and inversely proportional to BTE. The characteristics of BTE in the biogas run DFM engine is shown in Fig. 2.4. Researchers, in general, have noticed lower BTEs in biogas run DFM engine as compared to pure diesel mode (PDM). Bora and Saha (2016a) have studied the performance of a DFM engine at various ITs (26-32 CAD bTDC) and CRs (16 to 18) as portrayed in Fig. 2.4 using diesel as the pilot fuel. The BTE is found to increase with the increase of CR and it improved significantly with the advancement of IT from 26 to 29 CAD bTDC. The maximum BTE was achieved at IT = 29 CAD bTDC and CR = 18. At this setting, the BTE was found to be 25.44%, which is 12.17% and 10.32% higher in contrast to the ITs of 26 and 32 CAD bTDC. However, Bora and Saha (2017) found maximum efficiency at the IT = 32 CAD bTDC and CR = 18 with rice-bran biodiesel. Similar investigations have also been reported (Bora et al., 2014; Bora and Saha, 2015b; Bora and Saha, 2016b; Bora and Saha, 2016c). These investigators have used diesel and different biodiesel as the pilot fuels. The lower BTE in biogas run DFM engine

is attributed to the lower calorific value of biogas, residuals in biogas, lower combustion temperature, low flame speed, higher total fuel consumption, and enhancement of negative work due to induction of large volume of biogas. However, the investigators have used a naturally aspirated engine, hence, for a particular load, the induction of total volume (biogas-air mixture) remained the same, thereby keeping the negative work (compression) intact.

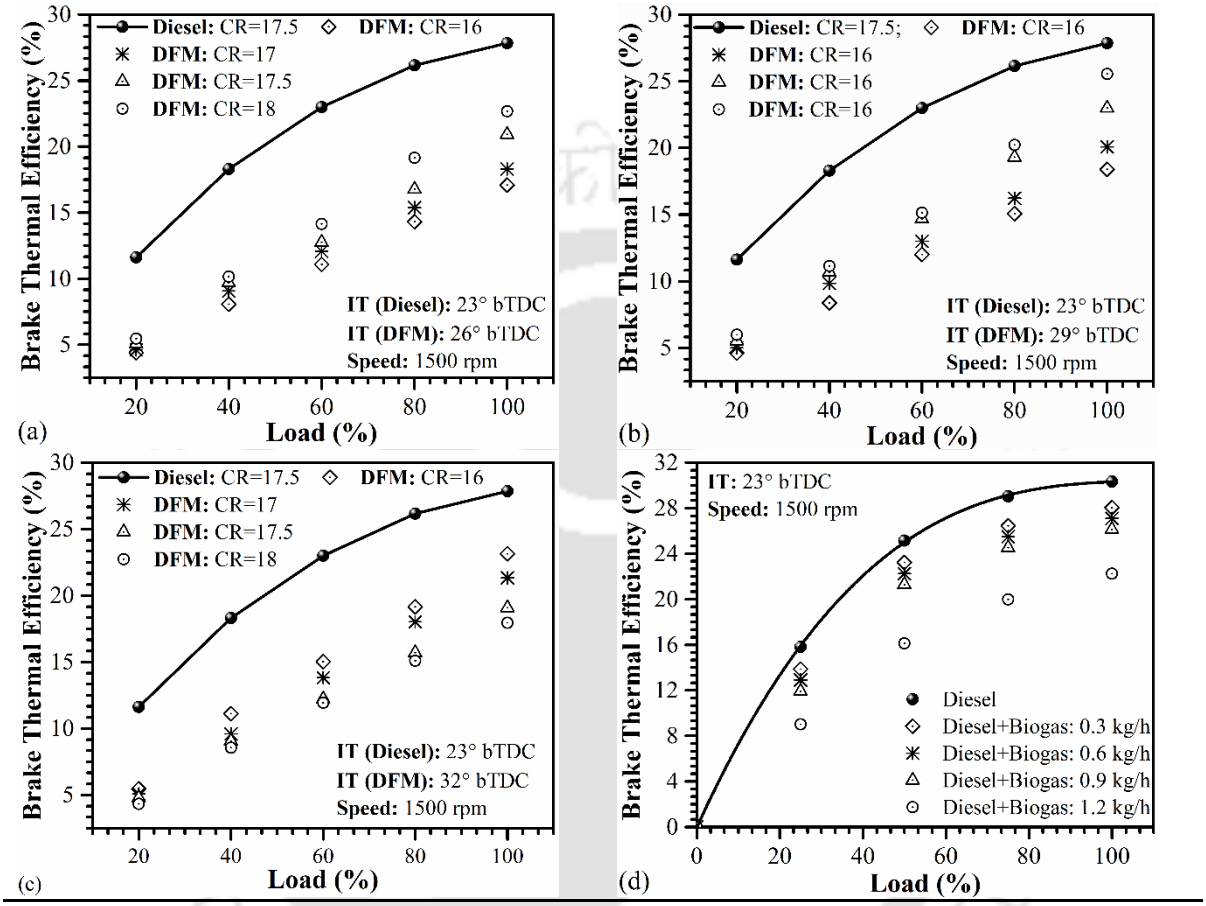

Fig. 2.4 Variations of BTE with load: (a)-(c) Bora and Saha (2016a), (d) Barik and Murugan (2016)

Debnath *et al*. (2014a) conducted the experiments (CR = 17.5 and IT = 23 CAD bTDC) using biogas as the primary and palm oil biodiesel-water emulsion as the pilot fuels. They noticed a 25% lower BTE in DFM as compared to PDM. However, they achieved 41% higher BTE in DFM than that obtained (uses jatropha oil methyl easter biodiesel as the pilot fuel) by Sahoo *et al*. (2012a). Similar experiments at different CRs (17, 17.5, and 18) and ITs (26-32 CAD bTDC) have been conducted by Bora and Saha (2015a) using water-rice-bran biodiesel emulsion as the pilot fuel. The maximum BTE was estimated at 23.62% at the CR = 18 and IT = 29 CAD bTDC. They explained the phenomena of micro-explosion as an efficient technique to improve the combustion strategy of the DFM engine. However, the BTE obtained in this study with emulsified fuel is found sufficiently lower in comparison to reported study (Bora and Saha, 2016a).

Barik and Murugan (2014, 2016) conducted experiments at various BFRs and ITs as seen in Fig 2.4 (d). They observed that the BTE decreases with the increase of BFR. However, the reverse trend of BTE was found with the advancement of IT. The maximum BTE was observed at IT = 26 CAD bTDC. At the standard IT = 23 CAD bTDC and at BFR = 0.3, 0.9 and 1.2 kg/h, the BTEs were estimated as 28.2%, 24.1 and 21.1%, respectively. At IT= 26 CAD bTDC and at BFR = 0.9 kg/h, the BTE was found to be 28.1%. It was inferred that the greater vaporization of pilot fuel and the improved inducted fuel-air mixture at advanced IT helps to raise the BTE. The comparative discussion of different performance parameters is presented in Tables 2.5 and 2.6 (Poonia *et al*. 1999, Abd-Alla *et al*., 2001; Masahiro *et al*., 2003; Wannatong *et al*., 2007; Papagiannakis and Hountalas, 2009; Paykani *et al*., 2012; Kumar and Raj, 2013; Papagiannakis, 2013; Pan *et al*., 2015).

2.6.4 Fuels Energy Share

The properties of liquid and gaseous fuels in DFM are different, and thus the proportion of individual energy share needs to be analyzed. The energy share is defined as the ratio of energy available in a particular fuel to the energy available in the total fuel consumed (Barik and Murugan, 2014; Kalsi and Subramanian, 2017). The variation of energy shares in different engine operating states is portrayed in Fig. 2.5.

Barik and Murugan (2016) conducted investigations at different ITs of a biogas run DFM engine as represented in Fig. 2.5. They set the BFR at 0.9 kg/h. Hence, at higher loads, the higher energy share was noticed with diesel fuel. However, at the advanced IT, the energy share of biogas was found to increase. The reason addressed was the early start of combustion at the advanced IT. Although, at 100% load and at IT of 27.5 CAD bTDC, the biogas energy share was found to decrease due to this prolong IT that reduced the in-cylinder air temperature. Consequently, a comparatively less fuel was burned at this IT relative to the ITs of 24.5 and 26 CAD bTDC, although there were the higher diesel fuel consumption and the corresponding higher cumulative LHV of the accumulated fuels.

Verma *et al*. (2017a) carried out the experiments with synthetic biogas with increasing methane percentage in the compositions (Fig. 2.5c). They observed an increase in diesel substitution with the increasing amount of methane in the biogas composition. Here, DS:BG93 (Fig. 2.5c) means diesel was used as the pilot fuel with 93% methane in biogas as the primary fuel. Hence, the study demonstrated that the diesel substitution and the energy share could be increased using biogas (as primary fuel) having higher methane quantity.

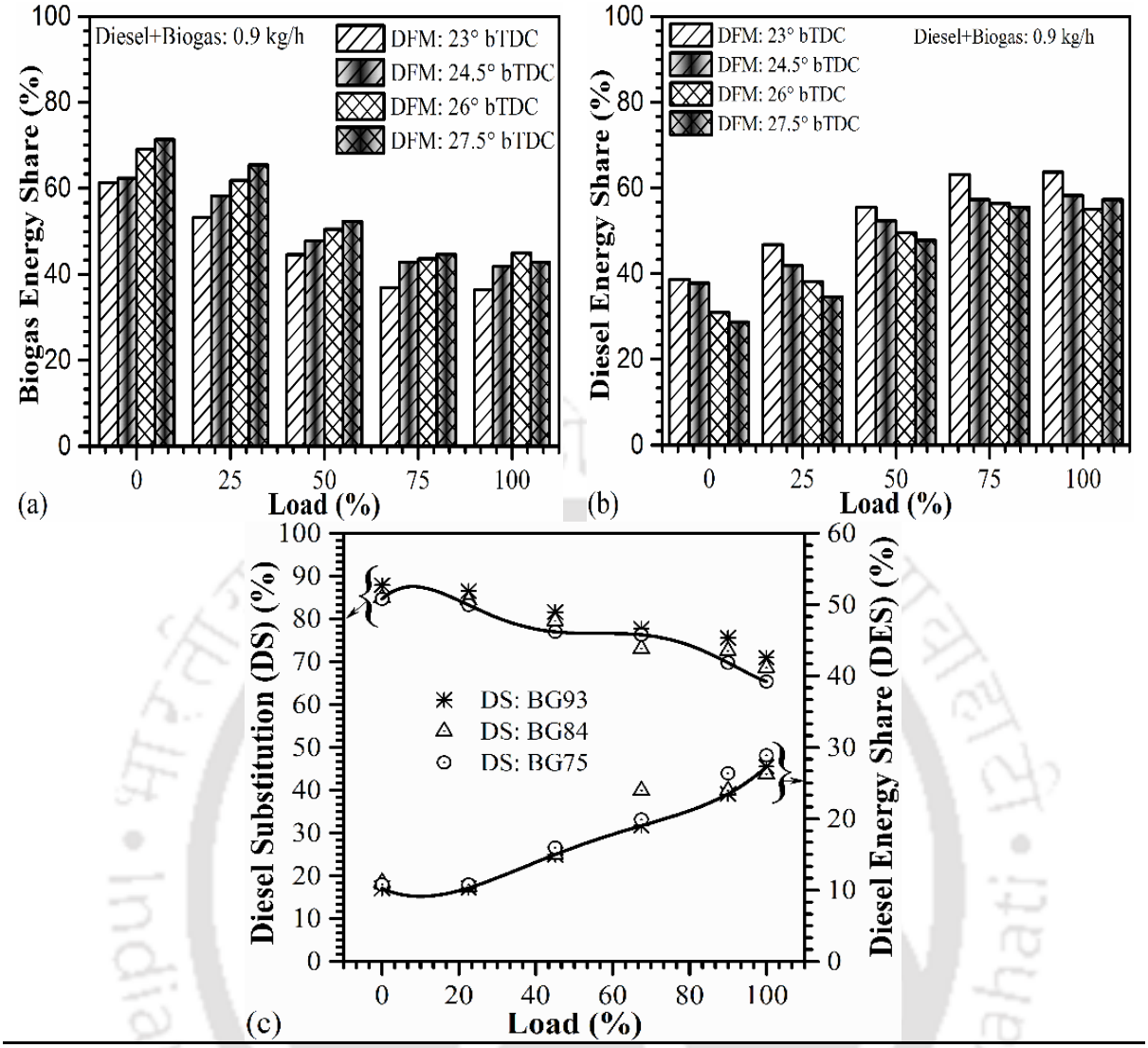

Fig. 2.5 Characteristics fuel energy share at different engine operating states: (a-b) Barik and Murugan (2016), (c) Verma *et al*. (2017a)

2.6.5 Fuel Conversion Efficiency

The parameter, fuel conversion efficiency (FCE) has a crucial influence on the engine performance and combustion. Krishnan (2001) and Krishnan et al. (2002) carried out extensive experimental investigations on the use of natural gas (NG) in a dual fuel diesel engine under various parametric conditions (Figs. 2.6 through 2.8) to study the characteristics of various dependent parameters including FCE and BSEC. In their study, the engine baseline conditions were set at medium engine speed, half load, and turbocharger intake and exhaust pressures at 1700 rpm, 21 kW, 181 kPa, and 171 kPa, respectively. It was observed in DFM that the higher consumption of NG increased the BSEC, reduced the FCE (Fig. 2.6) along with longer the ID (Fig. 2.9). However, at the same baseline condition, they found a remarkable increment of FCE and the reduction of BSEC with the enhancement of Φ_{global} (Fig. 2.7). Nevertheless, the enhancement of NG% in air-stream enhanced the corresponding Φ_{global}. At the maximum

Φ_{global} of 0.5, the efficiency was found even more than PDM. Further, the naturally aspirated engine in DFM was found to be more advantaegeous than the turbocharged DFM. On the other hand, with the increase of intake air temperature, there was a considerable increase of FCE and a considerable reduction of BSEC, respectively, (Fig. 2.8).

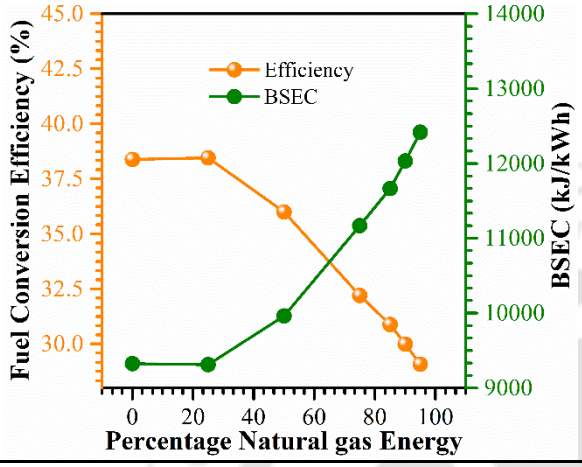

Fig. 2.6 FCE and BSEC versus percentage energy substituted by natural gas at half load

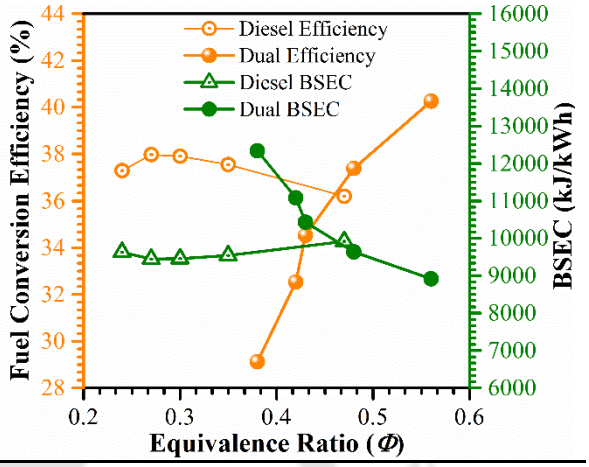

Fig. 2.7 FCE and BSEC versus equivalence ratio (Φ) at half load

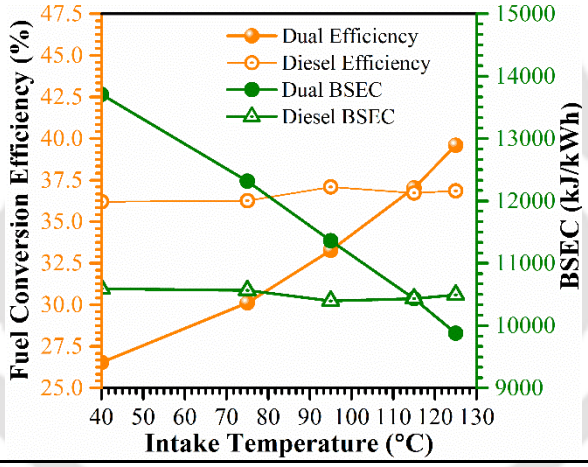

Fig. 2.8 FCE and BSEC versus intake manifold temperature at half load = 21 kW; Parameters considered: Turbocharger intake pressure (P_{in}) = 181 kPa, Intake temperature (T_{in}) = 75°C, Speed = 1700 rpm, half load = 21 kW, Turbocharger exhaust pressure (P_{ex}) = 171 kPa (Krishnan 2001, and Krishnan et al., 2002)

Krishnan (2005) carried out experimental and theoretical investigations considering wide variations of injection timings (ITs), intake charge preheating temeperature (T_{in}), and pilot fuels quantity (Q_{inj}) in a turburcharged advanced low-pilot-ignited natural gas (ALPING) engine. The ITs considered were 15, 20, 25, 30, 35, 40, 45, 50, 55 and 60 CAD, bTDC. At each of the IT, the T_{in} of 35 and 75°C at the loads of 42 kW (full load) and 21 kW (half load) were considered, respectively. The Q_{inj} for both of the loads were kept constant at 3.3 g/min. In this study, the turbocharger intake pressure (P_{in})/exit pressure (P_{ex}) at the loads of 21 kW and 42 kW were set at 1.84 bar/1.71 bar and 2.02 bar/1.91 bar, respectively. The trends of the FCE

and BSEC were found to be different with the advancement of ITs (Fig. 2.9). At full load, the FCE was found to increase with the advancement of IT from 15 to 45 CAD bTDC and upon further advancement, it was found to reduce until reaching the IT at 60 CAD bTDC. In PDM (baseline test), the FCE was estimated to be 41.3%. The reference IT in PDM was fixed at 22 CAD bTDC. At a particular load, the character of FCE was analyzed as a function of start of heat release, magnitude of peak heat relase rate, phasing of heat release relative to TDC and the duration of heat release. Consequently, several heat release patterns were obtained for the same power output; however, the FCE were found to be different at each of the heat release pattern. Krishnan (2005) opined that for a certain amount of fuel, a relatively higher amount of work could be extracted during the expansion process when there were higher realease of heat and shorter durartion of heat release and the heat release phasing was nearer to TDC. Therefore, at a particular load and engine speed, the investigator achieved a higher FCE at advanced and upto some particular range of ITs.

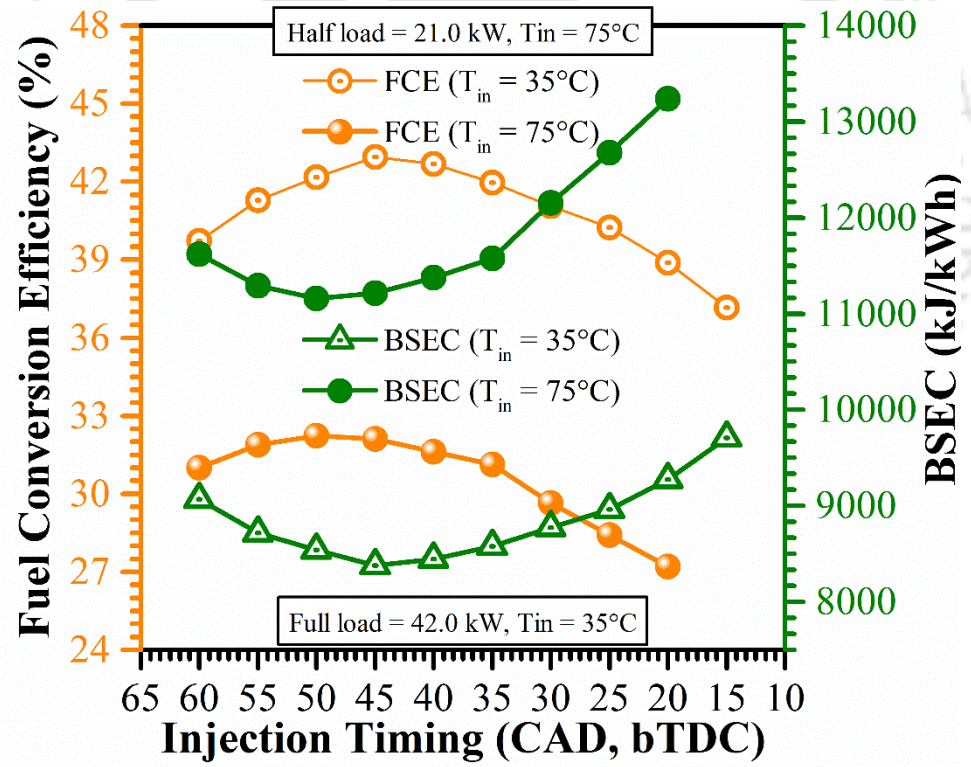

Fig. 2.9 Fuel conversion efficiency and brake specific energy consumption (BSEC) versus injection timing, speed = 1700 rpm, Q_{inj} = 3.3 g/min (Krishnan 2005)

At the half load, the FCE was found to increase from 27 to 32% upon advancing the IT from 20 to 50 CAD bTDC. It indicated that the increment of FCE was depicted at slightly higher advancement of IT relative to the case with full load. In the later stage of advancement of ITs, there was less reduction of FCE as compared to that of full load. The shifting of heat release phasing close to the TDC was stated as the physical reason behind this result. The BSEC was

noticed to have an opposite trend. Similar study was also conducted by Sing et al. (2004). They found a higher FCE at the higher pilot fuel quantity at all ITs. However, the significant increment of FCE was noticed beyond the advanced IT of 40 CAD bTDC due to the increment of the number of ignition centres attributed to the higher burning rates.

Srinivasan et al. (2006) studied the effects of pilot fuel quantity, intake charge preheating temperature, and injection timing (20-60 CAD bTDC) on a turbocharged ALPING engine. The engine was operated at constant speed of 1700 rpm and at engine quarter and half (21 kW) loads. They noticed an excellent NO_x-efficiency trade-offs at the advanced ITs of 55 and 60 CAD bTDC at the corresponding quarter and half loads, respectively. At these advanced ITs, the FCEs were found to be increased with the enhancement of T_{in} and pilot fuel quantity (Q_{inj}). However, there was a significant increase of FCE with enhancement of T_{in} relative to Q_{inj}. The physical reasons are already discussed above.

2.7 Combustion Analysis

In this section, the effects of ID, engine-cylinder pressure history, NHRR, CD, and CMGT are analyzed for the DFM engine run with biogas and with various oxygenated liquid fuels.

2.7.1 Variation of ID

The ID defines the point of ignition (POI) of fuel on the crank angle scale after the injection of the high cetane liquid fuel into the combustion chamber. The parameters that are allied with the ID are fuel characteristics, fuel-air equivalence ratio, engine speed, spray characteristics, states of the intake charge, IT, CR, and the cylinder pressure (Park *et al*., 2011; Satyanarayana and Muraleedharan, 2011; Mustafi *et al*., 2013). In a DFM, multi-phase fuels having different physical and chemical characteristics are used. Hence, the study of ID in DFM is important.

The variation of ID in the biogas run DFM engine is depicted in Fig. 2.10. Bora and Saha (2016a) investigated the effect of different CRs and ITs on ID using a very high BFR (Fig. 2.10a through 2.10c). They found a decrease of ID with the increase of loads and CRs. However, ID was found to increase with the advancement of ITs. It was found to be increased by 8.52% while advancing the IT from 26 to 32 CAD bTDC, whereas, it was noticed to be reduced by 8.2% while increasing the CRs from 16 to 18. Large BFR and higher heat capacity of biogas lowered the in-cylinder temperature causing this prolonged ID in DFM as compared to PDM. The reduction of ID at higher CR was due to the enhancement of biogas mixture temperature that accelerated the pre-ignition reaction. Further, the higher ID at advanced IT was due to the reduction of temperature of the inducted biogas-air mixture.

Table 2.5 Performance characteristics of biogas DFM engines

Investigators	Operating parameters	Liquid Fuel	BFR	BSFC	BTE	LFR	BES
Duc and Wattanavichien (2007)	rpm = 1000-2400; load = part and full	Diesel (primary at part loads)	-	↓with ↑rpm	↑with ↑rpm and ↑load	↓with ↑load; ↑with ↑rpm	↑with ↑load
Debnath et al. (2014a)	rpm = 1500; IT=23 CAD bTDC, CR=17.5; load = 0-3.65 kW; at misfire	Water biodiesel emulsion (WIP)	≈1.7-2.2 kg/h; ↑with ↑load	↓with ↑load; observed lower with WIP	↑with ↑load; observed higher with WIP	↑with ↑load; LFR=55%maximum noticed	-
Bora *et al*. (2014)	rpm = 1500; load=20%-100% IT = 23 CAD bTDC; CR = 16, 17, 17.5 and 18; at misfire	Diesel	↑with ↑load; ↓with ↑CR	↓with ↑load and CR	↑with ↑load and ↑CR; maximum of 20.04% at CR=18 was achieved	↑with ↑(load, IT and CR)	-
Barik and Murugan (2014)	rpm = 1500; load = 0% -100% (step =25%);	Diesel as the pilot fuel	0.3-1.2 (step = 0.3) Kg/h	↓with ↑load; ↑with ↑BFR	At load =100%, BFR = 0.3 and 1.2 kg/h, BTE=28.2 and 21.1%, respectively	↑with ↑BFR; ↓with ↑load	↑with ↑BFR; ↓ with ↑ load
Verma *et al*. (2014)	Up gradated biogas; rpm = 1500; Load = 20%-100%	Diesel	↑with ↑load	↓with ↑load	↑with ↑load and scrubbed biogas	↑with ↑load	-
Bora and Saha, (2015a)	rpm = 1500; load=20%-100% IT = 23-32 CAD bTDC; CR = 17, 17.5 and 18; at misfire	Water rice bran biodiesel emulsion (WIP)	↑with ↑load; ↓with ↑(CR and IT); varies from ≈2.2-2.9 kg/h	-	↑with ↑load, ↑CR and ↑IT up to 29° bTDC; at 100% load and at this IT maximum BTE of 23.62% was found	↑with ↑load, ↑IT and ↑CR	-
Bora and Saha (2015b)	rpm = 1500; load=20%-100% IT = 23 CAD bTDC; CR = 17.5; at misfire	Different biodiesels	↑with ↑load; varies from ≈2.3-3 kg/h	↓with ↑load	↑with ↑load at 100% load maximum BTE of 19.97% was found with RBME	↑with ↑load	-
Bora and Saha (2016a)	rpm = 1500; load=20%-100% IT = 26-32 CAD bTDC; CR = 16, 17, 17.5 and 18; at misfire	Diesel	↑with ↑load; ↓with ↑CR and ↑IT	-	↑with ↑load, ↑CR and ↑IT up to 29° bTDC; at 100% load and at this IT maximum BTE of 25.44% was found	↑with ↑load, ↑IT and ↑CR	-
Barik and Murugan (2016)	rpm = 1500; load = 0-100%; IT= 23 - 27.5 CAD bTDC (step = 1.5 CAD)	Diesel as the pilot fuel	0.9 kg/h	↓with ↑ load and IT	↑ with ↑load and ↑IT	-	↓with ↑ load; ↑with ↑IT
Barik and Murugan (2016a)	rpm = 1500; biodiesel IT = 23 and 24.5 CAD bTDC; DEE port injection	Biodiesel (pilot); DEE (port)	0.9 kg/h	↓with ↑load and ↑IT; ↓ up to 4% DEE	↑ with ↑load and ↑IT; ↑by 7.2 and 8% with 2% and 4% DEE, respectively, compared to biodiesel DFM	-	-

BES = Biogas Energy share, ↑ indicates the increasing and advancement trends; ↓ indicates the decreasing and retardation trends

Table 2.6 Performance of DFM engines with various gaseous fuels at various ICT

Investigators	Operating parameters	Fuels (Pilot/Primary)	ICT (°C)	BTE	PP	NHRR	CO	HC	NO_x
Poonia *et al*. (1999)	rpm = 1500; load = 20-100%; IT= 24 CAD bTDC (diesel) and 27.4 CAD bTDC (DFM)	Diesel (with varying quantity)/ LPG	34-70	↑with ↑ICT and ↑pilot quantity	↑with ↑ICT	↑with ↑ICT	↓(drastic) with ↑pilot quantity and ↓slightly with ↑ICT	↓with ↑ICT and ↑pilot quantity	-
Abd-Alla *et al*. (2001)	rpm = 1000; CR = 21; IT = 25 CAD bTDC	Diesel/gas mixture	28, 45 and 65	-	-	-	↓with ↑ICT	↓with ↑ICT	↑with ↑ICT
Ishida (2003)	rpm = 1700; load = 0.33 MPa and 0.66 MPa	Diesel/ CNG		-	-	↑with ↑ICT	-	↓with ↑ICT	↑with ↑ICT
Wannatong (2007)	rpm = 1200-2800; IT = 8, 17, 34	Diesel/ CNG	50-100	-	↑with ↑ICT	↑with ↑ICT	-	-	-
Papagiannakis *et al*. (2009)	load = 40% and 80%; IT = 14 and 16 CAD bTDC	Diesel/NG	47, 67, 87, 107	-	↑with ↑ICT	↑with ↑ICT	↓with ↑ICT, ↑load and ↑IT	-	↑with ↑ICT
Paykani *et al*. (2012)	CR = 17.5; IT = 20 CAD bTDC varying EGR	Diesel/ CNG	100-167	↑with ↑ICT	-	-	↓with ↑ICT	↓with ↑ICT	↑with ↑ICT
Kumar and Raj (2013)	rpm = 1500; varying IT	Biodiesel ethanol blend	40 and 60	-	↑with ↑IT and ↑ICT	↑with ↑IT and ↑ICT	↓with ↑ICT	↓with ↑ICT	↑with ↑ICT
Papagiannakis (2013)	load = 40% and 80%; IT = 14 and 16 CAD bTDC	Diesel/NG	50, 65 and 80	↑with ↑ICT	↑with ↑ICT	↑with ↑ICT	↓with ↑ICT	-	↑with ↑ICT
Pan et al. (2015)	rpm = 1500; IT = 2 CAD bTDC;	Diesel/port fuel is methanol	20, 40, 60, 70 and 80	-	↑with ↑ICT, and shifted towards TDC	↑with ↑ICT, shifted towards TDC	↓with ↑ICT	↓with ↑ICT	↑with ↑ICT

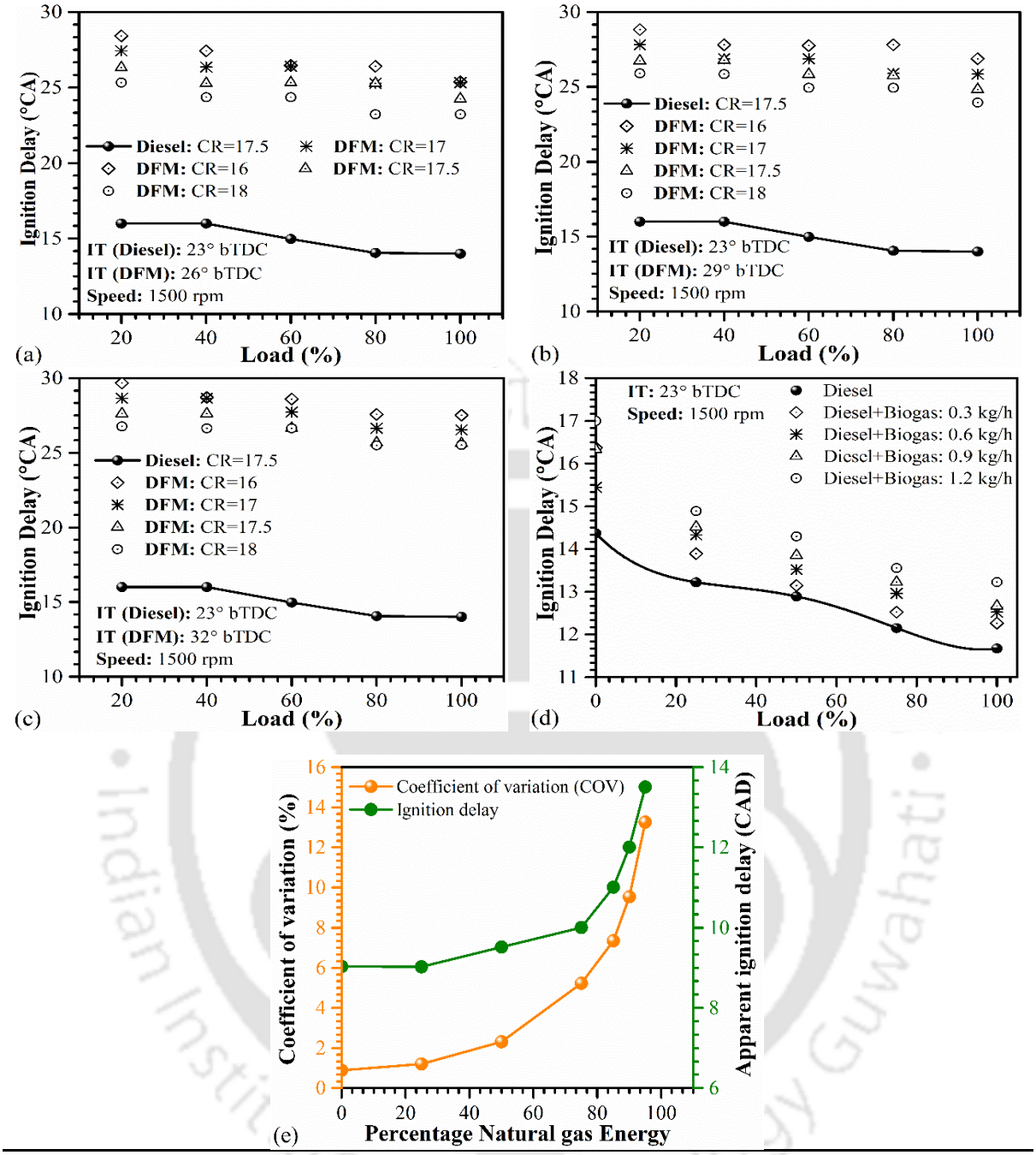

Fig. 2.10 Characteristics of ID: (a)-(c) Bora and Saha (2016a), (d) Barik and Murugan (2014), (e) COV of indicated mean effective pressure,and apparent ignition delay versus percentage energy substituted by natural gas (Krishnan 2001 and Krishnan et al., 2002)

Barik and Murugan (2014) while conducting investigations at standard IT = 23° bTDC and CR = 17.5 (Fig. 2.10d) observed a reduction of ID with the increase of loads. The ID estimated was found substantially lower in comparison to earlier reported data (Bora and Saha 2016a). The lower BFR was attributed as the physical reason behind it. At the optimized BFR = 0.9 kg/h, Barik and Murugan (2016) tested the DFM engine by advancing ITs, where a higher ID was observed. At 100% load and at IT= 24.5, 26, and 27.5, the IDs were estimated as 12.4,

12.7, and 13.6 CAD. Whereas, in PDM, it was calculated to be 11.8 CAD. The reduction of gas mixture temperature (at an advanced IT) and the deficiency of oxygen molecule (in the presence of biogas) that altered the nature of pre-ignition reaction of the gas mixture were signified as the main physical reasons behind the higher ID in DFM.

Krishnan (2001) and Krishnan et al. (2002) observed an enhacement of apparent ignition delay with the increment of percentage of NG energy in DFM (Fig. 2.10e). The reason behind this result was attributed to the progressively slower burning rates with increasing percentage of NG energy share that enhanced the ignition delay. It was also observed that higher energy share of NG enhanced the coefficient of cyclic variation (COV) remarkably (Fig. 2.10e).

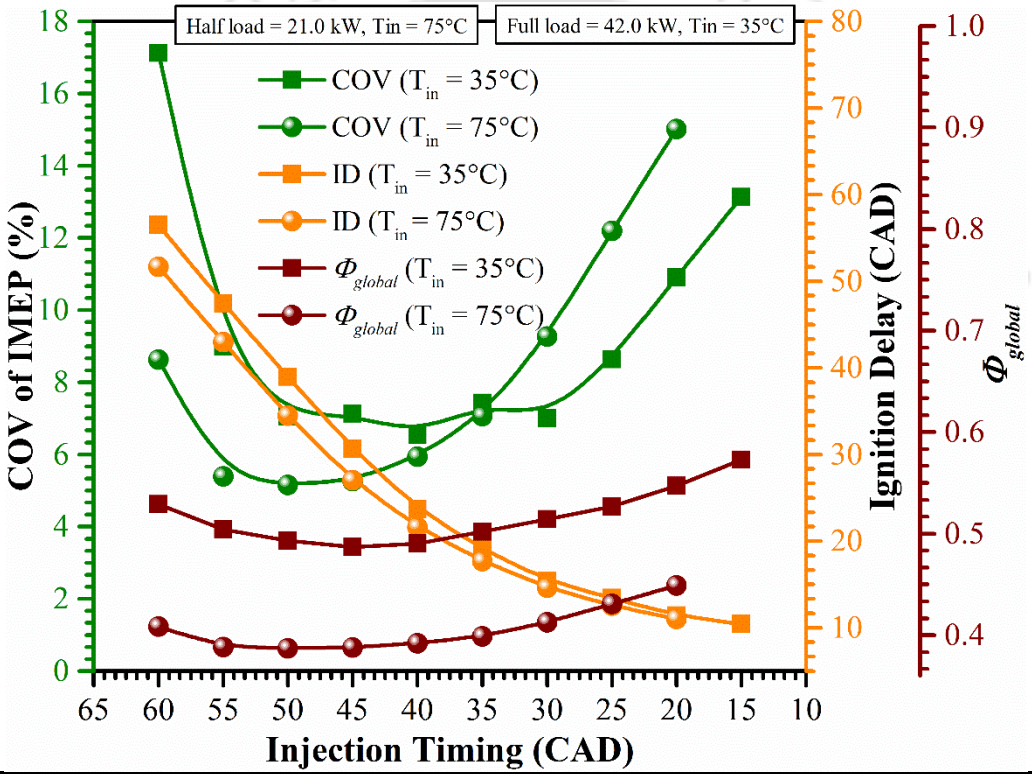

Fig. 2.11 Coefficient of variation of IMEP, ID (calculated from the onset of heat release), and overall equivalence ratio versus injection timing, speed = 1700 rpm, Q_{inj} = 3.3 g/min (Krishnan 2005)

In a separate study, Krishnan (2005) observed that the low pilot ignited NG dual fuel engine exihibited cycle-by-cycle variations. He made a graphical relations among the parameters viz., coefficient of cyclic variations of indicated mean effective pressure (COV of IMEP), ID, and Φ_{global} (Fig. 2.11). The engine was operated at different ITs, two T_{in} and two loads as indicated in Fig. 2.11. In the analysis of COV, a total of 150 successive engine cycles were consiederd. The Φ_{global} was limited to a maximum of 0.6. The lower and minor variations of COVs were noticed within the range of ITs of 30 to 50 CAD bTDC. The major reason of higher COV was stated to the inconsistencies in ignition or combustion phasing relative to TDC. The IDs within

the range of ITs of 30 to 50 CAD bTDC were observed to have a long enough delay period for the preparation of acceptable mixing of pilot and primary fuels and air prior to the start of ignition and this enhanced the probability of the repeatiablity from one operating cycle to the next one. However, beyond this range of IT (at advanced or retarded condtion), the variations in ignition or combustion phasing were found to be higher with the consequence of higher COV.

Srinivasan et al. (2006) noticed that the COV increased with the enhancement of pilot fuel quantity and reduced considerably with the enhancement of intake air tempereature in DFM. The experiments were conducted at the advanced IT of 60 CAD bTDC. However, the COV was found to be reduced to some extent with the increase of load. At increasing pilot quantity and therefore the higher rail pressure, the penetration was indicated to be higher. Hence, some quantity of pilot fuel in some cycles might reach the boundary layers or cooler areas that caused higher variations in ignition and combustion phasing. Thus, with higher pilot quantity, the investigator noticed a higher COV. However, with the intake charge preheating, the ignition was noticed to be advanced leading to faster and more repeatable origination of flame. On the other hand, the avaregae combustion phasing (CA50) was noticed to be advanced (closer to TDC) by 10 CAD, indicating a greater fraction of energy release near to TDC. This revealed a higher FCE and a lower COV. In this investigation, at half load (21 kW), 7% reduction of COV was estimated upon enhancement of intake charge temperature from 75 to 105°C.

2.7.2 Cylinder Pressure History

The cylinder pressure history is crucial to study the ID, NHRR, combustion phasing, cyclic variations of the engine, cylinder mean gas temperature (CMGT), combustion duration (CD) and the position of the peak pressure relative to the crank angle. In DFM, the probability of cyclic variation is more in comparison to PDM as higher-octane fuels are used in the former. The higher amount of gaseous fuel consumption, therefore, can lead to faster flame propagation thereby reducing the combustion duration with the penalty of undesirable cyclic variations. However, higher consumption of raw biogas that has the CO_2 (as the major component) can extinct the flame front.

The characteristics of the pressure history of biogas run DFM engine is shown in Fig. 2.12. Bora and Saha (2016a) discussed the in-cylinder pressure variation with engine crank angle at different CRs and ITs (Fig 2.12a and 2.12b). They observed a shifting of crank angle position of the cylinder peak pressure (CPP) towards TDC with the increase of CR and IT. At the IT =

26 CAD and BMEP = 4.24 bar, the relative crank angle position of CPP was found to be 10, 9, 8 and 8 CAD aTDCs at the CRs of 16, 17, 17.5 and 18, respectively. At these CRs and applied loads, the position of CPP was observed at 9, 9, 8 and 8 CAD aTDC at IT = 29 CAD bTDC and 8, 8, 7 and 6 CAD aTDC at IT = 32 CAD bTDC, respectively. The study demonstrated a pronounced effect of IT in comparison to the shifting the CPP towards TDC with the enhancement of CR. However, in the previous analysis (Bora and Saha 2017), a higher IDs was estimated at the advanced ITs in comparison to the ones that obtained by increasing the CRs. Moreover, the IDs were estimated relative to the static injection timing (SIT = 23 CAD bTDC). Thus, in this context, the shifting of CPPs with CRs should be more in comparison to ITs. The analysis of the combustion phasing can be used as the tool to clarify this conflict. Later experiments with emulsified fuels (Bora and Saha 2015a) demonstrated similar trends of cylinder pressure history. In general, a significantly lower CPP was noticed in DFM in comparison to PDM.

In the context of pressure history analysis, Barik and Murugan (2014) found a higher CPP in DFM than PDM (Fig. 2.12c). The CPP was found to have shifted from TDC with the increase of BFR. The higher CPP in biogas run DFM is only possible at the higher Φ_{global}. Hence, the engine speed would be higher in comparison to the constant speed (1500 rpm) of the diesel engine specified in this investigation. Consequently, the gaseous fuel promotes a faster flame propagation that helps to burn a higher quantity of liquid fuels as the higher cetane liquid fuels have the higher LHV. This, in turn, develops a higher pressure inside the combustion chamber (Karim and Wierzba, 1992; Liu and Karim, 1997; Mustafi *et al*., 2013). At an advanced IT, Barik and Murugan (2016) noticed a higher CPP (13.14% higher at BFR = 0.9 kg/h) in comparison to the standard IT = 23 CAD bTDC in DFM. At IT = 27.5 CAD bTDC and in comparison to PDM, the increment of 28.66% of CPP was noticed in DFM. The reasons for higher CPP at the advanced ITs were believed to be due to the formation of the rich fuel mixture, the occurrence of early combustion that caused a rapid premixed combustion. However, the investigators noticed a higher ID at the advanced IT, where the IDs were calculated with respect to the SIT = 23 CAD bTDC. On the other hand, the study did not report any analysis of combustion phasing. Hence, this higher pressure could be due to the higher Φ_{global} that caused a rapid reaction in premixed combustion phase. Later, Verma *et al*. (2017a) also found similar behaviour as observed in Fig. 2.12d.

Krishnan (2001) and Krishnan et al. (2002) carried out experimental investigations at various conditions as discussed above on the turbocharged dual fuel diesel engine performance using NG as the primary fuel (Fig. 2.12e). They found that with increasing of percentage of NG

energy share the in-cylinder pressure declined progressively. The physical reasons behind this would be discussed later in the heat release history of this section.

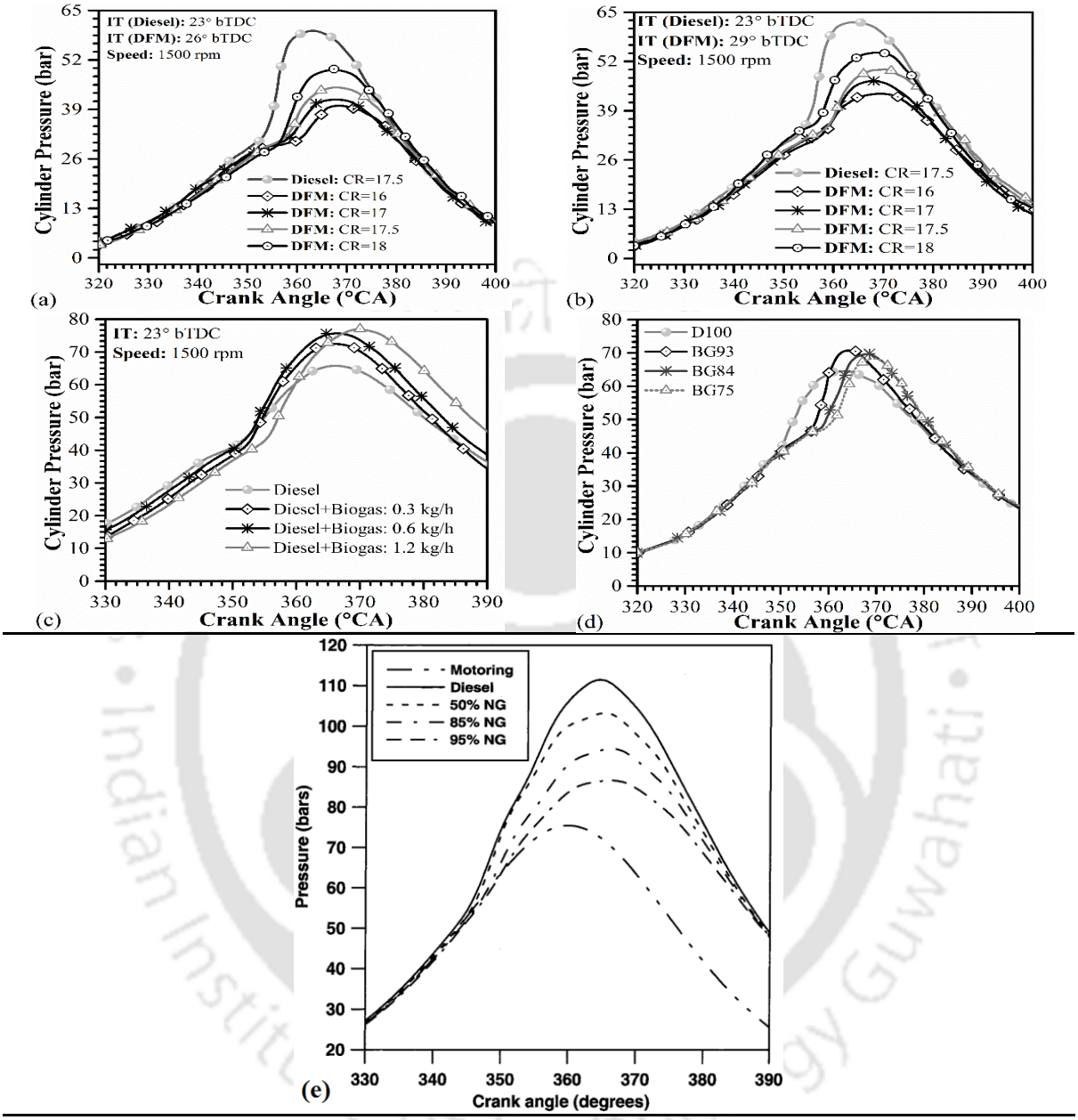

Fig. 2.12 In-cylinder pressure history: (a)-(b) Bora and Saha (2016a), (c) Barik and Murugan (2014), (d) Verma *et al*. (2017a), (e) Krishnan (2001) and Krishnan et al., (2002)

2.7.3 Variations of NHRR

The net heat release rate (NHRR) is the consequence of start of combustion (SOC) and rigorous ignition reaction of the fuel. Therefore, it is always desirable to release more heat by the combustion of fuel in a diesel engine. The NHRR is the function of cylinder pressure, volume, specific heat ratio and crank angle position (Heywood, 1988; Stone, 1999). Thus, the

parameters NHRR, cylinder pressure history, crank angle position, and fuel characteristics are internally related to each other.

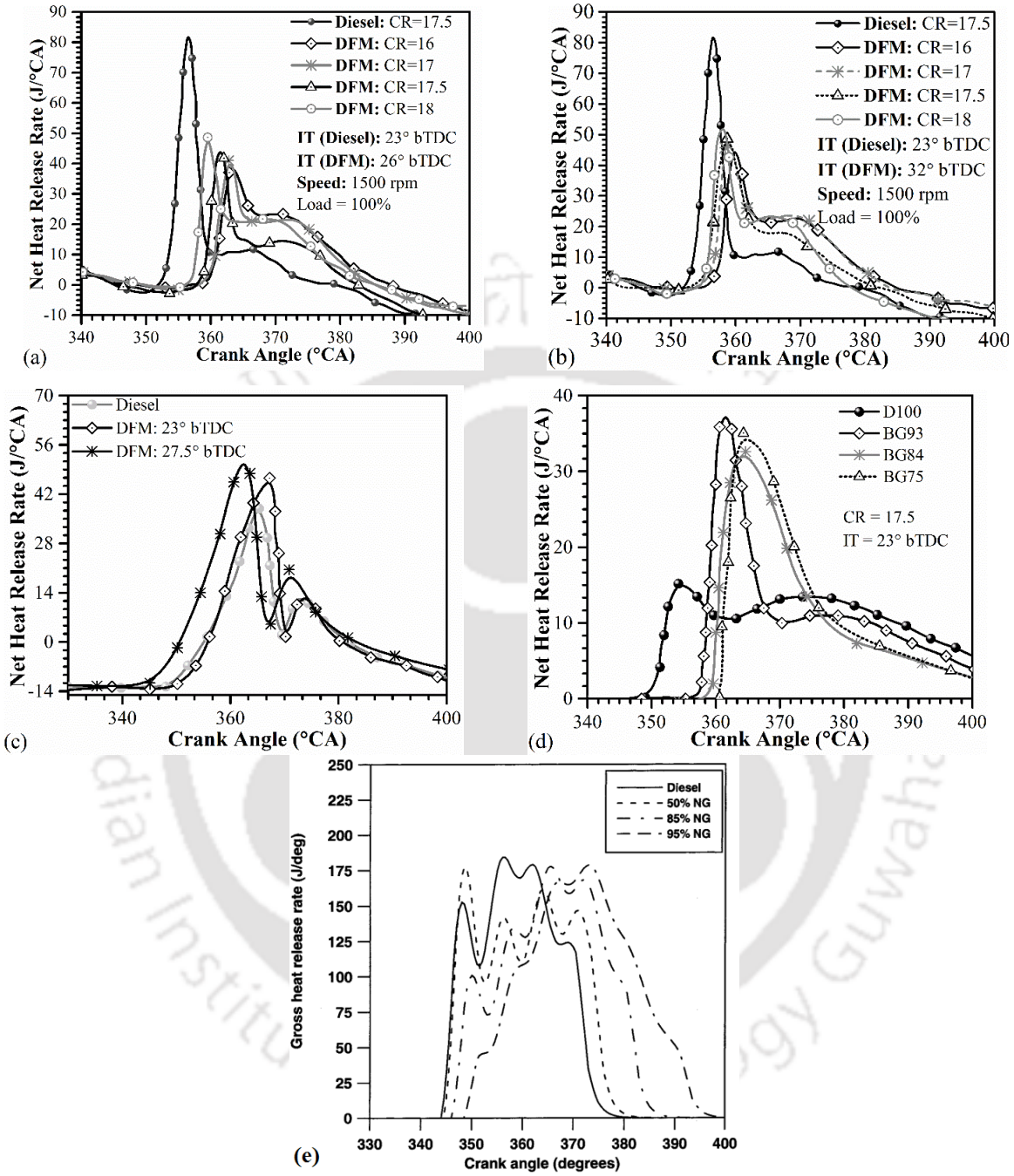

Fig. 2.13 Characteristics of NHRR: (a)-(b) Bora and Saha (2016a), (c) Barik and Murugan (2016), (d) Verma *et al*. (2017a), (e) Krishnan 2001 and Krishnan et al., 2002

The variation of NHHR is portrayed in Fig. 2.13. At various CRs and ITs, the NHRRs of a biogas run DFM engine were estimated by Bora and Saha (2016a) (Fig. 2.13a and 2.13b). The NHRR was found to increase with the increase of CRs and advancement of ITs. However, in DFM, the NHRR noticed to be substantially lower than PDM. In DFM with CR=16 and at the

maximum load of 4.24 bar, and IT = 26, 29 and 32 CAD bTDC, the reductions were estimated as 52.14%, 48.23%, and 45.74%, respectively. At this load and same ITs, (but at CR = 17.5) the reductions were calculated as 44.13%, 42.9%, and 41.35%, respectively. The only physical reason for this inferior NHRR in DFM might be due to the lower LHV of biogas in comparison to PDM. Similar results also were reported by Debnath *et al*. (2014a), Bora and Saha (2015a), Bora and Saha (2016b, 2016c, 2016d).

According to Barik and Murugan (2014, 2016), the NHRR is the combination of heat release rates caused by the combustion of injected pilot diesel fuel, combustion of inducted biogas in the immediate vicinity of the ignition kernel and the pre-ignition reaction due to subsequent flame propagation. It is understood that the NHRR in uncontrolled combustion phase (premixed) depends on ID, the formation of the mixture, and combustion rate at the preliminary stage of combustion. The investigators have found a higher NHRR in DFM than that in PDM (Fig. 2.13c). The reasons may be due to the increasing accumulation of total fuels due to prolonged ID, combined uncontrolled premixed combustion (of pilot and primary fuels) close to the pilot ignited combustion center. The NHRR is also referred as the dependent quantity of the parameters such as the quality of fuel mixture (diesel + biogas + air), fuel mass flow rate, and LHV of the liquid and gaseous fuels. At 100% load, (in PDM), the position of maximum NHRR of 8.5 CAD aTDC is found. At this load, in DFM, the positions of the maximum peak of NHRR with the BFRs of 0.3 kg/h, 0.6 kg/h, 0.9 kg/h, and 1.2 kg/h have been noticed at 7.8, 8.4, 10, and 11.6 CAD aTDC, respectively. On the other hand, at this load, and at standard IT = 23 CAD bTDC, the positions of the higher peak of NHRR in PDM have been observed at 7.3 CAD aTDC. Similarly, at this full load (in DFM), the positions of the maximum peak of NHRR at the ITs of 23, 24.5, 26, and 27.5 CAD bTDC are found at 7.7, 6, 4.9 and 3 CAD aTDC, respectively. Verma *et al*. (2017a) have also observed the similar trend of NHRR as shown in Fig. 2.13d. The lower oxygen concentration, lower polytropic index of methane in biogas as compared to air and the diluent CO_2 present in biogas also absorbs a considerable amount of heats with the consequence of higher ID. This causes the fuel to get accumulate progressively and burn rapidly in the premixed phase of combustion. All these physical interpretations are attributed to the higher NHRR than PDM. However, biogas has the lower calorific value (nearly 50% lower than that of the diesel fuel). Hence, it may be due to the rich fuel-air mixture.

Krishnan (2001) and Krishnan et al. (2002) in their combustion analysis observed that with the reduction of diesel and the corresponding enhancement of percentage of NG energy share, the

peaks of the heat release curve steadily reduced (Fig. 2.13e). It was due to the fact that the heat release curve first originated form the combustion of pilot diesel that evaporated and got mixed with gaseous fuel molecule surrounding the sprayed diesel during delay period. The investigators found an exception of the peak of heat realease curve at the 50% NG, which was noticed to be higher than that of peak of PDM at the same experimental conditions. They elaborated this with the help of the neddle lift curve. The same magnitude of neddle lift (indicating injection of diesel quantity) for diesel and 50% NG were noticed. This was attributed to the higher intial peak heat release than that of diesel. Besides, the heat release curves revealed that at higher percentage of NG energy share there was a shifiting towards right relative to the lower percentage of NG. This was probably due to the loss of energy to the exhaust at higher percentage NG energy share.

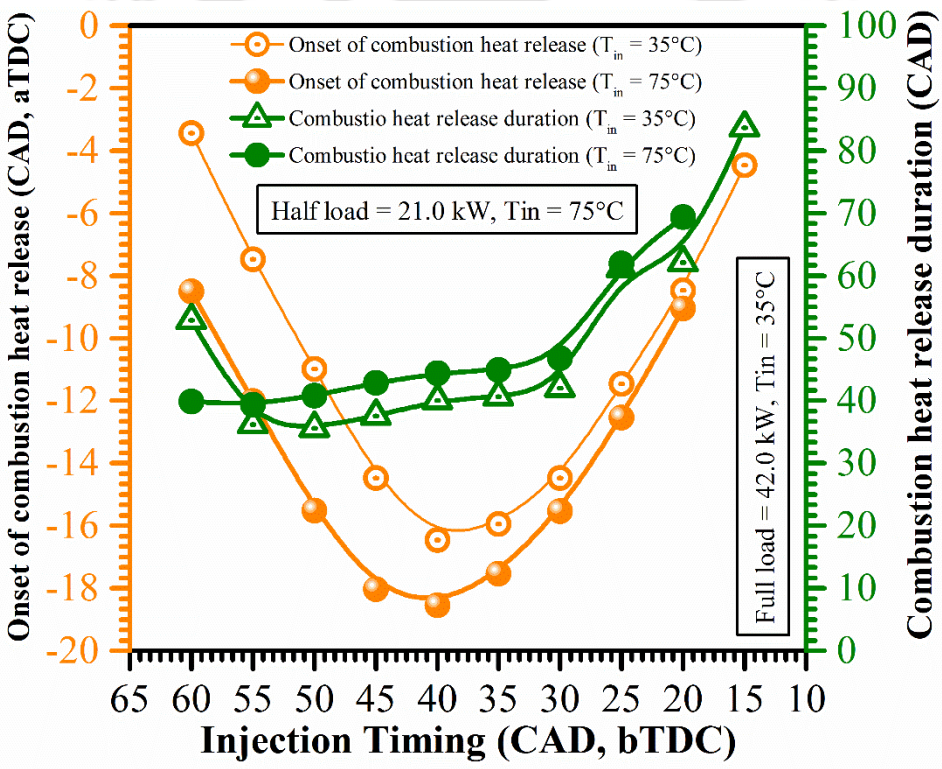

Fig. 2.14 Onset of combustion heat release and combustion heat release duration versus injection timing, rpm = 1700 rpm, Q_{inj} = 3.3 g/min (Krishnan 2005)

Krishnan (2005) studied the characteristics of onset of combustion heat release rate and combustion heat release duration with the variations of IT as shown in Fig. 2.14. The onset of combustion occurred earlier within the ITs of 30 to 45 CAD bTDC, while it was noticed to be progressively delayed beyond this range and started near to TDC. Nevertheless, the combustion duration was observed to have a different trend. The CD with the IT of 15 CAD bTDC was noticed to be higher than that with the IT of 60 CAD bTDC. Physically, the expansion stroke

associated with the longer CD indicated a reduction in FCE. In DFM, in order to achieve an efficient combustion performance, the investigator emphasized on the correct distribution of the ignition kernels in the combustion chamber. Hence, higher advanced IT was strongly recommended in this study. It was because, the advanced IT made the ID prolonged, which allowed a longer time to evaporate the droplets of diesel that helped to disperse the diesel fuel in the cylinder promoting a better mixing of total-fuel and air. Therefore, these well distributed ignition kernels led to rapid flame propagation through the sorrunding NG-air mixture and reduced the CD. The suitable range of IT to reduce the CD was found to be within 30 to 60 CAD bTDC.

2.7.4 Combustion Duration

The combustion duration (CD) is defined as the crank angle interval between the 10% (CA10) and 90% (CA90) cumulative heat release (Bedoya *et al*., 2011; Ryan *et al*., 2015). Physically, CA10 is used to identify the start of combustion (SOC) and CA90 is used to identify the end of combustion (Bedoya *et al*., 2011; Ryan *et al*., 2015; Wang *et al*., 2016). Hence, the combustion duration is the part of the analysis of the combustion phasing. The CD depends on the intake charge thermodynamic states and the fuel characteristics. The shorter CD is desirable in order to achieve more high-grade energy in diesel engines. Hitherto, the CD analyses in biogas run DFM engines have been very limited. Barik and Murugan (2014, 2016) analyzed the CD at various BFR and ITs as shown in Fig. 2.15 (a) to (b), and noticed a higher CD at higher BFR in DFM in comparison to PDM. At full load in PDM, the CD was found to be 37.4 CAD. At the same full load in DFM, the CD of 39, 39.5, 40.4, and 42.1 CAD were observed at BFRs of 0.3, 0.6, 0.9, and 1.2 kg/h, respectively. The reasons behind these results were attributed to the induction of biogas that altered the physical properties of the gas mixture during compression, and reduction of oxygen concentration that caused a slower diffusion combustion. At higher load, the consumption of higher fuel quantity raised the CD. Barik and Murugan (2016) observed to some extent a lower CD at the advanced ITs of 24.5 and 26 CAD (Fig. 2.15b). However, the drastic enhancement of CD was noticed at IT of 27.5 CAD bTDC.

The comparative performance and combustion analyses presented in Table 2.7 (Cacua *et al*. 2012, Mustafi *et al*. 2013, Park *et al*. 2014, Barik and Murugan 2014, Bora and Saha 2015b,

Barik and Murugan 2016, Barik and Murugan 2016a, Bora and Saha 2017) that give the useful information regarding biogas run DFM engine.

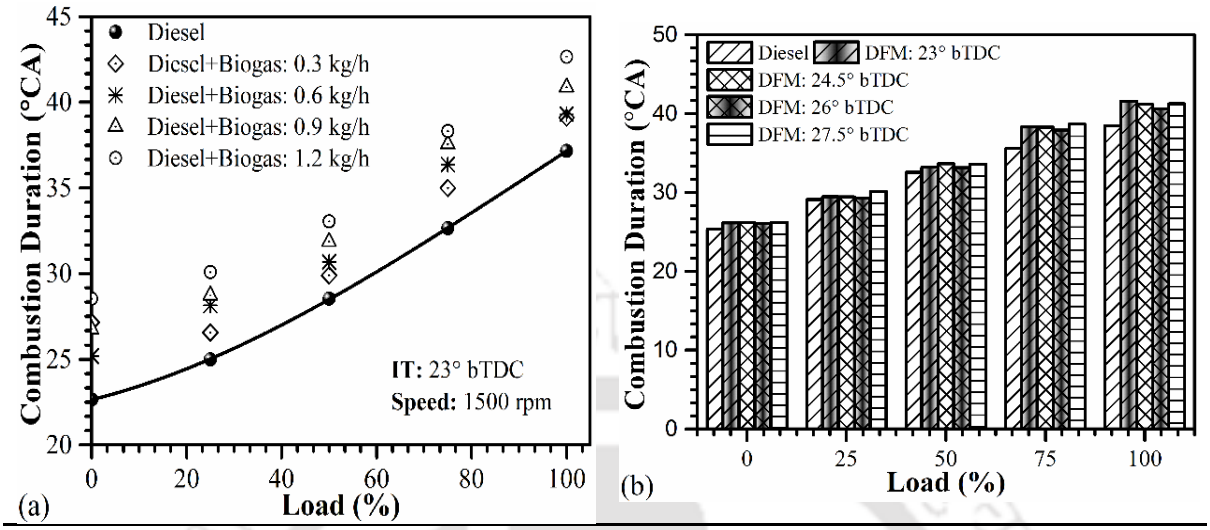

Fig. 2.15 Variation of combustion duration (a) Barik and Murugan (2014), (b) Barik and Murugan (2016)

2.7.5 Burned Mass Fraction

Burned mass fraction (BMF) is one of the most important parameter to understand the combustion history of the internal combustion engine. Krishnan (2001) and Krishnan et al. (2002) elaborated the BMF characteristics in details as a function of percentage of NG energy share, loads and intake preheating temperature at various CAD and parametric conditions as shown in Fig. 2.16. The BMF was defined as the instantaneous burned mass normalized by the total mass of charge in the cylinder. The investigators noticed a lower BMF at comparatively lean percentage of NG energy share as portrayed in Fig. 2.16a. In the investigation, the effect of loads on the variations of BMF was studied where the intake temperature at full load was reduced from 75°C to 55°C to prevent the knock (Fig. 2.16b). The higher BMF was noticed at higher loads due to the higher burning rates and burning of greater fractions of fuel were used. In the analysis of the effect of intake air temperature on BMF, three distinct temperatures namely 40, 75 and 125°C were considered (Fig. 2.16c). The experiments were carried out at half load to avoid knocking within the range of temperature (40 to 125°C). They noticed a similar trend for all the cases at the very early stage of BMF due to the fact that the combustion was dominated by burning of pilot diesel. However, in the later stage, the BMFs were remarkably differed to each other as it was dominated by the premixed combustion of NG. The analysis revealed the enhancement of BMF rates with the increase of intake charge preheating

temperature. The physical reasons were attributed to higher burning rates of fuels being used, which led to a more complete combustion associated with a higher intake charge preheating temperature.

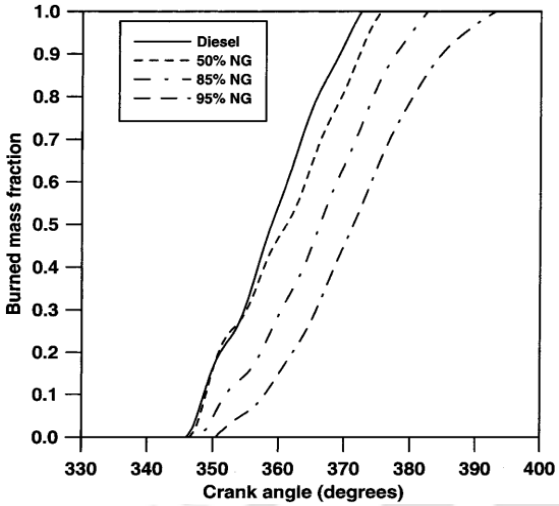

(a) BFM versus crank angle for different % of energy substituted by NG at half load = 21 kW

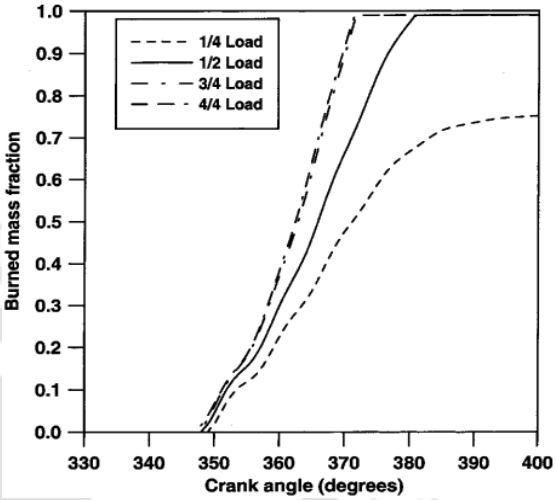

(b) BFM versus crank angle for different equivalence ratios

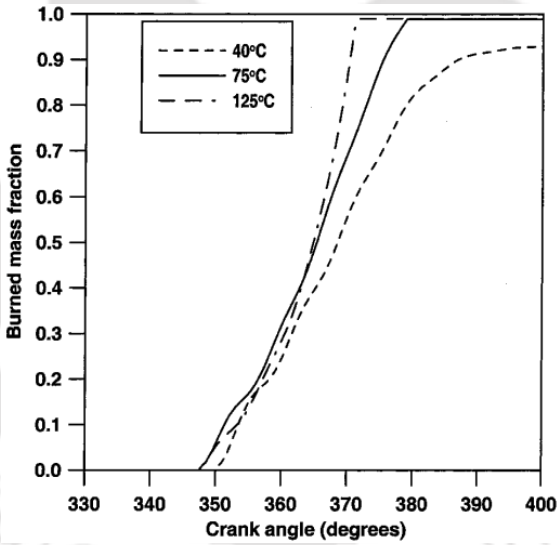

(c) BFM versus crank angle for different intake manifold temperatures at half load = 21 kW

Fig. 2.16 Parameters considered: Turbocharger intake pressure (P_{in}) = 181 kPa, Intake temperature (T_{in}) = 75°C, Speed = 1700 rpm, half load = 21 kW, Turbocharger exhaust pressure (P_{ex}) = 171 kPa (Krishnan 2001 and Krishnan et al., 2002)

2.8 Emission Analysis

Emission is the consequence of the burning of the input fuel-air mixtures. Therefore, the diagnosis of emission is essential concerning the severity of global warming and to sustain the healthy environment of the green ecosystem. Most importantly, the improvement in emission qualifies the engine performance and combustion characteristics.

Table 2.7 Combustion characteristics of the biogas run DFM engines

Investigators	Operating parameters	Fuels (Pilot/Primary)	BFR	ID	CD	Peak pressure	Peak NHRR
Cacua *et al.* (2012)	rpm = 1800; load = 40 to 100%; at different O_2-%	Diesel/ biogas	Maximum possible BFR is considered	↓with ↑load and O_2-%	-	↑with ↑load and O_2-%	Maximum at 70% load with 27% O_2,
Mustafi *et al.* (2013)	rpm = 1750; load = 8% and 75%; with different biogas compositions	Diesel/NG and biogas	Kept constant corresponding to 28 N.m load	Lowest with diesel; highest with biogas; ↑with ↑CO_2	shorter for DFM	Peaks are appeared later relative TDC due to higher ID	Peaks are appeared later due to higher ID and found higher in DFM
Barik and Murugan (2014)	rpm = 1500; load = 0% -100% (step =25%);	Diesel/ biogas	0.3-1.2 (step = 0.3) Kg/h	↓with ↑load; ↑with ↑BFR; 2-3 CAD higher than diesel	↑with ↑load and ↑BFR	at full load, ↑ with ↑BFR and shifted to the right of the TDC	Observed higher in DFM but delayed as compared to PDM
Park *et al.* (2014)	rpm = 1200; CR = 17.8; IT = 10-40 CAD bTDC	DME/ biogas	Controlled with the BES from 0.2 through 0.8	↑with ↑IT and ↑BES	-	↓with ↑BES and ↑IT due to formation of crevices	↓with ↑BES; the IT of 20° bTDC is found the best
Bora and Saha (2015b)	rpm = 1500; load=20%-100% IT = 23 CAD bTDC; CR = 17.5; at misfire	Different biodiesels/ biogas	Very high (≈2.3-3 kg/h)	Noticed very high in DFM (≈20-25° CA)	-	Throughout the test very low PP (at 100% load, reduction of 33.48% was observed) found in DFM compared to PD mode	Very low peak NHRR (at 100% load reduced by 63.82%) was noticed in DFM in comparison to PD mode
Barik and Murugan (2016)	rpm = 1500; load = 0-100%; IT= 23 - 27.5 CAD bTDC (step = 1.5 CAD)	Diesel/ biogas	0.9 kg/h	↓with ↑load; ↑with ↑IT	↑with ↑load; ↓with ↑IT	↑with ↑load and ↑IT; noticed higher peak pressure in DFM	↑with ↑load and ↑IT; peaks come closer to TDC with the ↑IT
Barik and Murugan (2016a)	rpm = 1500; biodiesel IT = 23 and 24.5 CAD bTDC; DEE port injection	Biodiesel/ DEE (port)/ biogas (primary)	0.9 kg/h	↑with ↑IT; ↓with DEE quantity	higher with biogas, ↓reduces with ↑DEE amount	Noticed higher peak pressure in DFM and found maximum with DEE	Found higher peak in PDM fuel; ↑with ↑load, ↑IT and ↑DEE amount; although the peaks positions are found after the positions of PP
Bora and Saha (2017)	rpm = 1500; load=20%-100% IT = 23-32 CAD bTDC; CR = 17, 17.5 and 18; at misfire	Biodiesel (rice bran)/ biogas	↑with ↑load and; ↓with ↑CR and ↑IT	↓with ↑load and ↑CR; ↑with ↑IT; at IT = 32 bTDC, ID of 27 CAD is noticed	-	↑with ↑load, ↑CR and ↑IT	Found very low NHRR in all states, however, slight improvements are noticed at maximum CR = 18 and at very ↑ITs

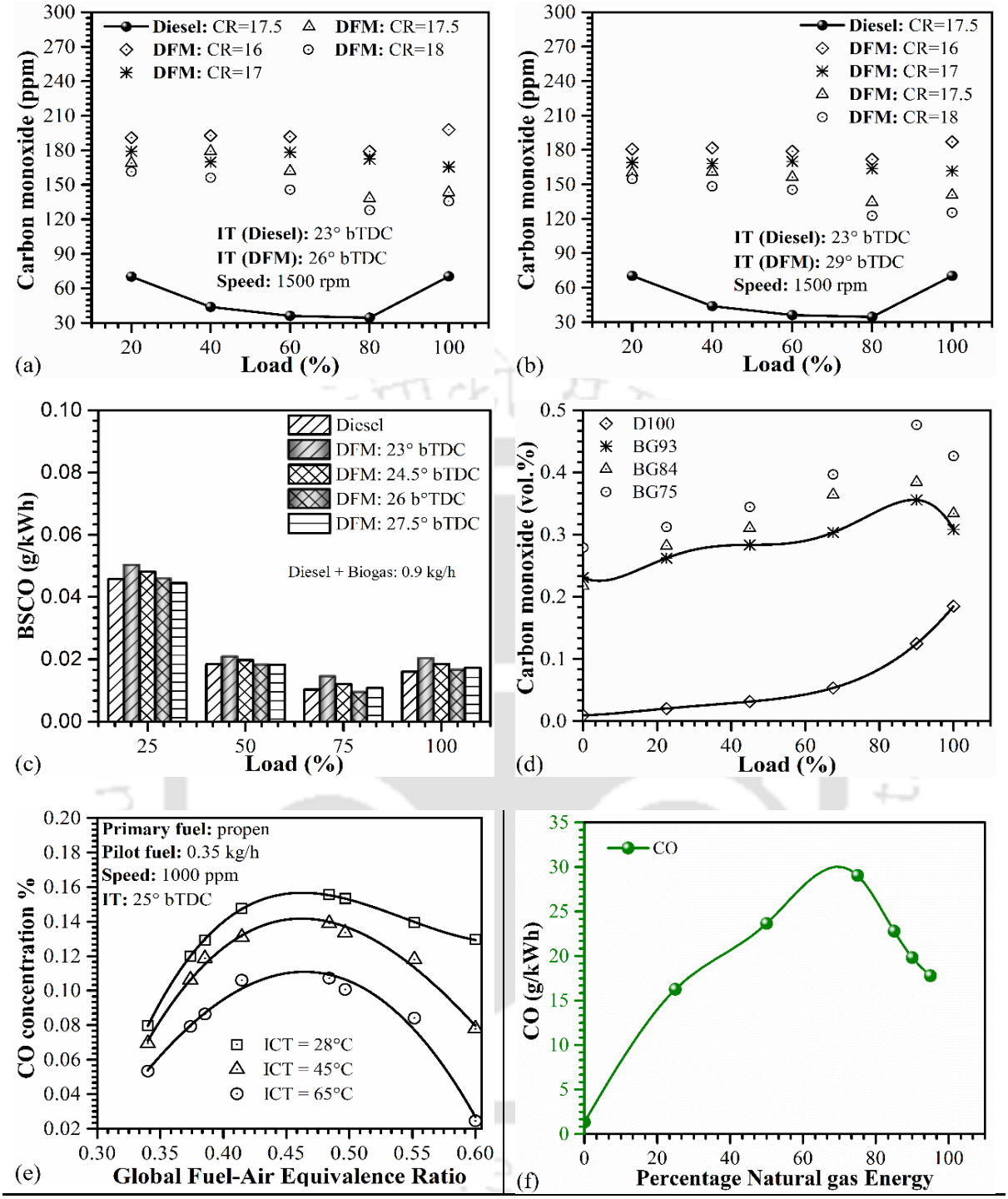

Fig. 2.17 Characteristics of CO emission: (a)-(b) Bora and Saha (2016a), (c) Barik and Murugan (2016), (d) Verma *et al*. (2017a), (e) Abd-Alla et al. (2001), (f) Krishnan (2001) and Krishnan et al. (2002)

2.8.1 CO Emission

The CO emission in internal combustion engines (petrol and diesel) are controlled primarily by the fuel-air equivalence ratio (Heywood, 1988). The characteristics of CO emission in biogas run DFM engines at different loads are represented in Fig. 2.17. Bora and Saha (2016a) observed a minor reduction in CO emission with the increase of loads with a pronounced effect

at 100% load. Nevertheless, with the increase of CRs and advancement of ITs, the CO emission declined (Fig. 2.17a and 2.17b). Irrespective of the change of parameters such as CR, IT and loads, a higher CO emission is demonstrated in DFM in comparison to PDM. The lower CO emission at higher CR was due to the generation of higher temperature that promoted combustion. The discrimination of lower CO on the advancement of IT is accredited to the increased time interval during expansion stroke that continued to enhance the high temperature and the oxidation of CO. However, due to rapid premixed combustion at higher BFR, the CD might have been lower as discussed in the previous section. This led to the oxidation time to be lower. As the lower CPP developed in the DFM was attributed to the lower CMGT, therefore, the CO emission reduction might be due to the faster flame propagation and rapid reaction of the fuel mixture. At CR = 18, when IT was advanced from 26 to 32 CAD bTDC, a reduction in CO emission by 5.59% (on an average) was noticed. Further, in the same range of IT, the average CO emission reductions for CR= 16, 17, and 17.5 were noticed to be 3.96%, 4.64%, and 4.91%, respectively.

Barik and Murugan (2014, 2016) found similar trends of CO emission as discussed above (Fig.2.17c). The reasons of higher CO in DFM were affected by the dilution of charge with the CO_2 present in biogas, the formation of the poor biogas-atomized liquid fuel mixture, and the paucity of oxygen. The higher CO at lower loads was observed due to the exceedingly leaner fuel-air mixture in the periphery of the fuel spray zone to sustain the flame propagation that reduced the local temperature. Hence, there was a substantial reduction of oxidation probability of CO. This was believed to be caused by the extinction of flame front in the pilot dominated ignition region until the reaching of the limiting states of auto-ignition. The higher CO was observed at the higher BFR. At full load and at BFR of 0.9 and 1.2 kg/h, the CO was found to be 17% and 24% higher, respectively in comparison to PDM. However, the lower CO with the advancement of ITs was qualified to the enhancement of cylinder temperature and the increasing oxidation reaction. At full load and with BFR = 0.9 kg/h, the CO emission was found to be reduced by 9.2, 19 and 17.3% at IT= 24.5, 26 and 27.5 CAD bTDC, respectively. This percentage of reduction was estimated in comparison to the one at standard IT = 23 CAD bTDC. However, Verma *et al*. (2017a) found a very high CO emission in a biogas run DFM using varying compositions of methane and CO_2 (Fig. 2.17d). The emission trends have been found to differ as compared to the emissions reported by Barik and Murugan (2014, 2016) and Bora and Saha (2016a). This happened because of the lower overall air-fuel ratio (AFR). At full load and in PDM, the AFR was calculated as 24.3. At the same load and at the biogas

composition of BG93 (volume percentage, methane =93%, and CO_2 = 7%), BG84, and BG75, the AFRs were estimated as 24.5, 17.8, and 14.2, respectively. This investigation demonstrated a higher CO_2 concentration in biogas to be associated with lower AFR. As a result, they found a higher CO with BG84 and BG75 in comparison to BG93. The variation of CO at different preheating temperatures is shown in Fig. 2.17d. As reported by Abd-Alla *et al*. (2001), the CO concentration as a function of Φ_{global} in the exhaust gas, got reduced with the increase of intake charge temperature (Fig. 2.17e). The faster reaction rates and wider flammability limits with preheating were illustrated as the physical reasons behind this effect. Krishnan (2001) and Krishnan et al. (2002) found an increase of CO emission with the increase in the percentage of NG energy share (Fig. 2.17f). However, beyond an approximat 70% of NG energy share, the CO emission was noticed to be reduced. This was attributed to the higher burning rate and higher flame speed at higher percentage of NG energy share of the total fuel used.

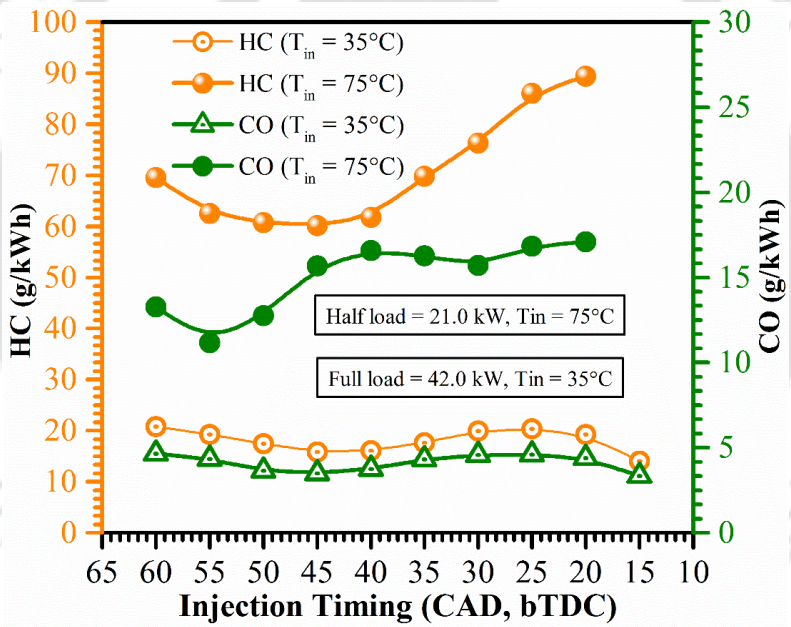

Fig. 2.18 HC and CO emissions versus injection timing, speed = 1700 rpm, Q_{inj} = 3.3 g/min (Krishnan 2005)

Krishnan et al. (2005) elaborated the physical reasons behind the HC and CO emissions. The typical sources of HC emission were indicated to (a) the in-cylinder crevices, (b) quenching of the flame front close to the cylinder walls, and (c) bulk quenching of the flame front in partially misfiring engine cycles. The last two reasons were pointed out as the dominant sources of HC emission in the NG run DFM engine. The controlling parameters to oxidize the HC were conferred as the charge temperature during expansion, the oxygen availability and the time available for oxidation. The conditions for the maximum oxidation of HC were stated as the requirement of sufficiently high temperature needed for a long time in the expansion stroke

and for ensuring the effective mixing of comparatively cool unburned gas with the hot burned gas. Whereas, the fuel-air equivalence ratio was stated to be the the key parameter to control the CO emission. The higher the equivalence ratio, the higher was the CO emission. However, the CO emission was found to be complex as it could be generated with the oxidation of HC under some certain combustion environment.

The investigator (Krishnan 2005) made a comprehensive analysis of HC and CO emissions at various ITs and parameteric states (Fig. 2.18). The ITs were varied from 15 to 60 CAD bTDC. The characteristics of emissions (HC and CO) were discussed in three ranges of ITs (advanced to retareded) such as 60-45, 45-25 and 25-15 CAD bTDC. In the first case, (IT=60 to 45 CAD bTDC) and at full load, both the HC and CO were found decrease. Beyond IT of 50 CAD bTDC, the COV was noticed to be significantly higher. This was attributed to the susceptibility towards exhibiting of partial misfiring cycles resulting the bulk quenching of flame front and the reduction of post combustion temperature. Upon the retardation of ITs from 45 to 25 CAD bTDC, the enhancements of HC and CO emissions were observed. However, a relatively lower COV was revealed in range of ITs = 45 to 25 CAD bTDC. Besides, there was the progressive delay of the onset of combustion upon retardation of ITs from 45 to 25 CAD bTDC that was discussed earlier. Consequently, a relatively lower HC and CO emissions as compared to the ones found within the ITs of 60 to 45 CAD bTDC were achieved. Interestingly, the investigator found a significant reduction in HC and CO emissions with the retardation of ITs from 25 to 15 CAD bTDC. However, within these ITs, there were sufficient lower heat release rate and higher heat release duration. These were attributed to the long oxidation time of fuel mixture resulting the lower HC and CO emissions. Nevertheless, the investigator noticed the different trends in HC and CO emissions at half load of engine operation as portrayed in Fig. 2.18. The primary reasons of these higher emissions at half load were pointed out as the phenomena of scavenging and the generation of lower in-cylinder temperature. The lowest CO was noticed at the advanced IT of 55 CAD bTDC.

At half load (21 kW), similar ternds of CO emission with ITs as discussed above were also depicted by Singh et al. (2004). However, the CO was noticed to be sufficiently lower at lower pilot quantity. Neverthless, the HC was found to be lower at the higher pilot fuel amount. The enhancement of the number of ignition centres and thereby the stable operations of engine in DFM were subjected to the reasons behind lower HC emission at higher pilot quantity. The relations of CO emission was linked with the HC emission and the physical reasons behind this were discussed above.

2.8.2 HC Emission

The unburnt hydrocarbons (HC) emission is the consequence of incomplete combustion of hydrocarbon fuel (Heywood 1988). The analysis of HC emission at various engine settings was carried out by Bora and Saha (2016a). The HC emission reduction was found minimal up to 60% load beyond which it increased significantly (Fig 2.19a and 2.19b). However, it was reduced with the increase of CRs and advancement of ITs. On an average, the reduction of 42.68% of HC emission was estimated upon increasing the CR from 16 to 18. On the other hand, when IT was advanced from 26 to 32 CAD bTDC, the average reduction of HC was found to be 8.36%. This indicated the effect of CR on HC emission to be more significant in contrast to IT. However, in all states, the investigators noticed higher HC emission in DFM than PDM. Barik and Murugan (2014, 2016) observed dissimilar trends of HC emission (Fig. 2.19c), where the HC emission got reduced with the increase of loads as well as with advancement of ITs. However, the emission was noticed to be higher at higher BFR. At full load, the increment of HC in DFM as compared to PDM at the BFRs of 1.2 kg/h and 0.9 kg/h, were found to be 41% and 30%, respectively. The lower oxygen amount caused by the induction of biogas, generation of the crevice, and scavenging due to the intake and exhaust valves opening were considered as the reasons behind the higher amount of HC emission in DFM. The lower HC emission at higher loads was attributed to the increase of ignition energy, improved spray characteristics, and turbulent intensity of the gas mixture, enhancement of heat transfer into the air-fuel mixture and increase in the number of ignition centers inside the combustion chamber. At full load and at the ITs of 24.5, 26 and 27.5 CAD bTDC, the HC emissions were found to be 5.7, 23, and 18.4% lower, respectively, than the emission at IT= 23 CAD bTDC.

Verma *et al*. (2017a) glimpsed a very high HC emission with the higher diesel fuel substitution and at the higher volume percentage of CO_2 in biogas (Fig. 2.19d). This reduced the potentiality to sustain the flame propagation. The higher ID with higher diesel substitution was also a reason to raise the HC emission. Similar results of HC emission were also reported (Nathan *et al*., 2010; Yoon *et al*., 2011; Mustafi *et al*., 2013; Barik and Murugan, 2014). Abd-Alla *et al*. (2001) stated an increase of HC emission with the increase of Φ_{global}. However, the emission level was lesser at higher Φ_{global}. With the intake charge preheating, this emission reduced significantly (Fig. 2.19e). The lower HC with intake charge preheating was connoted to the reduction of ID.

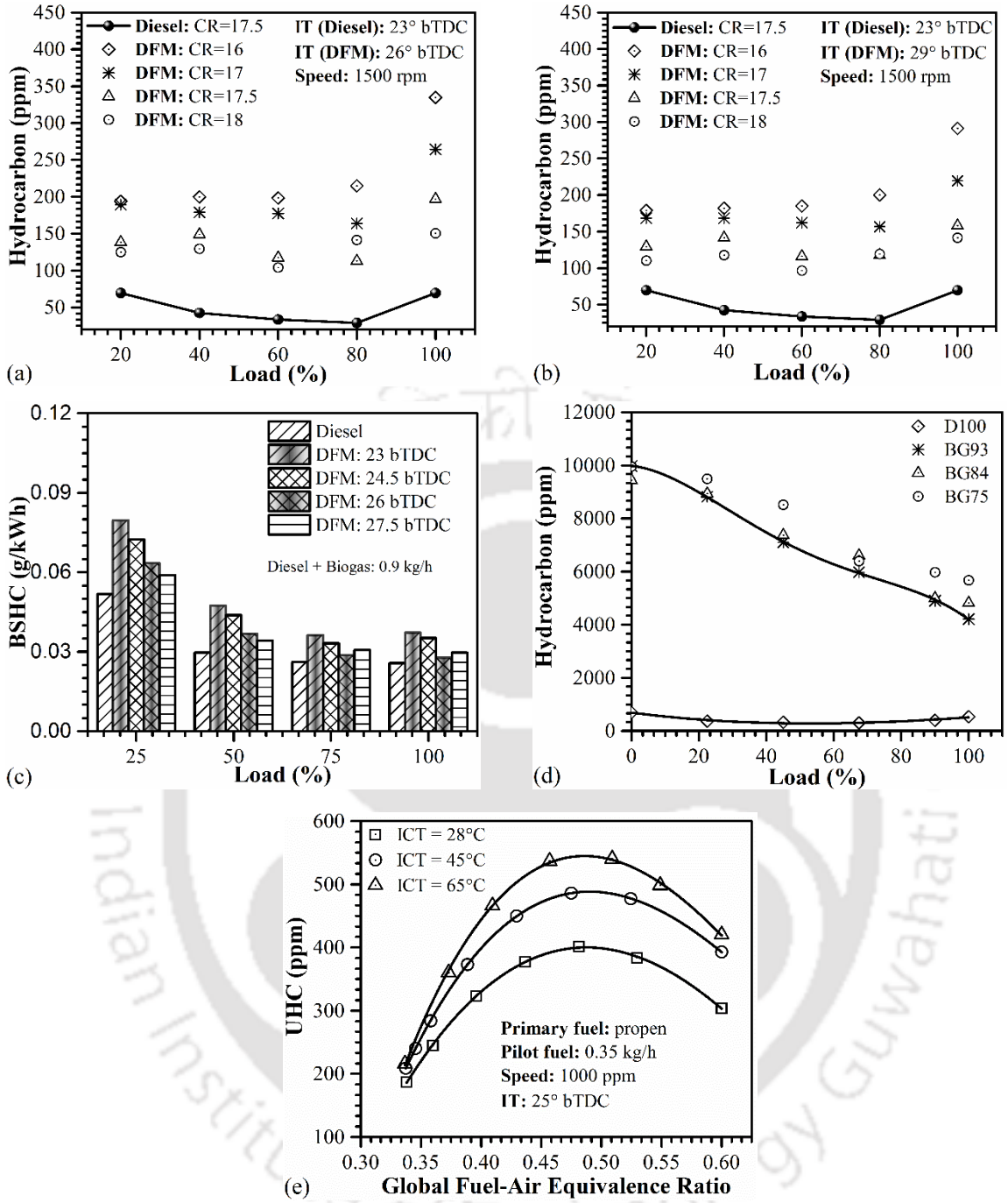

Fig. 2.19 Variations of HC: (a)-(b) Bora and Saha (2016a), (c) Barik and Murugan (2016), (d) Verma *et al*. (2017a)

Srinivasan et al. (2006) carried out the investigation at various intake charge preheating temperature (75, 95, and 105°C), pilot fuel quantities (3.3, 4.9, and 5.4 g/min) and at the advanced IT of 60 CAD bTDC. The significant reduction in HC with the increasing of intake charge preheating at all loads (at half load = 21 kW and quarter load) were observed. The enhancement of local temperature inside the combustion chamber and the reduction of COV at higher intake preheating temperature were demonstraded to be the reasons behind the lower

emission of HC. Whereas, the reasons behind the reduction of HC emission at higher quantity of pilot fuel were discussed earlier.

2.8.3 NO_x Emission

Concerning the detrimental effects on the environment, the researchers around the globe are seeking an efficient way to diminish the emission of NO_x. Most of the studies referred DFM of engine to be an effective technique to reduce NO_x.

Bora and Saha (2016a) noticed a very lower NO_x emission as compared to PDM. However, they found an increase in NO_x emission with the increase of CRs and advancement of ITs (Fig 2.20a and 2.20b). With the increase of CRs from 16 to 18, an average increment of 56.28% in NO_x was noticed due to the enhancement of cylinder temperature. However, with the advancement of ITs, a marginal increment of NO_x was observed owing to the improvement of biogas combustion.

Barik and Murugan (2014, 2016) observed a steep reduction of NO_x emission with the increasing of loads (Fig. 2.20c). The NO_x emission was found to be reduced with the increase of BFR and advancement of ITs. At full load, the maximum reduction in NO_x in DFM at the BFR of 1.2 kg/h with respect to PDM, was estimated at 42.8%. At the same load with the ITs of 24.5, 26, and 27.5 CAD bTDC, the NO_x was found to increase by 15.7, 33.8 and 39.4%, respectively, as compared to the one at IT = 23 CAD bTDC. The higher cylinder temperature, compression ratio, oxygen concentration and the retention time of reaction were designated as the general information behind the formation of NO_x. The lower NO_x emission in biogas run DFM engine was attributed to the higher molar specific heat of CO_2 that diluted the charge and reduced the engine cycle temperature. The higher NO_x at advanced IT was accredited to the development of higher temperature.

Verma *et al*. (2017a) found a very high NO_x emission in DFM as compared to the reported data (Barik and Murugan, 2014; Barik and Murugan, 2016; Verma *et al*., 2017b). They observed higher NO_x emission with a lower CO_2 concentration in biogas (Fig. 2.20d). However, the investigators achieved a lower NO_x emission in DFM than PDM. The shorter combustion duration in DFM was specified as one of the prominent reason behind the lower NO_x emission in DFM. Figure 2.20e shows the characteristics of NO_x with different engine operating parameters. In Fig. 2.20e, Abd-Alla *et al*. (2001) noticed that the NO_x emission increases with

the increase of intake charge preheating temperature owing to the enhancement of flame temperature.

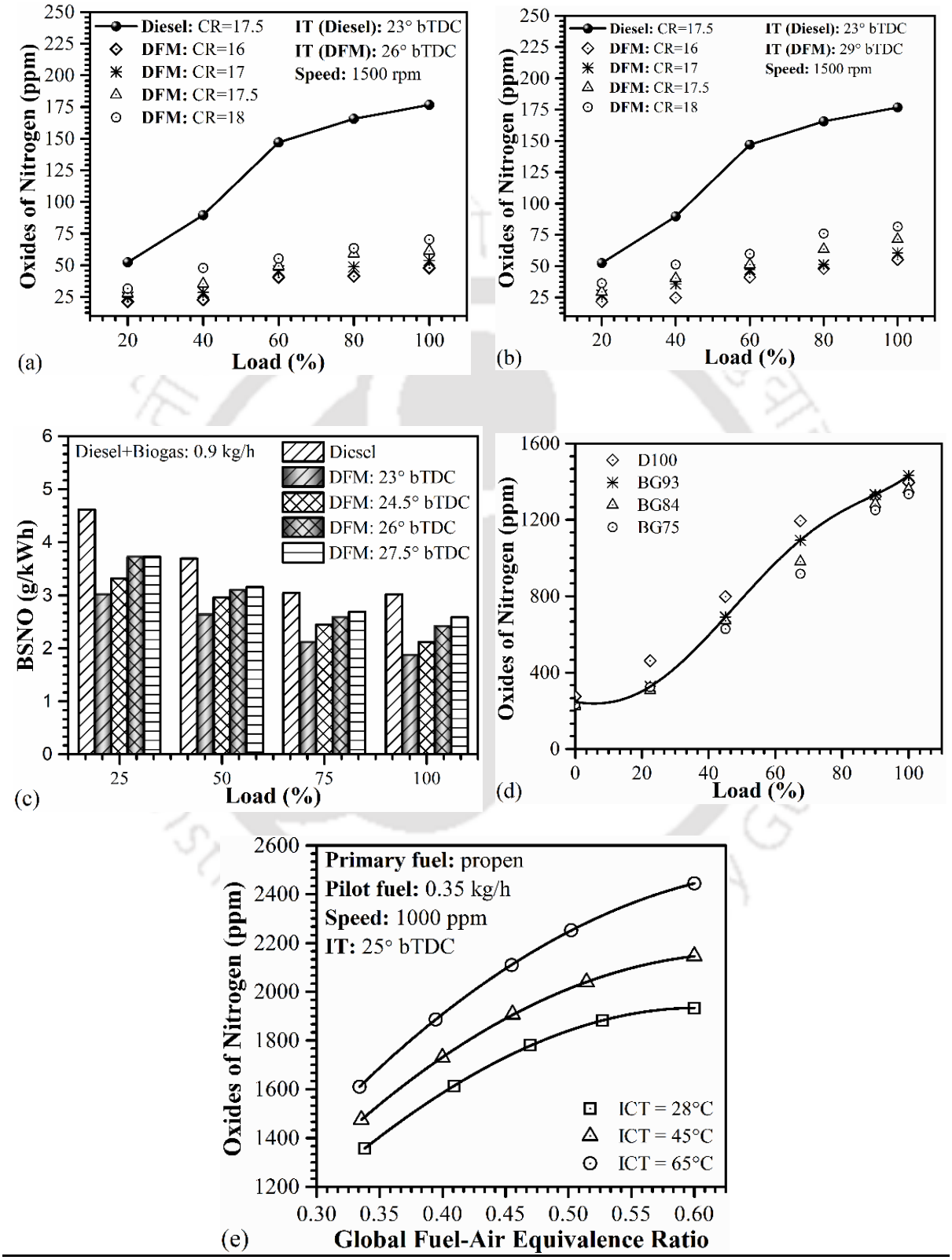

Fig. 2.20 Variations of emission of NO_x: (a)-(b) Bora and Saha (2016a), (c) Barik and Murugan (2016), (d) Verma et al. (2017b), (e) Abd-Alla *et* al. (2001)

The trade-off of NO_x and HC emissions (Fig. 2.21) at various states was elaborated by Krishnan (2001) and Krishnan et al. (2002). The investigators noticed a steady decrease of NO_x emission with increasing percentage NG energy share (increasing diesel substitution by NG), while at the same time the HC was found to increase remarkably (Fig. 2.21a). At higher substitutions (85-95 percentage NG), the low confidence level of HC emission data were measured due to the constraint of the gas analyser. The progressively higher ID and lower flame speed at higher level of substitution (at higher percentage of NG energy share) were the reasons behind the higher HC emission. Interestingly, the HC was found to be gradually and remarkably reduced with increasing loads, intake air temperature, and Φ_{global} (Figs. 2.21b and 2.21c). However, simulatenously there was the moderate enhancement of NO_x with the increase of loads, intake air temperature, and Φ_{global}. The higher consumptions of pilot (diesel) fuel and smaller near-wall "quenching volume" at higher loads were the reasons for the simulatenious reduction of HC emission and enhancement of NO_x emission. The HC was noticed to be reduced by 80% on increasing the intake air temperature from 40 to 125°C. This was accredited to the higher burning rates and smaller near-wall "quench volume" due to higher local charge temperature. At higher Φ_{global}, there was the distinct reduction of HC and corresponding enhancement of NO_x emissions. The reasons were conffered to the higher FCE at higher Φ_{global} that enhanced the fuel burning rates with the consequence of higher local temperature.

Krishnan (2005) studied the NO_x emission characteristics and the trade-off of the emissions of NO_x and HC at various ITs (Fig. 2.22) in a turbocharged DFM engine run on NG. The other operating parameters considered in this investigation were stated earlier. The high local temperature along with the adequate availability of nitrogen and oxygen were addressed to be the favorable reasons behind the emission of NO_x. Morever, as the NG run DFM engine was operated under the fuel-lean conditins (Φ_{global}~0.49 to 0.57); the local temperature was addressed to be the crtitical factor to form the NO_x. The peaks of NO_x emission were noticed within the ITs of 35 to 40 CAD bTDC (Fig. 2.22). Whereas, it reduced sharply with the advancement of ITs to 60 CAD bTDC. Further, there was a significant reduction in NO_x emission with the retardation of ITs beyond 35 to 15 CAD bTDC. Nevertheless, the twofold lower NO_x was noticed at the IT of 60 CAD bTDC relative to the IT of 15 CAD bTDC. The prolonged ID, small quantity of pilot fuel, availability of longer time for the homogeneous diesel-air mixture preparation were revealed to be the combustion environment at advanced IT of 60 CAD bTDC, which were addressed to be the probable reasons behind the lower local

temperature. Consequently, the lower NO_x was noticed at the advanced IT of 60 CAD bTDC. Whereas, at the retarted IT of 15 CAD bTDC, the shorter ID, availability of lesser time to prepare diesel and air mixture, start of ignition near to TDC, occurring of bulk combustion in the expansion stroke and releasing of lower heat over a long duration were pointed out to be the reasons behind the generation of lower local temperature. Thus, a lower NO_x was achived at the retarted IT of 15 CAD bTDC.

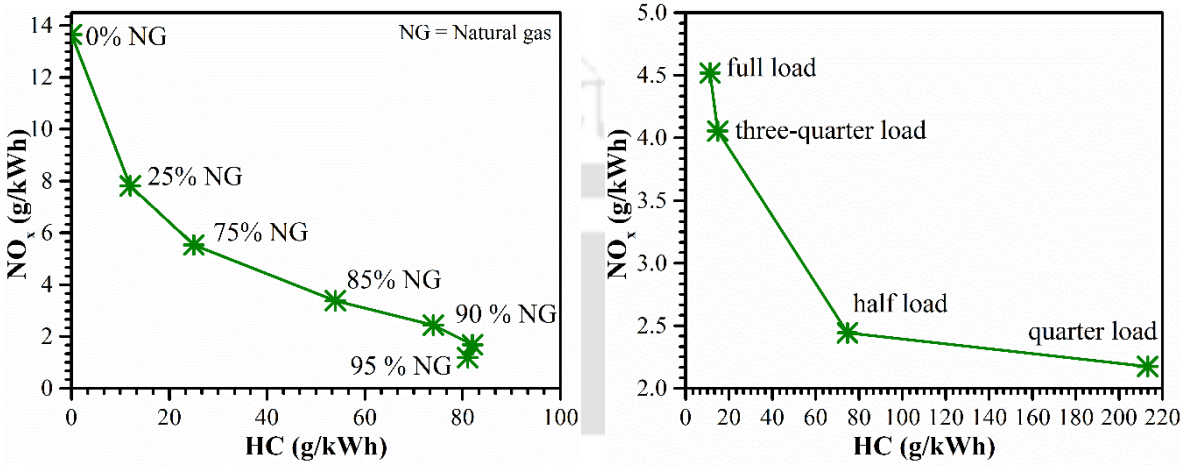

(a) NO_x versus HC emissions for different percentages ofenergy substituted by natural gas, half load = 21 kW

(b) NO_x versus HC emissions for different loads

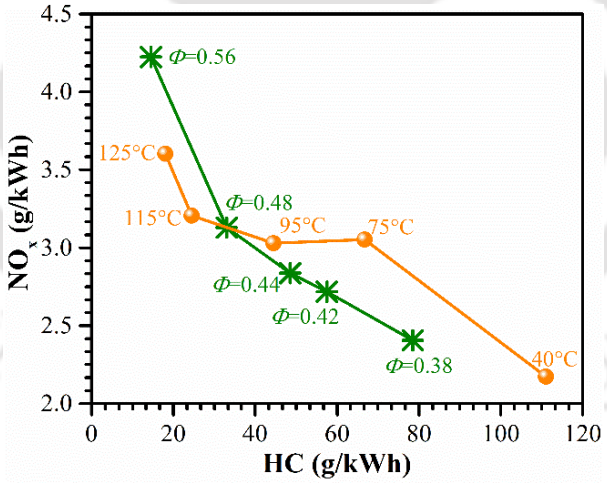

(c) NO_x versus HC emissions for different intake manifold temperatures and equivalence ratios: half load (21 kW)

Fig. 2.21 Parameters considered: Turbocharger intake pressure (P_{in}) = 181 kPa, Intake temperature (T_{in}) = 75°C, Speed = 1700 rpm, half load = 21 kW, Turbocharger exhaust pressure (P_{ex}) = 171 kPa (Krishnan 2001 and Krishnan et al., 2002)

Srinivasan et al. (2006) analyzed the characteristics of NO_x by increasing of intake charge preheating temperature (75, 95, and 105°C). They found a substantial enhancement of emission of NO_x with the increment of preheating temperature. The advancement of CA50 (15 to 5 CAD

aTDC), release of greater amount of energy near to TDC and the occurrence of the majority of combustion at higher local temperature were uncovered as the reasons behind the higher emission of NO_x at higher intake temperature. There was also the significant enhancement of NO_x at higher pilot quantity. The enhancement of high-temperature zone at higher pilot quantity was attributed to the higher NO_x at a greater amount of pilot fuel. The similar characteristics of NO_x with pilot quantity was also observed by Singh et al. (2004).

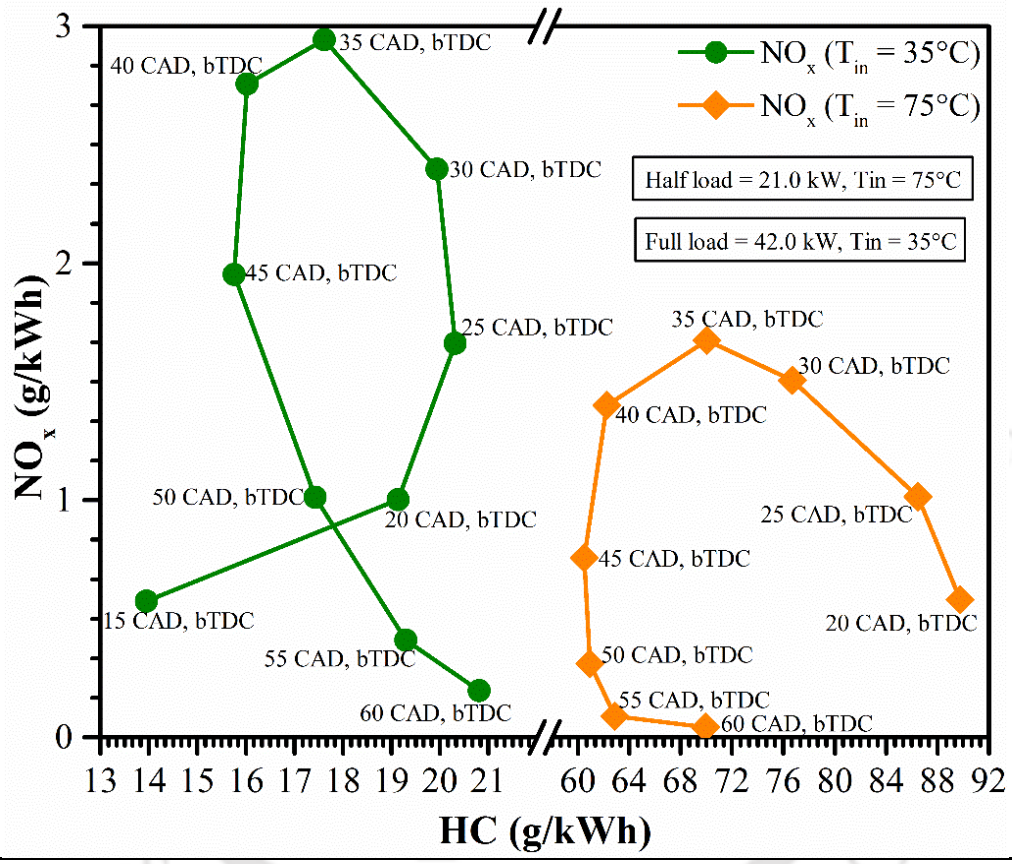

Fig. 2.22 NO_x-HC trade-off curve at different ITs, speed = 1700 rpm, Q_{inj} = 3.3 g/min (Krishnan 2005)

2.9 Smoke Emission

The visible black smoke in diesel engines is considered as the consequence of soot emission. The higher smoke emission at higher loads is attributed to the overall richer fuel-air ratios, longer duration of diffusion combustion, and the reduced oxygen concentration (Pundir 2010). The higher smoke emission is also caused by the fuels that have lesser hydrogen to carbon ratio (<2) (Heywood, 1988; Nagarajan *et al*., 2002). Researchers in general observed that the dual fuel technology would be viable to reduce the significant quantity of smoke emission from a DFM engine.

Table 2.8 Emission characteristics of the biogas run DFM engines

Investigators	Parameters	Fuels (Pilot /Primary)	BFR	CO emission	HC emission	NO_x emission	Soot/ Smoke
Mustafi and Raine (2008)	rpm = 1750; load = 3 Nm and 28 Nm; IT = 28 CAD bTDC; $0.61 \leq \Phi \leq 0.70$;	Diesel/ simulated biogas	controlled at the diesel substitution of 62%	Observed slightly higher in DFM than PD	Increased three times in DFM than PD	Reduced sharply with biogas	70% reduction was noticed in DFM
Yoon and Lee (2011)	rpm = 2000 load = 20-100%; IT = 12 CAD bTDC;	Diesel and biodiesel/ biogas	2.2±0.1 kg/h	Higher (~5-6 times) in DFM; slight reduction is noticed with biodiesel	Higher (~10-29 times) in DFM; slight reduction is noticed with biodiesel;	Drastic reduction of NO_x was observed	Reduced in DFM; as well as with the use of biodiesel
Makareviciene *et al*. (2013)	rpm = 2500; load = 20-100%; IT=20-24 CAD bTDC with and without EGR	Diesel/ different simulated biogas	20 and 40 liter/minute (lpm)	Worst results found with EGR; without EGR, ↓with ↓BFR and at ↑IT; ↑with ↑CH_4%	HC reduced considerably without EGR; at ↑IT, HC↓ with ↓CH_4% ↓BFR	Reduced in EGR; ↑with ↑load,↓CH_4% and with ↑IT	Found lower in the entire test
Verma *et al*. (2014)	Up gradated biogas; rpm = 1500; Load = 20%-100%	Diesel/ biogas	~1.1-2.4 kg/h	Found higher in DFM, reduced with scrubbed biogas	Noticed higher in DFM, reduced with scrubbed biogas	Observed lower in DFM; ↑a little with scrubbed biogas	-
Lounici *et al*. (2014)	rpm = 1500; IT = 13 CAD bTDC; load = 20-100%	Diesel/ simulated biogas	at which 90% of energy made from biogas	Very high (>1000 ppm) emission found in DFM	Very high (>2000 ppm) emission found in DFM	↑with ↑load; reduced in DFM, but ↑with CH_4 vol.%	Drastically reduced in DFM
Barik and Sivalingam, (2014)	rpm = 1500; load = 0-100%; IT = 23 CAD bTDC; CR = 17.5	Diesel, biodiesel/ biogas	0.3- 1.2 kg/h at a step of 0.3 kg/h	↑with ↑BFR; found higher than PD and maximum with 1.2 kg/h	The reasons are similar as CO	Drops by 32.17% in DFM, at the BFR of 1.2 kg/h at full load	Maximum drop noticed in DFM, but, ↑with ↑BFR
Bora and Saha (2015b)	Load=20%-100% IT = 23 CAD bTDC; CR = 17.5; at misfire	Biodiesels/ biogas	Very high (≈2.3-3 kg/h)	Noticed higher in DFM but the emission magnitudes are very small	Found higher in DFM but the emission magnitudes are very small	Negligible in DFM	-
Barik and Murugan (2016)	rpm = 1500; load = 0-100%; IT= 23 - 27.5 CAD bTDC	Diesel/ biogas	0.9 kg/h	↓with ↑load and at ↑IT; max. of 19% drop at the IT of 26° bTDC noted than PD mode	↓with ↑load and at ↑IT; max. of 23% drop at the IT of 26 CAD bTDC noted than PD mode	↓in DFM; ↑with ↑IT; max. 37.7% drop found (IT=23 CAD bTDC)	↑with ↑load; ↓with ↑IT
Bora and Saha (2017)	Load=20%-100%, IT = 23-32 CAD bTDC; CR = 17 to 18; at misfire	Biodiesel/ biogas	(~2-3.2 kg/h) ↑with ↑load and; ↓with ↑CR and IT	↓with ↑CR, at ↑IT and ↑ up to 80% load	Trend is found to be similar to CO emission	Negligible in DFM	-
Verma *et al*. (2017a)	rpm = 1500; varying load;	Diesel/ biogas	controlled at misfire limit	Very high in DFM (~0.24-0.47 vol.%); ↑with ↑load	Very high in DFM (~4000-10000 ppm); ↓with ↑load	Found significantly lower up to 80% load	Observed drastic reduction in DFM

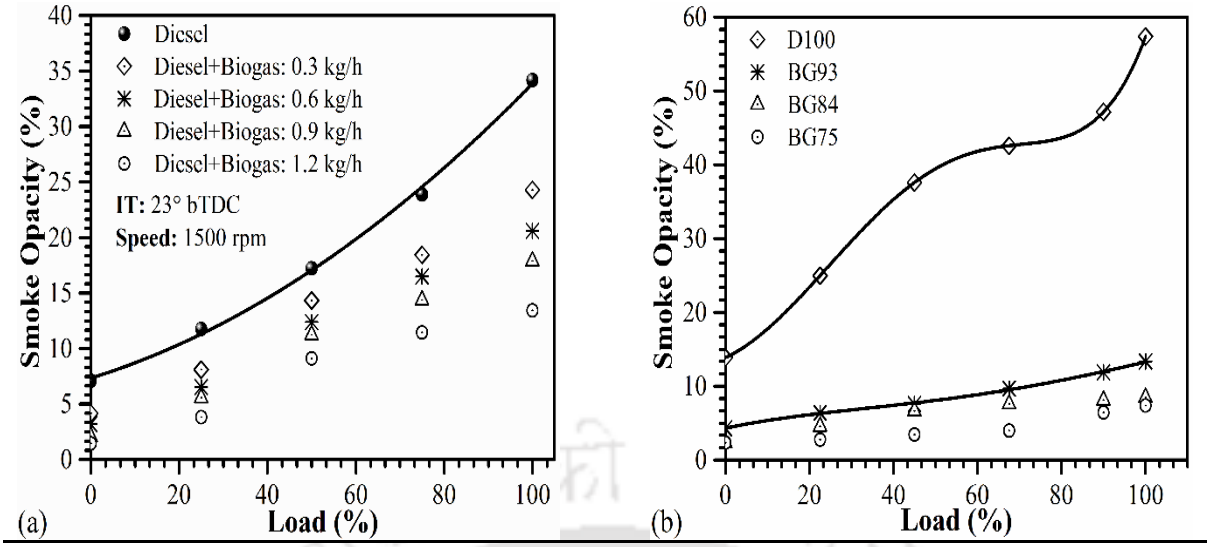

Fig. 2.23 Characteristics of smoke opacity: (a) Barik and Murugan (2014), (b) Verma *et al*. (2017a)

As depicted in Fig. 2.23a, Barik and Murugan (2014) noted a significant reduction of smoke opacity in DFM as compared to PDM. The smoke opacity reduced with the increase of BFR, while it increased with the increasing of loads. At full load, the smoke was noticed to be reduced by 30, 41, 49, and 62% at the BFRs of 0.3, 0.6, 0.9, and 1.2 kg/h, respectively. The lower smoke in DFM was accredited to the replacement of diesel fuel by the inducted biogas, reduction of flame temperature, and enhancement of oxidation of soot precursors in the soot prone zone by the increased concentration of O and OH around the flame generated from the CO_2 present in biogas. Verma *et al*. (2017a) noticed a similar trend of smoke emission (Fig. 2.23b), however, the emission level was found to be substantially lower in DFM than the reported data (Murugan 2014). The higher replacement of liquid fuel and the absence of aromatic compounds in biogas were specified as the reasons behind the lower smoke emission. The internal relations of the operating parameters, performance parameters and emission characteristics of biogas run DFM engine are presented in Table 2.8 (Mustafi and Raine, 2008; Yoon and Lee, 2011; Makareviciene *et al*., 2013; Barik and Sivalingam, 2014; Lounici *et al*., 2014; Verma *et al*., 2014; Bora and Saha, 2015b; Barik and Murugan, 2016; Bora and Saha, 2017; Verma *et al*., 2017a).

2.10 Exergy Analysis

Exergy analysis is essential in the field of applied science or in other words in engineering applications to achieve the number of benefits over energy analysis. This is to figure out the

quality of energy (Balmer, 1999), to utilize the maximum amount of energy and corresponding minimum loss of energy to the dead state (Heywood, 1988), to understand the fundamental physical phenomena (Borgnakke and Sonntag, 2013), to predict the best way of performance evaluation (Li *et al*. 2018) and to optimize the engineering devices (Lau *et al*., 1987; Dentice d'Accadiaa and Vanoli, 2004). The exergy analysis is vital in the production of energy from the internal combustion engines, as these heat engines are associated with the conversion of chemical to thermal energy of fuel, start and end of combustion, opening and closing of the engine ports (intake and exhaust), quality of fuels using, and allied with cooling and heating systems (Lior and Zhang 2007). Higher the exergy, higher is the possibility to utilize the energy produced or applied in a system. Therefore, the hunting of the sources of exergy destruction is essential to achieve the efficient performance (Li *et al*. 2018). Practically, the exergy is destructed due to the irreversibility owing to highest molecular disorders in a system that is attributed to the dissociation caused by friction. Rakopoulos and Giakoumis (2006) noticed that the main reasons of exergy destruction in engine due to the thermodynamic irreversibilities such as combustion, heat transfer, mixing, throttling, friction, and exergy wasted to the cylinder wall and to the dead state with exhaust. In engines, the sources of exergy destruction can be reduced substantially with the proper use of fuels and exact setting of the engine operating parameters. In the next sub-sections, the discussions on exergy destruction and utilization in the diesel engine in PDM and DFM have been made.

2.10.1 Exergy Analysis in PDM

Plenty of exergy studies have been carried out in PDM for an efficient use of various liquid renewable fuels as either pure or blended fossil diesel. Rakopoulos and Giakoumis (1997a) pursued a fashionable work on exergy in a turbocharged diesel engine. A very clear discussion was made on the states of various exergy equilibrium (thermal, mechanical and chemical). The investigators absorbed in to expose all practical reasons in all parts of the engine behind irreversibilities that caused the destruction of exergy. The maximum irreversibility was noticed to be associated with the combustion but there was a significant irreversibility in the intake and exhaust of the engine. Total irreversibilities were observed as much as 44.9% with the consideration of the loss of heat to the cylinder wall. In the exhaust port, the sources of irreversibilities are due to the fact of throttling during blowdown and friction.

Rakopoulos and Giakoumis (1997b) noticed a simultaneous enhancement of exhaust gas exergy as well as irreversibility in the exhaust gas with the increase of loads. Caton (2000) found that the combustion and chemical irreversibilities significantly reduces upon increasing of combustion temperature. Ayres *et al*. (2003) studied on the production of the engine, cost of production, production of energy during 1900 to 1998 in the light of exergy analysis and revealed its great impact on these parameters.

Parlak (2005) compared the exergy strategy in the exhaust gas of a standard diesel (STD) engine with a low heat rejection (LHR) diesel engine. The investigator observed the higher available energy in the exhaust gas of the LHR diesel engine than the STD one and suggested to use a turbine to recover the available energy in the exhaust. Giakoumis (2007) investigated the exergy performance of a transient LHR silicon nitride and plasma spray zirconia coated engine and compared with an STD engine. He found a significant enhancement of the combustion temperature of the coated LHR engine. Hence, this coating in LHR engine assisted to cut the combustion and total irreversibilities of the engine. However, there was no contribution of this enhanced heat energy to produce the extra amount of mechanical work and therefore, noticed a higher exergy in the exhaust gas and suggested the use of an expansion device to extract the exergy.

Som and Datta (2008) pointed out some crucial influencing factors of exergy during the entire combustion process. They noticed that the chemical reaction, the physical transport, and thermal energy exchange are the major sources of irreversibilities in any combustion process. The irreversibility due to the chemical reaction can be reduced significantly with the enhancing of flame temperature and that can be achieved with the oxygen-enriched environment. The irreversibility due to combustion can be reduced substantially with the reduction of the temperature gradient that can be done with the intake charge preheating, fuel-air enactment, and with the control of jet velocities. Abassi *et al*. (2010) found that the preheated intake charge helped to reduce the combustion irreversibility and enhances the exergy in the waste heat and exhaust gas of a direct injection diesel engine. Tat (2011) examined the effects of cetane number on exergy in a diesel engine using different biofuels. He concluded that the lower cetane number, higher ignition delay, and the corresponding long premixed combustion phase enhance the exergy of the engine. It is reported that the lean diesel engine operation with high

exhaust gas recirculation (EGR) is an efficient way to enhance the overall exergy of the engine (Caton, 2012).

Debnath *et al*. (2013a, 2014b) investigated the exergy of a variable compression ratio (CR) diesel engine using palm biodiesel and emulsified palm biodiesel as the fuels. They found that the shaft exergy and exergy efficiency were increased with the increasing of CR and advancement of ITs while exhaust gas exergy got reduced for the same. Jena and Misra (2014) noticed that the use of oxygenated fuels helped to enhance the exergy of the diesel engine. Mattson *et al*. (2016) in their numerical and experimental investigations on exergy using various quantity of biodiesel as the oxygenated fuel have observed that the use of biodiesel with some limits enhances the overall exergy due to the enhancement of the combustion temperature. However, they have found the loss of exergy to the dead state due to the enhancement of heat transfer from the system to the environment.

Khoobbakht *et al*. (2016), Paul *et al*. (2017) used various ternary blends of diesel, biodiesel, and ethanol to investigate the overall exergy of a diesel engine. They observed that the overall exergy enhances with the increasing of biodiesel and ethanol amount in the blend (up to some limits). Li *et al*. (2018) noticed that the overall exergy destruction reduced with the increase of combustion temperature with lower pollutant emission near to the stoichiometric fuel-air equivalence ratio.

2.10.2 Exergy Analysis in DFM

The above discussion of exergy in PDM revealed that the intake charge temperature, quality of fuel used, ignition delay, combustion temperature, combustion temperature gradient, physical transport of fresh charge and combustion products, combustion reaction etc. are the most influential parameters to efficient control the exergy of the engines. It is very clear that the dual fuel mode of engine operation is more complicated than the pure diesel mode of engine operation. The DFMs are more parametric dependent operation than the engine operation in PDM. The deficiency of the DFM engines is that the engine overall performance deteriorates in comparison to PDM. Consequently, it is essential to explore the parameters that are sensitive to decline the DFM engine overall performance in the light of the analysis on exergy. In this, an effort has been made to review the past work on exergy analysis of DFM engines (Table 2.9).

Table 2.9 Dual fuel engine exergy and sources of irreversibilities

Investigators	Operating Parameters	Fuels	Sources of Irreversibility	Exergy Enhancing Parameters
Rakopoulos and Kyritsis (2006)	Computational work Φ_{global} = 0.5, Lister LV1 diesel engine, rpm = 1500, IT = 22 CAD bTDC (static)	'$CH_4 - H_2$' and '$CH_4 - H_2 - CO_2$'	Complicated fuel chemical structure, Dilution of a higher amount of CO_2, Reduction of combustion temperature	Simpler fuel chemical structure, Higher combustion temperature, Supplementation of H_2
Sahoo *et al.* (2012b)	Experimental, Single cylinder 4-stroke diesel engine, rpm = 1500, Load = 0 to 100%	**Primary:** Biogas **Pilot:** Diesel, biodiesel	Qualities of pilot and primary fuels, Heat transfer, mixing, throttling, friction	Oxygenated pilot fuels, higher combustion temperature
Chintala and Subramanian (2014)	Theoretical and experimental, Single cylinder Diesel engine, rpm = 1500, Load = 50, 75 and 100%	**Primary:** H_2 **Pilot:** Diesel	Oxidation, Air-Fuel mixing, Heat transfer, Friction, Instantaneous chemical reaction, Heat transfer from intermediate products to reactants	Faster flame propagation, Enhancing of combustion temperature, Higher release of heat, Higher load levels, Optimum Fuel-air equivalence ratio
Bora and Saha (2016c)	Experimental, Single cylinder 4-stroke diesel engine (3.5 kW), rpm = 1500, Load = 0 to 100%, CRs = 16 – 18, ITs = 23 – 32 CAD bTDC	**Primary:** Biogas **Pilot:** Diesel, emulsified rice bran biodiesel	Mixing, friction, and combustion lower temperature	Noticed an improvement in exergy with the emulsified rice bran biodiesel
Bora and Saha (2016d)	Similar to Bora and Saha (2016c)	**Primary:** Biogas **Pilot:** Diesel	Mixing, friction	Advancement of injection timings and increasing of compression ratios, higher combustion temperature
Verma *et al.* (2017a); Verma *et al.* (2017b)	Single cylinder, four-stroke, diesel engine (4.4 kW), ITs = 20–32 CAD bTDC	**Primary:** Biogas, CNG, H_2 **Pilot:** Diesel	Knocking, misfire, lower load levels, Incomplete and lower temperature combustion	Advancement of injection timing, enhancement of flame speed, elevated combustion temperature, Supplementing the hydrogen with biogas

Rakopoulos and Kyritsis (2006) and Rakopoulos *et al*. (2008) have made a comparative analysis on exergy on the use of hydrogen and hydrocarbon (landfill gas) fuels for a single cylinder, naturally aspirated, direct injection diesel engine (Lister LV1). The investigators found a monotonic reduction in combustion irreversibility with the addition of H_2 with CH_4 as shown in Fig. 2.24 (a). The reason was attributed to the reduction of chemical irreversibility with the addition of H_2. During oxidation, H_2 produced only H_2O, whereas, hydrocarbons produced numerous complicated oxides of hydrocarbon, thereby enhancing the combustion irreversibility. It is seen in Fig. 2.24 (b) that the addition of CO_2 in the gas blends of CH_4 and H_2 reduced the fuel (55% CH_4 + 40% CO_2 + 5% H_2) input availability and increases the combustion irreversibility. The dilution of CO_2 in the gas blend reduces the combustion temperature and the dissociation of CO_2 to CO was stated as the main reason behind this findings.

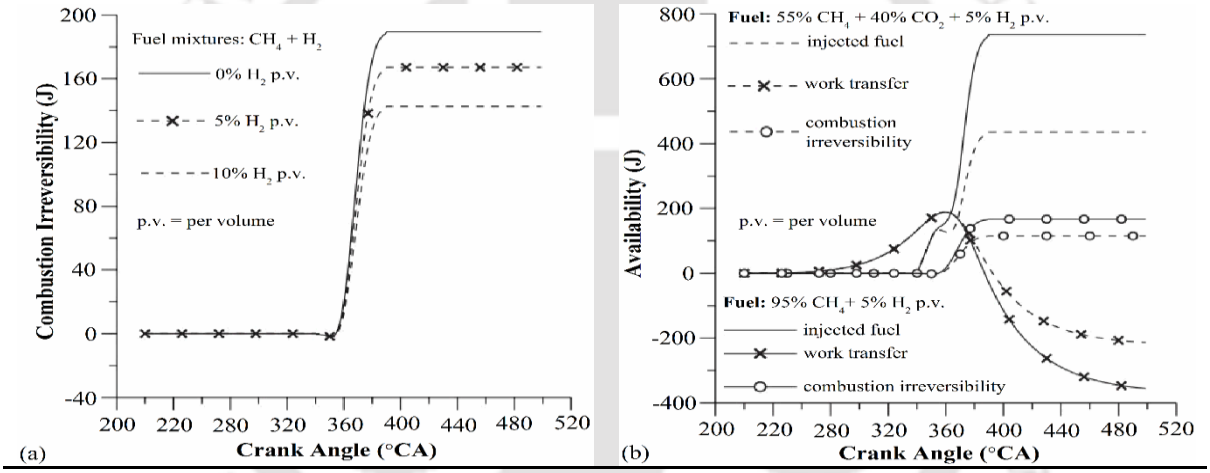

Fig. 2.24 (a) Effects of hydrogen components on combustion irreversibility, (b) Effects of CO_2 on exergy (Rakopoulos and Kyritsis, 2006)

Sahoo *et al*. (2011a) investigated the exergy behavior of a syngas-diesel DFM engine. They varied the H_2 and CO composition in the synthetic gas blend and found an enhancement of cumulative exergy of the engine with the increasing amount of H_2 in the gas blend. Due to the reduction of in-cylinder combustion temperature at lower loads (up to 40%), the destruction of exergy was noticed to be more in comparison to the higher loads. Ramôs da Costa *et al*. (2012) have carried out a theoretical and experimental investigation on exergy in a diesel engine using CH_4 - diesel fuels combination. They achieved a higher exergy efficiency in DFM than PDM. Besides, the lower exergy destruction in the exhaust was achieved in DFM than PDM. The results presented were found different in comparison to the reported data. Chintala and Subramanian (2014) investigated the exergy in an H_2-diesel DFM engine and observed a significant improvement in engine exergy.

Knizley et al. (2012) examined the effects of fuel type (CH_4, C_2H_5OH, and C_8H_{18}), reactant temperature (300 – 1200 K), reactant pressure (101.325 – 10132.5 kPa), equivalence ratio (0.3 – 1.5), and diluents (CO_2, H_2O, N_2, and O_2) on entropy generation (S_{gen}) in a constant internal energy – volume (UV) combustion process. With the increasing of reactant temperature by 100 K, 6-9% reduction in S_{gen} was estimated with CH_4, while there was a negligible influence of reactant pressure on S_{gen}. The similar trends in specific entropy generation (defined by per-unit-mixture-mass and per-unit-fuel-mass) with reactant temperature and pressure were also found. Nevertheless, the mixture-mass-specific S_{gen} was found to have a decreasing trend with decreasing equivalence ratio and increasing diluent fraction, while the total and fuel-mass-specific S_{gen} demonstrated the opposite trends. On the S_{gen}, a maximum of 65% and a minimum of 40% significant effects with species H_2O and CO_2 in the diluents were considered. The highest S_{gen} was calculated with the fuel C_8H_{18} (four and six times higher than that with C_2H_5OH and CH_4, respectively) was attributed to have a great influence of fuel characteristics on S_{gen}.

Mahabadipour et al. (2016) carried out the experimental and theoretical (multi-zone phenomenological simulation) investigations in a ALPING low temperature combustion (LTC) engine to characterize some important and interesting second law based parameters such as lost available IMEP (LAIMEP), fuel conversion irreversibility (FCI). The engine tested was a 2.4-liter single-cylinder research engine equipped with a dedicated pilot injection system. Other crucial parameters considered were the start of injection of diesel (SOI), T_{in} and intake boost pressure. The ALPING LTC engine was run at the constant engine speed of 1700 rpm, fixed diesel quantity of 3.3 g/min to keep NO_x emission low and at the BMEP of 6 bar at all SOIs. The investigation was conducted in two phases. In the first phase, SOI was varied from 300 to 340 CAD in steps of 5 CAD by keeping the intake manifold pressure and T_{in} at 1.81 bar and 75 °C, respectively. Whereas, in the second phase, T_{in} was varied from 50 to 150 °C, while the SOI was fixed at 310 CAD. In all cases, the fuel chemical energy input was kept constant. The key observation with diesel SOI sweeps (with the advancement) were found for the enhancement of IMEP, indicated fuel conversion efficiency (iFCE), LAIMEP, FCI, BMF and average in-cylinder gas temperature (T_{avg}) at exhaust valve opening (EVO). The major reasons were attributed to the occurrence of a more complete combustion with the advancement of SOI, which led to a higher mass of hot combustion products in the burned zone that caused a higher enetropy generation (irreversibility) and a higher lost available work within the burned zone.

Consequently, the investigators made an interesting and a cruicial statement regarding the requirement of the advancement of the parameters CA50 relative to TDC and a shorter combustion duration in order to avoid the unexpected irrversibilty and to achieve the best engine overall performance.

On the other hand, more efficient results were achieved with the the sweeps of T_{in}. It was noticed that with the increase of T_{in}, there was the significant reduction in the cumulative entropy generation indicating a lower lost available work, which got reflected to the lower FCI and LAIMP. There was also the significant advancement of CA50 with the increase of T_{in}. The physical reasons behind these improvements were attributed to the development of higher in-cylinder temperature at higher T_{in}, which helped to burn all the fuel elements and thereby ensuring a fairly high BMF. However, it was recommended to take care the volumetric efficiency, which was observed to be reduced with the increase of T_{in}. Thus, there might be the lost in power out put even at the advanced CA50. The different trends of LAIMP, FCI, and CA50 were noticed with the variations of intake boost pressure (P_{in}). The LAIMP and FCI were found to be increased monotonically with the increase in P_{in}, while the retarded CA50 was revealed with the increase in P_{in}. The investigator emphasized on further investigation to understand the correct physical reasons behind the charateristics of these parameters (LAIMP, FCI) with P_{in} sweeps. Nevertheless, the enhancement of exhaust gas enthalpy at EVO was attributed to the reasons behind the retardation of CA50.

At a later stage, an almost similar study was also carried out by the same group of investigators (Mahabadipour et al. 2017). In their study, the SOI was kept within 300 – 325 CAD and the T_{in} was varied from 75 – 115 °C. The trends of LAIMP, FCI, and CA50 with respect to the variables SOI, T_{in}, and P_{in} were noticed to be similar to their earlier work (Mahabadipour et al. (2016). They distributed the level of irreversibilities of the cumulative entropy generation in percentage at various zones with the sweeps of SOI, T_{in} and P_{in} as portrayed in Fig. 2.25. In all cases, the maximum, the significant, and the minimum entropy generations were observed in flame zone, burned zone and in packets, respectively. However, a comparatively lower irreversibility in flame zone was noticed with the sweeps of T_{in}. The entropy generation in flame zone was observed to be increased with the increase in T_{in}. However, the oppostive trends of entropy generation in burned zone and in packets with the T_{in} sweeps were noticed as compared to that in flame zone. The enhancement of instantenious flame temperature (T_f) with the increase of T_{in} (Fig. 2.26) was addressed to be the main reason behind the reduction in

irrversibity in flame zone with T_{in} sweeps. The parameter T_f which advanced the start of combustion (SOC) and CA50 and made favorable environment to reduce the entropy.

Cumulative entropy generation (100%)					
Variables		**Flame zone (%)**	**Burned zone (%)**	**Packets (%)**	**Unburned zone (%)**
T_{in} (°C) sweeps	75	58.2	37.4	4.4	0
	85	58.1	37.1	4.8	
	95	56.9	38.0	5.1	
	105	55.4	39.3	5.3	
	115	53.7	40.9	5.4	
SOI (CAD) sweeps	300	58.2	37.4	4.4	0
	305	57.7	37.4	4.8	
	310	56.7	38.5	4.8	
	315	58.1	37.5	4.4	
	320	60.2	35.8	4.0	
	325	65.8	30.6	3.6	
P_{in} (bar) sweeps	1.4	51.7	44.0	4.3	0
	1.6	56.0	39.6	4.4	
	1.8	58.2	37.4	4.4	
	2	59.3	36.3	4.4	
	2.2	60.0	35.6	4.4	
	2.4	60.7	35.0	4.3	

Fig. 2.25 Distrivution of cumulative entropy generation in different zones with sweeps of T_{in}, SOI, and P_{in} (Mahabadipour et al., 2017)

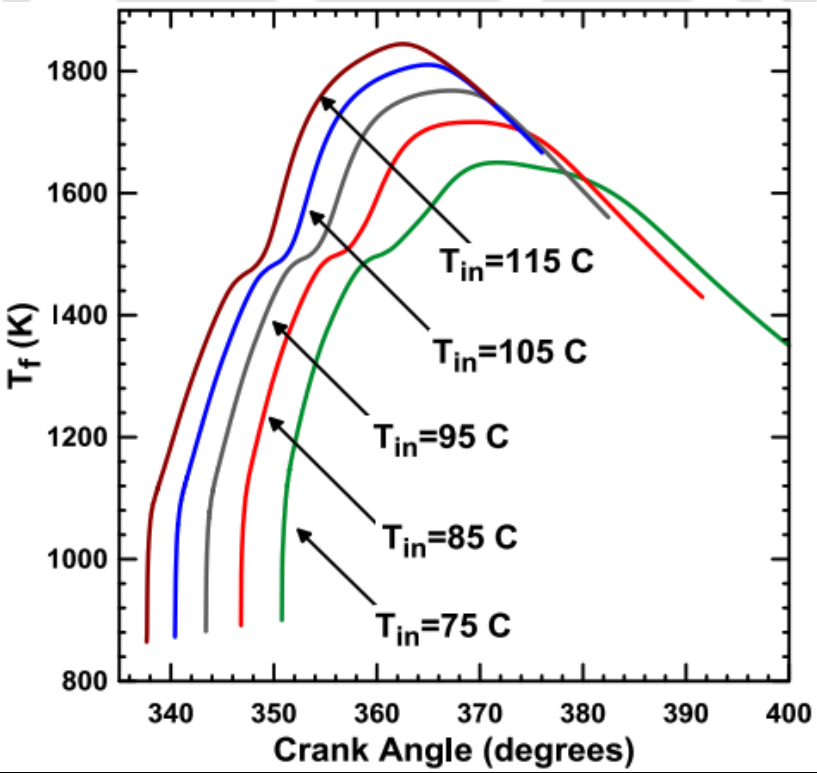

Fig. 2.26 Characteristics of T_f with CAD at various T_{in} (Mahabadipour et al., 2017)

In recent times, the biogas DFM engines have become popular, however, qualitative analyses based on the exergy are very few of such engines. Sahoo *et al*. (2012b) performed the exergy analysis of a biogas run DFM engine using diesel and biodiesel as the pilot fuels. They mainly investigated the effects of biodiesel as the pilot fuel on exergy. With biodiesel, a better exergy efficiency was achieved in comparison to pure diesel. It was also observed that the exergy in DFM improved beyond the applied load of 20%. However, a significantly lower exergy is achieved in DFM in comparison to PDM. Bora and Saha (2016d) investigated the exergy analysis of a biogas run DFM engine (at various CRs and ITs) using diesel as the pilot fuel. The CRs and ITs were optimized at 18 and 29 CAD bTDC, respectively. They found an increase of exergy with the increase of CRs and advancement of ITs (CR = 18 and IT = 29 CAD bTDC). However, the increasing advancement of ITs enhanced the cooling water exergy with the decreasing of exhaust gas exergy as compared to PDM. Bora and Saha (2016e) also made an exergy analysis of a biogas run DFM engine using emulsified rice bran biodiesel as the pilot fuel. The study found emulsified biodiesel as the promising fuel for the biogas DFM engine. Verma *et al*. (2017a) conducted a comparative experimental study on the use of synthetic biogas (varying composition) as the main fuel and diesel as the pilot fuel and observed the lower combustion irreversibility with higher CO_2 in the composition. However, total irreversibility was found to be increased with the increase of CO_2 concentration in the synthetic biogas. The optimum results competitive to PDM were obtained with a blend that contained maximum amount methane (93% by volume) and minimum amount of CO_2 (7% by volume). Verma *et al*. (2017b) examined the exergy in a DFM engine using biogas, compressed natural gas (CNG), and hydrogen respectively as the primary and diesel as the pilot fuels. The important findings in this investigation were the enhancement of exergy with the advancement of IT and, with the increase of loads and found maximum exergy with H_2 fuel. They estimated 2% more exergy efficiency with H_2 at maximum load. Verma *et al*. (2018) carried out an experimental investigation on the supplementation of H_2 with biogas to find the effects on exergy in a diesel piloted DFM engine. The investigators found a significant improvement in exergy with the addition of H_2 beyond 5% by volume.

2.11 Overall Findings

It is evident from the review study that the researchers have been trying to implement the dual fuel mode (DFM) in diesel engines using biogas and various injected oxygenated fuels. So far, the investigators have made serious efforts by altering the various operating and performance

parameters to improve the overall performance of biogas run engines. Some of the salient features accrued from the present literature review are summarized below:

2.11.1 Ethanol, Butanol, DEE, and Biodiesel as Oxygenated Fuels

- The present analysis mainly focused on the ternary blends of diesel-biodiesel-ethanol, diesel-biodiesel-butanol and, diesel-biodiesel-DEE. The attractive results reported and found suitable on the use of ternary blends in biogas run engines are: (a) the release of extra oxygen during combustion, (b) the reduction of premixed and total combustion duration, (c) the increase of NHRR, and (d) the significant reduction of CO and HC.

2.11.2 Performance Analysis in Biogas DFM Engines

- The BFR and the corresponding LFR are found to be very sensitive to performance, combustion, and emission characteristics. The significant reduction of BTE is noticed both at higher BFR and at higher LFR. However, a considerable increment of BTE is noted at higher CRs and at advanced ITs. The energy share is found to be higher at higher loads and at advanced ITs. BTE is always even at the higher CR and at advanced IT found to be significantly lower than the pure diesel mode.

2.11.3 Combustion Analysis in Biogas DFM Engines

- Irrespective of operating condition, the ID in biogas run DFM is found to be higher than PDM. The longer ID is reported at higher BFR. The significant reduction of ID is noticed at higher CRs and at advanced ITs. However, the IT was reported to be an influential parameter to reduce the ID. Although, few researchers notified that at advanced IT, the ID is actually increased. The balance of parameters CA50 and CD are demonstrated to be most inflencial parameters to achieve the best engine performance.

- Most of the studies report a significantly lower CPP in DFM as compared to PDM. However, a few reports a higher CPP at higher Φ_{global}. There is a drastic reduction of CPP at higher BFR. Nevertheless, the CPP is observed to be higher and shifts towards TDC at higher CRs and at advanced ITs.

- In general, there is a substantially lower NHRR in biogas run DFM engines. However, a higher NHHR is noted at the higher Φ_{global} than PDM. At higher CRs and at advanced ITs, the NHRR is found to be higher. Although, the CD in DFM is found to be lower, however, a higher CD at higher BFR is reported in some of the studies. Nonetheless, very few studies report a lower CD at higher BFR due to rapid premixed combustion.

2.11.4 Emission Analysis in Biogas DFM Engines

- The CO in biogas run DFM engine is found to be very high in all cases in comparison to PDM. However, with the increase of CRs and ITs, a significant reduction of CO is reported. Some studies reveal a higher CO at higher loads, while a few observe lower CO with the increase of load.
- The trends of HC emission with the increase of loads are found to be different. However, with the increasing of CRs and advancement of ITs, the HC emission reduces to some extent but significantly higher than that of PDM.
- The NO_x emission, in general, is found to be significantly lower in DFM than the PDM. However, there is a slight increment of NO_x in DFM with the increasing of CRs, and advancing of ITs. However, this increment is found much lower than PDM. There is a drastic reduction of smoke in biogas run DFM engines, and this is observed to be lesser at higher BFR.

2.11.5 Exergy and Irreversibility in DFM Engines

- In DFM the major sources of irreversibilities are: (i) complex chemical structure and mixtures of fuels are chosen, (ii) higher combustion temperature gradient, (iii) lower combustion temperature, (iv) deficiency of oxygen at the time of combustion, (v) mixing and throttling, (vi) heat transfer, (vii) friction, (viii) misfire, (ix) heat transfer from intermediate products to reactants, and (x) over dilution of CO_2 in the gas blend.
- The parameters that are crucial to improving the exergy of DFM engines are (i) fuels simple chemical structure to lessen the chemical irreversibility during combustion, (ii) preheating the intake charge to minimize the combustion temperature gradient, (iii) higher combustion temperature, (iv) enrichment of oxygen at the time of combustion to enhance the flame temperature and to increase the flame speed, (v) use of oxygenated liquid fuels as the pilot fuels but not as the secondary fuel, (vi) lowering the heat dissipation and frictional effects during the entire combustion process, and (vii) proper control of Φ_{global}.

2.12 Scope of Work

The state-of-the-art review implies that the researchers have been trying to implement biogas as the gaseous fuel in dual fuel diesel engines to produce the power. However, in the light of

energy and exergy analysis, it is observed that the biogas DFM engine overall performance substantially deteriorates due to some critical reasons which are not found in the reported works. Therefore, it is essential to search the reasons behind these limitations to make the biogas DFM engines as the viable option to sustain the balance of the ever-increasing demand and supply of the acute shortage of power particularly in rural areas of the developing countries. Consequently, the research gaps found in this contemporary review are as follows:

- The ample numbers of diesel engines throughout the world have been running to produce the power using fossil diesel fuel. These diesel engines have the single (standard) compression ratio and injection timing. Therefore, the utilization of this existing technology in the generation of power in DFM with the simplest modification will be a novel work. However, the investigators worldwide have not achieved the satisfactory results in a biogas run DFM engine at the engine standard CR and IT.

- The working principle of the DFM engine is the combination of CI and SI engines. The fuel-air equivalence ratio, therefore, will have a great impact to achieve an efficient DFM engine operation. On the other hand, biogas contains a very high amount of CO_2. Consequently, it is essential to run the biogas DFM engine with the optimized fuel-air equivalence ratio. However, there is no work found that takes the fuel-air equivalence ratio as a function to run the biogas DFM engine.

- The energy and exergy analysis reveal that the using of renewable liquid fuels in DFM would be an efficient technique to achieve an efficient engine performance. However, the implementations of the renewable fuels like ethanol, butanol, and DEE blended with diesel and biodiesel in a biogas run DFM are very rare. Since, these oxygenated liquid fuels help to enhance the flame temperature, flame speed and stimulate to improve the combustion process. Thereby the biogas DFM engine performance can be improved substantially by the use of these oxygenatyed fuel addressed above.

- Most of the investigators have used the biogas flow rate at the misfire limit and presents controversial results. Some investigators observed lower emission, while a few noticed very high emissions in a biogas run DFM.

- The exergy analysis demonstrates that the higher the combustion temperature gradient during the exchange of premixed combustion phase to diffusion combustion phase is the major source of combustion irreversibility. Some studies suggest that the intake charge

preheating technique can help to reduce the combustion temperature gradient significantly. However, there is no work found that elaborated the intake charge preheating effects on the overall performance of a biogas run DFM engine. Besides, the literature is almost silent about the thermodynamic potential study on the effects of intake charge preheating in such engines (biogas run DFM) using the various oxygenated fuels discussed above. However, very few but potential studies on second law in a LTC ALPING engine were observed. The studies on LTC ALPING engine revealed that the parameters such as quantity of pilot fuel, proper dispersion of sprayed pilot fuel, homogeneous distrubition of ignition kernels, IT, T_{in}, and P_{in} have the great influence on the overall engine performance.

- There is no state-of-the-art work found in any archived journal on the analysis of combustion considering the parameters such as global fuel-air equivalence ratio (Φ_{global}), oxygenated liquid fuels (such as the ternary blends of diesel-biodiesel with ethanol, butanol, and DEE, respectively) and the intake charge preheating in a biogas run DFM engine. The corresponding exergy analysis has also not been found.

2.13 Summary

In this literature survey, the parameters that have the direct or indirect influence on the performance, combustion, and emissions of biogas run DFM engines have been discussed. It is noticed that these engines can efficiently be performed at the standard CR and IT by

(a) optimizing the global fuel-air equivalence ratio (Φ_{global})
(b) using renewable oxygenated liquid fuels, and
(c) preheating the intake charge.

The efficient utilization of biogas in a DFM engine at the standard CR and IT is a challenging task as the use of excess fuel is an indication of the waste of energy into the environment. The combinations of optimum Φ_{global}, correct energy share of renewable liquid fuels and biogas at each of the load and preheating the intake charge will have a great impact on the engine overall performance.

Chapter-3

The Engine Test Bed and Instruments

Chapter

Highlights:	**Overview:** *It is clear that the generation of power from the existing diesel engines in DFM (at standard CR and IT) will be extremely beneficial in terms of lowering the dependency on imported fossil diesel fuels and reducing of GHG. The present research work has endeavored to unveil all the means to achieve an efficient DFM engine performance at standard CR = 17.5 and IT = 23 CAD bTDC. In order to reduce the detrimental pollutant emission in the green environment, the study emphasizes on the optimum and efficient implementation of the various renewable oxygenated liquid fuels in a biogas run DFM engine. In order to achieve these goals, it is necessary to identify and to recommend the specifications of the important influential parameters such as Φ_{global}, intake charge preheating temperature, biogas flow rate and fuels energy shares. In view of this, this chapter confers in details of the existing setup, its conversion to DFM, and the devices and instrumentations used.*
• *Existing VCR engine setup in PDM is described* • *Instruments and measurement devices are outlined* • *Outlines the method of conversion from PDM to DFM* • *Experimental procedure is explained* • *Selection criteria of binary and terniary blends along with preheating are explained.*	

***Chapter Layout*:**

3.1 The VCR Diesel Engine Test Bed

The experimental setup consists of a single-cylinder four-stroke, water-cooled, naturally aspirated direct injection variable compression ratio (VCR) diesel engine (Kirloskar, TV1). The specifications of the engine are presented in Table 3.1. An eddy current water-cooled dynamometer (Saj Test Plant, AG10) is coupled with the engine as the loading unit to measure the engine load in kg with a load cell (Sensotronics Sanmar, 60001). An ampere regulator attached to the control panel, is used to load the engine.

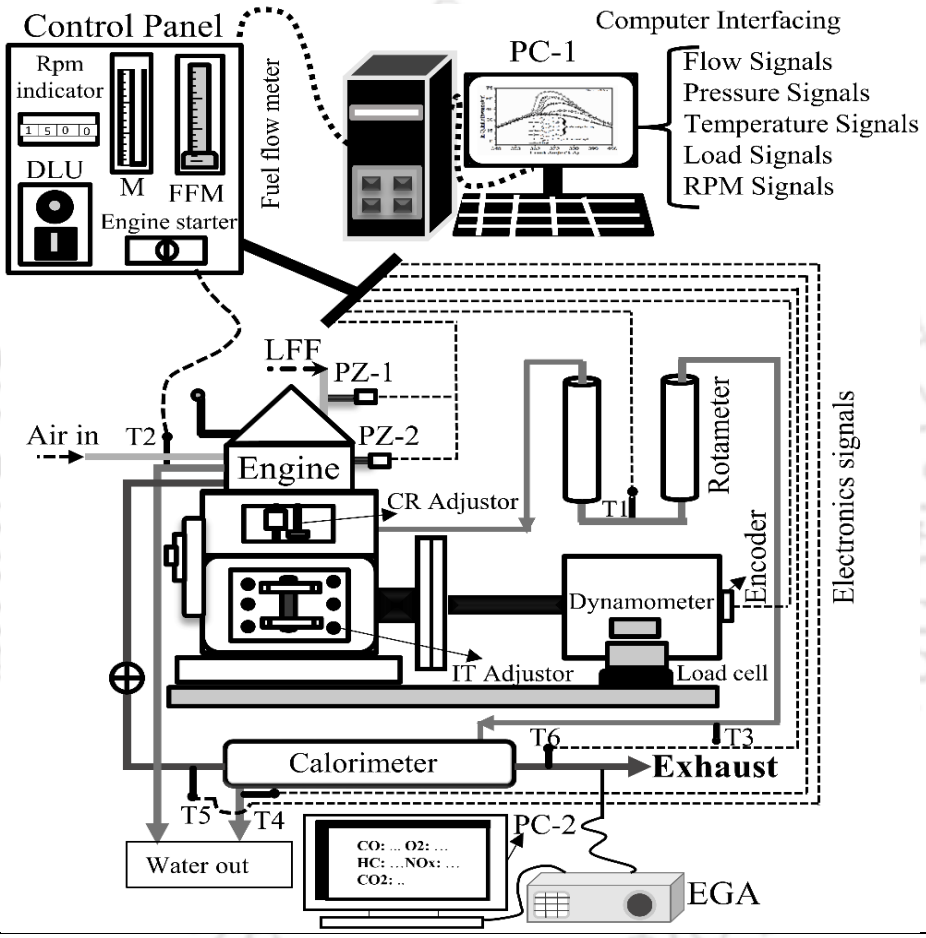

Fig. 3.1 Schematic diagram of the multi-fuel VCR diesel engine test rig
BFCV: Biogas flow control valve, **FFM:** Fuel flow meter, **EGA:** Exhaust gas analyzer; **M:** Manometer; **DLU:** Dynamometer loading unit, **LFF:** Liquid fuel flow, **PZ:** Pressure transducer, **T:** Thermocouple

The engine has the facility to vary the CR with the help of the tilting block mechanisms. The high pressure (opening pressure = 200-240 bar) liquid fuel injector (Bosch, 1035) firmed with the engine head has three circular holes (diameter = 0.3 mm) with the spray angle of 120°. The bowl shape of the piston top of the engine makes the combustion chamber hemispherical when the piston reaches the top dead center (TDC). The liquid fuel at the pump inlet reaches from the fuel tank by gravity. To measure the cylinder pressure and compressed liquid fuel pressure in the injector fuel line, two piezo type sensors are mounted on the engine head and injector

fuel line. The engine pressure-crank angle (P-θ) and pressure-volume (P-V) data can be acquired at each degree of rotation of the crank angle (360 CAD) in a complete cycle by interfacing of the signals with the piezo powering unit (Cuadra, AX-409). The crank angle encoder (Kubler, 8.3700.1321.0360) fixed with the dynamometer shaft, is used to measure the engine speed along with the crank angle position at each degree of rotation. The facilities to measure the fuel flow, airflow, and temperature are also provided along with the setup. Rotameters are used to maintain the mass flow rate of water as the coolant to eliminate the heat that develops in the engine cylinder wall and head. The schematic of the diesel engine test bed is shown in Fig. 3.1.

3.2 Measuring Instruments

The VCR test bed comprises a number of sensors, transmitters and, indicators. All these measuring accessories are interfaced with the computerized data acquisition system (DAS) to acquire automatically all most all the data to understand the engine performance characteristics. The essential parameters to apprehend the performance quality of the engine are discussed briefly in the following sections.

3.2.1 Performance Measurement

In the evaluation of various performance parameters at a particular applied load on the engine, the data are collected automatically from the computerized system. In order to have the correct results with the various fuels, the density and the calorific values of the respective fuels are included as per the requirement. The parameters estimated are air and fuel flow rates, air-fuel ratio, fuel-air equivalence ratio, efficiencies, energy share, power, mean effective pressure, and heat balance. The detailed discussions, in the evaluation of these parameters, have been made in Appendix-A.

3.2.2 Air and Fuel Flow Measurement

There is a provision for manual measurement of the air and fuel flow rates. For the airflow rate, the difference of the water column of the differential manometer is recorded. The manometer limbs are fitted with an orifice meter attached to the air-box, while, the fuel flow rate is measured by transferring the fuel from the storage tank through the measuring tube for the known volume. The automatic measurement of the airflow is associated with an airflow transmitter (WIKA Instruments, T19.10.3K0-4NK-Z). Similarly, automatic data for fuel flow rate can be acquired with a differential pressure transmitter (Yokogawa, EJA110-EMS-5A-92NN).

Table 3.1 The specifications of VCR diesel engine and elemental devices

System specifications	
Parameter	***Specification***
Product	Research engine test setup, Code 240
Type	Single cylinder, four-stroke, DI diesel engine
Power	3.5 kW (@ 1500±50 rpm)
Type of cooling	Water cooled
CR range	12:1 − 18:1
Injection variation	0 − 25 CAD bTDC
Combustion chamber	Hemispherical bowl in piston type
Dynamometer	Eddy current type, water cooled with loading unit
Air box	MS fabricated with orifice meter and manometer (100 - 0 - 100)
Fuel tank	Capacity 15 lit with measuring tube (0-450 ml)
Calorimeter	Pipe in pipe type
Rotameters	Engine cooling 40-400 lph, calorimeter 25-250 lph
Data acquisition Software	"Enginesoft" engine performance analysis software
Transmitters, sensors, and indicators	
Fuel flow meter	DP transmitter, range 0-500 mmWC
Air flow transmitter	Pressure transmitter (-) 250 mm WC
Pressure sensors	Piezo type, range 5000 PSI, with low noise cable
Temperature sensors and transmitter	PT100 (RTD) type, range 0-100° C, output 4-20 mA (4 nos) K (ungrounded) type, range 0-1200° C, output 4-20 mA (2 nos)
Load sensor and indicator	Strain gauge type load cell with digital indicator, range 0-50 kg
Speed sensor and indicator	Resolution 1° CA, range (5500 rpm) with TDC pulse
Data acquisition device	NI USB-6210, 16 bit, 250 kS/s
Setup constants	
Pulse per revolution	360°
No. of cycles	20
Fuel measuring interval	60 s
Speed scanning intervals	2000 ms
Bore × Stroke	87.5 mm × 110 mm
Capacity	661 cc
Orifice diameter	20 mm
Dynamometer	185 mm
Connecting rod length	234 mm
Theoretical constants	
Orifice coefficient of discharge	0.6
Specific heat of exhaust gas	1.00 − 1.25 kJ/kg-K
Specific heat of water	4.186 kJ/kg-K
Density of air	1.174 kg/m^3
Maximum permissible back pressure in the exhaust system	2.5 kPa
Maximum permissible intake depression	1 kPa

3.2.3 *P-θ* Measurement

In-cylinder pressure history is one of the vital parameters in the evaluation of combustion parameters and combustion characteristics of the engine. In order to measure the in-cylinder pressure data and liquid fuel pressure data in the high-pressure fuel line, two pressure sensors (PCB Piezotronics, S111A22) having identical specifications are mounted on the engine head and firmed with the fuel line, respectively. These sensors are able to distinguish the pressure

of compression, combustion, explosion, pulsation, cavitation's, blast, pneumatic, hydraulic, fluidic etc. An optical encoder (Kublar, 8.3700.1321.0360) is set to record the pressure data at each of the engine crank angles.

3.2.4 Temperature Measurement

The temperature at the four terminals of engine cooling water and calorimeter are measured with the four PT100 (RTD) temperature sensors. Whereas, the inlet and outlet temperatures of the exhaust gas are measured with the K-type thermocouple. All these temperature sensors are interfaced with a computer for automatic recording and online monitoring of the temperature data to arrive at the thermodynamic equilibrium state. The response time of the thermocouple used is higher than 0.08 seconds (for the 1500 rpm constant engine speed). Hence, the steady reading of temperature (approximately 5 minutes) instead of pulsation can be achieved with all fluids as discussed above.

3.2.5 Tuning of Compression Ratio and Injection Timing

The VCR diesel engine has the CR adjusting mechanism. The CR can be varied ranges from 12 to 18 with eight steps. However, to vary the CR, it is necessary to run the engine at the standard CR of 17.5. The adjustment of CR is done by tilting the cylinder block with the help of a locknut and stud arrangement. The tilting of the block can be done with loosening of the six Allen bolt that holds the cylinder block with supporting block. There is a scale on CR adjustor mechanism to fix the CR at a particular point. After fixing the CR at a particular point, it is necessary to insert this manually in the software for the data acquisition. The IT can be tuned online or manually. In either case of the tunning of IT, the six nuts should be loosened that holds the mechanism to change the position of the higher pair in-between lever and cam.

3.2.6 Emission Measurement

A flue gas analyzer (AVL, Digas 444n) is used to measure the emissions in the exhaust gas. At any time, without shutting down, the calibration of this device can be done. The measurement of emissions is carried out by letting the flue gas samples to rush through a probe in the steady-state operation of the engine. A condensation trap is used next, to dry out the gas sucked. Then the dry samples are investigated inside the analyzer for the analysis of the gases such as O_2, CO, CO_2, HC, and NO_x. The analyzer returns the values of CO, CO_2, and O_2 in percentage by volume, while the HC and NO_x are in ppm. CO and NO_x are measured through electrochemical measurement cells, whereas, CO_2 and HC are measured by infrared and Pellistor Head Affect

Detector, respectively. The device has the provision to interface with a computer through a USB cable to store and for online monitoring of emission data.

Table 3.2. Gas Analyzer Specification

Measured Gas	Resolution (vol.)	Accuracy		Range (vol.)
O_2	0.01%	±0.02% abs	1% rel	0-25%
CO	0.01%	0-10% ±0.02% abs 10.01%-15%	±3% rel ±15% rel	0-15%
CO_2	0.01%	0-16% ±0.3% abs 16.01%-20%	±3% rel ±5% rel	0-20%
NO	1 ppm	±5 ppm	1% rel	0-5000 ppm
HC	≤2000:1 ppm >2000:10 ppm	0-4000 ppm ±8 ppm 4001-10000 ppm 10001-30000 ppm	3% rel 5% rel 10% rel	0-30000 ppm

3.3 Modification in Diesel DFM Engine

There can be many ways to convert a diesel engine into a DFM engine. Bora and Saha (2014, 2015a, 2016a) attached a venturi-meter in the diesel engine intake manifold to convert it to a biogas run DFM engine. With this simple modification, the investigators carried out several experiments to utilize a very high amount of biogas in DFM. They mainly studied the influences of CR and IT at the maximum limit of the biogas flow rate where the misfire of the gas mixture inside the combustion chamber appears. Consequently, they attained poor results at the standard CR = 17.5 and IT = 23 CAD bTDC. In addition, the literature review also reveals that there is a performance penalty with such an engine at the standard CR and IT.

It is well known that ample numbers of diesel engines have been producing power throughout the globe at the standard CR and IT. The efficient utilization of the existing technologies to produce power can be a novel work. Keeping this panorama in mind, the present study intends to modify the diesel engine to a biogas run DFM engine by installing a cross-flow heat exchanger (CFHE) with the intake port as shown in Fig. 3.2. The CFHE consists of four headers. Two of headers are attached to the vertical channel of the CFHE through which the biogas-air mixture rushes into the combustion chamber due to suction. Another two headers are firmed to the horizontal channel. The one header of this pair is connected to the exhaust pipe and the other one is kept free to the atmosphere (Fig. 3.2). During the transportation of fluids, heat is transferred from the hot exhaust gas to the biogas-air mixture.

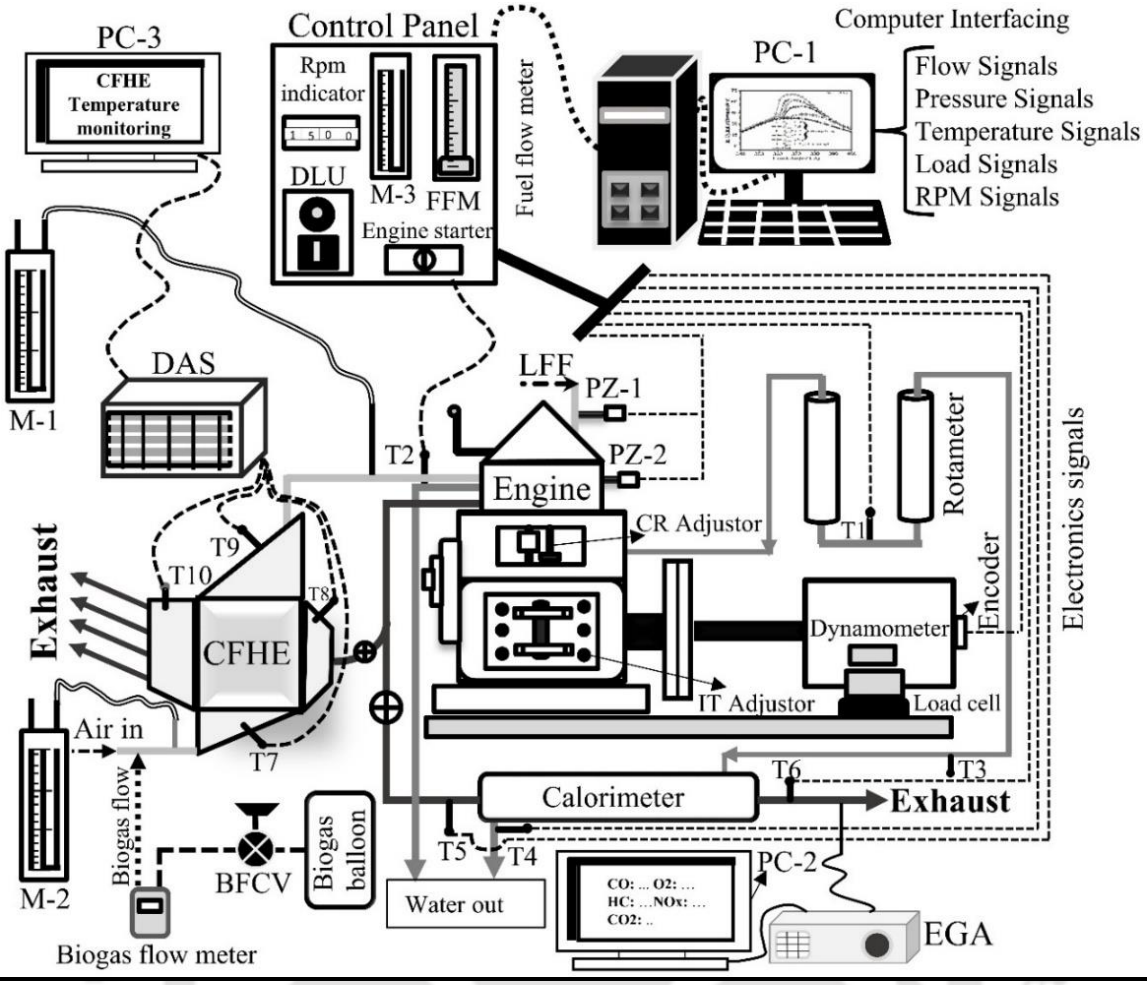

Fig. 3.2 Schematic diagram of the modified biogas run DFM engine

BFCV: Biogas flow control valve, **FFM:** Fuel flow meter, **EGA:** Exhaust gas analyzer; **M:** Manometer; **DLU:** Dynamometer loading unit, **LFF:** Liquid fuel flow, **PZ:** Pressure transducer, **T:** Thermocouple

The added advantage of using of CFHE is that it ensures a homogeneous mixture of the biogas-air mixture. The CFHE is designed in such a way that the depression of pressure is within the allowable limits as specified in the engine manual (Table 3.1). In DFM, the exhaust pipe outlet is divided into two segments by fabricating an angular (elbow shape) pipe attached to the CFHE. Another segment is fixed with the calorimeter (Fig. 3.2). In order to control the liquid fuel consumption, a fuel controlling mechanism is attached along with a damper. The damper helps to reduce the engine vibration. The existing dual fuel engine setup that identical to Fig. 3.2 and the modified components of setup are presented in Fig.3.3.The green thick arrow lines (Fig. 3.3) indicate the flow of the intake charge (biogas-air mixture) into the heat exchanger to preheat and finally introduce inside the combustion chamber. While the red thick arrow lines direct the exhaust gas flow through the CFHE and calorimeter. As the density of biogas is lower than the air, therefore, the pipe attached to the biogas balloon is firmed upward. This is to utilize the buoyancy effect to ensure the smooth flow of biogas into the main air stream.The valve-timing diagram of the engine is shown in Fig. 3.4.

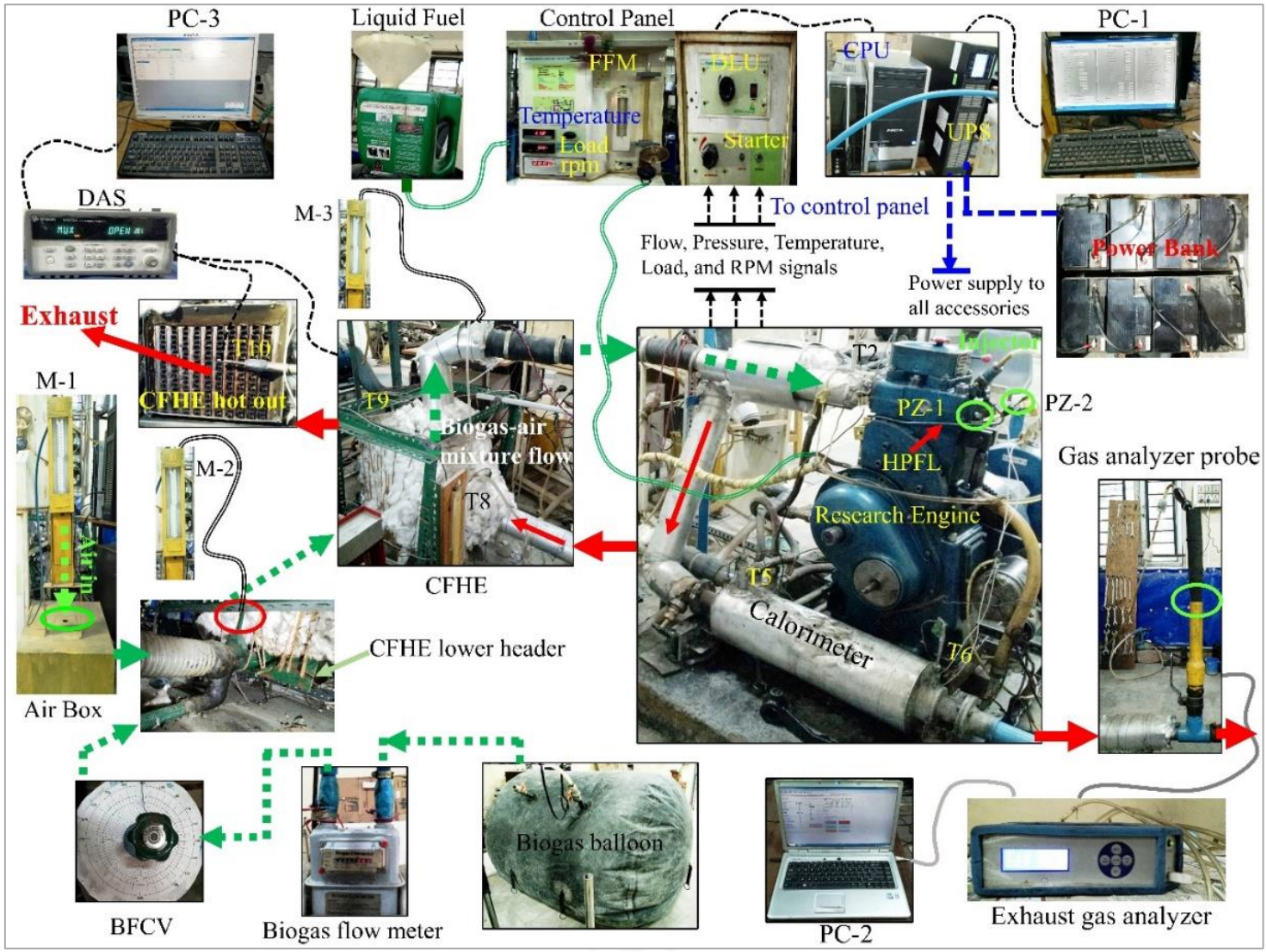

Fig. 3.3 Existing and modified experimental test setup

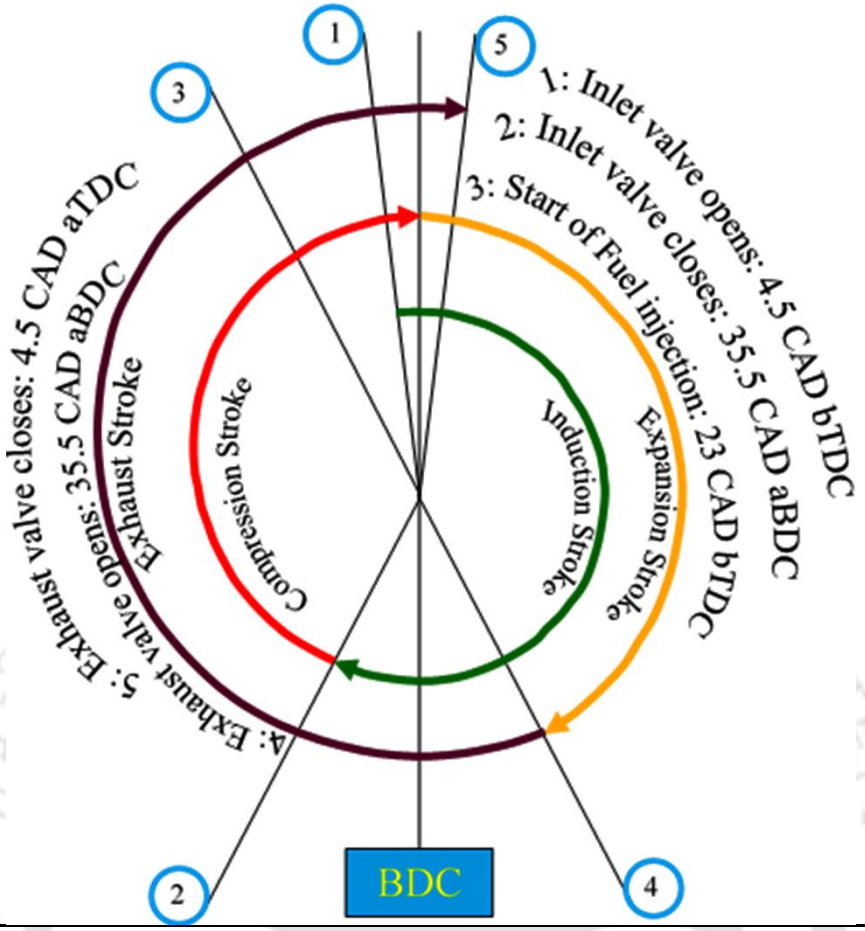

Fig. 3.4 Engine valve timing diagram

3.4 Experimental Procedure

The entire experimental investigation in the present study is divided into three parts as indicated below:

- Experiments in pure diesel mode (PDM)
- Experiments in DFM using biogas as the inducted fuel and diesel as the pilot fuel to optimize the global fuel-air equivalence ratio (Φ_{global}) from part to higher loads.
- Experiments in biogas DFM engine at the optimized Φ_{global} with intake charge preheating using various liquid oxygenated fuels blended with diesel as the pilot.

The oxygenated fuels that are chosen in the present investigation are biodiesel, ethanol, butanol, and diethyl ether (DEE). The blends prepared for their use as pilot fuel are:

- Binary blends (BB) of diesel-ethanol
- Ternary blends (TB) of diesel-biodiesel-ethanol (D-B-E)
- TB of diesel-biodiesel-butanol (D-B-BT), and
- TB of diesel-biodiesel-DEE (D-B-DEE).

3.4.1 Engine Tests in PDM

The PDM operation is executed to make the foundation for the later experiments in DFM. In PDM, pure diesel fuel is used to investigate the overall performance (performance, combustion, and emission). The loads in terms of brake mean effective pressure (BMEP, bar) are considered as 0.83 bar, 1.65 bar, 2.48 bar, 3.31 bar and, 4.14 bar (=100% load). The standard setting of CR = 17.5 and IT = 23 CAD bTDC are maintained throughout the investigation. The water follows into the engine and calorimeter are adjusted at 300 kg/h and 100 kg/h, respectively, as instructed in the engine manual. During the trial runs, it is observed that the whole system takes about 15 minutes to arrive at the steady states. Consequently, to attain the states of thermodynamic equilibrium, this time duration is maintained at each of the two successive loads. After reaching to the thermodynamic equilibrium states, the data such as engine load, rpm, temperature, air, and fuel flow rates, fuel line and cylinder pressure history are automatically acquired through DAS. The sample of flue gas is then examined with a gas analyzer (AVL, DiGas444n) by inserting the probe into the exhaust gas stream. The pollutants quantify this analyzer are O_2, CO, CO_2, HC, and NO_x.

3.4.2 Engine Tests in DFM to Optimize the Φ_{global}

In order to achieve an efficient DFM engine performance at the standard CR and IT of the existing diesel engine, Φ_{global} is targeted as the crucial parameter. Therefore, in this section, Φ_{global} is optimized where the experiments are carried out without preheating of the intake charge. While the preheating has been done with the optimized Φ_{global} to improve the DFM engine performance. In all the tests, loads (BMEP) are varied from 0.83 to 4.14 bar and at the engine standard CR = 17.5 and IT=23^o bTDC. In DFM, biogas and diesel are used as the primary and pilot fuels, respectively. A series of tests are conducted at different Φ_{global} as represented in Table 3.3 to optimize this parameter (Φ_{global}). The minimum Φ_{global} is considered based on the minimum biogas consumption (pilot fuel replacement > 20%). At the same load during the trial run of biogas DFM engine, a drastic reduction in CPP is observed with the increasing of Φ_{global}. Consequently, the maximum Φ_{global} is considered at the point where the biogas mass flow rate is maximum, and there is no enhancement of CPP from part to higher loads. In addition, at this maximum Φ_{global}, there are the appearances of misfire sounds, engine vibration due to the rate of change of acceleration, abrupt fluctuation of cylinder pressure and engine speed.

The aim of the investigation thus is to optimize the biogas mass flow rate and Φ_{global} depending upon the engine overall performance at each of the load at which the engine would give the

comparable overall performance between part loads and higher loads. The investigation conducted without preheating in DFM with the optimized Φ_{global} is designated as *nr*-DFM (WOP). Whereas, for the case of with preheating, it is designated as *nr*-DFM (WP). In DFM, the engine speed enhances upon supplementing of inducted gaseous fuel. Hence, a sophisticated manual mechanism is attached to the engine governor to control the liquid fuel consumption and the engine speed. The BFR is controlled with a biogas valve and biogas flowmeter (Fig. 3.2). The preheating has been done with the optimized Φ_{global}. The preheating temperature of 55±2° C is chosen at the point where there is no appearance of knocking. Moreover, the preheating temperature and the higher values of optimum Φ_{global} are restricted depending upon the maximum reduction of volumetric effeicency (VE) of 10%. This is to ensure enough oxygen in the fuel-air mixture. The A CFHE is attached to preheat the intake charge (biogas-air mixture) using exhaust gas as the hot fluid. It is observed that the whole system between two successive loads takes about 30 minutes to arrive at the thermodynamic equilibrium states. The composition of biogas used in this work is analyzed through gas chromatography (GC). In the GC analysis, an approximate composition of biogas is found to be consists of 40% CO_2 and 60% CH_4 by volume. The data for all the independent parameters are recorded three times both in PDM and in DFM, and the average data are presented in the study.

Table 3.3 Optimization of Φ_{global} in DFM

Load in BMEP (bar)				
0.83	1.65	2.48	3.31	4.14
Φ_{global}				
0.29	0.35	0.40	0.47	0.53
0.30	0.36	0.41	0.48	0.54
0.32	0.38	0.43	0.49	0.55
0.34	0.39	0.44	0.50	0.56
0.35	0.40	0.45	0.51	0.58
0.38	0.43	0.50	0.52	0.59
0.40	0.44	0.52	0.56	0.61
0.42	0.46	0.53	0.60	0.63
0.50	0.50	0.56	0.63	0.65
0.60	0.63	0.62	0.66	0.67
0.69	0.71	0.72	0.73	0.75
0.74	0.76	0.78	0.79	0.80
0.87	0.87	0.88	0.89	0.89

3.4.3 Engine Tests with Preheating and with Binary Blend

The experiments in PDM are conducted similarly to that discussed earlier. The tests are carried out in *nr*-DFM (WOP/WP) at the optimized Φ_{global} are also similar as discuss above. The same

preheating temperature is maintained throughout the investigation as discussed above. In this study, 5% ethanol by volume (chosen as the oxygenated fuel) is blended with 95% diesel fuel to investigate the biogas DFM engine performance with preheating of the intake charge. The blend is designated as E5. The engine operating parameters are similar to that have discussed above.

3.4.4 Engine Tests with Preheating and with TBs

In the present investigation, the ternary blends (TB) are considered as D-B-E, D-B-BT, and D-B-DEE. The experimental procedure to study the DFM engine performance, combustion, and emission are discussed below.

(a) ***Engine Tests with D-B-E Blends***

Here the comparative analysis has been made among the PDM, *nr*-DFM (WOP/WP) and the DFM with various blends of diesel biodiesel and ethanol (D-B-E). Six blends of the TB of D-B-E are chosen to optimize the best ternary blends of D-B-E to achieve the best results with the preheating and at the optimized Φ_{global}. The optimized blend is designated as TB-E and it uses in the next comparative analysis. The detail discussion of the optimization of blends has been made later in the respective chapters.

(b) ***Engine Tests with D-B-BT and D-B-DEE Blends***

In this investigation, the overall comparative analysis has been made among PDM, *nr*-DFM (WOP/WP), TB-E, TB-BT, and TB-DEE. The TB-BT and TB-DEE blends are prepared with respect to the TB-E blend. The volume percentage of BT and DEE in TBs are considered depending upon the amount of oxygen that is equal to that in ethanol in TB-E blend. The biodiesel volume percentage is kept fixed in all the blends.

The design of experiments and the details of all fuel properties are discussed in the subsequent chapters. The exergy analysis considering PDM, *nr*-DFM (WOP/WP), and ternary blends in DFM have been done.

3.5 Summary

This chapter discusses the details of engine test bed both in PDM and in DFM. In order to achieve the efficient results in DFM at the engine standard CR and IT, the necessary modifications in DFM are also discussed in detailed. Finally, the conceptual techniques that adopted to achieve the efficient engine overall performance with the implementation of the various liquid renewable oxygenated fuels, have been introduced.

Chapter-4

Results of Biogas Run DFM Engine Using Diesel and the Optimization of Φ_{global}

Chapter

Highlights:	**Overview:** *The main objective of this chapter is to optimize the global fuel-air equivalence ratio (Φ_{global}) and to perform the biogas DFM engine with preheating of intake charge (biogas-air mixture). The overall performance of the biogas DFM engine is found to be very sensitive to Φ_{global}. At the optimum Φ_{global} with intake charge preheating, the diesel-like performance is achieved in DFM. The cycle-by-cycle variations of cylinder peak pressure (CPP) are found to be increased with the increase of Φ_{global}. The CPP and NHRR are also found to be very low at the higher Φ_{global}. At the maximum limit of Φ_{global} (= 0.89), there is an abrupt fluctuation of engine speed (rpm) and cylinder pressure with the appearance of misfire and engine vibration. The lower DR (diesel replacements) and BES (biogas energy share) at the optimum Φ_{global} are necessary in order to achieve an efficient engine performance in biogas DFM.*
• *Φ_{global} is noticed to be the most influential parameter in biogas DFM engine* • *Higher Φ_{global} enhances the cycle-by-cycle variations of the CPPs* • *Defining of Φ_{global} from part to higher loads is necessary to achieve an efficient engine data* • *Preheating is a good technique to improve the DFM engine performance* • *There is a scope to use a higher amount of liquid renewable fuel to replace fossil diesel fuel*	

***Chapter Layout*:**

4.1 Selection of Fuels

The analysis in this chapter is considered as the base study of the present entire research work. The previous analysis and key findings from the literature review revealed that the parameter Φ_{global} will have the acute influences on the overall performance of biogas run DFM engines. Therefore, an assessment on the parametric study on impacts of Φ_{global} over the other various operating and performance parameters is essential. Hence, diesel is considered as the injected (pilot) fuel, whereas biogas is used as the inducted fuel. It is to be noted that the biogas can be used as the primary or secondary fuel. Hence, for biogas the term 'inducted' fuel is used. Most of the properties of these fuels are quantified with the use of existing facilities available at various laboratories in Indian Institute Technology Guwahati. In addition, some of the properties of these fuels are collected from the reported work as shown in Table 4.1.

Table 4.1 Fuels Properties used in the present study (Porpatham, 2007; Nathan et al., 2010; Yoon and Lee, 2011; Chen et al., 2013; Tutak, 2014; Rakopoulos et al., 2014; Zhang, 2016)

Properties	Diesel	Biogas
Chemical structure	$C_{12}H_{26}$	Approximately (vol.) 60% CH_4, 40% CO2
C (wt.%)	84.7	-
H (wt.%)	15.3	-
O (wt.%)	-	-
Density (kg/m^3), at 32.2^{o}C	824.91[a]	1.096[a]
Lower heating value (MJ/kg)	42.10[a]	19.1[a]
Cetane number	50	-
Kinematic viscosity (mm^2/s, at 40^{o}C)	2.54[b]	-
Stoichiometric air-fuel ratio	14.94[a]	6.17[a]
Auto Ignition temperature (^{o}C)	200-220	632-813
Flammability limits (% by volume of air)	1.5-7.6	7.5-14
Flame speed (m/s)	0.86	0.25

[a]calculated, [b]measured

4.2 Design of Experiments

The literature demonstrates that the dual fuel diesel engine performance significantly deteriorates in comparison to the PDM. The major deterioration of the engine performance has been notified in the reported work at the part loads in comparison to higher loads in DFM. The researchers conducted the investigation in biogas DFM with the aim of the consumption of a higher amount of biogas. Consequently, they never found an efficient engine performance at the engine standard CR and IT (Bora and Saha 2014, Bora and Saha 2015a, Bora and Saha 2016a). All most all the researchers use biogas as the primary fuel and liquid fuel (pilot) as the

secondary fuel. Literature also reveals that the quantity and quality of the liquid fuel have the great impact on DFM engine performance (Sahoo *et al*. 2009). It is also evident from the literature that a higher rate of gaseous fuel mass consumption cannot improve the engine performance, rather it deteriorates at some limits of pilot fuel replacement (Abd Alla *et al*., 2000; Papagiannakis *et al*., 2003). In a DFM engine operation, higher the pilot fuel replacement higher is the rate of consumption of the inducted gaseous fuel (Bora and Saha, 2015a; Bora and Saha, 2016a). This attributes to the higher substitution of air with the induction of higher amount gaseous fuel. Thus, the parameter Φ_{global} that is the function of the mass of total fuels (injected + inducted) along with the inducted air quantity, is chosen to optimize to achieve the efficient biogas DFM engine performance from part to higher loads. Therefore, the aim of this study is to optimize the parameter Φ_{global} at all applied loads from part to higher. In order to arrive at the aim and to resolve the problem in biogas DFM discuss above a set of Φ_{global} is considered at each of the loads from part to higher as shown in Fig. 4.1.

BMEP (bar)				
0.83	**1.65**	**2.48**	**3.31**	**4.14**
Φ_{global}				
0.29	0.35	0.40	0.47	0.53
0.30	0.36	0.41	0.48	0.54
0.32	0.38	0.43	0.49	0.55
0.34	0.39	0.44	0.50	0.56
0.35	0.40	0.45	0.51	0.58
0.38	0.43	0.50	0.52	0.59
0.40	0.44	0.52	0.56	0.61
0.42	0.46	0.53	0.60	0.63
0.50	0.50	0.56	0.63	0.65
0.60	0.63	0.62	0.66	0.67
0.69	0.71	0.72	0.73	0.75
0.74	0.76	0.78	0.79	0.80
0.87	0.87	0.88	0.89	0.89
Optimization of Φ_{global} depending upon the DFM engine performance, combustion and emission				
Experiments with preheating (55±2°C) with the optimized Φ_{global}				
Comparison the results in DFM with PDM				

The zone indicated inside concentric grey box is the values of Φ_{global} at which there is no improvement of engine performance, combustion, and emission and discuss later

Direction of investigation

Fig. 4.1 Experimental matrix (at CR = 17.5, IT = 23 CAD bTDC)

The minimum Φ_{global} is considered based on the minimum biogas consumption (pilot fuel replacement should not be lower than the 20%). At the same load during the trial run of the engine in DFM, a drastic reduction in CPP with the increasing of Φ_{global}, is observed. Consequently, the maximum Φ_{global} is considered at the point where the biogas mass flow rate

is maximum, and there is no improvement of CPP from part to higher loads. In addition, at this maximum value of Φ_{global}, there are the appearances of misfire sounds, engine vibration due to the rate of change of acceleration, abrupt fluctuation of cylinder pressure and engine speed. At the optimize Φ_{global}, the experiments are conducted with the preheating of the intake charge. The temperature limit is considered depending upon the zero appearance of knocking.

4.3 Optimization of Φ_{global}

Figures 4.2 through 4.6 show the behaviour of performance parameters at various Φ_{global} and at various loads in DFM mode. It can be seen in Fig. 4.2 (at the load = 0.83 bar) that with the increase of Φ_{global}, the diesel replacement (DR), biogas flow rate (BFR), biogas energy share (BES), CO and HC emissions are increased. However, there is a reduction of BTE with the increase of Φ_{global}. Nevertheless, in PDM, CO and HC emissions are found to be lower, while the BTE is observed to be higher as compared to DFM. Therefore, in order to achieve the efficient engine performance, the characteristic curves in Fig. 4.2 indicate that the Φ_{global} (in terms of DR, gaseous fuel consumption, and other performance parameters) must be lower at lower loads. Another crucial issue is the inefficient engine performances in DFM at lower loads with higher Φ_{global} in comparison to higher loads. Thus, it is necessary to confine Φ_{global} as the key parameter within some limits at which a comparable overall engine performance can be achieved between the part and higher loads. Moreover, at this limit of Φ_{global} and under different conditions (e.g., use of oxygenated liquid fuel and preheating of the intake charge), there is a prospect to achieve a PDM (base results) like overall performance in biogas run DFM engine.

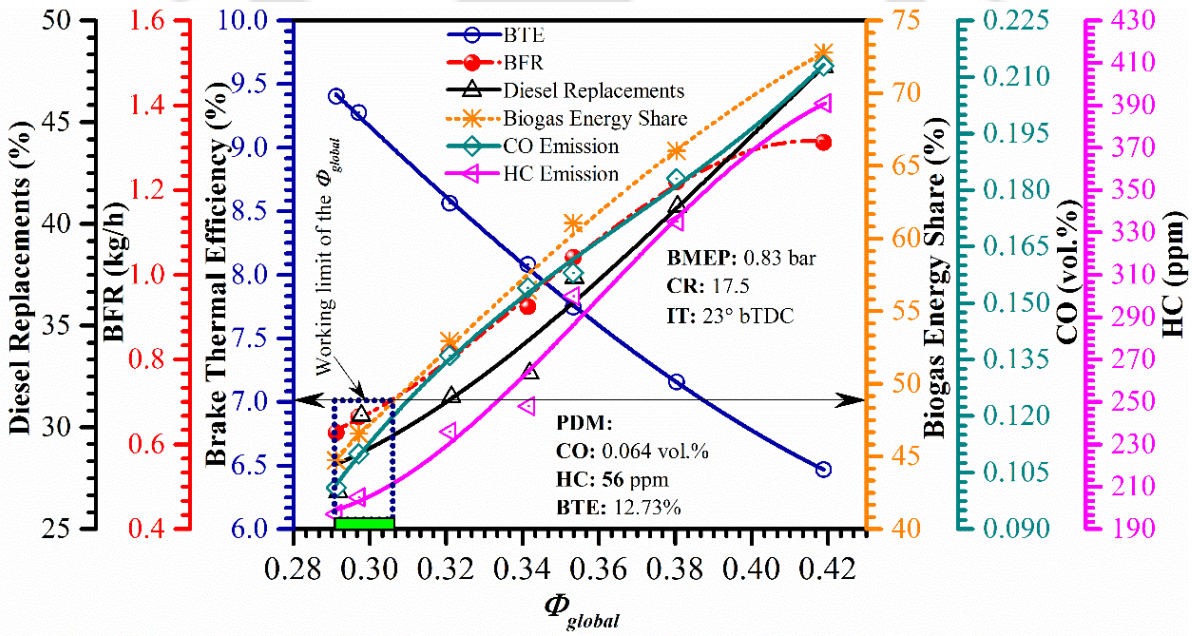

Fig. 4.2 Variations of DR, BFR, BTE, BES, CO, and HC with Φ_{global} (**BMEP:** 0.83 bar)

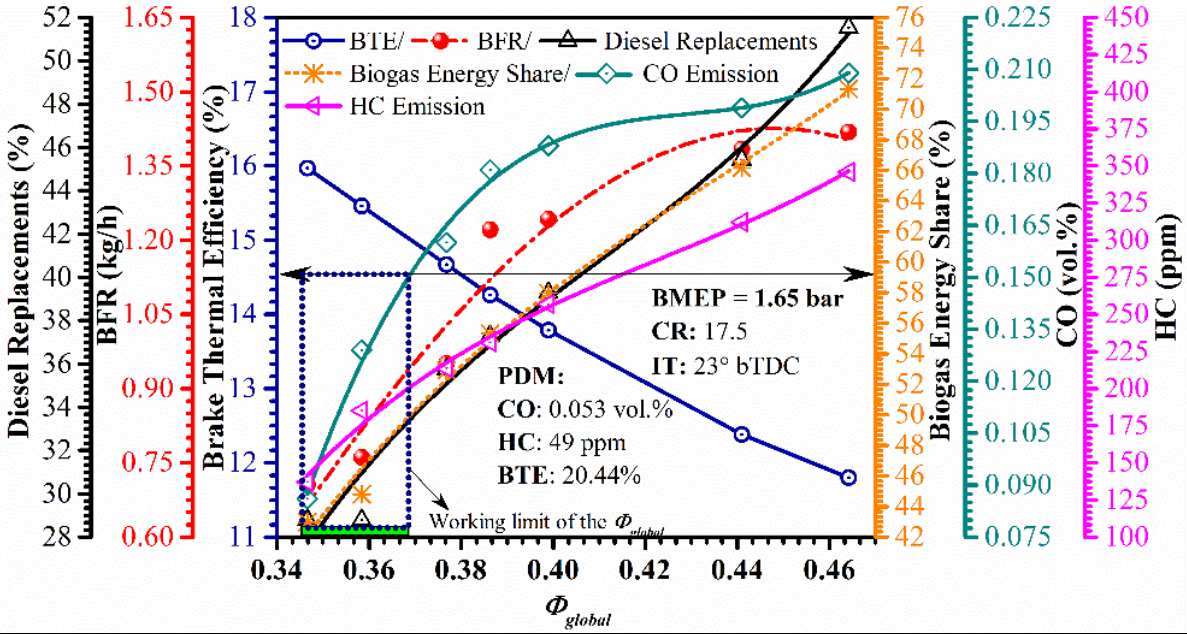

Fig. 4.3 Variations of DR, BFR, BTE, BES, CO, and HC with Φ_{global} (**BMEP:** 1.65 bar)

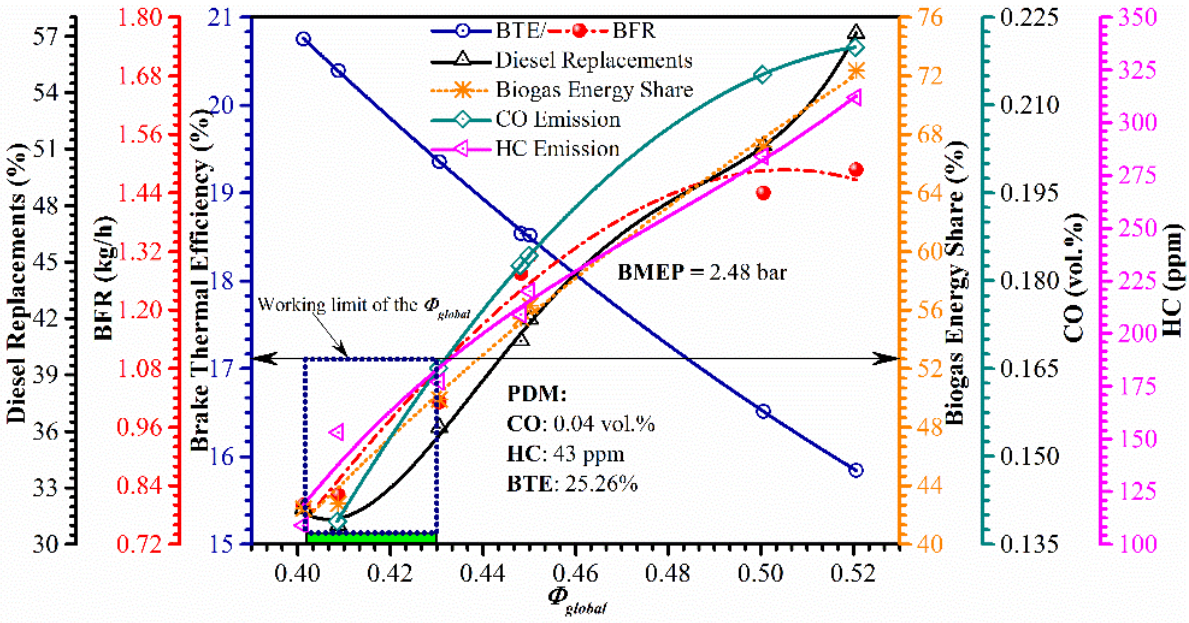

Fig. 4.4 Variations of DR, BFR, BTE, BES, CO, and HC with Φ_{global} (**BMEP:** 2.48 bar)

The investigation in DFM with repeated (three times) experiments at each of the applied load implied that the controlling of Φ_{global} at a single point is impossible due to change of the experimental environment with respect to time and space. In addition, Φ_{global} can be increased in a warm atmosphere of the intake charge and with the use of liquid fuel (e.g., ethanol, butanol) which has the lower heating value. Thus, the best practice would be to identify the ranges of Φ_{global} at each of the applied load where an efficient engine performance can be achieved. At the load of 0.83 bar (Fig. 4.2), the range of Φ_{global} (= 0.29–0.31) is indicated by the rectangular green colored band (lower left corner). At this range of Φ_{global}, the emission is found to be lower

(indicated in dotted grey box), but sufficiently higher than the PD. However, with preheating, the emission is found to be substantially lower than that of the without preheating. With the preheating, the trends of the emissions (CO and HC) within this range of Φ_{global} are observed to be decreasing in comparison to the case without preheating. The preheating effects are discussed later in the following sections. However, due to higher emission and abrupt reduction of BTE, there is no sufficient improvement in performance of DFM engine beyond this range of Φ_{global} even with the intake charge preheating.

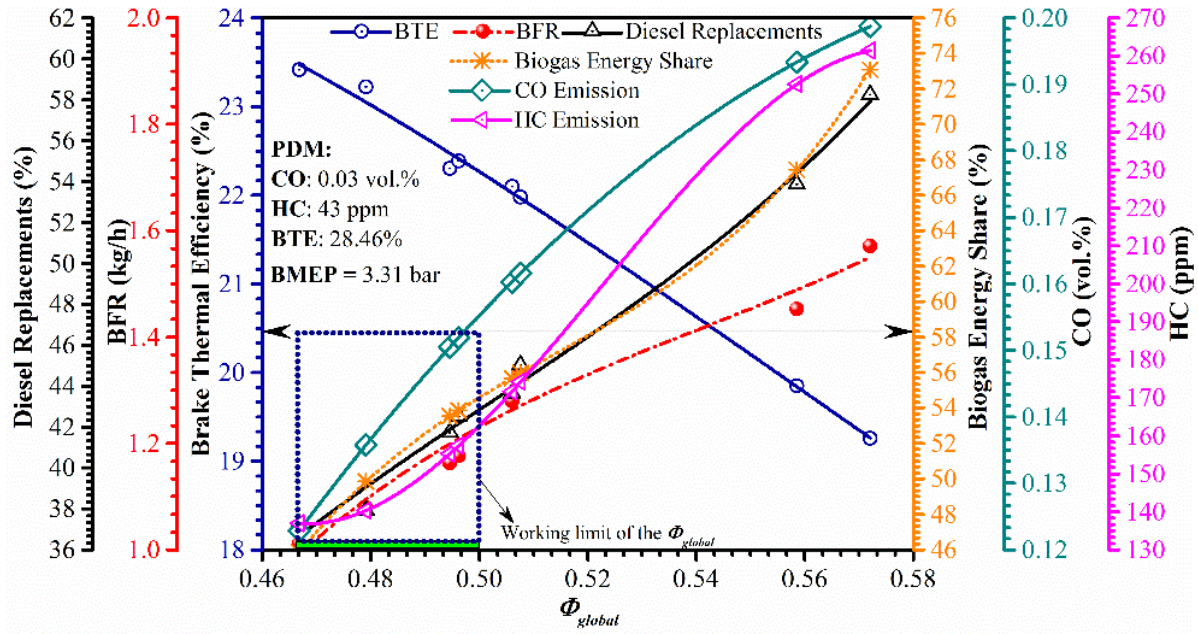

Fig. 4.5 Variations of DR, BFR, BTE, BES, CO, and HC with Φ_{global} (**BMEP:** 3.31 bar)

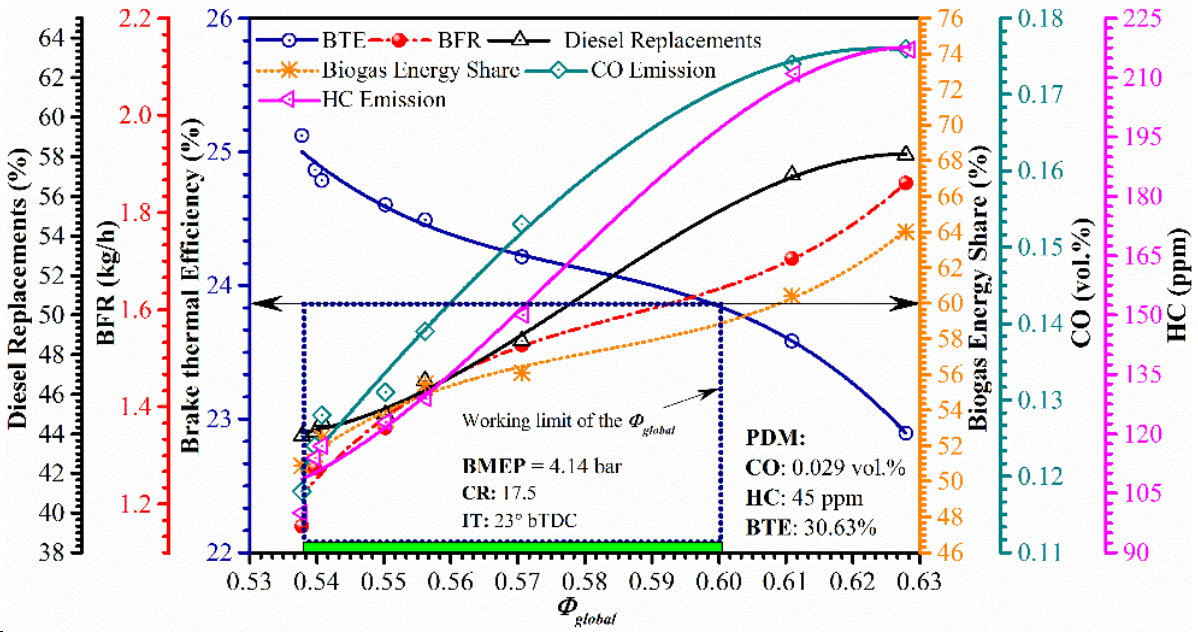

Fig. 4.6 Variations of DR, BFR, BTE, BES, CO, and HC with Φ_{global} (**BMEP:** 4.14 bar)

The emissions of CO and HC are kept approximately at 0.1–0.15 vol.% and 100-200 ppm, respectively, at the specified range of Φ_{global} at all the imposed loads (Fig. 4.2 through 4.6) to achieve the comparable results between the part and higher loads. The ranges of Φ_{global} at loads = 0.83, 1.65, 2.48, 3.31 and 4.14 bar are shown in Figs. 4.3 through 4.6 and the magnitudes are found approximately as 0.29–0.31, 0.35–0.36; 0.40–0.43; 0.47–0.50 and 0.53–0.60, respectively. The most interesting and important matter is that with the increase of applied loads on the engine, the bandwidth of Φ_{global} increases and the overall engine performance is found to be improved. This means that the usability of gaseous fuel with the increase of applied loads increases in DFM engine operation. The main reason of increasing bandwidth may be due to the enhancement of average in-cylinder temperature that allows burning more fuels.

4.4 Results at Very High and at Optimize Φ_{global} with and without Preheating

In the previous section, the maximum of 0.63 of Φ_{global} is considered to be sufficient in the analysis of the optimization of Φ_{global}. However, it is necessary to unveil the biogas DFM engine behavior beyond this limit and up to some higher values. The criteria of the maximum allowable values of Φ_{global} are discussed in the section "Design of Experiments." The results obtained for the case without preheating with optimizing Φ_{global} is also compared with the case of intake charge preheating. In this section, engine performance, combustion and, emissions are elaborated in the light of various important performance, combustion and emission parameters.

4.4.1 Role of Φ_{global} on Engine Performance

The BFR, diesel replacements (DR), BES, and brake thermal efficiency (BTE) are considered as the important parameters to explore the DFM engine performance as a function of Φ_{global} and intake charge preheating.

The characteristics of BFR in various conditions are shown in Fig. 4.7. The load of 0.83 bar is considered as the part load and 4.14 bar (maximum) is chosen as the

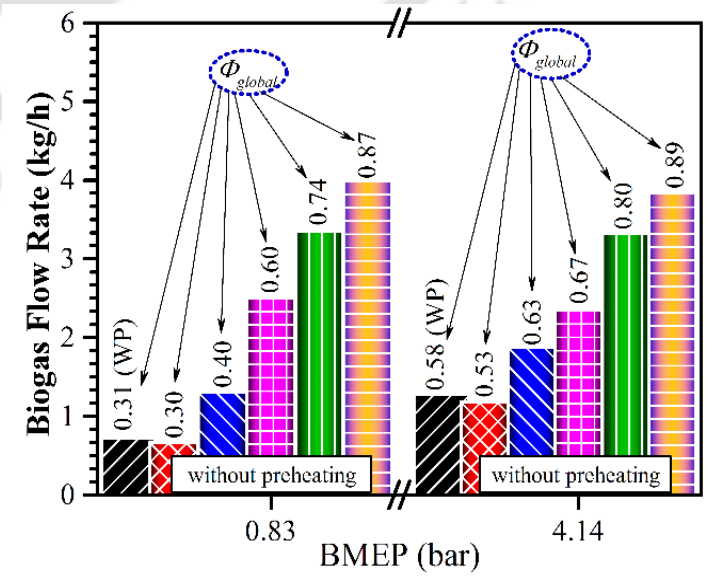

Fig. 4.7 Variations of BFR with loads at various Φ_{global}

higher load. This is to compare the results among parts and higher loads. The variations of BFR in the intermediate loads are observed within the range of loads of 0.83 to 4.14 bar. At the part load, the lower Φ_{global} is considered depending upon the value of DR>20%. The consideration of the higher value of Φ_{global} is already discussed in the previous section. On the other hand, as the ability to consumption of biogas enhances at higher loads, hence, the initial values of Φ_{global} are kept higher as compared to that of the part load (Fig. 4.7). The Φ_{global} with the intake charge preheating is observed to be higher as compared to the case without preheating. It may be due to the enhancement of the specific volume of the air inducted. At part loads, the BFR is also observed to be higher in comparison to higher loads with reference to the Φ_{global}. It may be due to the enhancement of cylinder mean gas temperature (CMGT) at higher loads as compared to lower loads. At 0.83 bar, the BFR of 0.67, 0.73 (with preheating) and 3.99 kg/h are noticed at the Φ_{global} of 0.30, 0.31 (with preheating) and 0.87, respectively. Whereas, at 4.14 bar the BFRs of 1.18, 1.27 (with preheating) and 3.83 kg/h at the Φ_{global} of 0.53, 0.58 (with preheating) and 0.89, respectively, are estimated.

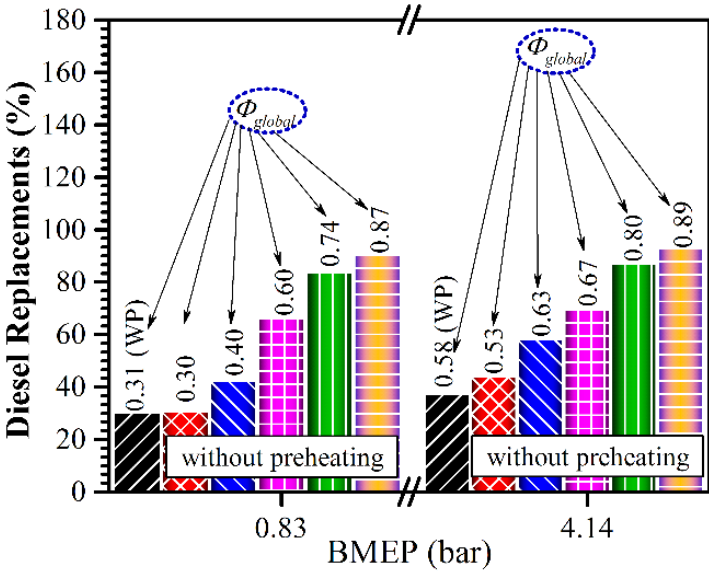

Fig. 4.8 Variations of DR with loads at various Φ_{global}

The variations of DR with loads are portrayed in Fig. 4.8. The DR increases abruptly with the increase of Φ_{global}. However, with the preheating the slight reduction of DR is noticed. It can be seen in Fig. 4.8 that the DR is very sensitive to the Φ_{global} rather than

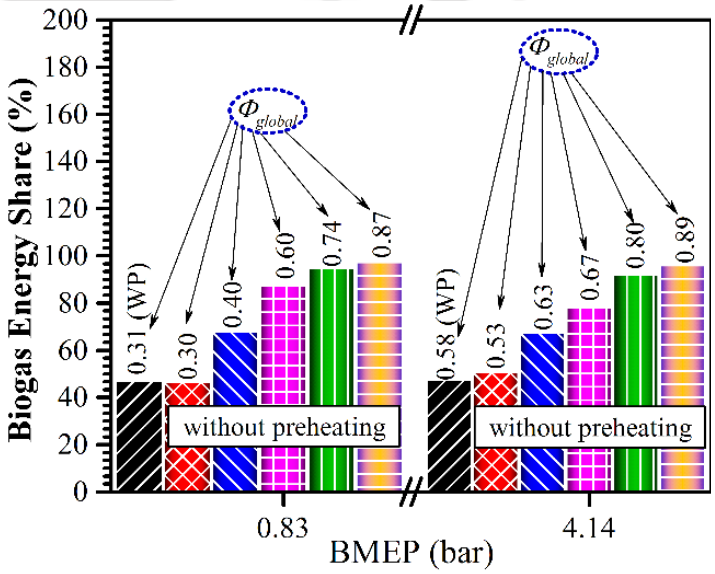

Fig. 4.9 Variations of BES with loads at various Φ_{global}

the loads. At 0.83 bar, the DRs of 30.69, 30.29, 66.43, and 90.56% are estimated at the Φ_{global} of 0.30, 0.31 (with preheating), 0.60, and 0.87, respectively. Whereas, at the higher load of 4.14 bar, the DR are estimated as 44.06, 37.37, 69.76 and 92.49% at the Φ_{global} of 0.53, 0.58 (with preheating), 0.67 and 0.89, respectively. The characteristic of BES is represented in Fig. 4.9, which is similar to that of the DR. The BES increases with the increase of Φ_{global}. It may be due to the higher amount of biogas consumption at higher Φ_{global} and at higher DR. At the part load of 0.83 bar, the BESs are found to be 46.69, 47.38, 87.57, and 97.55% at the corresponding Φ_{global} of 0.30, 0.31 (with preheating), 0.60, and 0.87. While, at 4.14 bar, the BES are found as 50.68, 47.58, 78.42 and 96.24% at the Φ_{global} of 0.53, 0.58 (with preheating), 0.67 and 0.89, respectively.

The variations of BTE with Φ_{global} at different load are shown in Fig. 4.10. The analysis reveals that the BTE reduces drastically with the increase of Φ_{global}. Hence, the results demonstrate that there is a performance penalty of the biogas run DFM engine with the increase of Φ_{global}. At 0.83 bar, the reduction of 65.31% of BTE is estimated with the increment of Φ_{global} from 0.30 to 0.87, relative to the Φ_{global} of 0.87. However, at 0.83 bar, with preheating (Φ_{global} = 0.31), there is an increment of BTE of 5.72% as compared to the case without preheating (Φ_{global} = 0.30). On the other hand, at 4.14 bar, the BTE is found to be reduced by 55.21% for the enhancement of Φ_{global} from 0.53 to 0.89, relative to the Φ_{global} of 0.89. However, at this higher load, the increment of BTE of 2.60% is noticed for the case with preheating at Φ_{global} of 0.58 with respect to Φ_{global} of 0.53 (without preheating). The BTE in PDM is always observed to be higher than that in DFM. However, the maximum and similar trend of BTE is noticed at the Φ_{global}/load (bar) of 0.31/0.83, 0.35/1.65, 0.42/2.48, 0.48/3.31 and 0.58/4.14 (bar) with preheating. Therefore, the Φ_{global} of 0.31, 0.35, 0.42, 0.48, and 0.58 are considered to be the optimum with the intake charge preheating. The increment of Φ_{global} is attributed to the increase in biogas consumption that has a very high self-ignition temperature

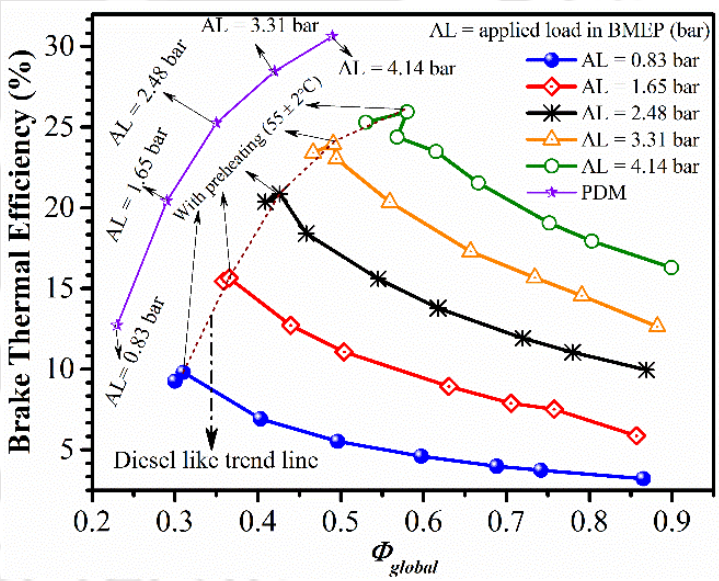

Fig. 4.10 Variations of BTE with loads at various Φ_{global}

and lower LHV as compared to diesel. Thus higher the consumption of biogas means there will be reduction of the cylinder mean gas temperature (CMGT), that slow down the pre-ignition reaction rate and flame propagation (Hinton and Stone 2014, Nonaka and Pereira 2016). Hence, the combustion efficiency deteriorates at higher Φ_{global}. The behaviour of CMGT with Φ_{global} is discussed later. Consequently, the BTE reduces with the rise of Φ_{global}. At the optimum Φ_{global} and with preheating, the higher BTE, lower DR and BES attribute to the higher liquid fuel energy share at all loads from part to higher. Therefore, there will be a huge scope to use various promising liquid renewable fuels in a biogas run DFM engine to achieve more efficient engine performance.

4.4.2 Role of Φ_{global} on Engine Combustion

The combustion parameters such as ID, in-cylinder pressure and NHRR history, CD, CMGT and cyclic variations of CPP are chosen to perform an in-depth analysis on the combustion characteristics as a function of Φ_{global}, preheating temperature and applied load on the dual fuel engine.

The characteristic of ID with load, Φ_{global}, and preheating is shown in Fig. 4.11. The ID is found to increase with the increase of Φ_{global}. However, it reduces with the increase of load and with the intake charge preheating. The higher Φ_{global} for a particular load and at a constant engine speed indicates the higher consumption of biogas. It is known that the CO_2 present as the major component in biogas has higher specific heat. Therefore, higher consumption of raw biogas reduces the CMGT that slows the pre-ignition reaction, thereby reducing the adiabatic flame temperature (Pizzuti et *al*. 2016). These attribute to the reduction of ID. At the part load of 0.83 bar, the drastic increment of 81.42% of ID is found upon increase of Φ_{global} from 0.31 to 0.87. While, at the higher load of 4.14 bar, the ID at the Φ_{global} of 0.53, 0.58 (with preheating), 0.67 and 0.89 are observed to be 14, 12.8, 15.5, and 19.2 CAD, respectively.

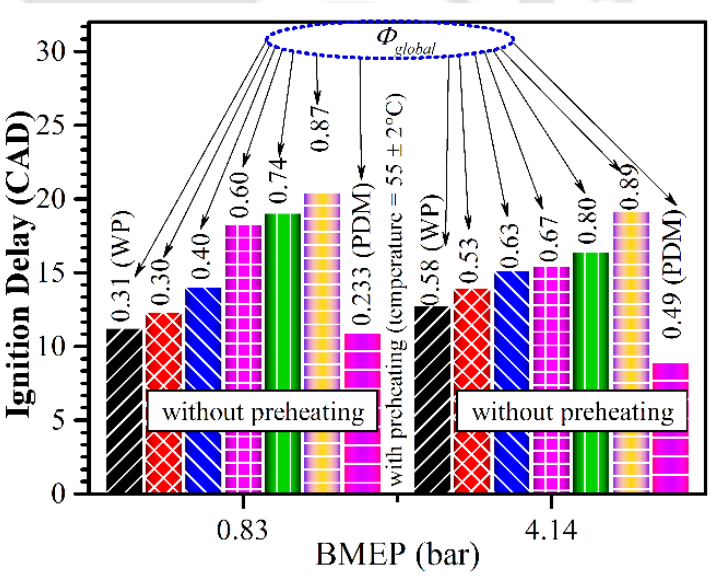

Fig. 4.11 Characteristics of ID at various loads

The in-cylinder pressure history at the load of 0.83 and 4.14 bar relative to the engine crank angle at various Φ_{global} and at preheating temperature = 55 ± 2° C are depicted in Figs. 4.12 and 4.13, respectively. The analysis of pressure history reveals that the cylinder peak pressure (CPP) enhances with the applied loads and falls drastically with the increment of Φ_{global}. It is also observed that the crank angle position of CPP with the increment of Φ_{global} shifts towards the right side with respect to top dead center (TDC) of the engine. At the part load of 0.83 bar, the CPP (bar)/crank angle positions (CAD) are found as 52.56/368 (with preheating), 52.07/369, 49.37/369 and 43.19/372 at the Φ_{global} of 0.31 (with preheating), 0.30, 0.40 and 0.60, respectively (Fig. 4.12). At this part load and within the range of Φ_{global} of 0.74-0.87, the prediction of CPP (bar)/crank angle position (CAD) are observed to be uncertained. It may be due to the higher biogas consumption at higher Φ_{global} that stimulate to occur more cycle-by-cycle variations of the CPPs.

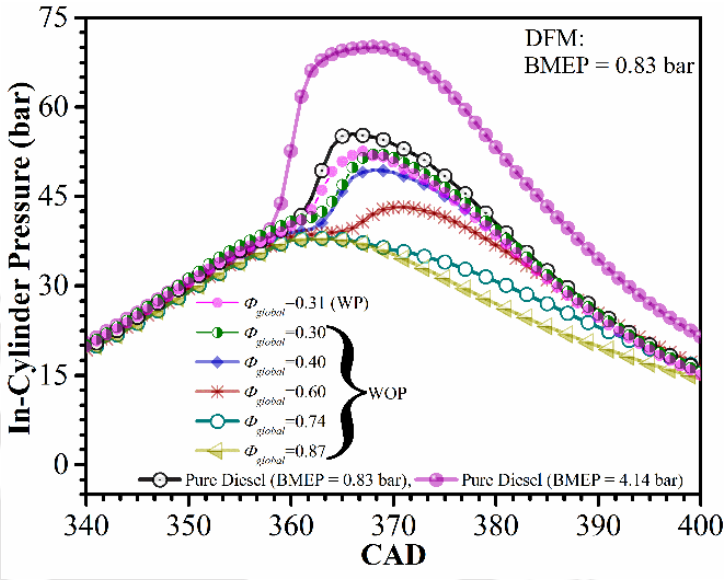

Fig. 4.12 Characteristics of in-cylinder pressure at various CAD (AL = 0.83 bar)

The above discussion of the pressure history at the part loads revealed that the Φ_{global} must be lower in order to achieve an efficient DFM engine performance. At 4.14 bar, the CPP (bar)/crank angle positions (CAD) are observed as 62.84/367, 62.75/369, 60.65/370, 53.68/373 and 43.01/375 at the Φ_{global} of 0.58 (with preheating), 0.53, 0.63, 0.67 and 0.80, respectively as

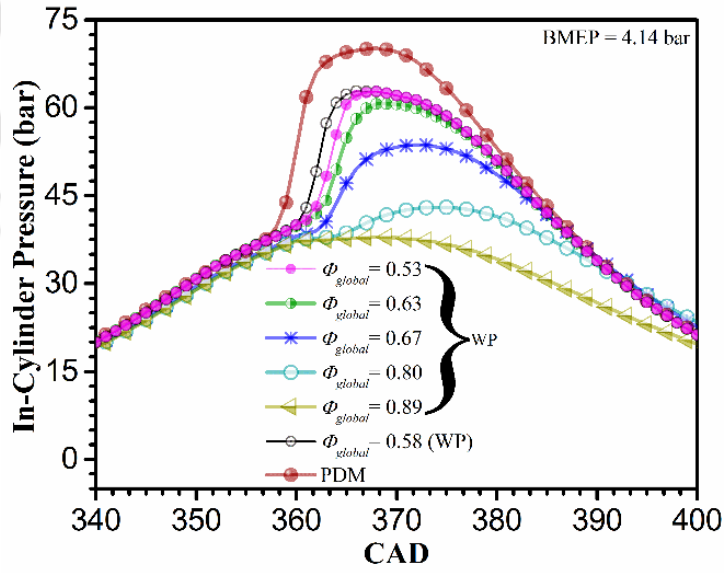

Fig. 4.13 Characteristics of in-cylinder pressure at various CAD (AL = 4.14 bar)

shown in Fig. 4.13. At this higher load, the position and magnitude of CPP at the Φ_{global} of 0.89 are noticed to be uncertained due to the higher biogas consumption, which leads to occur higher cycle-by-cycle variations that are discussed later in this section. Consequently, the maximum Φ_{global} of 0.80 can be considered as the limiting point to run the stable biogas run engine. However, at this Φ_{global}, the parameters like BTE and NHRR are observed to be substantially lower in comparison to PDM. Therefore, it is not possible to improve the quality of the performance of biogas run engine at the Φ_{global} of 0.80. It may be due to the lower LHV, higher self-ignition temperature, and CO_2 present in biogas reduce the CMGT that retard the pre-ignition reaction rate and flame speed. Consequently, at higher Φ_{global}, the CPP reduces drastically and the position of the crank angle shifts from TDC (right side). However, the preheating significantly heals these adverse effects of using biogas in DFM and this improves the CPP. Nevertheless, with preheating, the shifting of CPP towards the TDC is a clear indication to improve the combustion characteristics of the biogas run DFM engine. The present analysis demonstrates that the DFM engines have to be run at some suitable range of Φ_{global} from lower to higher loads at which comparable results in comparison to PDM can be achieved. The present study will define this range of Φ_{global} at the end of the overall discussion.

At 0.83 and 4.14 bar, the variations of NHRR history (at various Φ_{global} and with preheating) with the crank angle are shown in Figs. 4.14 and 4.15, respectively. Since, in the estimation of NHRR, the pressure is the independent variable. Hence, as a function of Φ_{global} and preheating, the similar trend of CPP in NHRR history is observed. Consequently, the physical reasons of NHRR history are the similar to that of the in-cylinder pressure history. At 0.83 bar, the NHRR peaks (J/CAD)/crank angle position (CAD) are found as 48.47/363 (with preheating), 47.72/365, 46.61/366, 30.42/368,

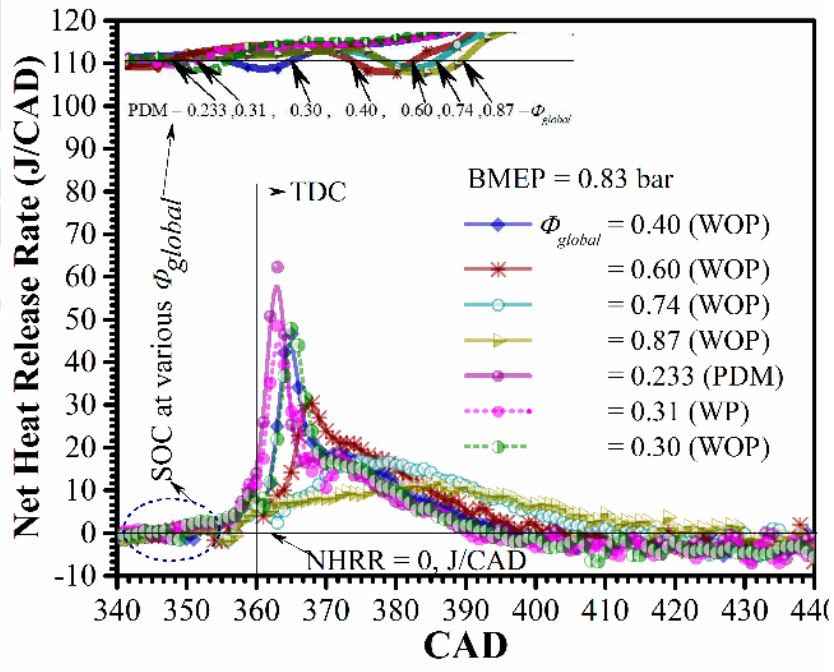

Fig. 4.14 Characteristics of NHRR at various CAD (AL = 0.83 bar)

16.96/375 and 11.12/382 at the Φ_{global} of 0.31 (with preheating), 0.30, 0.40, 0.60, 0.74 and 0.87 respectively. At this load, the peak value of NHRR in PDM is found to be 62.18 J/CAD at the crank angle of 363 CAD. It is a noticeable matter that the crank angle position of the peaks of NHRR in PDM and in DFM with preheating is found to be identical. This is a clear indication of the improvement of DFM engine combustion. At 4.14 bar, the NHRR peaks (J/CAD)/crank angle position (CAD) are obtained as 96.77/362 (with preheating), 88.17/364, 78.08/365, 48.52/366, 30.44/377 and 21.71/378 at the Φ_{global} of 0.58 (with preheating), 0.53, 0.63, 0.67, 0.80, and 0.89, respectively. Whereas at 4.14 bar, the NHRR peaks (J/CAD) and the corresponding position of peaks (CAD) in PDM are found as 113.02 J/CAD and 360 CAD, respectively (Fig. 4.15). At 4.14 bar, the peak values of NHRR in DFM are estimated to be substantially lower as compared PDM at the Φ_{global} of 0.80 and 0.89. Although, the previous analysis of CPP shows the possibility of a smooth run of the biogas DFM engine at the Φ_{global} of 0.80 as compared to 0.89, however, the present study does not recommend this Φ_{global} (=0.80) as the performance parameter because of the attainment of unsatisfactory results.

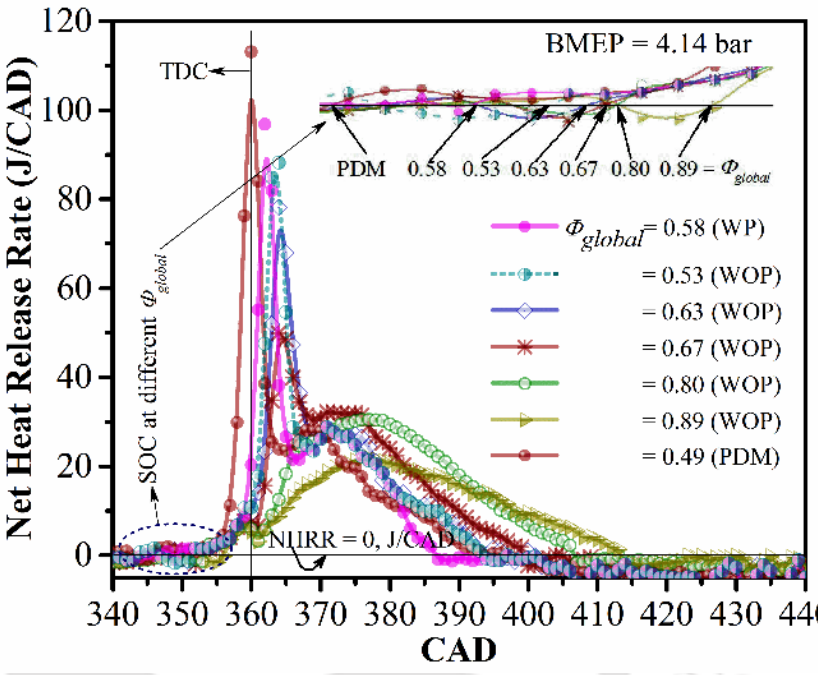

Fig. 4.15 Characteristics of NHRR at various CAD (AL = 4.14 bar)

The characteristics of the CD as a function of Φ_{global}, preheating temperature, and applied load, is portrayed in Fig. 4.16. To calculate the CD, the start of combustion (SOC) is considered at a point where the first NHRR = 0, J/CAD as can be seen in Figs. 4.14 and 4.15. The end of combustion (EOC) is considered where the pressure rise due to combustion is equal to zero (Stone, 1999). The CD in DFM is observed to be lower than the PDM with preheating. However, at all loads in DFM, with the increase of Φ_{global}, the CD is observed to increase in comparison to PDM. Nontheless, the CD is observed to be lower at higher loads in comparison to part loads. In general, the CD in DFM decreases with the increase of the gaseous fuel flow

rate due to the faster-premixed combustion in presence of clean gaseous fuel (Mustafi *et al.*, 2013). Owing to the higher self-ignition temperature of biogas and deficiency of oxygen, there is a reduction of CMGT. Hence, the pre-ignition reaction rate slows down and flame speed reduces in presence of CO_2 in biogas with the consequence of higher CD (Barik and Murugan, 2014; 2016). However, the investigators (Barik and Murugan, 2014; 2016) found higher CD at higher loads due to the accumulation of the higher amount of total fuel. Further, they achieved a higher peak pressure in the DFM in comparison to PDM. This is only possible when the weighted average of LHV in duel fuel (biogas + diesel) is higher than the diesel fuel, else, there would be the accumulation of the higher amount of total fuel. Consequently, the CD will be higher at higher load. Nevertheless, with the preheating the CMGT increases (Fig. 4.17) that helps to occur the efficient combustion. Accordingly, the CD reduces with the preheating of the intake charge.

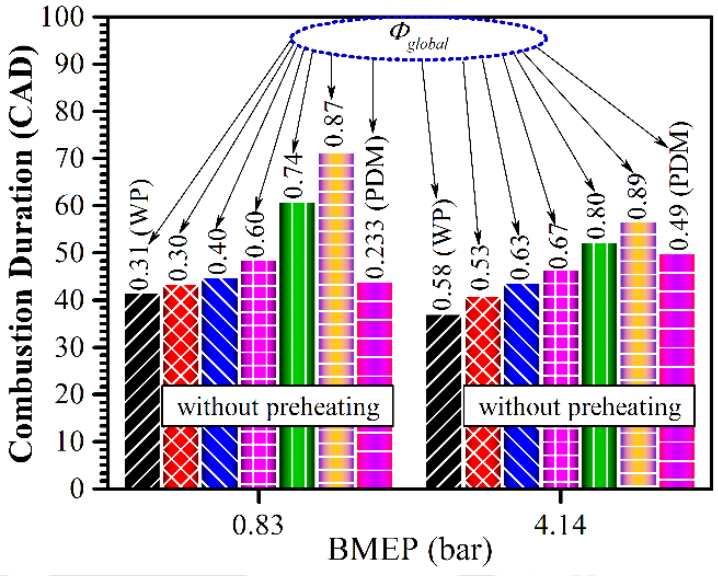

Fig. 4.16 Characteristics of CD with loads at different Φ_{global}

The characteristics of the CD as a function of Φ_{global}, preheating temperature, and applied load, is portrayed in Fig. 4.16. To calculate the CD, the start of combustion (SOC) is considered at a point where the first NHRR = 0, J/CAD as can be seen in Figs. 4.14 and 4.15. The end of combustion (EOC) is considered where the pressure due to combustion is equal to zero (Stone, 1999). The CD in DFM is observed to be lower than the PDM with preheating. However, at all loads in DFM, with the increase of Φ_{global}, the CD is observed to increase in comparison to PDM. Nontheless, the CD is observed to be lower at higher loads in comparison to part loads. In general, the CD in DFM decreases with the increase of the gaseous fuel flow rate due to the faster-premixed combustion in presence of clean gaseous fuel (Mustafi *et al.*, 2013). Owing to the higher self-ignition temperature of biogas and deficiency of oxygen, there is a reduction of CMGT. Hence, the pre-ignition reaction rate slows down and flame speed reduces in presence of CO_2 in biogas with the consequence of higher CD (Barik and Murugan, 2014; 2016). However, the investigators (Barik and Murugan, 2014; 2016) found higher CD at higher loads

due to the accumulation of the higher amount of total fuel. Further, they achieved a higher peak pressure in the DFM in comparison to PDM. This is only possible when the weighted average of LHV in duel fuel (biogas + diesel) is higher than the diesel fuel, else, there would be the accumulation of the higher amount of total fuel. Consequently, the CD will be higher at higher load. Nevertheless, with the preheating the CMGT increases (Fig. 4.17) that helps to occur the efficient combustion. Accordingly, the CD reduces with the preheating of the intake charge.

At 0.83 bar, the CDs are found to be 41.7 (with preheating), 43.6, 44.9, 48.7, 60.9, and 71.5 CAD at the Φ_{global} of 0.31 (with preheating), 0.30, 0.40, 0.60, 0.74, and 0.87, respectively. At the same load and in PDM, the CD is estimated at 44 CAD. At 4.14 bar, the CD is observed to be 37.2, 41, 43.8, 46.5, 52.5, and 56.8 CAD at the Φ_{global} of 0.58 (with preheating), 0.53, 0.63, 0.67, 0.80 and 0.89, respectively. At this load, the CD in PDM is found to be 50 CAD. The higher CD in PDM at higher load may due to the accumulation of the higher amount of liquid fuel. The lower CD in DFM may be due to the faster flame propagation at the elevated CMGT.

The variations of CMGT as a function of load, Φ_{global} and preheating temperature is shown in Fig. 4.17. It is observed that the CMGT reduces substantially with the increase of Φ_{global}, while it is found to increase with preheating and with the increase of applied load. The parameter, CMGT is the function of cylinder pressure, initial thermodynamic states of the intake charge and volume. Therefore, the higher the in-cylinder pressure, higher will be the CMGT. Hence, the physical reasons behind the development of CMGT are similar to that of the in-cylinder pressure history. However, the initial states of the intake charge in DFM would have the great role in the development of CMGT. Thus, with preheating of the intake charge in DFM, the study achieves a higher CMGT in comparison to without preheating. At 0.83 bar, the CMGTs of 1281.28 (with preheating), 1262.18, 1202.53 and 955.47 K at the Φ_{global} of 0.31 (with preheating), 0.30, 0.60 and 0.87, respectively are estimated. At 4.14 bar, the CMGTs of 1679.67, 1649.61, 1615.18,

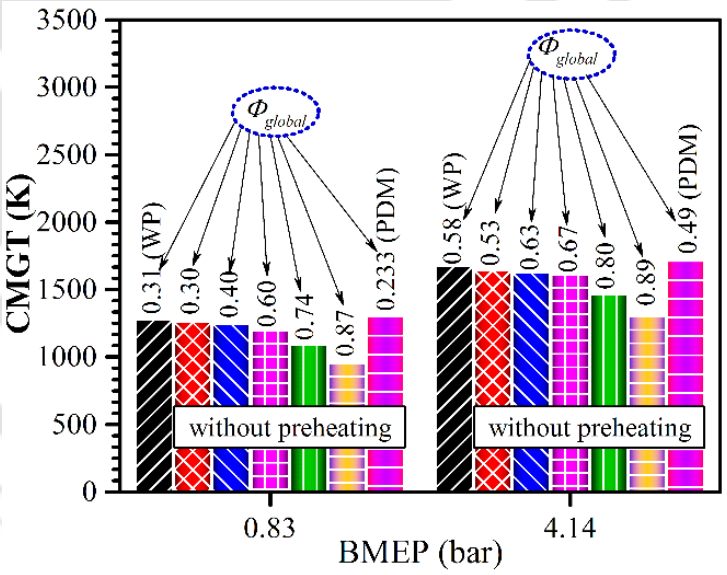

Fig. 4.17 Characteristics of Peak CMGT with loads and at different Φ_{global}

1305.64 K at the Φ_{global} of 0.58 (with preheating), 0.53, 0.67, and 0.89, respectively, are found. In PDM, the CMGTs of 1303.22 and 1718.39 K are estimated at the loads of 0.83 and 4.14 bar, respectively.

The coefficient of variation (COV) of indicated mean effective pressure is noticed to be reduced monotonically with loads as shown in Fig. 4.18. In the evaluation of COV of IMEP (Krishnan 2001), 100 cycles for the instanteous pressure have been chosen. Nevertheless, very high COV is noticed with higher Φ_{global}, while it is found to be signically lower at the optimized and sufficiently lower Φ_{global}. Moreover, there is the drastic reduction of COV of IMEP at optimum Φ_{global} and with the intake charge preheating. At higher Φ_{global}, very high substitution of pilot fuel is observed (order of ~80-95%) as portrayed in Fig. 4.8. Therefore, there will be the heterogeneous distribution of ignition kernles (distribution of atomized pilot fuel). Nonetheless, at higher Φ_{global}, misfire seemed to occur (as perceived from the engine speed and cylinder peak pressure variation, and vibration) indicating the partial combustion of the gas mixture and slowdown of the reaction rates in presence of CO_2. It is to

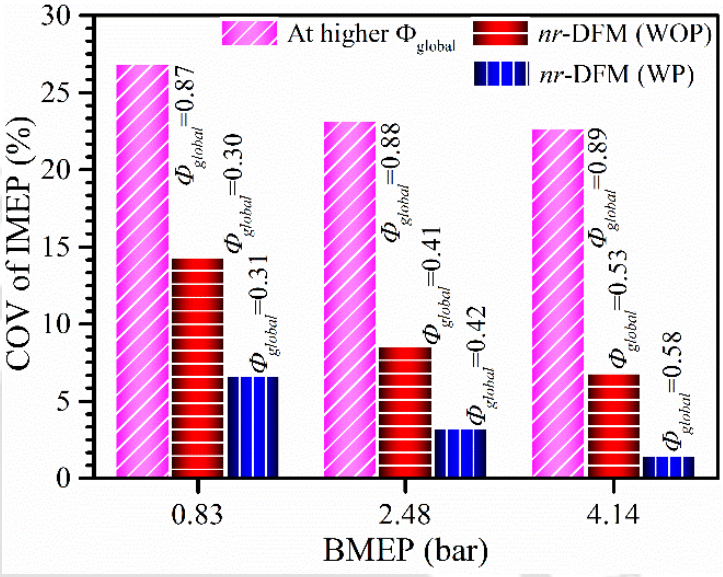

Fig. 4.18 Characteristics of COV of IMEP with loads and at different Φ_{global}

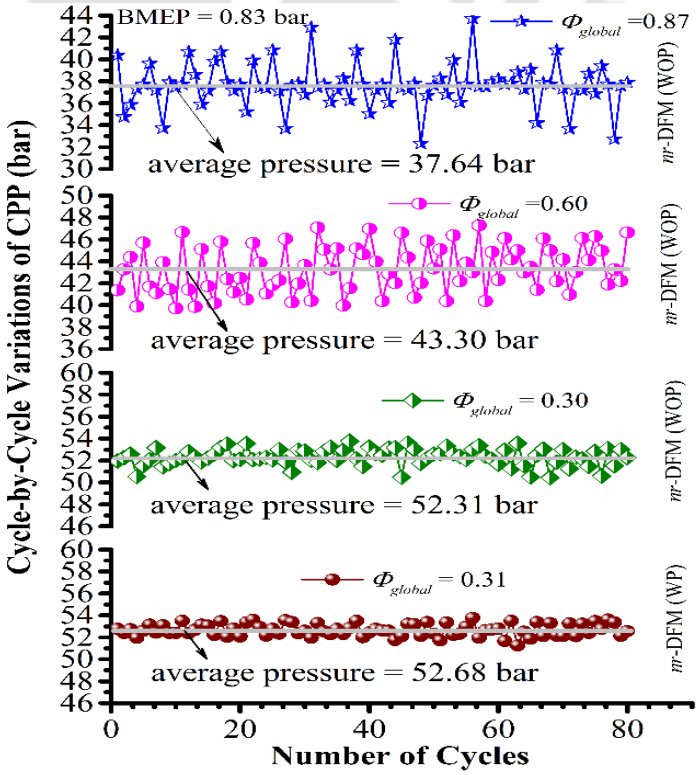

Fig. 4.19 Characteristics of Cyclic variations of CPP (AL: 0.83 bar) at different Φ_{global}

be noted that higher Φ_{global} means higher substitution of pilot fuel and corresponding higher use of biogas amount. Thus, the CO_2 quantity in biogas will be higher at higher Φ_{global}. Hence, these associated phenomena are attributed to the higher COV at higher Φ_{global}. On the other hand, the Φ_{global} has been optimized in such a way that there is not only the sufficient amount of pilot quantity but also the engine gives an oveall improved performance under satble condition. Consequently, the number ignition centres definitely will be more for the case of optimum Φ_{global}. The physical reasons behind the reduction of COV of IMEP with intake charge preheating was clearly addressed by Srinivasan et al. (2006).

The lower cyclic variation physically indicates the stable engine operation. The analysis of the cycle-by-cycle variation of CPP is therefore essential regarding the use of higher-octane gaseous fuels like biogas in DFM. The characteristics of cycle-by-cycle variations of CPP is depicted in Figs. 4.19 and 4.20 at the loads of 0.83 and 4.14 bar, respectively. In the analysis, a total of 80 cycles are taken to predict the cycle-by-cycle variations of CPP. At a particular load, the variation is observed to be higher at the higher Φ_{global}. However, it is noticed to be lower at higher load. The analysis reveals that the Φ_{global} should be as minimum as possible to achieve the stable biogas DFM engine operation. Another important finding is that the cyclic variation reduces considerably with the preheating. The higher CMGT at higher load and with preheating are the probable reasons to reduce the cyclic variations of the CPP.

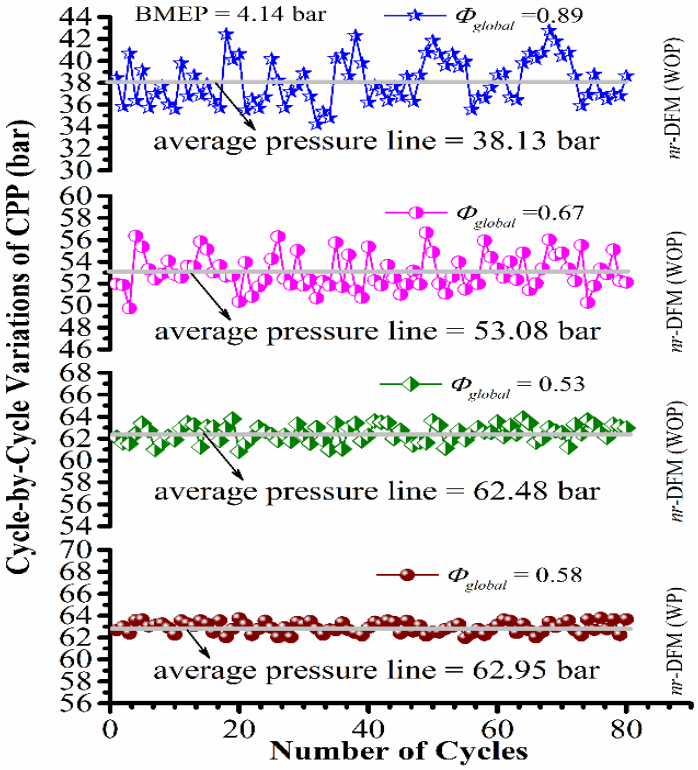

Fig. 4.20 Characteristics of cyclic variations of CPP (AL: 4.14 bar) at different Φ_{global}

4.4.3 Role of Φ_{global} on Engine Emission

Emission is the consequence of the burning of the fuels used to generate the power in engines. The careful diagnosis of emission to sustain the healthy environment of the green ecosystem is thus necessary concerning the severity of the global warming and pollutants emitted in the

environment. In this study, the emissions of CO, CO_2, HC, and NO_x considered to be the important parameters to diagnose the biogas DFM engine emission characteristics.

The CO emission in internal combustion engines is controlled primarily by the fuel-air equivalence ratio (Heywood 1988). In presence of sufficient quantity of oxygen molecules, the threshold temperature of 1450 K is required to initiate the oxidation of CO to CO_2 (Liu et *al*. 2013, Karagöz et *al*. 2016). The temperature of 1500 K is also noticed to be the equilibrium reaction temperature of the reaction CO + OH = CO_2 + H (Glassman and Yetter, 2008). Hence, the CO emission is the function of the fuel-air equivalence ratio, CMGT, and availability of oxygen atoms. The characteristics of the CO emission as a function of Φ_{global}, preheating and applied load is shown in Fig. 4.21. The CO emission is found to increase with the increase of Φ_{global} and reach a maximum value at some magnitude of Φ_{global} after this the emission is observed to be reduced. However, the cyclic variation at higher Φ_{global} is noticed to be higher. The similar trend of CO emission is also noticed by Badar et *al*. (1999). It can be seen in Fig. 4.21 that the CO at lower Φ_{global} is sufficiently lower and at this Φ_{global}, the CMGT is higher (Fig. 4.17) in comparison to higher Φ_{global}. The lower values of Φ_{global} (or initial values) are observed to be increased with the increase of

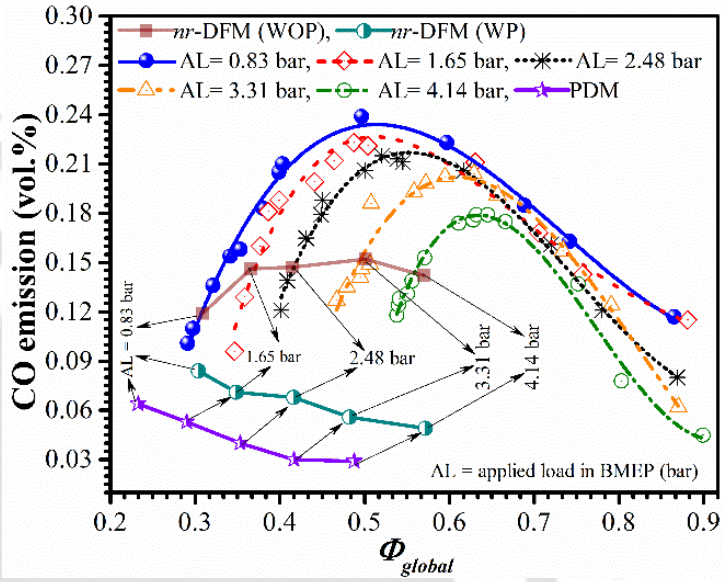

Fig. 4.21 Characteristics of CO emission with Φ_{global} and loads

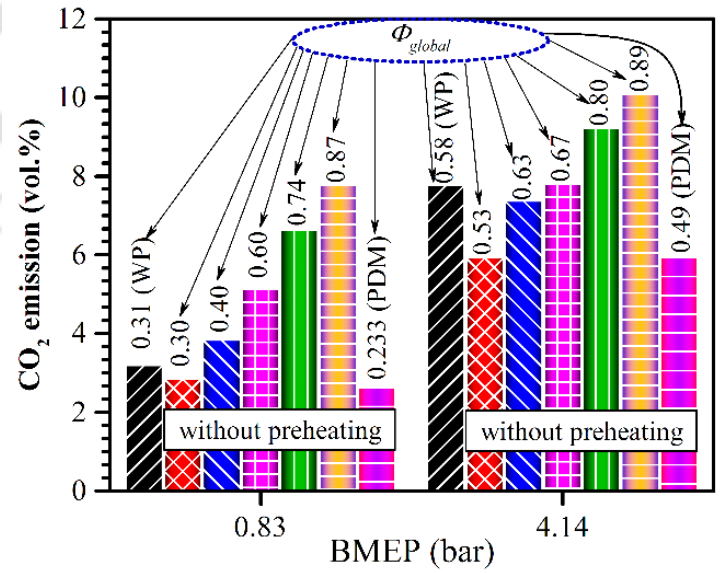

Fig. 4.22 Characteristics of CO_2 emission with Φ_{global} and loads

loads. It indicates that the ability of the biogas consumption in DFM increases with the increase of loads. These initial values of Φ_{global} at each of the loads are identified and conducted an investigation to examine the nature of CO emission without preheating the intake charge (Fig. 4.21). These Φ_{global}/CO (vol. %) emission/load (bar) are found as 0.30/0.119/0.83, 0.36/0.146/1.65, 0.42/0.147/2.48, 0.50/0.152/3.31 and 0.57/0.142/4.14. Badar et al. (1999) find similar trends of CO emission. At these nearest values of Φ_{global}, another investigation has been carried out with intake charge preheating where a substantially lower CO emission is observed. At 0.83 bar, the reduction of CO = 29.41% with the case of preheating is noticed in comparison to the one for without preheating. While at 4.14 bar, with preheating, the CO is found to be reduced by 65.49% in comparison to the one for without preheating. Hence, emission performance of the biogas DFM engine can be improved from part to higher loads with preheating and with the controlling of Φ_{global}. With preheating, the Φ_{global}/load (bar) are estimated as 0.31/0.83, 0.35/1.65, 0.42/2.48, 0.48/3.31 and 0.58/4.14. However, at all loads, the higher CO emission is noticed in DFM as compared to PDM. It may be due to insufficient oxygen quantity, and the lower CMGT developed during combustion.

The variations of CO_2 emission are portrayed in Fig. 4.22. In the present investigation, CO_2 is found to increase with the increase of applied loads as well as with increasing of Φ_{global}. The increasing of CO_2 with the increasing of loads in PDM at a particular Φ_{global} in DFM is the clear indication of the improvement of the combustion efficiency. While the CO_2 present in biogas as the major constiunts causes a higher CO_2 emission at higher Φ_{global}. There is a significant improvement in CO_2 emission with the intake charge preheating from part to higher loads. The preheating stimulates the combustion process with the consequence of higher CO_2 emission in DFM. In PDM, the emission of CO_2 at the loads of 0.83 bar and at 4.14 bar are observed at 2.64%, and 5.95% by volume. In DFM, at 0.83 bar., the CO_2 (vol.%)/Φ_{global} are found as 3.21/0.31 (with

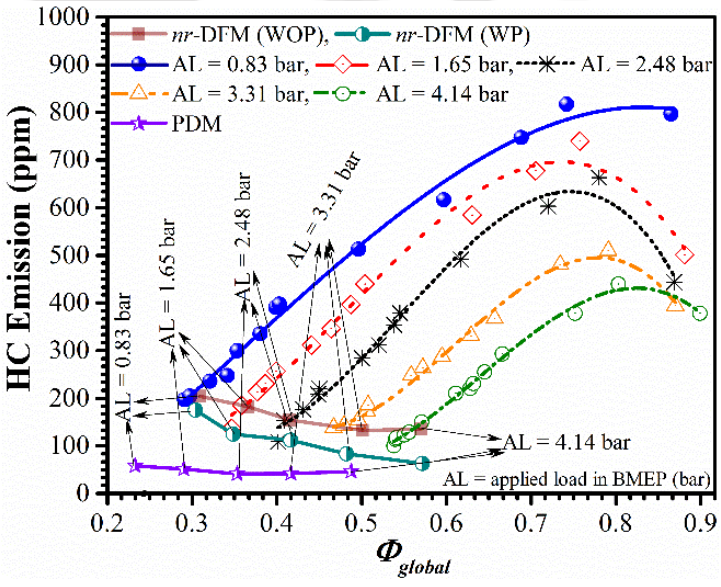

Fig. 4.23 Characteristics of HC emission with Φ_{global} and loads

preheating), while without preheating, they are found to be 2.86/0.30, 3.85/0.40, 5.14/0.60, 6.65/0.74 and 7.79/0.87. Similarly, at 4.14 bar, the CO_2 (vol.%)/Φ_{global} are noticed to be 7.79/0.58 (with preheating), and without preheating, they are found to be 5.94/0.53, 7.39/0.63, 7.82/0.67, 9.23/0.80 and 0.89/10.1.

The variations of HC emission with Φ_{global}, preheating, and the load is depicted in Fig 4.23. The increasing trends of HC emission with the increase of Φ_{global} is noticed with an exception of slightly lower emission at the load of 4.14 bar. At 0.83 bar, the HC emission at the Φ_{global} of 0.30 and 0.89 are found as 197 and 797 ppm, respectively. The lower CMGT and deficiency of oxygen enhance the HC emission at part load. At 4.14 bar, the HC emissions are found as 100 and 378 ppm at the Φ_{global} of 0.53 and 0.89 respectively. The lower HC emission at higher load may be due to the faster pre-ignition reaction, faster flame propagation and the corresponding development of higher CMGT. Due to the lower magnitudes of defined Φ_{global} (0.30, 0.34, 0.42, 0.48, and 0.57) as discussed above, the HC emission (without preheating) is found to be lower. Further reduction of HC emission is observed with the preheating. At 0.83 bar (with preheating), the reduction of 14.21% of HC emission at the Φ_{global} of 0.30 in comparison to without preheating. At 4.14 bar and with preheating, the reduction of HC is noticed to be 53.33% at the Φ_{global} of 0.57 as compared to the one without preheating.

Figure 4.24 shows the emission of NO_x at various Φ_{global}, preheating, and load. The emission of NO_x in DFM is found to be lower in all conditions. The emission is observed to have been reduced with the increase of Φ_{global}. At a higher value of Φ_{global}, a drastic reduction of NO_x emission is observed (Fig. 4.24). However, at the defined values of Φ_{global} (at each of the load), the diesel like trends of CO emission is noticed. The emission is found to be more with the preheating in comparison to without preheating. Nevertheless, at the load of 4.14 bar., a reduction of 39.48% in DFM with preheating

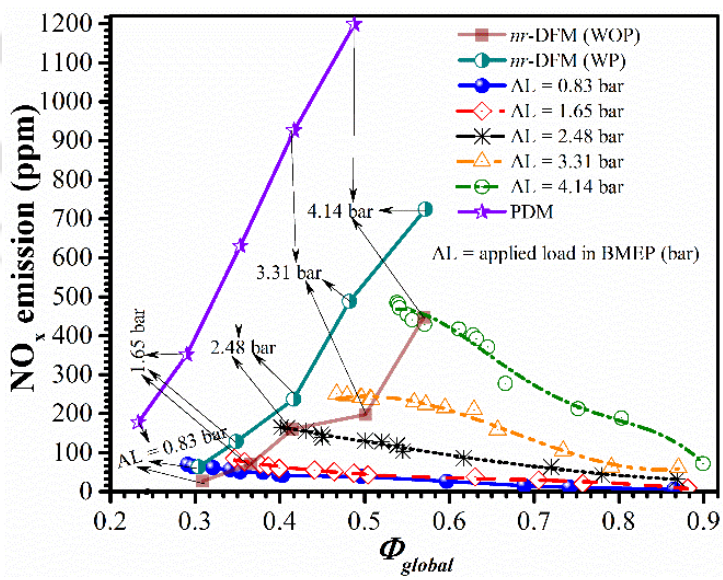

Fig. 4.24 Characteristics of NO_x emission with Φ_{global} and loads

is achieved in comparison to PDM. The insufficient amount of oxygen, development of lower CMGT and lower retention time of the combustion product in DFM make favourable atmosphere to generate lower NO_x in DFM as compared to PDM. The conversion of emissions data measured in ppm and vol.% units to gm/kWh unit are presented in Appendix-D.

4.5 Summary

This study attempts to achieve a reduced emission characteristic of the dual fuel engine while maintaining its performance competitive to its pure diesel mode. The key findings obtained in this part of study at various Φ_{global} and with intake charge preheating are summarized below:

Role of Φ_{global} on Engine Performace:

- The results obtained in *nr*-DFM (WOP/WP) mode reveal the decisive influence of Φ_{global} on engine performance and pollutant emission. The ranges of optimum Φ_{global}/load (bar.) are assesed as 0.29–0.31/0.83, 0.35–0.36/1.65, 0.40–0.43/2.48, 0.47–0.5/3.31, and 0.53–0.60/4.14.
- The BFR (kg/h)/Φ_{global} are varied within the range of 0.67/0.30 to 3.99/0.89. Within this range of BFR (kg/h)/ Φ_{global}, the DR (%)/BES (%) are found in the range of 30.69%/46.69% to 92.49%/97.55%, respectively. At 0.83 bar, there is an increment of BTE by 5.72% with preheating. At 4.14 bar, a reduction of BTE by 55.21% is noticed (without preheating) on increasing the Φ_{global} from 0.53 to 0.89; while with preheating, there is an increment of BTE by 2.60% in comparison to the one without preheating.
- The analysis reveals that a lower Φ_{global} at part load and higher Φ_{global} at higher load is suitable for improving the biogas DFM engine performance. With preheating, the optimum Φ_{global}/load (bar) are observed as 0.31/0.83, 0.35/1.65, 0.42/2.48, 0.48/3.31, and 0.58/4.14.

Role of Φ_{global} on Engine Combustion

- In the tested range of loads, the IDs are found to increase drastically with the increase of Φ_{global}. At 4.14 bar, the increment of ID with the increase of Φ_{global} from 0.53 to 0.89 is is found as 37.14%. However, with preheating, the ID is found to decrease.
- The CPPs are observed to be reduced drastically with the increase of Φ_{global}. With the increase of Φ_{global}, the crank angle positions of the CPPs are shifted toward right sides of the TDC. However, with preheating, it shifts towards TDC. A drastic reduction of NHRR is noticed at higher Φ_{global}. At 0.83 bar, the peaks of NHRR (J/CAD)/Φ_{global} are observed

to be 47.72/0.30, 11.12/0.87. At 4.14 bar, the maximum (with preheating) and minimum peaks of NHRR (J/CAD)/Φ_{global} are noticed to be 88.17/0.53 and 21.71/0.89, respectively.

- The CD is found to increase with the increase of Φ_{global}. There is a drastic reduction of CMGT at higher Φ_{global}. At 4.14 bar, the reduction of CMGT is estimated at 20.99% on increase of Φ_{global} from 0.53 to 0.89 relative to the Φ_{global} of 0.53. The COV of IMEP and cycle-by-cycle variations of CPP are found to be higher at the higher Φ_{global}. However, it reduces with the increase of loads and preheating.

Role of Φ_{global} on Engine Emission

- At 0.83 bar (with preheating and at Φ_{global} = 0.31), the reduction of CO by 29.41% is noticed in comparison to the one without preheating. While, at 4.14 bar, there is a reduction of CO (with preheating and Φ_{global} = 0.58) by 65.49% as compared to the one without preheating. The emission of CO_2 is observed to increase with an increase of Φ_{global} and with intake charge preheating.
- The HC is found to very high at higher Φ_{global}. However, at optimum Φ_{global}, with preheating, the HC is found to reduce. At higher load (4.14 bar) and with preheating, a reduction of HC by 53.33% is recorded. A drastic reduction of NO_x is observed with the increment of Φ_{global}. While, with preheating, the NO_x is found to increase.

Chapter-5

Results of Biogas Run DFM Engine Using Binary Blend (Diesel and Ethanol)

Chapter

Highlights:	**Overview:** *An exhaustive investigation has been carried out to study the effects of preheating and the role of ethanol as the oxygenated fuel blended with diesel. With preheating and with E-5 blend, adequate improvements in engine performance and combustion have been attained, whereas, there is a substantial reduction of emissions with these combinations of parameters. In combustion, the reduction of ID, enhancement of CPP, and the higher peak of NHRR and CMGT are noted with preheating and with E-5 blend. There is also a drastic reductions in CO and HC emissions. A very low emission of NO_x is noticed in DFM as comparec to PDM. However, a marginal increment in NOx emission is noticed. Overall, the preheating and the implementation of the renewable oxygenated fuel are unveiled as the most influential parameters to improve the DFM engine performance.*
• *Ethanol as biofuel is chosen to implement in DFM* • *Preheating and E-5 blend are chosen as the main parameters* • *There is a shifting of the peak of net heat release rate (NHRR) towards left relative to TDC* • *With intake charge preheating, various renewable liquid fuels blended with diesel can be used in the biogas run DFM engine*	

***Chapter Layout*:**

5.1 E-5 (5% ethanol + 95% diesel) as Pilot Fuel

The analysis in the previous chapter reveals that there is a huge scope to use the renewable oxygenated liquid fuels in a biogas run DFM engine to achieve the results competitive to PDM. Hence, in the present study, ethanol is considered as the oxygenated fuel blended with the diesel fuel. The properties of the individual fuels used in this investigation are presented in Table 5.1. The volume percentage of ethanol is chosen as 5% (E-5) to blend with diesel fuel at which there is no separation. The blend is prepared to observe the effects of oxygenated liquid fuel on the performance of biogas run DFM engine. The properties of the blended fuel have been evaluated with the use of Lever Law (Rakopoulos et *al*. 2016a).

Table 5.1 Fuels Properties used in the present study (Porpatham et *al*., 2007; Nathan et *al*., 2010; Sahoo et *al*., 2011b; Yoon and Lee, 2011; Chen et *al*., 2013; Rakopoulos et *al*., 2014; Tutak, 2014; Aleiferis and Behringer, 2015; Zhang et *al*., 2016)

Properties	**Biogas**	**Diesel**	**Ethanol**
Chemical structure	Approximately 60% **CH_4**, 40% **CO_2** (vol.%)	**$C_{12}H_{26}$**	**C_2H_6O**
C (wt.%)	-	84.7	52.18%
H (wt.%)	-	15.3	13.04%
O (wt.%)	-	-	34.78%
Density (kg/m^3), at 32.2^{o}C	1.096[a]	824.91[a]	778[a]
Lower heating value (MJ/kg)	19.1[a]	42.10[a]	26.8
Cetane number	-	50	~8.0
Kinematic viscosity (mm^2/s, at 40^{o}C)	-	2.54[b]	1.2
Stoichiometric air-fuel ratio	6.17[a]	14.94[a]	9.0
Auto Ignition temperature (^{o}C)	632-813	200-220	423
Flammability limits (% by volume of air)	7.5-14	1.5-7.6	4.3-19.0
Flame speed (m/s)	0.25	0.86	0.42
Latent heat of evaporation (kJ/kg)	-	250	840

[a]calculated, [b]measured

5.2 Design of Experiments

The experiments are conducted in PDM, *nr*-DFM (without and with preheating), and in DFM with preheating with the E5 blend as the pilot fuel. The parameters considered in the study are defined in the experimental matrix as shown in Table 5.2. In PDM, only pure diesel is used as the fuel. Here, the term *nr*-DFM means the investigations are carried out with pure diesel as the pilot and biogas as the inducted fuel. Therefore, in *nr*-DFM, the experiments conducted without and with preheating are designated as *nr*-DFM (WOP) and *nr*-DFM (WP), respectively. Besides, in DFM, with E-5 blend, the experiment is also carried out with intake

charge preheating. The preheating temperature of 55 ± 2° C is considered by following the same criterions that have discussed in the previous chapter. The investigation in PDM is considered to be the base or target experiment. All the tests are carried out at loads of 0.83, 1.65, 2.48, 3.31 and 4.14 bar. At all loads, the test are conducted at the engine standard CR = 17.5 and IT = 23 CAD bTDC. Further, in DFM, experiments have been carried out at different optimum global fuel-air equivalence ratios (Φ_{global}) at each of the applied load that is illustrated in the previous chapter. The optimum Φ_{global}/load (bar) are found as 0.29–0.42/0.83, 0.35–0.46/1.65, 0.40–0.52/2.48, 0.47–0.57/3.31, and 0.54–0.63/4.14 (=100%), respectively. The estimated optimum Φ_{global} in *nr*-DFM (WOP) are used as a basis to investigate the engine performance, combustion, and emission in *nr*-DFM (WP) and E-5 with the preheating of the intake charge.

Table 5.2 Experimental Matrix

Parameters	**PDM**	***nr*-DFM (WOP)**	***nr*-DFM (WP)**	**E-5**
Fuel	Pure diesel	Diesel + Biogas	Diesel + Biogas	E5 blend + Biogas
Φ_{global}/Load (bar)	0.23/0.83-0.48/4.14	0.29-0.42/0.83, 0.35-0.46/1.65, 0.40-0.52/2.48, 0.47-0.57/3.31 and 0.54-0.63/4.14 only for the DFM		
Preheating Temperature	Atmospheric	Atmospheric	55 ± 2° C	55 ± 2° C

5.3 Performance Analysis

The performance parameters are chosen as global fuel-air equivalence ratio (Φ_{global}), premixed fuel-air equivalence ratio ($\Phi_{premixed}$), BFR, BES, BSEC, BTE, and volumetric efficiency (VE) to study the behaviour of the engine performance. In this investigation, E-5 blend and the intake charge preheating are considered to be the key parameters. The experiments from part to higher loads have been carried out at the specified ranges of Φ_{global} (Table 5.2).

The variations of Φ_{global} and $\Phi_{premixed}$ with the applied load on the engine at different states are presented in Fig. 5.1. The Φ_{global} is noticed to be slightly higher with preheating in *nr*-DFM (WP) than the *nr*-DFM (WOP), and for E-5 it is observed to be maximum. This is because of the lower heating value of ethanol and the enhancement of specific volume of the intake charge, which in turn, reduces the volume flow rate of air as well as biogas in contrast to *nr*-DFM (WOP). However, to sustain the engine rpm, the liquid fuel consumption increases with the consequence of an increment of Φ_{global}. Nevertheless, the $\Phi_{premixed}$ reduces due to the reduction of the gas volume flow rate at the engine intake port. On the other hand, the equivalence ratio for PDM is found to be lower because of a very high quantity of air consumption. This implies

that the diesel engine work always in the lean atmosphere. The Φ_{global} obtained in this analysis is presented in Fig. 5.1.

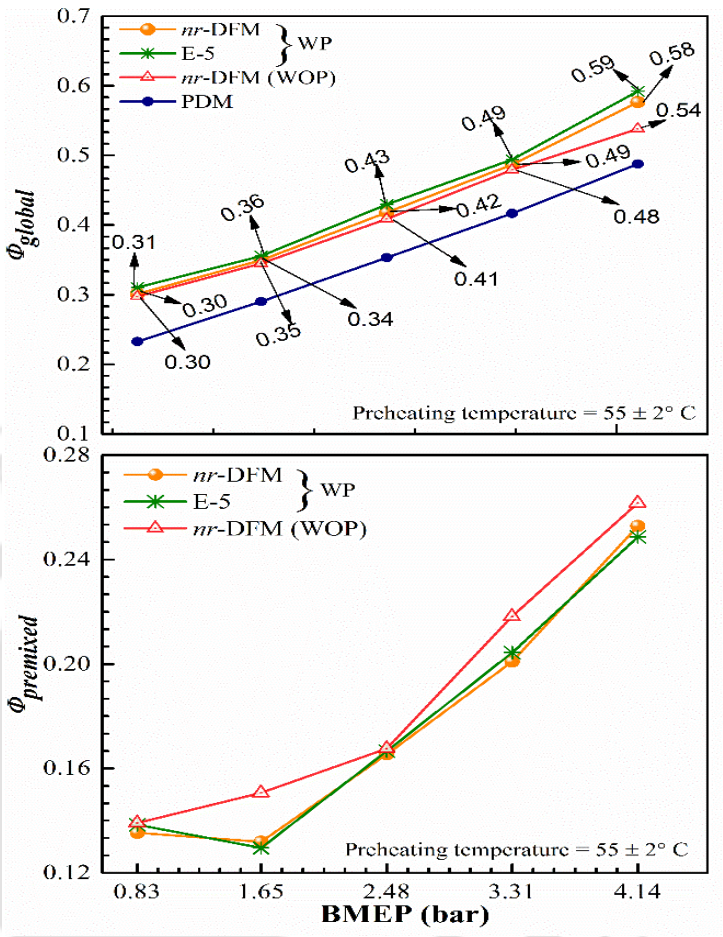

Fig. 5.1 Variations of equivalence ratios with loads

The characteristics curve in Fig. 5.2 depicts the variation of BFR with loads at different operating conditions. The BFR is found to increase with the increase of imposed loads, except that, it reduces slightly at the load of 1.65 bar. This may be due to the reduction of engine speed. Though the study is carried out with a constant speed engine, however, the engine speed from the applied load of 0 – 4.14 bar is found to drop roughly by 50 rpm (Debnath et al. 2013a). This drop is found to be comparatively more at an applied load of 1.65 bar. As a result, the liquid fuel consumption enhances which is evident in Fig. 5.3. It shows that at 1.65 bar, the energy share by biogas is lower than that of liquid fuels used in the investigation. On the other hand, the BFRs in *nr*-DFM (WP) and with E-5 blend are found to be nearer to each other. This is because of the same preheating temperature of the intake charge. The BFR is kept lower at part loads and higher at higher loads to acquire the efficient utilization of the gaseous fuel. With preheating and at the loads of 1.65 and 4.14

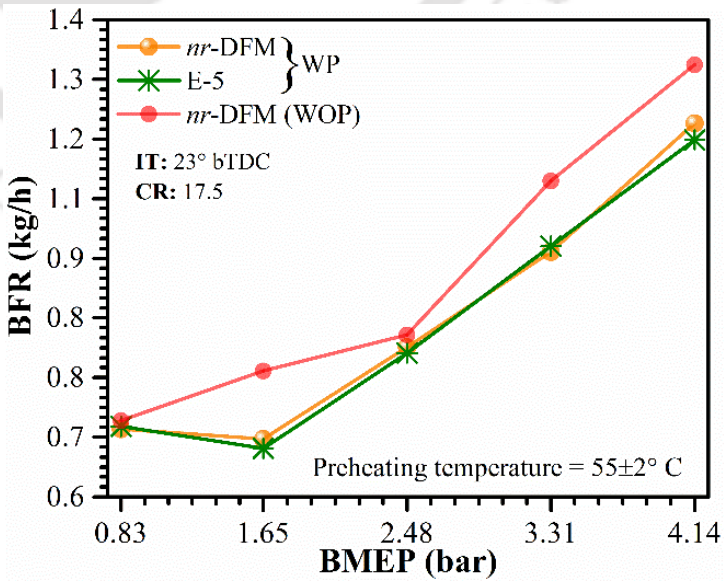

Fig. 5.2 Variations of BFR with loads

bar, the minimum and maximum BFRs are found to be 0.65 kg/h and 1.18 kg/h, respectively. Whereas, in *nr*-DFM (WOP), the minimum and maximum BFRs are observed as 0.66 kg/h and 1.27 kg/h at loads of 0.83 and 1.65 bar, respectively.

Figure 5.3 shows the variation energy shares with loads. At all loads, the BESs are observed to be lower than that of liquid fuel. However, with the increase of loads, there is a simultaneous increment of BES and decrement of the liquid fuel enrgy share. These energy shares of the liquid and gaseous fuels have been manifested on Φ_{global} as discussed above. At all the applied loads, the energy shares with preheating in *nr*-DFM (WP) and E-5 blend are found to closer to each other. The maximum BES is evaluated as 51.48% at 4.14 bar in *nr*-DFM (WOP), while the minimum is 39.52% at 1.65 bar with E-5 blend. At 4.14 bar with E-5 blend, the energy share by biogas is found to be 45.23%. Whereas, the energy shares with the liquid fuels at all the applied loads on the engine are noticed to be above 50%. However, at the load of 4.14 bar and in *nr*-DFM (WOP), the minimum energy share of the diesel fuel is found to be 48.52%. Therefore, the study identifies biogas as the secondary fuel and the liquid fuel as the primary fuel to achieve the efficient utilization of the fuels in DFM.

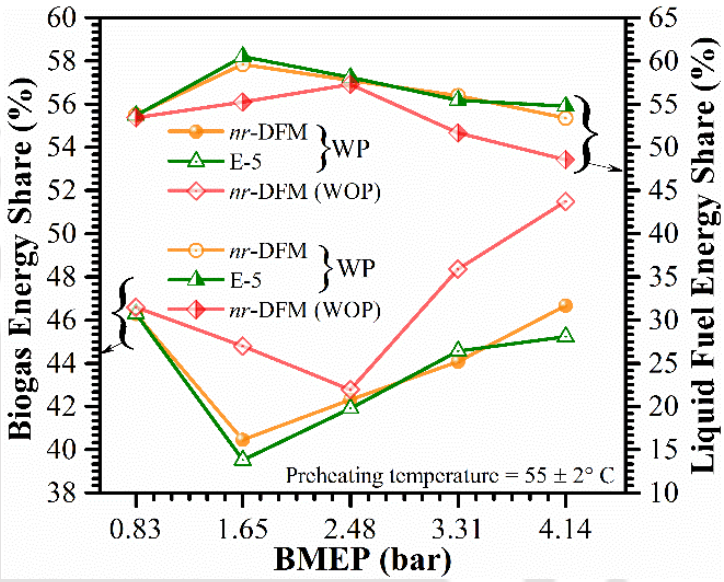

Fig. 5.3 Variations of BES and liquid fuel energy share with loads

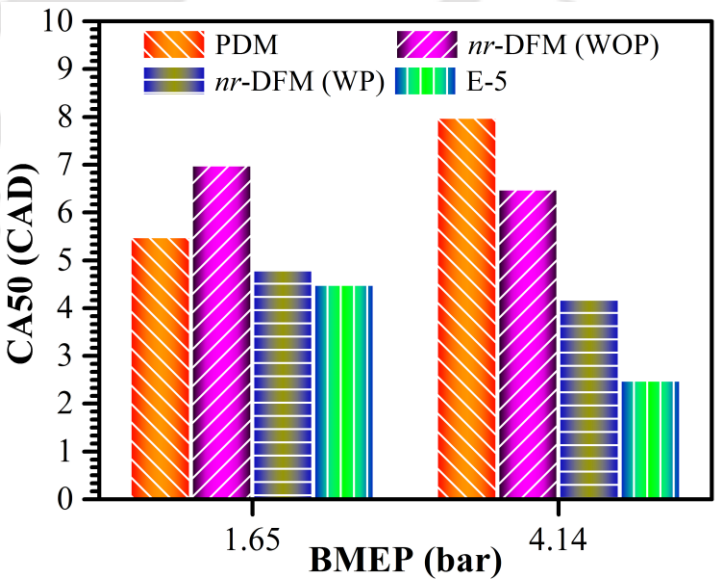

Fig. 5.4 Characteristics of CA50 with the load

The charateristics of CA50 (defined as the crank angle of 50% cumulative heat release)

with loads is shown in Fig. 5.4. In PDM, the CA50 is noticed to increase with the increase of load. It may be due to the enhancement of diesel consumption with load. The similar results have also been observed by Li et al. (2018). Whereas, in DFM, the CA50 is found to reduce with the increase of load. The advanced CA50 is observed with E-5 as compared to one with *nr*-DFM (WOP) and (WP). It is to be noted that the investigation with E-5 in DFM is associated with the preheating of intake charge. The advancing of combustion phasing (CA50) with ethanol addition has also been observed by Masimalai and Nandagopal (2016) and Kanga et al. (2019). Although, the engine in DFM is operated at sufficiently lean conditions (Φ_{global} ~0.32-0.59), however, there might be the slowdown of reaction rate in presence of CO_2 in biogas. Thus, the oxygenated fuel (ethanol) blended with diesel improves the combustion quality in the preheated atmosphere of the intake charge and helps to advance the CA50.

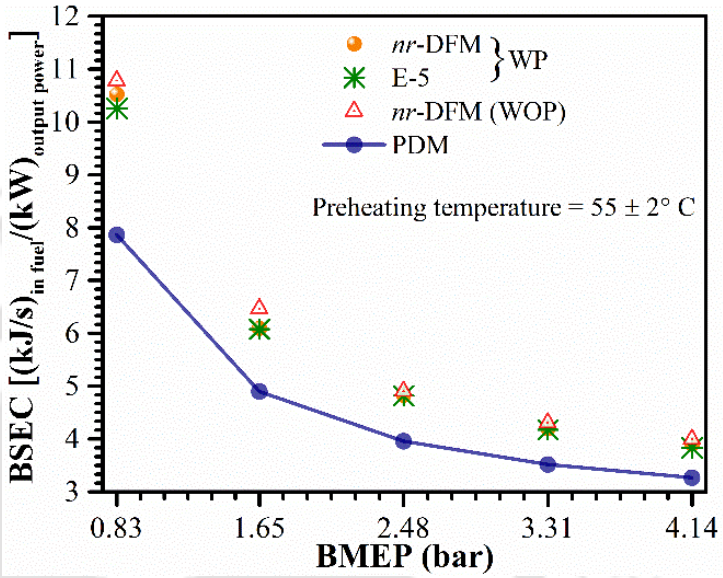

Fig. 5.5 Characteristics of BSEC with the load

The variations of BSEC in different states are illustrated in Fig. 5.5. At all the applied loads, the lower value of BSEC is observed in PDM and higher in *nr*-DFM (WOP). The BSECs in *nr*-DFM (WP) and with E-5 blend are found to lie in between PDM and *nr*-DFM (WOP) engine operation. With preheating, the BSEC with E-5 blend is found to be slightly lower than that in *nr*-DFM (WP). It may be due to the improvement of combustion in

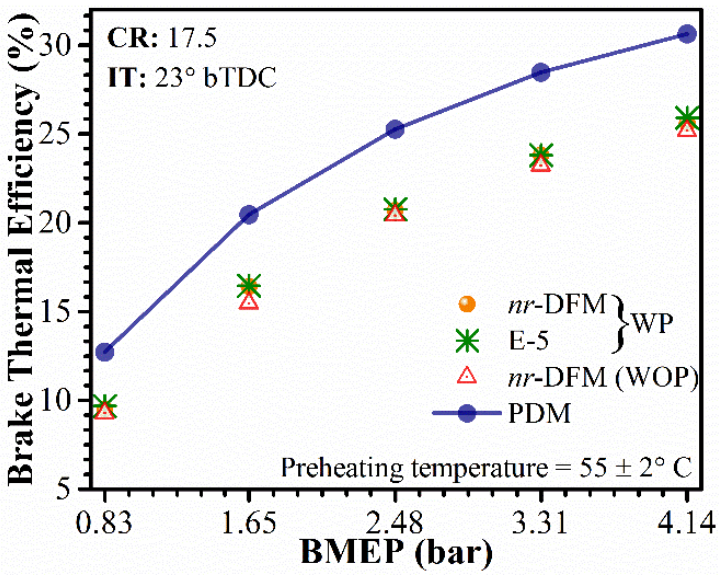

Fig. 5.6 Characteristics of BTE with the load

the presence of ethanol in the warm environment. At 4.14 bar, the BSEC in PDM, *nr*-DFM (WOP), *nr*-DFM (WP) and with E-5 blend are found to be 3.27, 3.99, 3.91, and 3.84 kJs^{-1}/kW, respectively.

Figure 5.6 shows the variations of BTE with loads in PDM and in DFM engine operation. The BTEs in PDM in comparison to DFM are noticed to be higher at all imposed loads on the engine. The major factor for the lower BTE in DFM in contrast to PDM is the lower volumetric efficiency and the higher specific heat of CO_2 present in biogas that reduces the adiabatic flame temperature with the consequence of lower laminar flame speed (Pizzuti et al. 2016), higher auto-ignition temperature of biogas that cools the combustion chamber walls. However, at the applied load of 4.14 bar, BTE in *nr*-DFM (WP) and with E-5 blend with respect to *nr*-DFM (WOP) are evaluated as 1.75% and 2.98% higher. The BTEs with E-5 blend are found as 9.70%, 16.45%, 20.76%, 23.82%, and 25.91% at the corresponding loads of 0.83, 1.65, 2.48, 3.31 and 4.14 bar, respectively. Whereas, in *nr*-DFM (WP), the BTEs (%)/load (bar), are estimated as 9.51%/0.83, 16.41%/1.65, 20.71%/2.48, 23.81/3.31 and 25.60%/4.14. The higher efficiencies with E-5 blend may be due to the release of extra oxygen during the combustion process. The properties of biogas and ethanol indicate that both the fuels have the higher self-ignition temperature. Hence, the preheating of intake charge helps to augment the combustion process inside the cylinder. As a result, the advanced CA50 is noticed with E-5 as compared to *nr*-DFM (WOP)/(WP) in DFM. Nevrtheless, the CD with E-5 is observed to be marginally higher than the one in *nr*-DFM (WP). This probably helps in sustaining the reaction over the short period. The BTEs achieved in the present study are substantially higher than those obtained by Debnath et *al.* (2014a) and Bora and Saha (2014). However, the authors had done their investigation with a very high mass consumption rate of biogas.

The VEs are noticed to be decreased with the applied load on the engine in all mode of engine operation (Fig. 5.7). The reasons are the slight drop in engine speed, trapping of

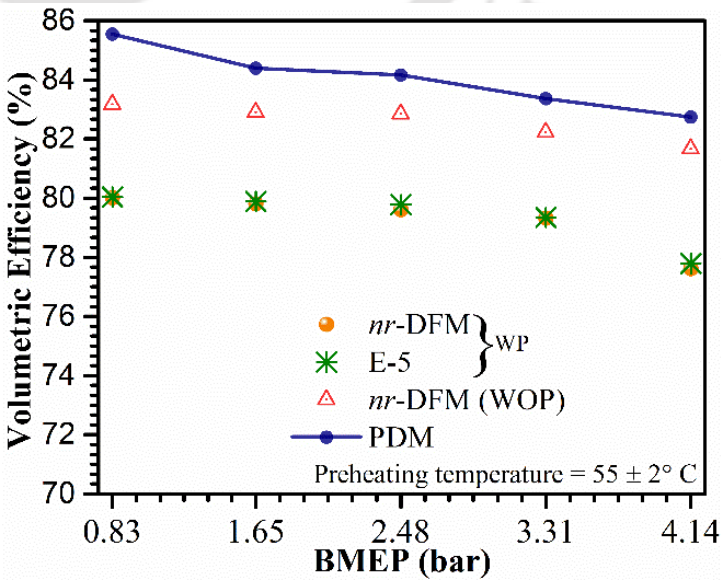

Fig. 5.7 Characteristics of VE with the load

residual gas in the engine clearance volume, enhancement of cylinder mean gas temperature (CMGT) and boost of heat flow into the inducted air-stream with the increase of loads. However, the drop in VE is found to be more in DFM and observed higher with preheating. In DFM, the same volume of air is replaced with an equivalent amount of inducted biogas. On the other hand, preheating enhances the specific volume of the inducted air. Hence, in DFM and with preheating, the reduction of VEs are found to be more in comparison to without preheating. On the other hand, owing to the same intake charge temperature, the VEs in *nr*-DFM (WP) and with E-5 blend are found to be closer to each other. Physically, the VE does not depend on the characteristics of fuel rather it depends on the physical states (thermodynamics) of experiments. The same characteristics curves of VEs are also observed with *nr*-DFM (WP) and with E-5 blend. At 4.14 bar, the reductions of 6.19% and 5.98% are noticed with *nr*-DFM (WP) and with E-5 blend, respectively with respect to the PDM, whereas in *nr*-DFM (WOP) the reduction is found to be 1.31% only.

5.4 Combustion Analysis

The parameters considered in the combustion analysis are ignition delay (ID), cylinder pressure, net heat release rate (NHRR), combustion duration (CD) and peak cylinder mean gas temperature (PCMGT).

The ID is the ignition time duration in between the end of liquid fuel injection and the start of combustion (SOC). This ID is true for the liquid fuel only. Hence, there is another ID for the gaseous fuel in DFM that is defined as the ignition time difference between the end of premixed combustion phase of the liquid fuel and the SOC of the gaseous fuel (Nwafor 2003). The ID in DFM is indicated between the points where the cylinder pressure starts to decrease (end of premixed combustion phase of the liquid fuel) and reach at lowest value from which the pressure again start to rise (SOC of the gaseous fuel) (Nwafor 2003). However, there is a

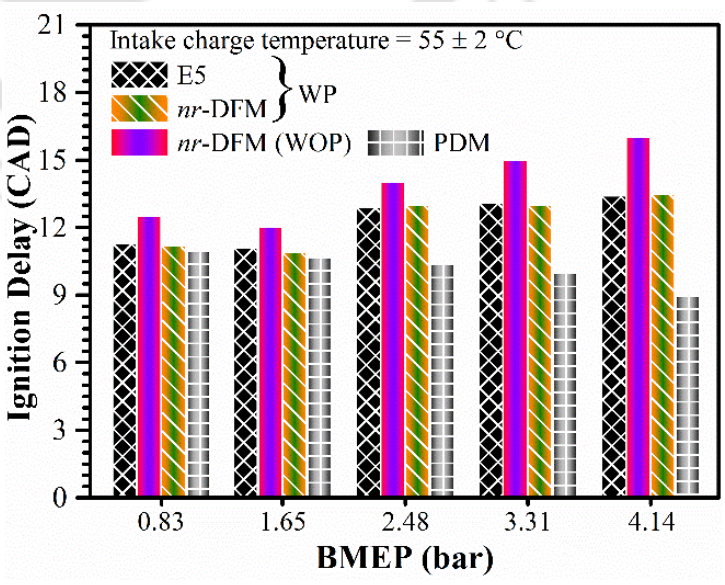

Fig. 5.8 Variations of ID with the load

probability to origin the flame front from pilot fuel after immediate SOC. Therefore, the SOC of gaseous fuel can be started before the end of the premixed combustion phase of liquid (pilot) fuel. Consequently, it is very difficult to identify the ID of the gaseous fuel. Therefore, in the present study, the point of the ID of the gaseous fuel on the cylinder pressure history curve remains unidentified. Hence, the SOC in the present study is considered at the point where the NHRR = 0, J/CAD and from which rises to its maximum magnitude (Figs. 5.11 and 5.12).

The variations of ID with loads are shown in Fig. 5.8. The ID in PDM is found in decreasing trend with the increasing of loads. In PDM, a reduction of 18.2% of ID is noticed on increasing the load from 0.83 to 4.14 bar. While, in DFM, the ID is noticed an increasing trend with the increasing of loads. It is due to the effects of optimization of Φ_{global} on engine combustion. The parameter Φ_{global} is optimized with the consideration of improvement of combustion with the switching of part loads to higher loads. Consequently, the Φ_{global} is kept in an increasing trend with the increase of loads to increase the corresponding biogas consumption rates. Besides biogas has very high self-ignition temperature and ignition inhibitor CO_2 presents as the major constituents in biogas. These attribute the higher IDs in DFM and also the higher IDs at the higher loads. The maximum increase of ID is observed to be 28% in *nr*-DFM (WOP) with the increase of loads from 0.83 to 4.14 bar, relative to 0.83 bar. The IDs in *nr*-DFM (WP) and with E-5 blend are noticed to be similar. However, it is found to be 7.46% lesser than that in *nr*-DFM (WOP).

At the optimum Φ_{global}, the characteristics of the engine (in PDM and DFM) in-cylinder pressure history at the loads of 1.65 and 4.14 bar are shown in Figs. 5.9 and 5.10 respectively. The lowest pressures at all loads are depicted in *nr*-DFM (WOP). It may be due to the higher self-ignition temperature of biogas, higher amount CO_2 in biogas that behaves like a flame extinction agent and lower LHV of biogas. Therefore, more shifting of the corresponding crank angle position of the CPP towards the right side (relative to TDC) is also noticed at all operating loads in *nr*-DFM

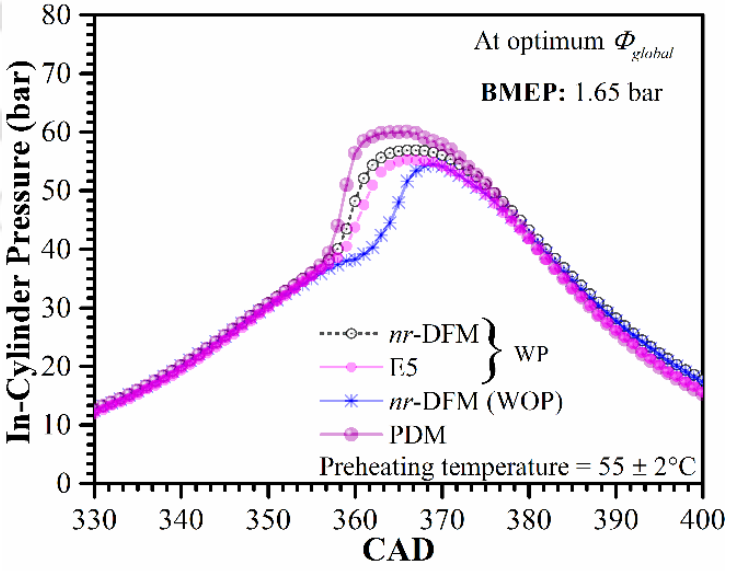

Fig. 5.9 Variations of in-cylinder pressure with CAD (AL: 1.65 bar)

(WOP). However, at 1.65 bar, in *nr*-DFM (WP), there is a rise of CPP of 2.4 bar is noticed as compared to *nr*-DFM (WOP). This attributes that the preheating augmented the combustion in *nr*-DFM (WP). At 1.65 bar, the intermediate but sufficiently higher pressure with E-5 blend than in *nr*-DFM (WOP) is achieved. With E-5 blend, the maximum CPP is found to be 55.3 bar, which is 1.6 bar lower than that of *nr*-DFM (WP). It may be due to the lower LHV and higher heat of vaporization of ethanol than diesel fuel. However, the position of the peak with E-5 blend is noticed to be similar to that of PDM. The reason may be the effects of preheating which reduces the ID of the E-5 fuel in DFM. Nevertheless, at the maximum load of 4.14 bar, the CPP with E-5 blend is found to closer to that of the CPP with preheating in *nr*-DFM (WP). The shifting of CPP at higher loads from the TDC towards right side is noticed to be higher as compared to the crank angle position of the CPP at the part loads. It may be due to the increasing diesel consumption with the increase of loads in PDM. While, in DFM, this shifting of CPP may be due to the simultaneous increasing consumption of liquid (diesel and blended fuel) and biogas with the increase of loads. At 4.14 bar, the CPP (bar)/CAD in *nr*-DFM (WOP), *nr*-DFM (WP), with E-5 blend and in PDM are found as 65.1/371, 68.1/370, 66.2/369 and 72.3/368, respectively.

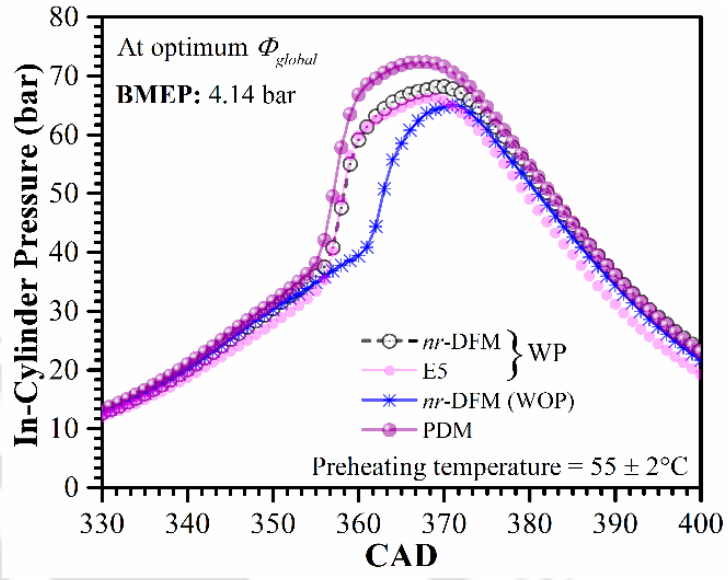

Fig. 5.10 Variations of in-cylinder pressure with CAD (AL: 4.14 bar)

The NHRR is the consequence of the rigorous ignition reaction of the fuel. The NHRR starts at some suitable thermodynamic states that prevail in the combustion chamber. It is ended either after the complete burning of the fuel or due to the bulk extinction of the flame front. The maximum release of NHRR is always desirable.

The NHRR history inside the cylinder is portrayed in Figs. 5.11 and 5.12. The release of heat and the development of pressure are physically interrelated to each other. Nevertheless, the physical reasons behind the release of heat and development pressure inside the cylinder are similar. However, the position of the crank angle of the NHRR peak has the crucial role in the development of the CPP and the corresponding utilization of higher expansion energy. At the

part load of 1.65 bar and in DFM, the lowest, maximum, and intermediate NHRRs are noticed in *nr*-DFM (WOP), *nr*-DFM (WP) and with E-5 blend, respectively. At this load, the maximum NHRR of 74.93 J/CAD is observed in PDM. At the load of 1.65 bar, there is an increment of NHRR of 0.74% and 12% estimated with the E-5 blend and in *nr*-DFM (WP), respectively, in comparison to the *nr*-DFM (WOP). The marginal increment of NHRR with the E-5 blend may be due to the lower LHV and higher heat of vaporization, higher self-ignition temperature of biogas that already has been discussed above. On the other hand, the significant improvement of NHRR in *nr*-DFM (WP) is due to the augmentation of combustion with the intake charge preheating. However, the reductions of NHRR in *nr*-DFM (WOP), with E-5 blend and in *nr*-DFM (WP) in comparison to that of PDM are assessed as 39%, 38.45%, and 31.50%, respectively. The crank angle positions of the peaks (CAD) of the NHRR are found as 363, 361, 360, and 359 in *nr*-DFM (WOP), with E-5 blend, in *nr*-DFM (WP) and PDM, respectively. At the higher loads, the substantial improvement in NHRRs is noticed. At the load of 4.14 bar, the NHRRs (J/CAD)/CAD are attained as 79.12/364, 80.12/358, 81.25/357 and 91.6/357 in *nr*-DFM (WOP), with E-5 blend, in *nr*-DFM (WP) and PDM, respectively. It is reflected in the results at this higher load that there is more shifting of the crank angle positions of the NHRR peaks

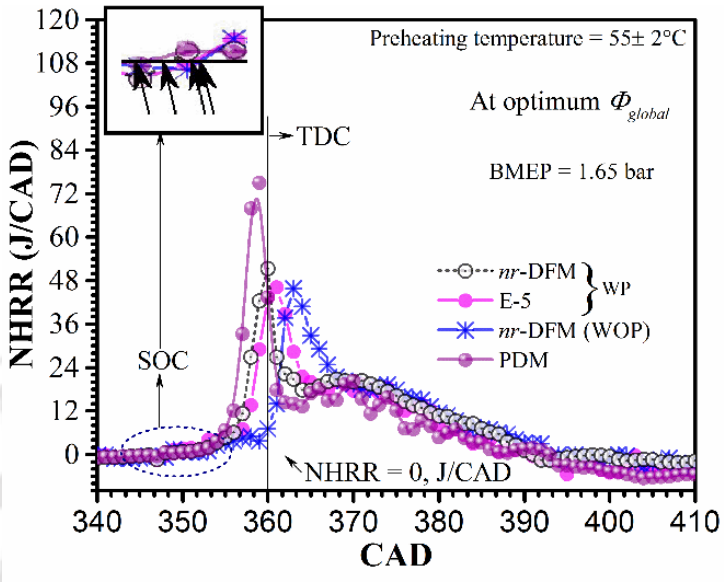

Fig. 5.11 Variations of NHRR with CAD (AL: 1.65 bar)

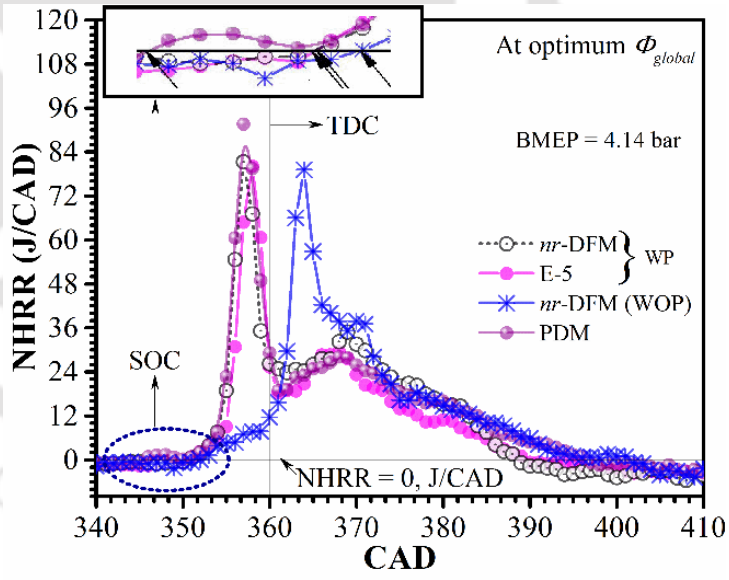

Fig. 5.12 Variations of NHRR with CAD (AL: 4.14 bar)

to the left side relative to TDC. This attributes the higher utilization of the expansion energy at higher loads.

The variations of CD are shown in Fig. 5.13. The lowest CD is noticed with the preheating in comparison to that in *nr*-DFM (WOP), with E-5 blend, and in PDM. In addition, with preheating CD is noticed to reduce with the increase of loads. However, the CDs are observed to increase with the increase of loads in PDM and in *nr*-DFM (WOP). Overall, the lower CDs are attained in DFM than PDM. As there is no flame propagation and due to the longer diffusion combustion in PDM, the CD is found to be higher in PDM than DFM. In DFM, with preheating the CDs with E-5 blend and in *nr*-DFM (WP) are estimated to reduce by 14.3% and 10.79% upon increasing of loads from 0.83 to 4.14 bar, respectively. Whereas there are the increment of CDs of 11.63% and 13.64% in *nr*-DFM (WOP) and in PDM relative to *nr*-DFM (WP) respectively, are noticed.

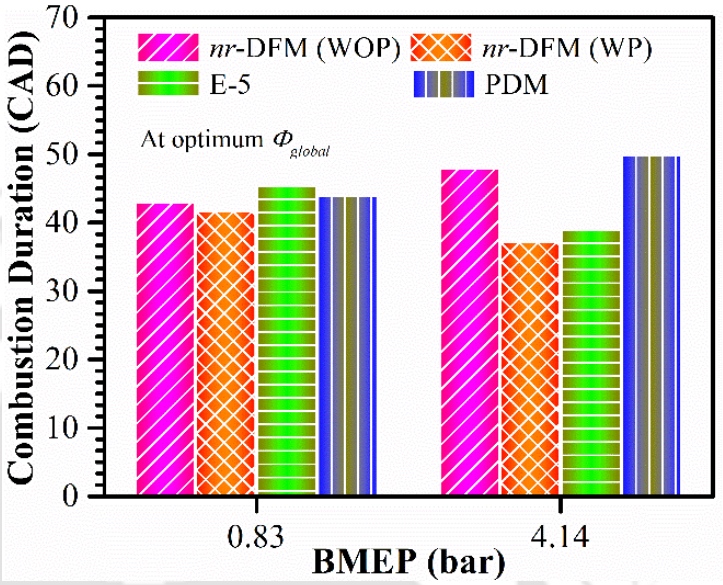

Fig. 5.13 Variations of CD with lad

The variations of the PCMGT with loads are shown in Fig. 5.14. The PCMGT is one of the crucial parameters in the analysis of the combustion characteristics of the internal combustion engines. The PCMGT has the proportional relation with the development of CPP. Hence, the higher the CPP higher will be the PCMGT. The higher values of PCMGT is desirable in order to have the lower combustion irreversibility

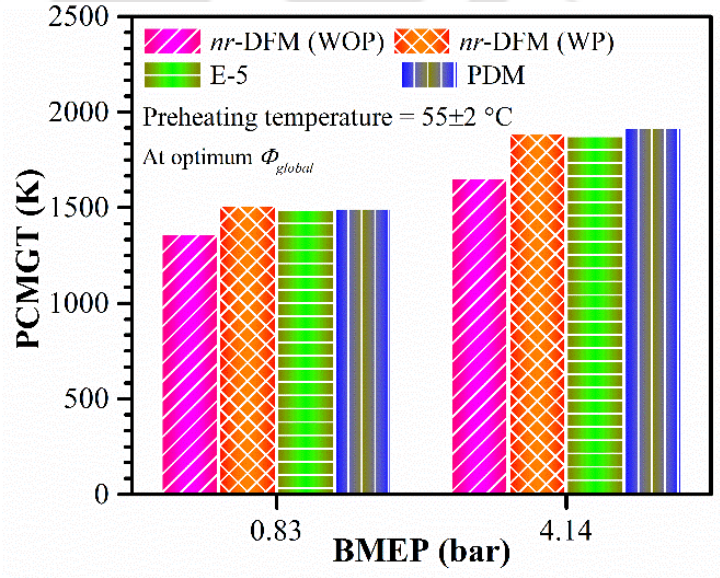

Fig. 5.14 Variations of PCMGT with lad

(Som and Datta 2008), higher flame speeds, to curtail the pollutant emission except for the case of NO_x emission. The preheating is found to be an efficient technique to enhance the PCMGT. In all the modes of engine operation, PCMGT is noticed to increase with the increasing loads. However, at a particular load, there is an increment of PCMGT with preheating. At 0.83 bar, the increment of PCMGTs with E-5 blend and in *nr*-DFM (WP) than in *nr*-DFM (WOP) are found as 9.43% and 11.07%, respectively. While at the maximum load of 4.14 bar, these increments are observed as 13.28% and 14.03%, respectively. The PCMGT in all loads are found to be higher in PDM.

5.5 Emission Analysis

The variations of carbon monoxide (CO), unburnt hydrocarbon (HC) and oxides of nitrogen (NO_x) are depicted in Figs. 5.15, 5.16 and 5.17, respectively. The emission of CO in DFM reduces with preheating along with the applied load. Whereas in PDM, it is reduced with the increase of applied loads on the engine (Fig. 5.15). However, in *nr*-DFM (WOP), the CO emission is found to increase with the increase of loads, which reduces slightly at the maximum load of 4.14 bar. In *nr*-DFM (WP) and with E5 blend, the CO emission is found to be slightly higher than that of PDM. Nevertheless, the CO at the maximum load of 4.14 bar with E-5 blend is noticed to be marginally lower than the emission in PDM. Although, the CO emission in *nr*-DFM (WP) is found to be higher than that in PDM, however, it is observed to be substantially lower than that in *nr*-DFM (WOP). At 4.14 bar, the reduction of CO emissions in *nr*-DFM (WP) and with E-5 blend in comparison to *nr*-DFM (WOP) are noticed to as 65% and 82.9%. At this load, with E-5 blend the CO is found to be reduced by 17.2% in comparison to PDM. At the part load of 0.83 bar, the CO emission with *nr*-DFM (WP) and with E-5 blend are observed to be reduced by 23.6% and 34.5% relative to one in *nr*-DFM (WOP). At this part

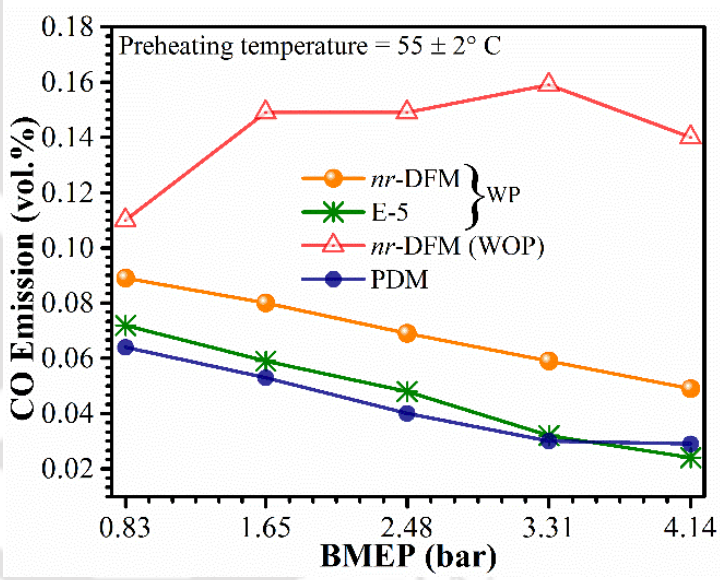

Fig. 5.15 Variations of CO emission with load

load, however, the CO with E-5 blend is noticed to be 12.5% higher as compared to one in PDM.

The main reasons of CO emission in a diesel engine are due to the effects of blowdown (Heywood 1988), lower peak cylinder means gas temperature (PCMGT) (>1450 K) (Heywood 1988). The blowdown drastically reduces the peak cylinder pressure as well as PCMGT at the exhaust port that breaks down the chemical equilibrium reactions (Heywood 1988) in which CO is converted into CO_2. However, the key reasons of CO emission in DFM engine may be due to the lower PCMGT, higher gaseous fuel consumptions, and deficiency of oxygen.

The reported studies (Liu et *al*. 2013, Karagöz et *al*. 2016) notified the PCMGT of 1450 K as the threshold temperature at which the oxidation of CO to CO_2 starts and the PCMGT 1500 K is considered to be the temperature at which the reaction ($CO + OH = CO_2 + H$) comes at the equilibrium state (Glassman and Yetter, 2008). Sjöberg and Dec (2005) noticed a negligible emissionof CO within the range of PCMGT of 1500 –1800 K. The effects of Φ_{global} on PCMGT has also been discussed in the previous chapter. It is observed that there is a drastic reduction of PCMGT with the increase of Φ_{global}. Hence, the present study achieves best results with the optimization of Φ_{global} from part to higher loads under the influence of preheating and with the use of oxygenated fuel. It is known that the use of higher-octane gaseous fuels in diesel engine reduces both cylinder peak pressure and PCMGT. Therefore, it is essential to take special care whenever the gaseous fuels are chosen to perform the investigation in DFM engine operation. Moreover, in *nr*-DFM (WOP), the CO emission generally increases due to the lack of oxygen. Hence, the analysis reveals that with preheating and with the E-5 blend, the emission of CO reduces due to higher cylinder peak pressure, higher PCMGT, and release of extra oxygen in the presence of ethanol.

The emission of unburnt hydrocarbon (HC) is the consequence of the incomplete combustion of the fuels used to run the engine. The reasons, favor to generate the emission of HC, are the formation of locally over-rich or over-lean mixture, bulk quenching or extinction of the flame front at the wall of the combustion chamber due to the formation of boundary layer, formation of the crevice volumes inside the combustion chamber (Heywood 1988) and the insufficient oxygen present during combustion process. In crevice volume, the compressed fuel is trapped at the corner of the cylinder during compression process and do not take part in the primary combustion process and emits as the unburnt HC (Barik and Murugan 2014). The detailed discussion of the crevices in the combustion chamber is elaborated by Alkidas (1999). The

emission of HC in Fig. 5.16 is shown in decreasing trends with the increasing of applied load on the engine. At higher load, the lowest emission of HC is observed with the E-5 blend in comparison to the one in PDM. However, this emission with E-5 blend is found to be higher at part loads than that in PDM. The maximum emission of HC is observed in *nr*-DFM (WOP) and intermediate in *nr*-DFM (WP) as compared to PDM. At the load of 4.14 bar, the reduction of 31.11% of HC with E-5 blend is noticed in contrast to PDM. However, at this load, the increments of HC emission in *nr*-DFM (WP) and in *nr*-DFM (WOP) with respect to the one in PDM, are found as 75.6% and 191.11, respectively. The higher HC emission in *nr*-DFM (WOP) may be due to the lower LHV of biogas, the higher self-ignition temperature of biogas that cools the combustion chamber wall, substitution of air by same volume of inducted biogas and deficiency of oxygen at the time of combustion. The lower HC emission in DFM with preheating and with E-5 blend is due to preheating of intake charge and release of extra oxygen in the presence of ethanol, promoting an efficient combustion.

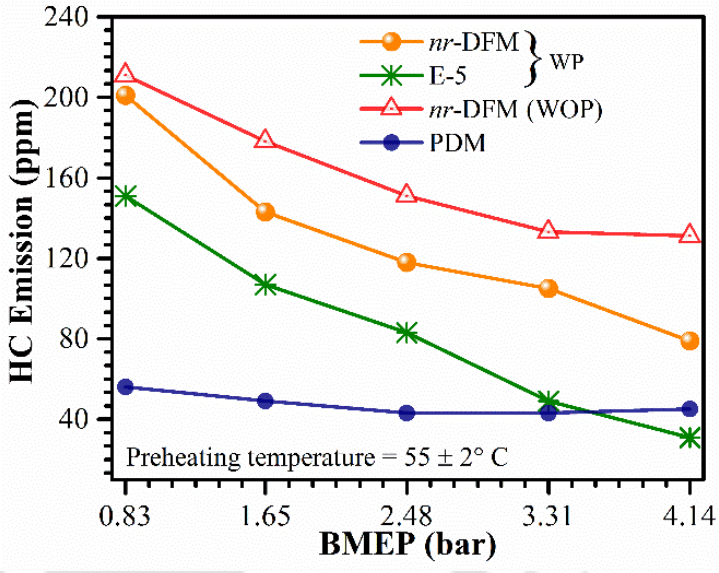

Fig. 5.16 Variations of HC emission with load

The emission of NO_x is found to increase with the increase of load as shown in Fig. 5.17. The emission in DFM in comparison to PDM is found to be lower in all conditions. However, the NO_x emission is found to be higher in DFM with preheating and with E-5 blend and lower in *nr*-DFM (WOP). At the load

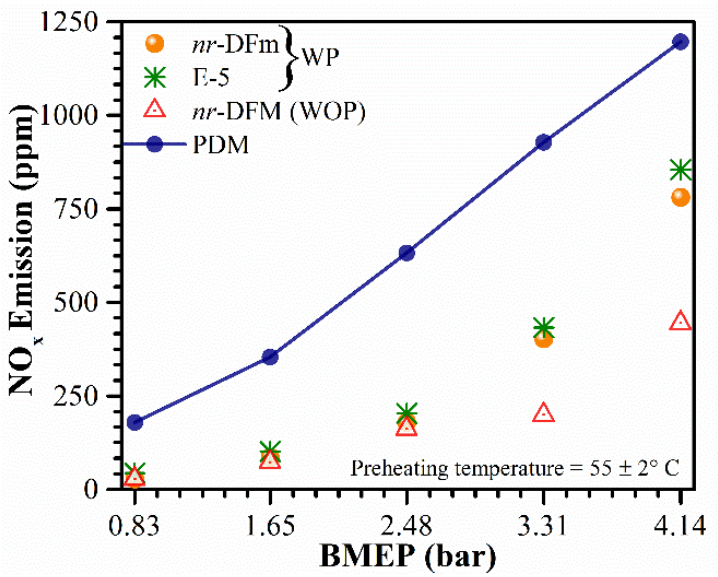

Fig. 5.17 Variations of NO_x emission with load

of 4.14 bar, the reduction of NO_x in *nr*-DFM (WOP), *nr*-DFM (WP) and with E-5 blend are found 62.87%, 34.70%, and 28.51%, respectively in comparison to one in PDM. The NO_x is formed mainly due to richer oxygen amount, higher flame temperature and the residence time of the burnt gas at the high temperature at oxygen-rich atmosphere (Heywood 1998). Consequently, the NO_x in PDM and in DFM with preheating and with E-5 blend are increased in comparison to one in *nr*-DFM (WOP).

5.6 Summary

In this chapter, results of *nr*-DFM (WOP/WP), with E-5 blend at the optimized Φ_{global} are summarized. The investigation mainly has been carried out to examine the usability of the oxygenated fuel like ethanol and effects of preheating in biogas DFM engine.

Performance Analysis

- At the loads of 1.65/4.14 bar, the BFRs with E-5 blend are noticed to be 0.66 kg/h/1.18 kg/h, respectively. At 4.14 bar, the BES in all states (except for the case of without preheating) are found to lesser than 50%.
- At all loads, the retarded CA50 is noticed in PDM, while the advanced one is found with E-5. The BSEC in *nr*-DFM (WP) and with E-5 blend are found to be closer to each other, while it is observed to be lower than that in *nr*-DFM (WOP). At 4.14 bar, in *nr*-DFM (WP) and with E-5 blend, the BTEs are observed as 1.75% and 2.98% higher in comparison to one in *nr*-DFM (WOP).
- A higher reduction of VE is noticed in DFM. With preheating, this drop is found to be more. At 4.14 bar, in *nr*-DFM (WP) and with E-5 blend, the VEs are found to reduce by 6.19% and 5.98%, respectively.

Combustion Analysis

- The ID in PDM reduces with increasing of loads, while the reverse trends are noticed in DFM. The IDs with *nr*-DFM (WP) and E-5 blend are noticed to be closer to each other. However, on an average, it is found to lesser by 7.46% than that in *nr*-DFM (WOP).
- In general, there is an increment of CPP with the preheating and shifting of the crank angle position of CPP towards TDC. At 4.14 bar, the CPP (bar)/CAD in *nr*-DFM (WOP), *nr*-DFM (WP) and with E-5 blend are found as 65.1/371, 68.1/370 and 66.2/369, respectively.

- At 1.65 bar, there is an increment of NHRR of 0.74% and 12% attained with the E-5 blend and in *nr*-DFM (WP), respectively, in comparison to *nr*-DFM (WOP). At higher loads, more shifting of peaks of NHRR towards left from the TDC is noticed.

Emission Analysis

- There is a significant reduction of CO emission with preheating and with E-5 blend. At 4.14 bar, the reduction of 17.2% of CO emission with E-5 blend relative to PDM, is estimated.
- The lower emission of HC at the higher load is achieved with the E-5 blend. However, at part loads, the emissions of HC are found to be higher in comparison to PDM. At 4.14 bar, the reduction of 31.11% of HC with E-5 in contrast to PDM blend is evaluated.
- The NO_x emission is found to increase with increase of loads, preheating and with E-5 blend. Substantial reduction in NO_x emission in DFM relative to PDM is attained. At 4.14 bar, the reduction of NO_x in *nr*-DFM (WOP), *nr*-DFM (WP) and with E-5 blend in comparison to PDM are found to be 62.87%, 34.70% and 28.51%, respectively.

Chapter-6

Results of Biogas Run DFM Engine Using Ternary Blends (Diesel, Biodiesel and Ethanol)

Chapter

Highlights:

- *Preheating and various ternary blends (TB-Es) (D-B-E) are chosen as the key parameters*
- *There is a gain of energy with preheating as compared to without preheating*
- *Cylinder mean gas temperature (CMGT) increases due to preheating and with the use of oxygenated fuels*
- *The diesel (PDM) like trends in CO and HC emissions are achived in DFM*

Overview: *In the previous chapter, it is demonstrated that the use of renewable oxygenated liquid fuels with the intake charge preheating can be beneficial to improve the DFM engine performance. In this chapter, ethanol and biodiesel (as the oxygenated fuel) blended with diesel (ternary blend) is considered as the injected pilot fuel. The five ternary blends of Diesel-Biodiesel-Ethanol (D-B-E) have been prepared to obtain the optimum one. The blends are designated as TB-E1 (D70-B20-E10), TB-E2 (D75-B20-E5), TB-E3 (D72-B20-E8), TB-E4 (D77-B15-E8) and TB-E5 (D67-B25-E8). All the investigations are carried out at the engine standard CR=17.5 and IT=23 CAD bTDC. The various performance, combustion and emission parameters are considered to make a comparative analysis of PDM, nr-DFM (WOP) and nr-DFM (WP) and DFM with the ternary blends with preheating. The adequate improvement in DFM engine performance and combustion are achieved, while, a drastic reduction in CO and HC emission found with the marginal increment of NO_x for the cases with preheating and with blended fuels.*

***Chapter Layout*:**

6.1 Selection of Pilot Fuel

It is evident in the previous chapter that the liquid renewable oxygenated fuels blended with fossil diesel can be beneficial in terms of efficient overall engine performance, mainly in the significant reduction of emissions in a biogas run DFM engine. The study in this chapter considers ethanol and biodiesel as the renewable oxygenated fuels, which are blended with diesel to form the ternary blends (TB). The various TBs of Diesel-Biodiesel-Ethanol (D-B-E) are considered to optimize composition in the blends in order to have an efficient engine performance. The optimization process of the blend composition in TBs is described in the following section. The properties of the individual fuels selected in this investigation are presented in Table 6.1.

Table 6.1 Properties of fuels used in the present study (Nathan et *al*. 2010; Luijten and Kerkhof 2011; Sahoo et *al*. 2011b; Rakopoulos et *al*. 2014; Aleiferis and Behringer 2015)

Properties	**Biogas**	**Diesel**	**Jatropha Biodiesel**	**Bio-Ethanol**
Chemical structure	-	$C_{12}H_{26}$	$C_{18.8}H_{35.1}O_2$	C_2H_5OH
C (wt.%)	-	84.7	77.08	52.2
H (wt.%)	-	15.3	11.99	13
O (wt.%)	-	-	10.93	34.8
Density (kg/m^3), at 32.2^{o}C	1.096[a]	824.91[a]	873.36[a]	765.36[a]
Heat of vaporization (kJ/kg)	-	250-270	-	840-904
Lower heating value (MJ/kg)	19.1[a]	42.1[a]	38.17 [a]	26.97[a]
Cetane number	-	50-53	51-58	5-11
Kinematic viscosity (mm^2/s, at 40^{o}C)	-	2.54[b]	4.218[b]	1.137[b]
Bulk modulus of elasticity (bar)	-	16,000	-	13,200
Stoichiometric air-fuel ratio	6.17[a]	15.01[a]	12.52[a]	9.0[a]
Flash point (^{o}C)	-	67.5-71	147-191	13-14
Auto ignition temperature (^{o}C)	632-813	200-220	-	-
Flammability limits (% by volume of air)	7.5-14	1.5-7.6	-	-

[a]calculated; [b]measured

6.2 Design of Experiments

The investigations are carried out in dual fuel mode (DFM), however, pure diesel mode (PDM) is also considered to have a direct comparison of the engine performance. Five different blends (TB-E1 through TB-E5) with preheating, pure diesel-biogas in *nr*-DFM (WP) and pure diesel-biogas in *nr*-DFM (WOP) have been investigated as detailed in Table 6.2. It is evident from Table 6.1 that biogas has the very high self-ignition temperature and ethanol has a higher heat of vaporization than other liquid fuels (diesel and biodiesel). Besides, the analysis in the previous chapter demonstrates that the preheating helps to obtain a significant improvement in

the engine's overall performance of the biogas run DFM engine. In the present study, all the experiments in DFM except *nr*-DFM (WOP) are conducted with the intake charge preheating. The preheating temperature is chosen and optimized at 55 (±2) °C, depending upon zero appearance of knocking and engine overall performance characteristics. According to Karim (1980), to achieve an optimum performance in DFM, the liquid and gaseous fuel consumption at part load should be higher and lower respectively, while at higher load, it should be vice versa. Based on this consideration, the variable Φ_{global} is optimized at all the operating loads (from part to higher) and without/with preheating. Since the values of Φ_{global} vary from one experimental environment to another, it is not possible to achieve the same Φ_{global} at the same load. Hence, the optimum Φ_{global} is indicated with the range at each of the operating load. In *nr*-DFM (WOP), the optimum ranges of Φ_{global}/load (bar) are identified as 0.29-0.31/0.83, 0.35-0.36/1.65, 0.40-0.43/2.48, 0.47-0.5/3.31 and, 0.53-0.60/4.14. Whereas, with the blended fuel and with intake charge preheating, the optimum ranges of Φ_{global}/ load (bar) are estimated as 0.29-0.33/0.83, 0.35-0.8/1.65, 0.42-0.45/2.48, 0.48-0.51/3.31 and 0.56-0.61/4.14.

Table 6.2 Experimental Matrix

Parameters	**PDM**	**DFM (Raw biogas)**						
		With preheating (WP) (55 ±2° C)						**WOP**
Fuel/ Blended Fuel	Diesel	*nr*-DFM	TB-E1	TB-E2	TB-E3	TB-E4	TB-E5	*nr*-DFM (WOP)
Φ_{global}/Load (bar)	0.23/0.83-0.48/4.14	0.29-0.42/0.83, 0.35-0.46/1.65, 0.40-0.52/2.48, 0.47-0.57/3.31 and 0.54-0.61/4.14						

6.2.1 Optimization of the TB-Es

The blends are optimized and the flow diagram of optimization is presented in Fig. 6.1. Experiments with the blended fuels are started with TB-E1 (D70-B20-E10) and ended with TB-E5 (Fig. 6.1). In TB-E1, 20% biodiesel has been selected as per the U.S. Environmental Protection Agency (EPA 2002) report. According to EPA, in a diesel engine, the combustion of 20% biodiesel blended with diesel produces minimum pollutant emissions. Again, Rakopoulos et *al*. (2015) in their

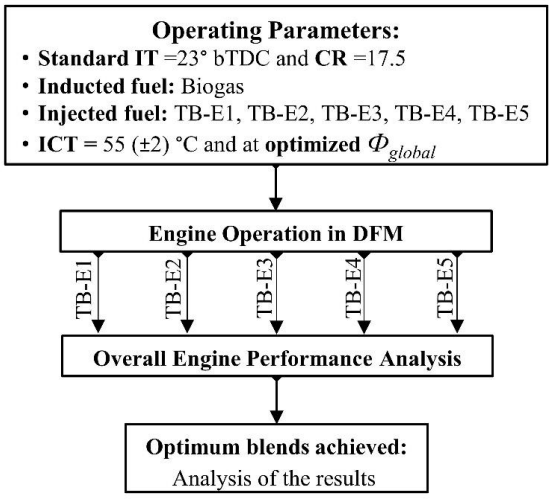

Fig. 6.1 Flowchart to optimize the ternary blends (TB) of diesel-biodiesel-ethanol (TB-E)

experiments, have noticed that 10% ethanol blended with diesel can be efficiently used to run the diesel engine. However, TB-E1 is a ternary blend and further optimization of the composition in the TB-E1 blend (composition) is essential. In this regard, the ethanol percentage is reduced to 5% (TB-E2: D75-B20-E5) to apprehend the effects of ethanol percentage in the mixture, by keeping the amount of biodiesel intact. The results obtained are found to be better than the 10% ethanol in the blends. Nonetheless, it is not possible to recognize that TB-E2 is an optimized blend. As a result, in TB-E2 blend (mixture), the ethanol percentage is increased from 5% to 8%. This new blend is designated as TB-E3 (D72-B20-E8) and is found to be superior over TB-E2 and TB-E1 in terms of overall performance.

Table 6.3 Properties of the blended fuel

Properties	Blended Fuel				
	TB-E1	TB-E2	TB-E3	TB-E4	TB-E5
Density (kg/m^3)	828.65	831.62	829.84	827.41	832.26
LHV (kJ/kg)	39874.2	40578.3	40156.4	40358.1	39955.9
Viscosity (mm^2/s)	2.76	2.83	2.79	2.70	2.88
Oxygen content (wt.%)	5.52	3.89	4.87	4.31	5.43

Finally, to study the effect of biodiesel amount in the blend of TB-E3, it is necessary to reduce and increase the biodiesel amount in the blend. Consequently, TB-E4 (D77-B15-E8) and TB-E5 (D67-B25-E8) blends are prepared and experiments are conducted. Nevertheless, the optimum results (engine overall performance) are once again confirmed with the TB-E3 blend as compared to other blends. The properties of all the blended fuels are presented in Table 6.3. The properties of blended fuels are calculated with use of the Lever law (Rakopoulos et *al*. 2016a). A careful inspection of Table 6.3 indicates that the TB-E3 blend has the better cumulative physical properties than the other fuels.

6.3 Engine Performance Analysis

In the present experimental facility, the biogas volume flow rate is measured with a biogas flow meter, in which, the engine suction is the driving force to flow the gas into the engine cylinder. Consequently, it is practically impossible to retain the same flow rate of biogas in all individual experiments in DFM. Nevertheless, with a proper control, it is possible to confine the nearest mass flow rates of biogas at the same load but among different tests in DFM. Hence, an optimum but average Φ_{global} is considered to describe the engine parameters. Since all the liquid fuels (diesel and blended fuels) in the present investigation are considered as a pilot (but primary) fuel. Hence, in the study, more stress is given on Φ_{global} rather than $\Phi_{premixed}$.

Figure 6.2 shows the variation of BFR with engine load and average but optimum Φ_{global}. The minor variations of BFR at all individual loads (from part to higher) for all the blended fuels (TB-E1 to TB-E5) and in *nr*-DFM (WP) are depicted in Fig. 6.2. The variations may be due to the different cumulative fuel properties (Table 6.3) and different experimental environments like humidity in the air, the initial temperature of engine coolant etc. The blended fuel properties in Table 6.3 are calculated by picking up the data from the Table 6.1 and using the "Lever" law (Rakopoulos et al. 2016a). The approximate BFRs for *nr*-DFM (WP) (diesel-biogas combination) are found as 0.722, 0.718, 0.856, 0.996 and 1.173 kg/h at the load of 0.83, 1.65, 2.48, 3.31 and 4.14 bar, respectively. Whereas, the average BFRs for the blended fuels (average of TB-E1, TB-E2, TB-E3, TB-E4, and TB-E5 blends) are measured as 0.731, 0.728, 0.856, 1.002 and 1.180 kg/h (at the same load interval as stated above), respectively. The higher BFRs with the blended fuels (TB-E1 through TB-E5) in comparison to that in PDM and in *nr*-DFM (WP) may be due to the lower LHVs of the blended fuel than diesel fuel.

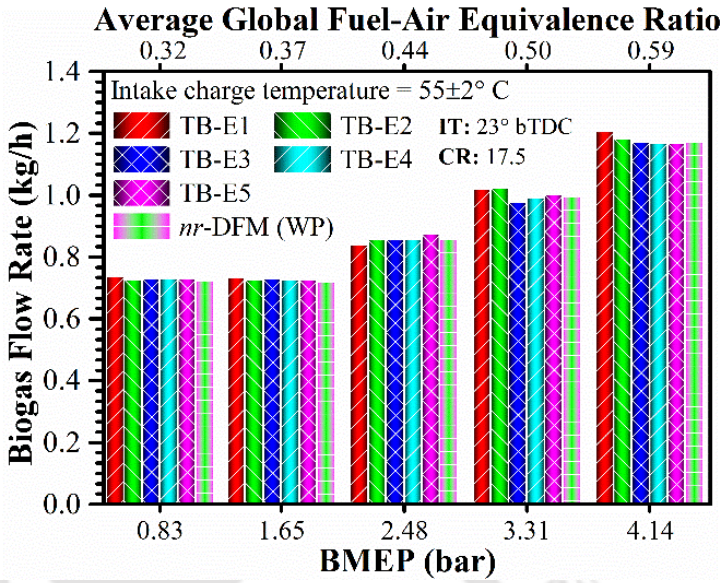

Fig. 6.2 Variations of BFR with load and at optimum Φ_{global}

The characteristics curves of BSEC, BTE, and VE with load and average (optimum) Φ_{global} are shown in Fig. 6.3 through 6.5, respectively. At all load, the lowest BSEC is noticed with the TB-E3 blend in comparison to TB-E1, TB-E2, TB-E4, and TB-E5. However, the BSEC is found to be lower in *nr*-DFM (WP) and in PDM (in ascending order, PDM > *nr*-DFM (WP) >DFM with TB-E3) than DFM with TB-E3 blend. It may be due to the lower LHV of blended fuel as compared to LHV of the diesel fuels used in *nr*-DFM (WP) and in PDM. As BSEC is inversely proportional to BTE, hence, a lower BSEC means a higher BTE. Hence, the higher BTE is found with the TB-E3 as compared to that of other blends (Fig. 6.4). It is seen in Table 6.3 that the cumulative properties (density, LHV, viscosity, and oxygen content) of the blend TB-E3 is much better (as a fuel) than the other blends. Consequently, the BTEs with TB-E3 at

all loads are observed to be higher as compared to other blends. Hence, it can be ascertained that the composition in the blend of TB-E3 (72% diesel, 20% biodiesel and 8% diesel) is optimum. As a result, it releases optimum oxygen molecules, which support an efficient combustion. However, at all loads, the BTE in PDM is noted to be higher than the BTE in DFM. The reasons are the lower LHV, the higher self-ignition temperature of biogas, higher heat of vaporization of ethanol and higher viscosity of biodiesel than diesel fuel. Besides, the higher specific heat of CO_2 present in biogas reduces the adiabatic flame temperature with the consequence of lower laminar flame speed (Pizzuti et al., 2016). At 4.14 bar, the minimum and maximum increment of BTE (of 1.29% and 5.04%) are observed with the TB-E3 blend in contrast to BTE in *nr*-DFM (WP) and with TB-E1 blends. At 100% load (= 4.14 bar), the BTE with TB-E3 blend is estimated to be 26.73%. Whereas at the same load, the maximum of 14.58% increment of BTE is observed in PDM in comparison to DFM with TB-E3 blend. Nonetheless, in this study, the efficiency achieved at engine standard CR = 17.5 and IT = 23 CAD bTDC, is found to be substantially higher than earlier reported data (Bora and Saha 2014, Bora and Saha 2015a, Bora and Saha 2016b).

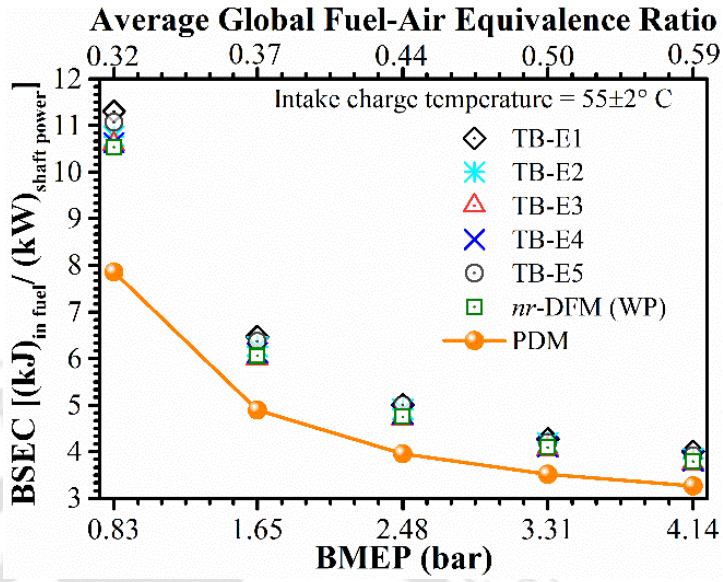

Fig. 6.3 Variations of BSEC with load and at optimum Φ_{global}

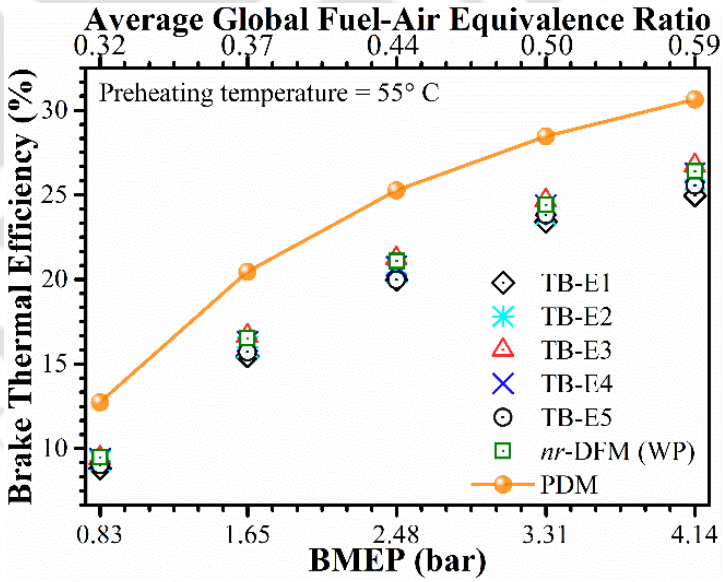

Fig. 6.4 Variations of BTE with load and at optimum Φ_{global}

The variations of VEs in DFM are found to be lesser but nearer to each other as shown in Fig. 6.5. It may be due to the close controlling of biogas flow rate and intake charge temperature. Moreover, the VE does not depend on the liquid fuel characteristics. The lower VE in DFM than PDM is due to the replacement of air volume by biogas. The reason behind the reduction of VE with a load in all modes of engine operations may be due to the enhancement of specific volume (with the increase of cylinder mean gas temperature) of the trapped residual gas inside the engine cylinder.

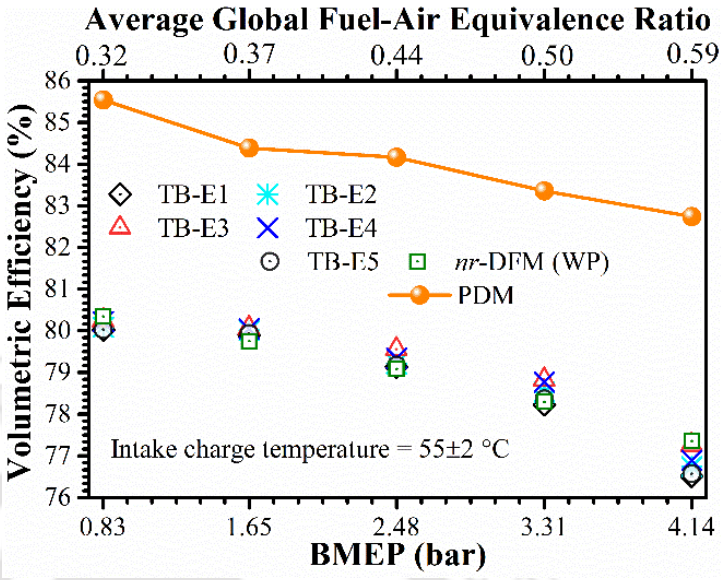

Fig. 6.5 Variations of VE with load and at optimum Φ_{global}

Figures 6.6 and 6.7 show the variations of Φ_{global} and $\Phi_{premixed}$ with loads. Φ_{global} is evaluated by considering both liquids (diesel and blended) as well as gaseous fuels. Further, in the estimation the $\Phi_{premixed}$, only biogas quantity is considered. Conversly, as there is a variations of LHV in different blended fuels including biogas, the variations of Φ_{global} are noticed to be higher in comparison to $\Phi_{premixed}$. It is because the fuel mass consumption is inversely proportional to fuel LHV. Here, the Φ_{global} is considered as the crucial parameter and constrained from lower to higher loads, in such a way that the consumption of liquid fuels in DFM at part loads and higher loads can be higher and lower, respectively. Simultaneously, the

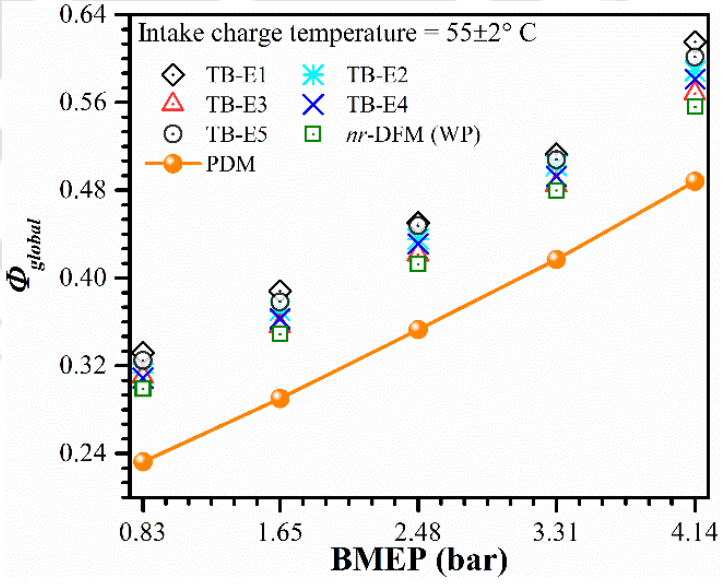

Fig. 6.6 Variations of Φ_{global} with load

biogas consumption from lower to higher loads can be vice versa to that of the consumption of the liquid fuel (Karim 1980). The confinement of the magnitudes of Φ_{global} from lower to higher loads, are already referred to in the previous section and can be seen in Fig. 6.6.

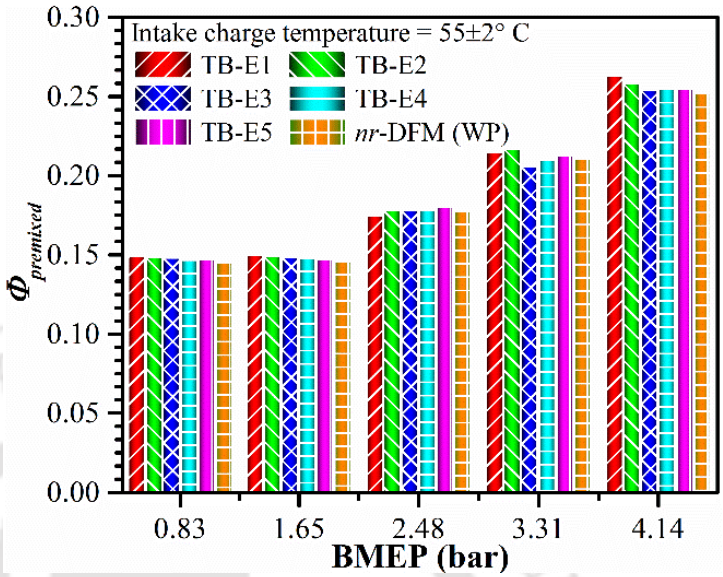

Fig. 6.7 Variations of $\Phi_{premixed}$ with load

The variations of blended and actual diesel replacements (ADR) are depicted in Fig. 6.8. Apart from the load of 0.83 bar, the replacements of blended fuel increase with the increase of load (1.65-4.14 bar). Experimentally, it is observed that a slight increment of biogas consumption at the load of 1.65 bar (relative to the load of 0.83 bar), increases the pollutant emission in the exhaust. Accordingly, at the load of 1.65 bar, the liquid fuel consumption increases that reduces the replacements of blended fuels. Another reason may be due to the lower engine speed at 1.65 bar as compared to the load of 0.83 bar. At all load, the maximum replacement is observed in *nr*-DFM (WP). Thus, it can be said that the maximum replacement within the blended fuels is attained with the TB-E3 blend (Fig. 6.8). The minimum and maximum replacements with TB-E3 blend are estimated as 31.16% and 39.64% at the load of 1.65 and 4.14 bar, respectively. Conversely, by considering the biofuel quantity in the blend, the ADRs are evaluated and presented in Fig. 6.8. The ADRs at the loads of 1.65 and 4.14 bar with the TB-

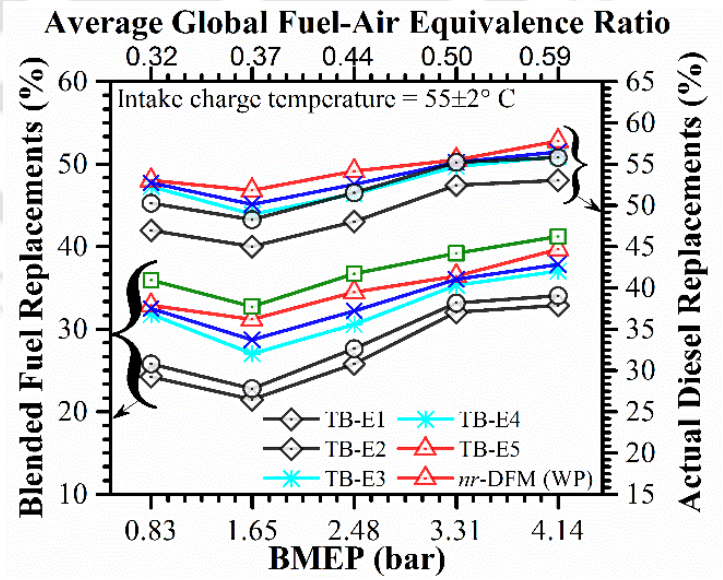

Fig. 6.8 Variations of fuel replacements with load

E3 blend are found as 51.81% and 57.75%, respectively, which are higher in comparison to the other blends. Although, in most of the cases, the ADRs achieved are greater than 50% (Fig. 6.8). Hence, the biofuels not only promote an efficient engine performance but also replace a substantial amount of petrodiesel. The results demonstrated that the biofuels have the great prospects to reduce the dependency on the imported fossil diesel fuel.

Figure 6.9 shows the biogas and blended fuel energy share with the applied load on the engine and average Φ_{global}. Biogas energy share at the load of 0.83 bar, is noticed to be higher for all the blended fuels. It may be due to the lower liquid fuel consumption at lower load. However, at this load, the BFR in the present study is found to be substantially lower (approximately 71.2%) in contrast to the reported data (Bora and Saha, 2016b). The trends of fuels energy share (i.e., lower BES at lower load and higher at higher loads) are maintained correctly from the load of 1.65 to 4.14 bar (= 100%). The higher BES at the load of 0.83 bar, may be due to the higher engine speed. Nevertheless, from the load of 1.65 bar, biogas and the blended fuel energy share increases and decreases, respectively, with the increase of the load. The maximum biogas energy share of 48.68% is observed at the load of 4.14 bar with TB-E3 blend. Simultaneously, at this condition (at 4.14 bar load and with TB-E3 blend), the blended fuel energy share will be lower and calculated as 51.32% as compared to other blends. The lower blended fuel energy share with the TB-E3 blend in DFM is the consequence of the improved engine performance with optimum cumulative properties of this blend.

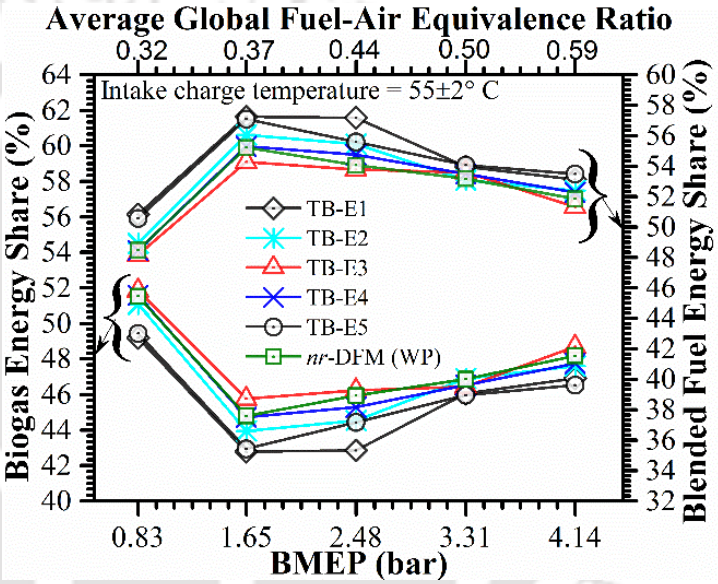

Fig. 6.9 Variations of fuel energy share with load

6.4 Combustion Analysis

The parameters considered in the discussion of combustion analysis are ID, cylinder pressure and NHRR history, CMGT and cycle-by-cycle variations of CPP.

The variations of ignition delay (ID) with engine load and average Φ_{global} is shown in Fig. 6.10. In the evaluation of ID, the engine static injection timing (23 CAD bTDC) is used as the start of injection of the fuel into the cylinder. In addition, the motoring curve (Figs. 6.11 and 6.12) is used to identify the start of combustion (SOC) of the fuel mixture inside the combustion chamber. The SOC can also be identified at a point where the NHRR (J/CAD) is equal to zero and rises abruptly after this point as indicated in Figs. 6.14 and 6.15. The ID is found to be lower with diesel fuel in PDM and it reduces with the increase of load. However, in DFM and with all the blended fuels, the IDs are found to increase with the increase of load (except the load of 1.65 bar) and Φ_{global}. The reasons may be due to the higher biogas consumption at higher loads (excluding the load of 1.65 bar), the higher self-ignition temperature of biogas and higher heat of vaporization of ethanol present in the blended fuels. Experimentally, it is observed that the BFR at the load of 1.65 bar is lower than that at the load of 0.83 bar. At the load of 0.83 bar and 4.14 bar, the maximum and minimum IDs in PDM are found as 11 and 9 CAD, respectively. Whereas, the lower IDs in DFM are observed in *nr*-DFM (WP) and with TB-E3 blend. Since, in *nr*-DFM (WP) pure diesel is used as the pilot fuel, having the lowest heat of vaporization and higher LHV. On the other hand, the intake charge preheating and the best cumulative properties of the blend TB-E3, assist in reducing the ID. Further, the higher IDs in DFM are observed in *nr*-DFM (WOP) and TB-E1 blends. The higher density of biogas (for the case without the intake charge preheating) enhances the mass consumption of this gaseous fuel, which has the very high self-ignition temperature thereby enhancing the ID. As well, the higher volume percentage of ethanol in TB-E1 blend makes it suitable to increase the ID as ethanol has the higher heat of vaporization than the diesel fuel. At the load of 4.14 bar, in *nr*-DFM (WP), with TB-E3, and TB-E1 blends, the IDs are approximately estimated as 13.5,

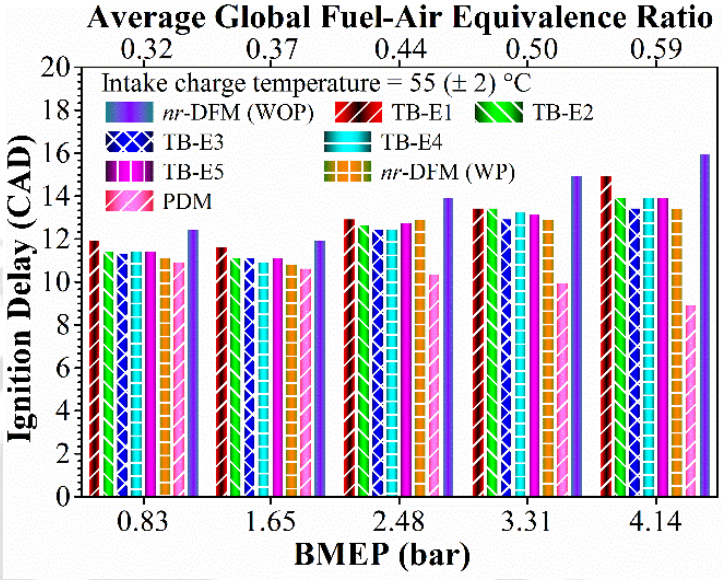

Fig. 6.10 Variations of ID with load

13.5, and 15 CAD respectively. While in *nr*-DFM (WOP), the IDs at loads of 1.65, 3.31 and 4.14 (=100%) bar, are evaluated as 12, 15, and 16 CAD, respectively.

Table 6.4 Peak pressure and corresponding positions of peak pressures with different fuels

Parameters	Load (bar)	Biogas-DFM				PDM
		WP			WOP	
		TB-E1	TB-E3	Pure diesel	Pure diesel	Pure diesel
Peak pressure (bar)	1.65	54.96	56.20	56.90	54.49	60.08
	3.31	61.00	62.82	64.04	60.46	70.07
	4.14	66.91	68.75	68.11	65.06	72.32
Positions (CAD)	1.65	367	367	367	369	366
	3.31	368	368	368	370	368
	4.14	369	369	369	371	368

Figures 6.11 and 6.12 show the variations of cylinder pressure distribution with the engine crank angle at the load of 1.65 and 4.14 bar, respectively. The magnitude of the peak pressure and the corresponding crank angle position of the peak pressure are important, as these are the essential criteria for an efficient combustion. The development of peak pressure nearer to the TDC means, the higher utilization of the engine expansion energy, better combustion, and lower loss of energy into the environment (Heywood 1988). Table 6.4 shows the values of peak pressure and the positions of the peak pressure with different blends and without/with preheating in DFM and in PDM.

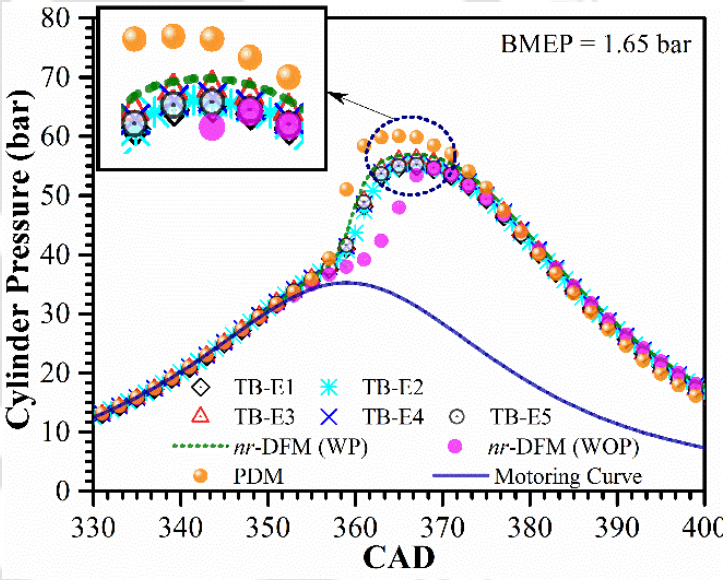

Fig. 6.11 Variations of (b) in-cylinder pressure with CAD (AL: 1.65 bar)

The minimum pressure peaks at all the loads are observed in *nr*-DFM (WOP). Further, these pressure peaks in *nr*-DFM (WOP) at different loads are found at a significant angular distance (degree of crank angle) to the right side of the TDC as compared to with preheating (Table 6.4). The reason may be due to the atmospheric state of the intake charge (in the case of without preheating), higher self-ignition temperature and lower LHV of biogas. The improvement of combustion efficiency with the intake charge preheating and with ternary blends of biofuels as

the pilot fuels can be discussed with respect to Fig. 6.12 and Fig. 6.13. Figure 6.13 shows the variations of pressure (*P*) distribution with the cylinder volume (*V*), where, the areas inside the *P*-*V* curves represent the work done by the engine in DFM and in PDM at different states. It is noticed in Fig 6.13 that the engine in *nr*-DFM (WOP) has done the minimum work as compared to the one with preheating. The loss of work, without preheating and the corresponding gain of work with preheating in *nr*-DFM (WP) and other ternary blends, is also indicated in Figs. 6.12 and 6.13. The similar loss and gain of work can also be seen in the Fig. 6.11. At all the loads, the maximum gain of energy is observed with the TB-E3 blend and minimum in *nr*-DFM (WP). As a result, more energy is gained in DFM with the intake charge preheating in contrast to the one without preheating. In addition, the extra oxygen in the blends of biofuels (biodiesel-ethanol blended with diesel) helps to burn more fuel molecules. Hence, the energy gained from the blended fuels is found to be more as compared to *nr*-DFM (WOP). Thus, in the study, the magnitude of peak pressures, the position of peak pressures and the trends of the history of pressures inside the cylinder in DFM with preheating and with biofuels are noticed to be very much similar to PDM operation (Figs. 6.11 through 6.13). Therefore, it can be said that at the engine standard CR and IT, the present investigation

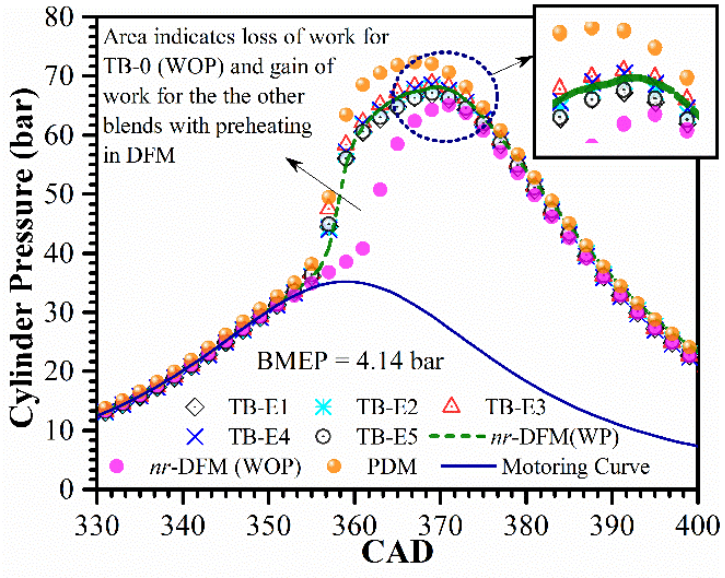

Fig. 6.12 Variations of in-cylinder pressure with CAD (AL: 4.14 bar)

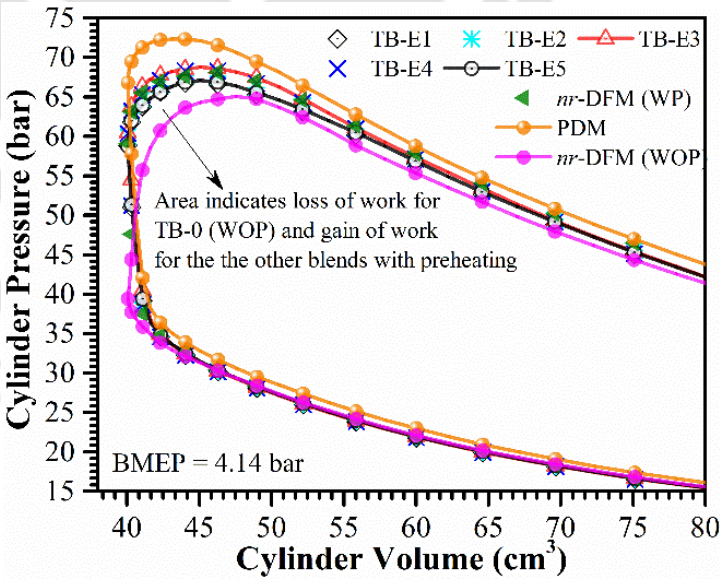

Fig. 6.13 Variations of in-cylinder pressure with vombustion chamber volume (AL: 4.14 bar)

achieves approximately the same diesel-like performance in DFM with ethanol and biodiesel blended with diesel and with intake charge preheating.

The characteristics curves of NHRR with engine crank angle at different states are shown in Figs. 6.14 and 6.15. It is a well-known fact that the development of NHRR and pressure inside the cylinder are internally related to each other. However, the NHRR greatly depends on the fuel characteristics and the experimental environment such as the state of air that is introduced inside the cylinder during engine suction. This is because the SOC is very much dependent on intake charge initial states. Furthermore, the SOC and the distribution of NHRR are internally related to each other. The peaks of the NHRRs, in *nr*-DFM (WOP), are found to be lower at all loads as compared to the one with preheating in DFM. With preheating, the peaks of the NHRRs are observed to be very close to the TDC (at 3 CAD bTDC). Whereas, without preheating and at all loads, the peaks of the NHRRs are noticed to occur after TDC. At the load of 1.65, 3.31, and 4.14 bar and without preheating, the positions of the peak of the NHRRs are identified at the CAD of 363, 364, and 365, respectively. Consequently, in the previous

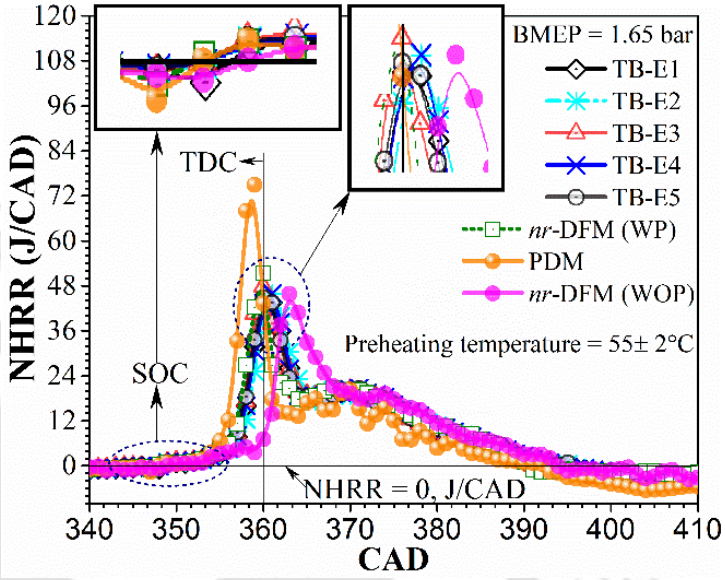

Fig. 6.14 Variations of NHRR with CAD (AL: 1.65 bar)

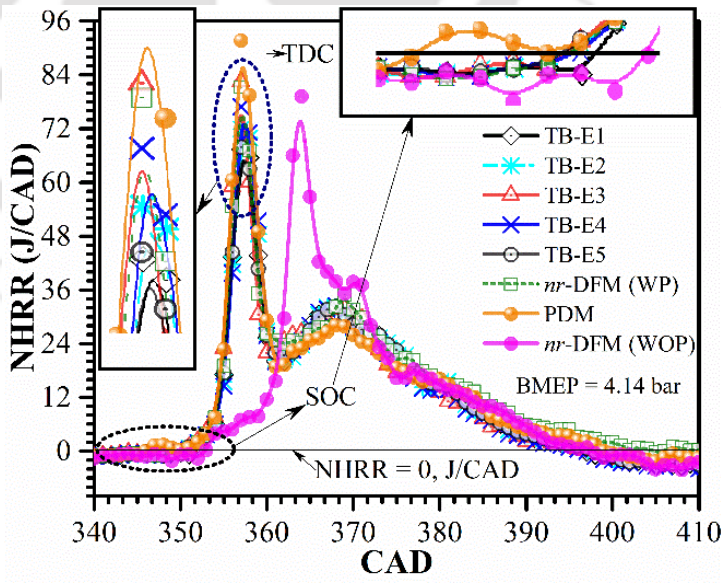

Fig. 6.15 Variations of NHRR with CAD (AL: 4.14 bar)

analysis, the work done without preheating is found to be lower as compared to the one with preheating and in the presence of biofuels in the blends. The maximum peak of NHRRs at part loads is found in *nr*-DFM (WP).

Throughout the investigation, at a particular load, there have been close controls of BFRs in all conditions. Therefore, the physical reasons for the variation of NHRR peaks at different states may be attributed to the varying properties of liquid fuels used in the study and the preheating of the intake charge. Thus, the maximum peaks of NHRR in *nr*-DFM (WP) may be due to higher LHV, lower viscosity and lower heat of vaporization of diesel fuel and preheating that helps to release more heat at part loads as compared to others blended fuels. While at higher loads, the maximum peaks are observed with the TB-E3 blends. It may be due to the release of more oxygen at higher loads in comparison to part loads that helps to release more heat. This is why there is a shifting of pressure and NHRR curves towards the TDC with preheating, thereby indicating an improvement of engine combustion from the part to higher loads. At the load of 4.14 bar, the maximum peak of the NHRR of 91.6 J/CAD is noticed in PDM. At the same load, the maximum peak of NHRR of 82.5 J/CAD is observed in DFM with TB-E3 blend.

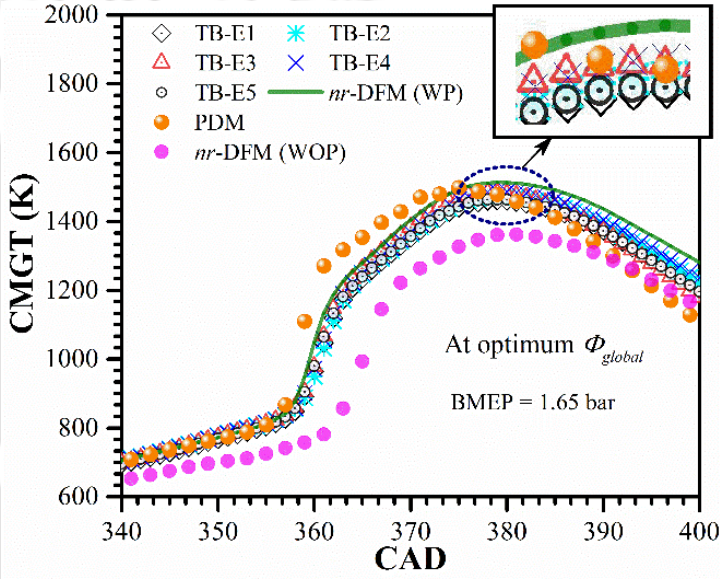

Fig. 6.16 Variations of CMGT with CAD (AL: 1.65 bar)

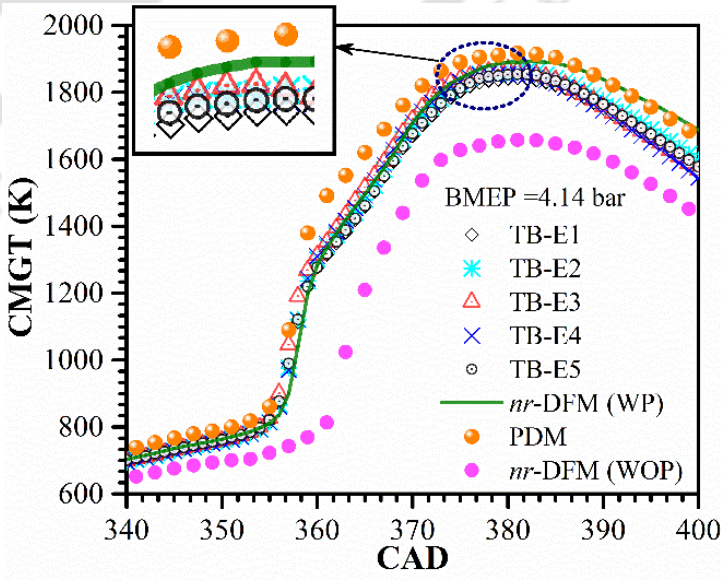

Fig. 6.17 Variations of (d) CMGT with CAD (AL: 4.14 bar)

Figures 6.16 and 6.17 show the history of cylinder mean gas

temperature (CMGT) with the engine crank angle. The higher the release of heat and the development of peak pressure inside the cylinder, the higher will be the peak of the CMGT inside the cylinder. Therefore, the physical reasons behind the development of CMGT are similar to that of the development of pressure and NHRR inside the cylinder. However, the preheating is identified as the key parameter to enhance the CMGT in contrast to the one without preheating in DFM (Figs. 6.14 through 6.17). As a result, at all loads, the minimum CMGT is evaluated in *nr*-DFM (WOP). At the load of 4.14 bar, the maximum CMGT of 1868.64 K is noticed with TB-E3 blend. At 4.14 bar (=100%), the values of the CMGTs with other blended fuels except TB-E3 and in *nr*-DFM (WOP/WP), are observed to be lesser concerning to that in PDM. However, the value of CMGT nearer to PDM is attained with TB-E3 blend. At this load, in PDM the maximum CMGT is calculated at 1917.27 K. At 4.14 bar, the CMGT in *nr*-DFM (WOP) is estimated to be 1657.37 K, which is minimum in contrast to other blends in DFM.

The cyclic variations are caused mainly due to the cycle-by-cycle variations in gas motion in the cylinder during combustion, variations in proportions of fuel and air in the mixture, and variations in mixture composition within the cylinder (Heywood 1988). Consequently, the cyclic variations in SI engine will be higher than the CI engine. Hence, owing to the use of gaseous fuels, there are comparatively higher cycle-by-cycle variations in DFM as compared to PDM. If there is a possibility to eliminate all the cyclic variations, then there would be a 10% increase in the power output for the same fuel consumption with weak mixtures (Stone 1999). The cyclic variation is generally identified with the distribution of the CPP relative to the number of cycles under investigation. The cycle-by-cycle variations of CPP with

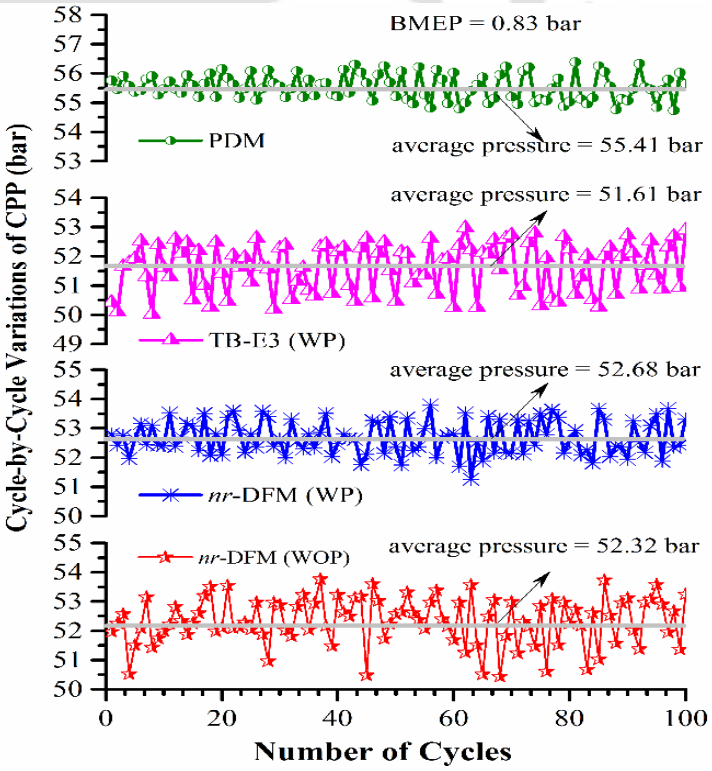

Fig. 6.18 Characteristics of Cyclic variations of CPP (AL: 0.83 bar)

various fuels and at different states in DFM and in PDM are shown in Figs. 6.18 and 6.19. The above discussion reveals that the lower cyclic variations are beneficial in terms of energy utilization along with the stable engine operation. In the present investigation, lower variations of CPPs with cycles are noticed with preheating in comparison to the one without preheating. It also reduces with the increase of loads. The lowest variation is noticed in PDM. The cyclic variations with the blended fuels are observed to be higher relative to that in *nr*-DFM (WP). However, it is noted to be lower than that in *nr*-DFM (WOP). The lower cyclic variation with blended fuels used in the present investigation is attained with the TB-E3 blend. The heat exchanger (CFHE) in the study assists not only to preheat but also it works like an efficient mixing device. That ensures preparing a homogeneous mixture of biogas-air and reduces the cyclic variations. The higher heat of vaporization of ethanol may assist to form a heterogeneous mixture and thereby exhibits higher cycle-by-cycle variations relative to pure diesel and with preheating.

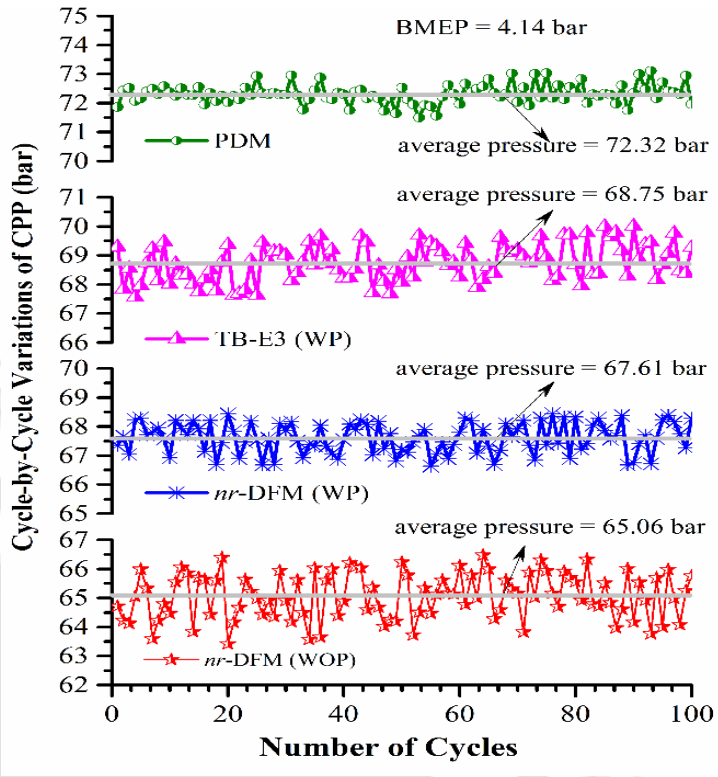

Fig. 6.19 Characteristics of cyclic variations of CPP (AL: 4.14 bar)

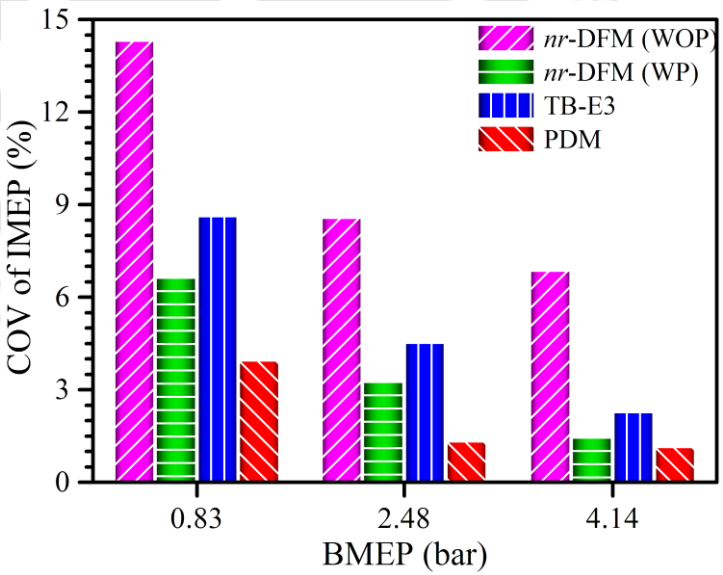

Fig. 6.20 Variations of COV of IMEP with load

The variations of COV of IMEP with load in PDM and in DFM are shown in Fig. 6.20. The COV is noticed to reduce with loads in all the cases. The lowest

COV is noticed in PDM, while the higher one is with *nr*-DFM (WOP). On the other hand, a slightly higher COV is noticed with TB-E3 as compared to *nr*-DFM (WP). Although, there are enough ignition centres (pilot fuel energy share ~50%) that help to enhance the flame speed, however, more homogeneuous dispersion of ignition kernels are necessary to reduce the COV with TB-E3. Therefore, an advanced and an optimized injection timing (IT) would reduce the COV to improve the engine performance.

6.5 Emission Analysis

The emission characteristics of CO, HC, and NO_x with engine loads and average Φ_{global}, are shown in Figs. 6.21 through 6.23. The CO emission in Fig. 6.21 shows the decreasing trends with the increasing of loads at different conditions except the emission in *nr*-DFM (WOP). In *nr*-DFM (WOP), CO is found to increase with the increase of load. However, at the load of 4.14 bar, the slight drop in CO emission is observed. In the investigation, minimum CO emission is achieved with the TB-E3 blend. The CO emission with TB-E3 is found to be approximately identical and adequately lower (at the loads of 3.31 and at 4.14 bar) than the PDM. It may be due to the proper controlling of fuel-air equivalence ratios at different loads, development of higher CMGT at the preheated atmosphere and release of extra oxygen during combustion of the oxygenated fuels present in the ternary blends.

At the load of 4.14 bar, the maximum CMGT of 1868.64, 1657.37 and 1917.27 K with TB-E3, in *nr*-DFM (WOP) and in PDM, respectively, are estimated. The CMGTs at all loads in *nr*-DFM (WOP) are found to be minimal in comparison to preheated biogas and with the other blends. The required threshold temperature to start the oxidation of CO to CO_2 is 1450 K as reported by Liu et al. (2013) and Karagoz et al. (2016). On the other hand, Glassman and Yetter (2008) has identified 1500 K to be the equilibrium reaction temperature for the reaction CO + OH = CO_2 + H. Irrespective of the quality of the fuels, Sjoberg

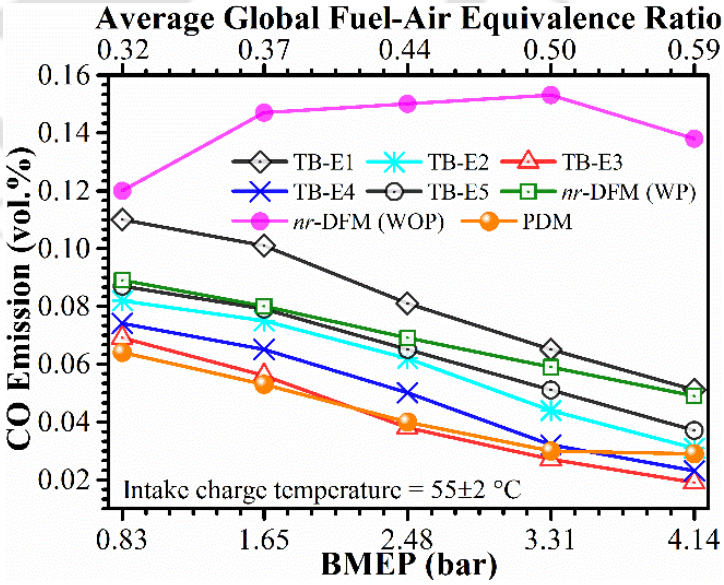

Fig. 6.21 Characteristics of CO emission with load and at optimum (average) Φ_{global}

and Dec (2005) in their experiments find that the CO emission drastically reduces from 1500 K to a higher temperature. Thus, due to the higher self-ignition temperature of biogas the CO emission in *nr*-DFM (WOP) is noticed to be higher in comparison to emission with preheated intake charge. At the load of 4.14 bar, the drastic reduction of CO emission with TB-E1, TB-E2, TB-E3, TB-E4, TB-E5, in *nr*-DFM (WP) and in PDM in comparison to *nr*-DFM (WOP) are found as 63.04, 77.54, 86.23, 83.33, 73.19, 64.49 and 78.99%, respectively. At the part load of 1.65 bar, the significant reduction of CO emission with TB-E1, TB-E2, TB-E3, TB-E4, TB-E5, in *nr*-DFM (WP) and in PDM in comparison to *nr*-DFM (WOP) are estimated as 31.29, 48.98, 61.90, 55.78, 46.26, 45.58 and 63.95%, respectively.

The unburned hydrocarbon (HC) emission is the consequence of incomplete combustion of hydrocarbon fuels. The most favorable circumstances that help to generate the emission of HC are locally over-rich or over-lean mixture, which makes the reaction rate slower. Other reasons are attributed to the very high self-ignition temperature of fuels, bulk quenching or extinction of the flame front due to the formation of the boundary layer at the cold cylinder wall and along with the effects of crevice volumes (Heywood 1988, Rakopoulos et al. 2016). In DFM, biogas having a very high self-ignition temperature can cool the combustion chamber wall with the consequence of higher HC emission. Moreover, the higher specific heat of CO_2 present in biogas (nearly 40% composition by volume) slows down the laminar flame velocity and makes a suitable environment to generate the HC (Pizzuti et *al*. 2016). It is known that the air in DFM is replaced by the same volume of inducted gaseous fuel. Thus, another reason for higher HC production may due to the lack of oxygen that needs to oxidize the hydrocarbon fuel. However, with intake charge preheating and use of oxygenated fuel can reduce the HC emission.

The HC is found to be lower with the increase of loads as seen in Fig. 6.22. The higher HC emission is found in *nr*-DFM (WOP), whereas, there is a lower HC with TB-E3 blend. In addition, the HC is found to be

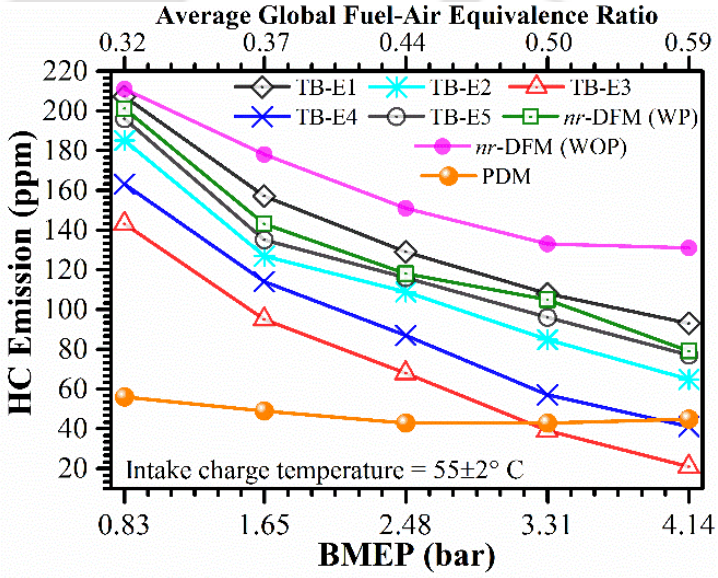

Fig. 6.22 Characteristics of HC emission with load and at optimum (average) Φ_{global}

lower with intake charge preheating with blended fuels in comparison to *nr*-DFM (WOP). It may be due to the release of extra oxygen at the hot (preheated) atmospheric condition that enhances the flame speed and improves the combustion of the fuel mixture. At the load of 4.14 bar, a substantial reduction of HC is achieved with the TB-E3 blend and it is about 83.97% relative to *nr*-DFM (WOP). While at this same load, HC emission drops by 29.01, 50.38, 68.70, 41.22, 39.69 and 65.65%, for TB-E1, TB-E2, TB-E4, TB-E5, in *nr*-DFM (WP) and in PDM, respectively, with respect to *nr*-DFM (WOP). The higher HC emission with TB-E1 blend is possibly due to the higher volume percentage of ethanol present in the blend. The reductions of HC emission with all the blended fuel in comparison to *nr*-DFM (WOP) are observed to be lower at part loads with respect to higher loads. It may be due to the higher auto-ignition temperature of biogas and higher heat of vaporization of ethanol that cools the cylinder wall temperature.

The NO_x emission is found to increase with the increase of loads (Fig. 6.23). The emission is noticed to be higher with the blended fuels and at the preheated state of the intake charge. According to the Zeldovich mechanism of NO_x formation (Heywood 1988), the nitrogen is oxidized mainly due to the oxygen-enriched atmosphere, higher flame temperature and a higher residence time of the burnt gas at the high temperature at oxygen-rich atmosphere. However, a more advanced mechanism of NO_x formation proposed by Kosmadakis et al. (2016), gives an extensive discussion on this issue under the various environmental temperatures inside the engine cylinder. Subsequently, the oxides of nitrogen are found to be more with the pure diesel mode and in DFM with the oxygenated fuels (different ternary blends of diesel-biodiesel-ethanol) along with the preheating of the intake charge. As well, the NO_x emission is observed to be lower in *nr*-DFM (WOP). However, with respect to PDM, the emission of NO_x in DFM is noticed to be lower in all states. It may be due to the lower temperature developed inside the cylinder in the presence of biogas that has the higher self-ignition temperature. At the load of 4.14 bar (=100%), the emission is found to be

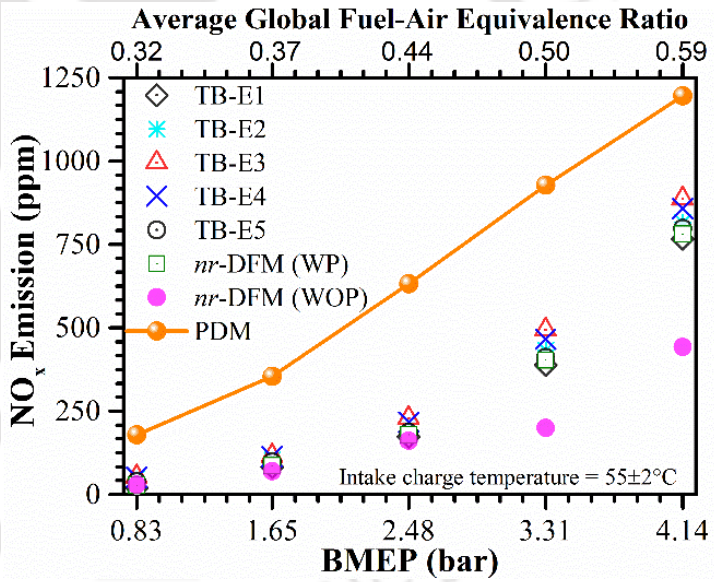

Fig. 6.23 Characteristics of NO_x emission with load and at optimum (average) Φ_{global}

maximum in all cases. Again, at this same load, the reduction of NO_x is calculated as 35.87, 31.77, 25.84, 28.34, 33.28 and 63.04%, with TB-E1, TB-E2, TB-E3, TB-E4, TB-E5, (WP) and *nr*-DFM (WOP), respectively. The emissions data (measured in ppm and vol.%) for the best belnd (TB-E3) are presented in Appendix-D.

6.6 Summary

In this chapter, the results of DFM (at the optimum Φ_{global} and with preheating) with ternary blends of diesel-biodiesel-ethanol (viz. TB-E1, TB-E2, TB-E3, TB-E4 and TB-E5) are summarized below:

Performance:

- The BFRs are observed to be confined within the ranges of 0.722-0.731 to 1.173-1.180 kg/h from the part (0.83 bar) to higher (4.14 bar) loads. Due to lower cumulative LHV than the pure diesel fuel, the higher BFRs are observed with the TB-Es fuel.
- The lower BSEC achieved with the TB-E3 blend in comparison to other blends. The BSEC achieved in ascending order can be expressed as PDM > *nr*-DFM (WP) >DFM with TB-E3. At 4.14 bar (=100% load), with TB-E3, the BTE is evaluated as 26.73% which is 1.29% and 5.04% higher than that in *nr*-DFM (WP) and with TB-E1 blends, respectively. At this load, the BTE in PDM is found to be higher by 14.58% than that in DFM with TB-E3 blend. A lower VE is found in DFM and higher reduction is found with preheating.
- At the loads of 1.65/4.14 bar, the higher LFRs are observed with TB-E3 blend and they are estimated to be 31.16%/39.64%. The maximum ADR is also noticed with TB-E3 blend. At the loads of 1.65/4.14 bar, the ADRs are found as 51.81%/57.75%. At 4.14 bar, the maximum BES is noticed to be 48.68% with TB-E3 blend and the corresponding BFES is found as 51.32%.

Combustion:

- The ID in PDM is found lower and reduces with the increase of loads, whereas in DFM the reverse trends are noticed. At the loads of 0.83 bar/4.14 bar, IDs in PDM are found as 11/9 CAD. In DFM, the ID reduces with the intake chare preheating. The lower IDs in DFM are achieved in *nr*-DFM (WP) and with TB-E3 blend. At 4.14 bar, the reductions of IDs in *nr*-DFM (WP) and with TB-E3 blend as compared to the one in *nr*-DFM (WP) are found to be 15.63%.

- In DFM, there is a shifting of CPP (CAD) as compared to the case of without preheating. The higher gain of energy is noticed with TB-E3 blend and in *nr*-DFM (WP) relative to that in *nr*-DFM (WOP). The peak of the NHRR in *nr*-DFM (WOP) is found to be lower and gets shifted towards the right of TDC. While, with preheating, the peak of NHRR is noticed to be closer to TDC (3 CAD bTDC). In DFM, at 4.14 bar, the maximum peak of NHRR of 82.5 J/CAD is observed in DFM with TB-E3 blend.
- The CMGTs are observed to be higher for preheating as well as with the blended fuels. At 4.14 bar, the higher CMGT of 1868.64 K is observed with TB-E3 blend. The cyclic variations with preheating, with the increasing of loads and with TB-E3 are noticed to be lower. The higher cyclic variations are attained in *nr*-DFM (WOP). The higher COV of IMEP is noticed with *nr*-DFM (WOP), and the lower one with (WP). A slightly higher COV as compared to *nr*-DFM (WP) is noticed with TB-E3. Therefore, it is recommended to advance the IT to lower the COV and improve the engine performance in DFM.

Emission:

- Overall, there is a substantial reduction of CO emission in DFM at the preheated state of the intake charge and with the use of oxygenated liquid fuels. At the loads of 1.65/4.14 bar, the maximum reduction of CO of 61.90/86.23% are noticed with TB-E3 blend as compared to *nr*-DFM (WOP). The trend of CO emission with the TB-E3 blend is found similar to that with PDM.
- Similar results for HC emission are also noticed with preheating and with the blended fuels. At 4.14 bar, a substantial reduction of 83.97% of HC with the TB-E3 blend relative to *nr*-DFM (WOP) is achieved. At the higher loads (>3.31 bar), the HC with the TB-E3 is found to be lower even than that in PDM. The lower NO_x is attained in DFM, however, found higher with preheating and with the blended fuels. A negligible emission of NO_x is attained at part loads and increases with the increase of loads. At 4.14 bar, the reductions of NO_x with TB-E1, TB-E2, TB-E3, TB-E4, TB-E5, *nr*-DFM (WP) and *nr*-DFM (WOP) as compared to PDM are estimated as 35.87, 31.77, 25.84, 28.34, 33.28 and 63.04%, respectively.

Chapter-7

Results of Biogas Run DFM Engine Using Ternary Blends (Diesel-Biodiesel-Butanol/ Diesel-Biodiesel-Diethyl Ether)

Chapter

Highlights:

- *Optimum Φ_{global}, preheating and the ternary blends of oxygenated fuels are found crucial parameters in DFM*
- *The shorter ID and CD and higher CMGT is observed with high cetane fuel (TB-DEE)*
- *Overall, the emissions in DFM are found to be lower than that in PDM*
- *The investigation recommends the oxygenated fuels blended with diesel for biogas DFM engine*

Overview: *In the previous chapter, various ternary blends (TB) of diesel-biodiesel-ethanol (D-B-E) are found to be beneficial to improve the overall performance of the biogas DFM engine. In this chapter, ternary blends of diesel-biodiesel-butanol (D-B-BT) (TB-BT) and diesel-biodiesel-diethyl ether (D-B-DEE) (TB-DEE) are considered. The optimum ternary blend (diesel-biodiesel-ethanol) in the previous chapter is brought in this chapter to compare the results and designated as TB-E. The volumes of butanol (BT) and diethyl ether (DEE) in the TB blends are prepared based on identical oxygen quantity (that is with the volume quantity of ethanol) in the optimum blend of TB-E. In TB-BT and TB-DEE, the compositions are estimated as D67-B20-BT13 and D67-B20-DEE13, respectively. The experiments have been carried out at the engine standard CR = 17.5 and IT = 23 bTDC. The results in nr-DFM (WOP), nr-DFM (WP), with the blends of TB-BT, TB-E, and TB-DEE are compared to each other along with the results of PDM. It is revealed that the biogas DFM engine overall performance at the optimum Φ_{global}, with the intake charge preheating and with the implementations of the oxygenated liquid fuels blended with diesel can be improved substantially from the part to higher loads. The results of DFM with the oxygenated fuels are found suitable and competitive to PDM, however, the best results are achieved with TB-DEE.*

Chapter Layout:

7.1 Selection of Pilot Fuels

It is evident from the results represent in the previous chapter that with the use of biodiesel and ethanol, blended with diesel (TB) fuel with the intake charge preheating, there is a significant improvement in the performance, combustion, and emissions of biogas run DFM engines. Therefore, in this study, butanol, diethyl ether (DEE), and biodiesel are considered as the oxygenated fuels blended with diesel. The TBs are considered and prepared as diesel-biodiesel-butanol (designated as TB-BT) and diesel-biodiesel-DEE (designated as TB-DEE). The properties of the individual fuels used in this study are presented in Table 7.1.

Table 7.1 Properties of fuels used in the present investigation (Nathan et *al*. 2010; Luijten and Kerkhof 2011; Sahoo et *al*. 2011b; Rakopoulos et *al*. 2014; Aleiferis and Behringer 2015)

Properties	**Biogas**	**Diesel**	**Jatropha Biodiesel**	**Bio-Ethanol**	**Butanol**	**DEE**
Chemical structure	-	$C_{12}H_{26}$	$C_{18.8}H_{35.1}O_2$	C_2H_5OH	$C_4H_{10}O$	$C_4H_{10}O$
C (wt.%)	-	84.7	77.08	52.2	64.87	64.87
H (wt.%)	-	15.3	11.99	13	13.51	13.51
O (wt.%)	-	-	10.93	34.8	21.62	21.62
Density (kg/m^3), at 32.2°C	1.096[a]	824.91[a]	873.36[a]	765.36[a]	809.48[a]	713
Heat of vaporization (kJ/kg)	-	250-270	-	840-904	585	355
Lower heating value (MJ/kg)	19.1[a]	42.1[a]	38.17[a]	26.97[a]	33.09[a]	33.9
Cetane number	-	50-53	51-58	5-11	25	>125
Kinematic viscosity (mm^2/s, at 40°C)	-	2.54[b]	4.218[b]	1.137[b]	3.7[a]	0.23
Bulk modulus of elasticity (bar)	-	16,000	-	13,200	15,000	13,000
Stoichiometric air-fuel ratio	6.17[a]	15.01[a]	12.52[a]	9.0[a]	11.2[a]	11.2[a]
Flashpoint (°C)	-	67.5-71	147-191	13-14	35	-40
Auto-ignition temperature (°C)	632-813	200-220	-	-	385	160
Flammability limits (% by volume of air)	7.5-14	1.5-7.6	-	-	1.4-11.2	-

[a]calculated; [b]measured

7.2 Design of Experiments

The design of experiments in the present study is almost similar to that discussed in the previous chapter. The tests are conducted at the same ranges of the optimum Φ_{global} and loads. However, the pilot-fuels chosen are TB-BT and TB-DEE, and the experiments are carried out with these

blends with intake charge preheating. The results of the optimum blend TB-E3 (here it is designate as TB-E) in the previous chapter (Chapter 6) are brought to compare the results that obtained with TB-BT and TB-DEE. The experimental matrix is represented in Table 7.2.

Table 7.2 Experimental Matrix

Parameters	**PDM**	**DFM (Raw biogas)**				
		With preheating (WP) (55 ±2° C)				**WOP**
Fuel/ Blended Fuel	Diesel	*nr*-DFM	TB-E	TB-BT	TB-DEE	*nr*-DFM (WOP)
Φ_{global}/Load (bar)	0.23/0.83-0.48/4.14	0.29-0.42/0.83, 0.35-0.46/1.65, 0.40-0.52/2.48, 0.47-0.57/3.31 and 0.54-0.61/4.14				

The blends, TB-BT and TB-DEE are prepared with reference to TB-E. The volume percentage of butanol (BT) and DEE in TB-BT and TB-DEE are considered depending upon the oxygen amount, which is equal to that of ethanol in TB-E, respectively. While, in all blends, the volume percentage of biodiesel is kept intact. Therefore, the total oxygen in each blend will remain the same. The properties of the blended fuels estimated with the Lever law (Rakopoulos et *al.* 2016a) are shown in Table 7.3.

Table 7.3 Properties of the blended fuels

Properties	**Blended Fuels**		
	TB-E (D72-B20-E8)	**TB-BT (D67-B20-BT13)**	**TB-DEE (D67-B20-DEE13)**
Density (kg/m^3)	828.65	832.59	820.05
LHV (kJ/kg)	39874.2	40136.73	40336.06
Viscosity (mm^2/s)	2.76	3.04	2.64

7.3 Performance Analysis

The parameters considered here are BFR, BSEC, BTE, fuel energy share, liquid fuel replacements, global and premixed fuel-air equivalence ratios.

The variations of BFR at the part load of 0.83 bar and the higher load of 4.14 bar are depicted in Fig. 7.1. The BFRs from part to higher loads are modulated depending upon the parameter Φ_{global} (optimum). Here, Φ_{global} is the function of the mass of air and biogas inducted, and the mass of fuel (pilot) injected into the combustion chamber. The aim of the investigation is to achieve the efficient overall performance (performance, combustion, and emission) of a biogas DFM engine. As the experiments are carried out at the optimum Φ_{global} (at each of the applied load on the engine), hence, at a particular load, the marginal variations of BFRs with various TBs are observed (Fig. 7.1). These nominal variations of BFR might be due to the experimental

uncertainties. At the part load of 0.83 bar, the higher BFRa are noticed with the TB-DEE blend and in *nr*-DFM (WOP). The BFRs with other blended fuels are found to be more or less similar. However, the higher BFR with TB-DEE indicates an improvement of the engine performance. Because of the case of without preheating, more biogas is inducted inside the cylinder, hence, in *nr*-DFM (WOP), the BFR rises as compared to other states in DFM. At all loads, the BFR with TB-BT is estimated to be lower than TB-E and TB-DEE. It may be due to the higher viscosity and density of this blended fuel (TB-BT) as indicated in Table 7.3. The consequence is the higher liquid droplet size that hinders complete combustion. This reduces the ability to take more biogas in DFM with TB-BT blend. The effects of higher viscosity and density are discussed later in the analysis of combustion of the engine.

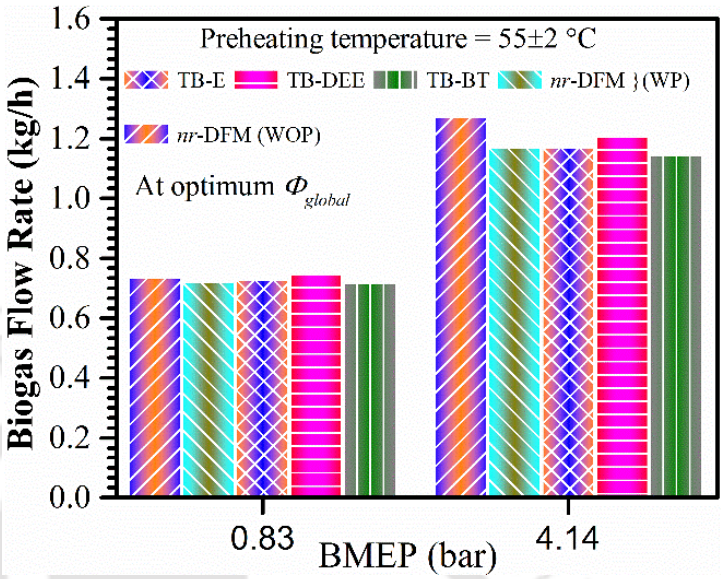

Fig. 7.1 Characteristics of BFR with load

At higher loads, due to the enhancement of in-cylinder pressure and corresponding augmentation of cylinder mean gas temperature (CMGT), the ability to burn the higher-octane fuel in DFM engine increases substantially. This attributes the increasing capability to consume biogas at higher loads of the DFM engine. At 0.83 bar, in *nr*-DFM (WOP), the BFR is noticed as 0.736 kg/h. At this load, the reductions of BFRs with TB-BT, in *nr*-DFM (WP), and with TB-E as compared to *nr*-DFM (WOP) are found as 2.13%, 1.96%, and 0.77%, respectively. Whereas, there is an increment of 1.68% of BFR with TB-DEE blend relative to *nr*-DFM (WOP) is found. At the higher load of 4.14 bar, the BFR with *nr*-DFM (WOP) is estimated to be 1.27 kg/h which is higher in DFM. Whereas, at this higher load, the corresponding reductions of BFRs with TB-BT, in *nr*-DFM (WP), with TB-E and TB-DEE in comparison to *nr*-DFM (WOP) are estimated as 10.14%, 8.01%, 7.94%, and 5.16%, respectively. The variations of BFRs in the present investigation are somewhat similar to that have been reported by Makareviciene et al. (2013), Barik and Murugan (2014), Barik and Murugan (2016), and, Barik and Murugan (2016a). Most of the researchers (Sahoo, 2011; Debnath, 2013; Bora, 2015;

Verma et al. 2017a) carried out the investigation in DFM at very high BFR (~1.8-3.5 kg/h, at which the misfire appeared) to replace a very high amount of diesel fuel.

The BSEC is defined as the ratio of input fuel energy per unit time to engine power output. Therefore, this parameter has the ability to qualify the suitability of fuel in an engine. The lower input power and the corresponding higher output power is always desirable. Consequently, the higher BSEC means an inefficient utilization of fuel and vice versa. Thus, the reduction of BSEC at higher loads indicates efficient utilization of the fuel input energy. However, the inducted fuel biogas has a very high self-ignition temperature, lower LHV, and CO_2 (the ignition inhibitor agent) present in biogas as the major constituent (Luijten and Kerkhof, 2011). Hence, the internal relations among the parameters such as inducted air and biogas, and the injected pilot fuel is crucial, which can be expressed in terms of Φ_{global} (Bedoya et al. 2009). Besides, the DFM engines generally suffer from the deficiency of oxygen due to the replacement of fresh air with the inducted gaseous fuel (Sahoo 2011, Bora 2015, Barik and Murugan 2016a). Hence, optimization of Φ_{global}, preheating of the intake charge and using of renewable oxygenated fuels can ensure the efficient utilization of the fuels in DFM. The variation of BSEC with loads is portrayed in Fig. 7.2 in which the effects of the optimization of Φ_{global}, preheating of the intake charge and using of renewable oxygenated fuels are considered. With these combinations (with optimum Φ_{global}, preheating, and using of renewable oxygenated fuels), the BSEC is noticed to be sufficiently lower even at part loads as compared to the reported data (Bora and Saha, 2014; Bora and Saha, 2015a; Bora and Saha, 2016a; Verma et al., 2017a). The BSEC is observed to be higher at part loads and reduces with the increase of loads. In ascending order, the BSECs in PDM< with TB-DEE< with TB-E< in *nr*-DFM (WP)< with TB-BT< in *nr*-DFM (WOP), are noticed. At the part and higher loads of 0.83 and 4.14 bar, the BSEC in *nr*-DFM (WOP) are evaluated as 10.87 and 3.97 kJs^{-1} in

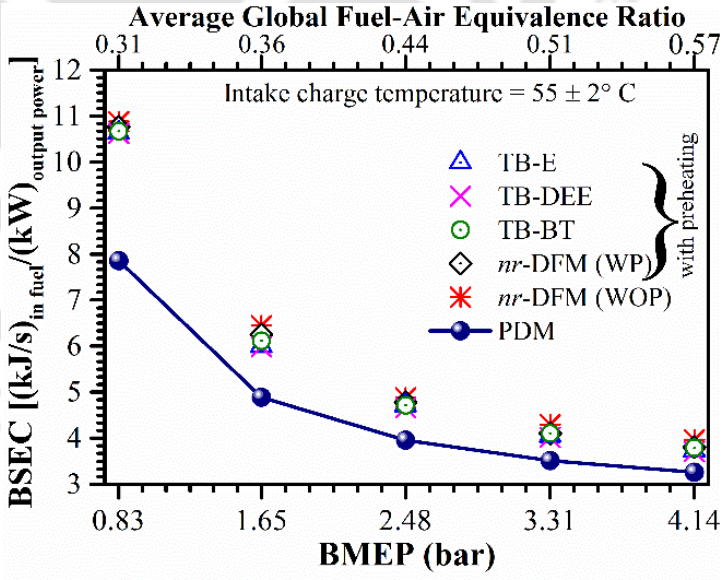

Fig. 7.2 Characteristics of BSEC with load

fuel/kW, respectively, which are higher in comparison to the BSECs in *nr*-DFM (WP), with the blends of the oxygenated fuels (TB-BT, TB-E and TB-DEE) and in PDM. At 0.83 bar, the reductions of 1.01% , 1.88% , 2.20% , 2.26% and 27.73% of BSECs are noticed in *nr*-DFM (WP), with TB-BT, TB-E, TB-DEE and in PDM with reference to *nr*-DFM (WOP), respectively. At 4.14 bar, the similar order of reductions of BSECs in *nr*-DFM (WP), with TB-BT, TB-E, TB-DEE and in PDM relative to the one in *nr*-DFM (WOP) are estimated as 3.91%, 4.31%, 5.66%, 6.27%, and 17.67%, respectively. Hence, the results indicate that with preheating and with the use of the oxygenated fuels in comparison to *nr*-DFM (WOP) there is a marginal improvement of fuel utilization at part loads and sufficiently higher at higher loads.

The characteristics of CA50 with loads in PDM and in DFM with various pilot fuels are portrayed in Fig. 7.3. In DFM, the CA50 is noticed to have advanced with loads. However, there is a little variation of CA50 with load for the case without preheating. For the blended oxygenated fuels, a relatively retarted CA50 is noticed with TB-BT, and the advanced CA50 is observed with TB-DEE, whereas the itermediate one is obtained with TB-E. The advanced CA50 with TB-DEE may be due to the very high cetane number of DEE (>125), which promotes the occurrence of early stage of SOC. On the other hand, a comparatively retarted CA50 with TB-BT is probably due to the higher viscosity of butanol that leads to the bigger fuel droplet size and therby taking longer time to evaporate.

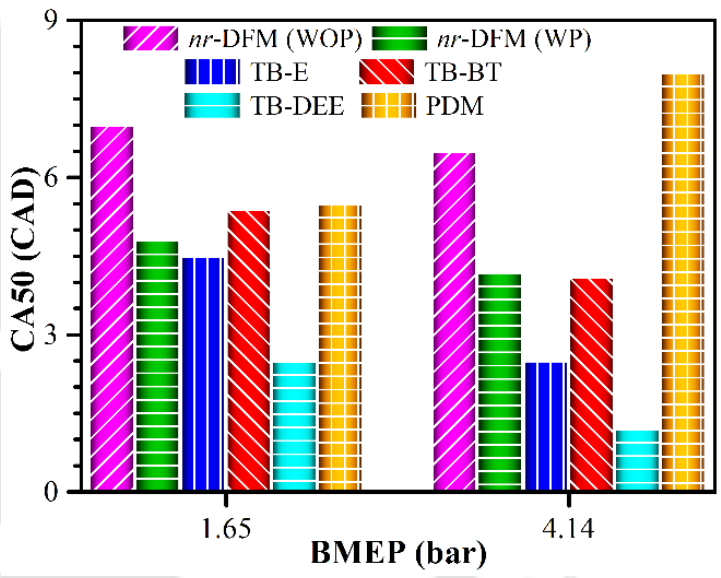

Fig. 7.3 Characteristics of CA50 with load

The parameter BTE is inversely proportional to the parameter BSEC. Therefore, the physical reasons for the variations of BTE with loads (Fig. 7.4) are similar to that with BSEC. In all cases, the lower BTE is observed in *nr*-DFM (WOP). At the loads of 0.83 and 4.14 bar, the BTEs in *nr*-DFM (WOP) are calculated as 9.20% and 25.22%, respectively. At 0.83 bar, in comparison to *nr*-DFM (WOP), the increment of BTEs in *nr*-DFM (WP), with the blends of TB-BT, TB-E, TB-DEE and in PDM is estimated as 1.02%, 1.91%, 2.13%, 2.31% and 38.37%,

respectively. At 4.14 bar, the enhancement of BTEs in *nr*-DFM (WP), with the blends of TB-BT, TB-E, TB-DEE and in PDM as compared to the one in *nr*-DFM (WOP) are found as 4.07%, 4.50%, 6.00%, 6.69% and 21.46%, respectively. In the present research work, a sufficiently higher BTE is found than the one obtained (at optimum advanced IT = 29 CAD bTDC and CR = 18 using pure rice bran biodiesel as the pilot fuel) by Bora (2015). The reasons may be attributable to the very higher rate of biogas consumption at which misfire has been encountered. Besides, he has used pure biodiesel as the pilot fuel. However, according to IEA report (OECD/2011), up to 20% of biodiesel by volume blended with diesel can efficiently be used in diesel engines. Nevertheless, pure biodiesel has a considerably higher viscosity (approximately two times) and density than diesel fuel (Table 7.1). Hence, due to higher surface tension, there could be the formation of coarse droplets at the end of injection of the pilot fuel instead of a fine one. It is to be noted that the investigator (Bora, 2015) has carried out a contemporary investigation in a DFM engine at various advanced ITs and CRs with the aim of maximum use of biogas and 100% replacement of diesel fuel with biodiesel fuel. In the present investigation, the higher BTE in DFM with TB-DEE may be due to the relatively higher advancement of CA50 than the ones with TB-E and TB-BT. However, the lower increment of BTE may be due to the higher CD associated with the advanced CA50.

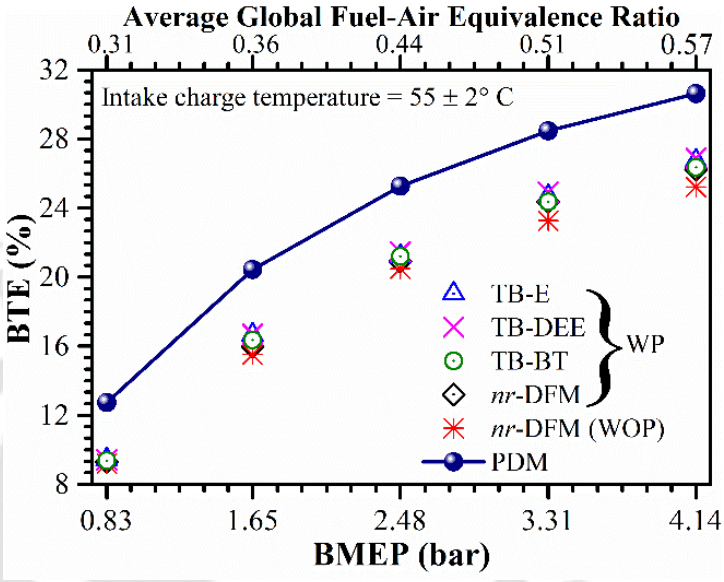

Fig. 7.4 Characteristics of BTE with load

The variations of biogas energy share (BES) and blended fuel energy share (BFES) are shown in Fig. 7.5. In all states, higher BES is noticed at the minimum applied load of 0.83 bar. While, at the load of 1.65 bar, it comes to the lowest level. Thereafter, the BES increases with the increase of loads. The higher BES at, the lower load of 0.83 bar may be due to higher engine speed and lower in-cylinder temperature (CMGT) that allow consuming more amount of biogas. Further, in the trial run of the engine in DFM, higher emissions of CO and HC are observed at the load of 1.65 bar. Hence, the BFR is reduced in such a way that there could be

a reduction of CO and HC emissions with preheating as compared to the one without preheating. Besides, there is a reduction of engine speed at the load of 1.65 bar than 0.83 bar. Therefore, these reasons are attributed to the reduction of BES at the load of 1.65 bar than the other applied loads. Thus, the trends of the BES and BFES are found as that can be seen in Fig. 7.5. In the analysis, the energy shares at various loads with *nr*-DFM (WOP) are considered as the reference frame. At all loads, the higher BES is noticed with TB-DEE, and lower is found with TB-BT.

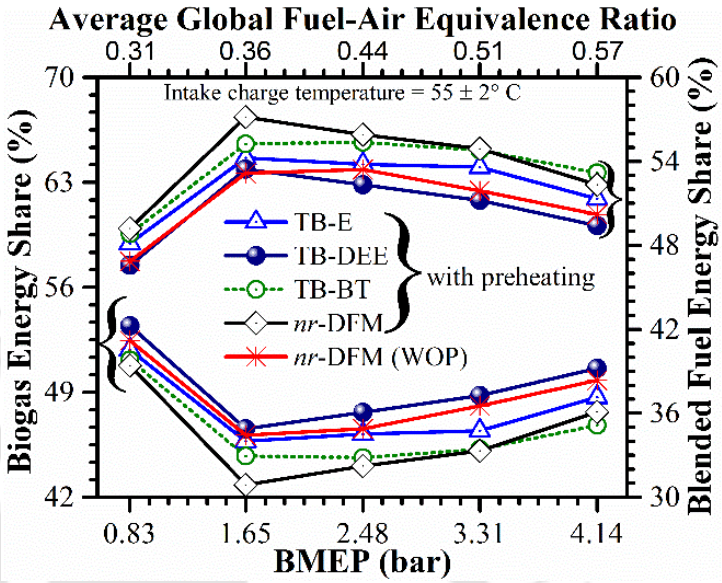

Fig. 7.5 Variations of biogas and blended fuel energy shares with load

At the load of 0.83 bar, the BES and BFES in *nr*-DFM (WOP) are attained as 52.45% and 46.85%, respectively. Whereas, at 4.14 bar, the BES and BFES are observed at 49.80% and 50.20%, respectively. At 0.83 bar/4.14 bar, the BESs are estimated to be reduced by 3.17%/4.24%, 2.44%/5.99%, and 1.16%/2.24% in *nr*-DFM (WP), with the blends of TB-BT, and TB-E, as compared to *nr*-DFM (WOP), respectively. Whereas, at 0.83 bar/4.14 bar, the increment of BESs with TB-DEE blend relative to the one in *nr*-DFM (WOP) are found to be 1.89%/1.63%. The reduction or increment of BES means the vice versa of BFES. Thus, at 0.83 bar/4.14 bar, the BFES in *nr*-DFM (WP), with TB-BT, and TB-E, are assessed to increase by 5.04%/5.95%, 4.23%/4.21%, and 2.80%/2.22%, respectively, as compared to *nr*-DFM (WOP). While, at these loads (0.83 bar/4.14 bar) the BFESs are observed to increase by 0.61%/1.61% as compared to *nr*-DFM (WOP), respectively. The higher cetane number of DEE in TB-DEE helps to augment the combustion process. Hence, with the increase of loads the BES and the corresponding BFES with the blend TB-DEE are observed to increase and decreased, respectively. A similar trend of energy share is also observed by Barik and Murugan (2014).

The variations of liquid fuel replacements (LFR) and actual diesel replacements (ADR) are depicted in Fig. 7.6. The LFR (blended and diesel fuel replacements) is the consequence of consumption of gaseous fuels and both are balanced to keep the engine speed intact to that of PDM at a particular load. Therefore, the trend of LFR will be more or less similar to that of

gaseous fuel (biogas) energy share as reflected in Fig. 7.6. The replacements in *nr*-DFM (WP) and with the blended fuels are found to be higher than that in *nr*-DFM (WOP). The reasons are attributed to the effects of preheating at optimized Φ_{global} that helps to faster the reaction and to accelerate the flame propagation upon releasing of extra oxygen on combustion of oxygenated fuels. At 0.83 bar, the LFR in *nr*-DFM (WOP) is acquired as 28.04%. With reference to these combinations (LFR at 0.83 bar in *nr*-DFM (WOP)), the replacements in *nr*-DFM (WP), with TB-BT, TB-E, and TB-DEE are noticed to rise by 5.86%, 3.92%, 4.84%, and 7.74%, respectively. At 4.14 bar, the LFR in *nr*-DFM (WP), with the blends of TB-BT, TB-E, and TB-DEE are found to increase by 5.08%, 0.27%, 3.50%, and 6.50%, respectively as compared to *nr*-DFM (WOP). However, there is a lucrative amount of ADR (considering, the mass of liquid renewable oxygenated fuels blended with the diesel). It is a noticeable matter that the benefits of higher replacements (70%-90%) of liquid fuels are termed as the higher use of biogas (Sahoo, 2011; Bora and Saha, 2014; Bora, 2015; Verma et al., 2017a) as the cheaper renewable fuels. However, liquid fuel inside the injector serves as a coolant to maintain the nozzle tip temperature within a limit. Hence, a very high replacement of liquid fuel can lead to burnout of the nozzle tip concerning the long-term run of the DFM engine, and there will be a higher probability of incomplete combustion. At

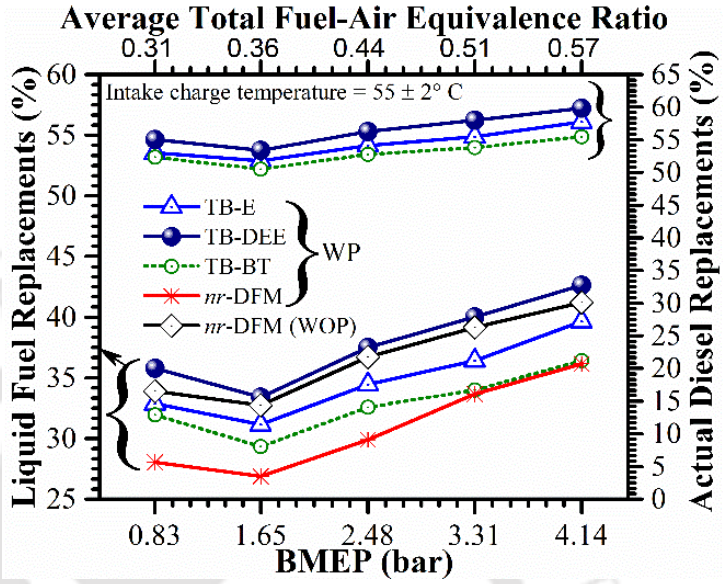

Fig. 7.6 Variations of LFR and ADR with load

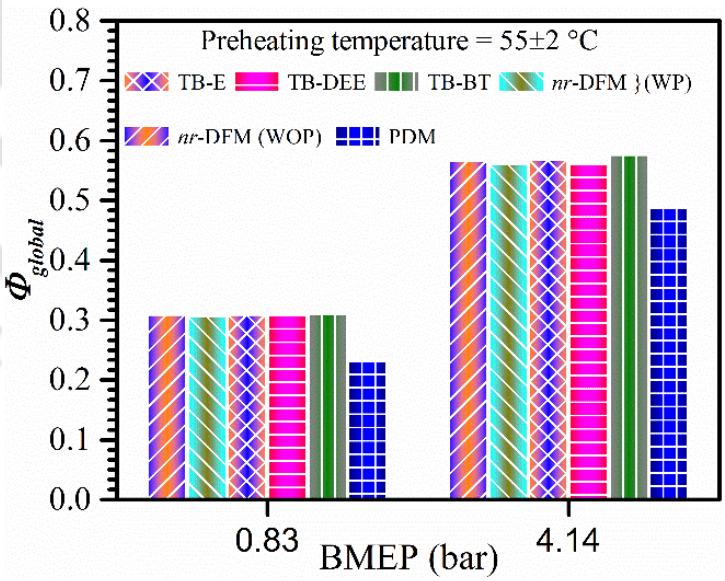

Fig. 7.7 Variations of Φ_{global} with load

0.83 bar, the ADRs are estimated as 52.37%, 53.01% and 55.04% with TB-BT, TB-E, and TB-DEE, respectively. At 4.14 bar, the ADRs with TB-BT, TB-E, and TB-DEE, are calculated as 55.49%, 57.75%, and 59.84%, respectively. The higher ADR with TB-DEE may be due to an improvement of combustion in engine in DFM. It may be due to very high cetane number and the better cumulative properties of TB-DEE (Table 7.3).

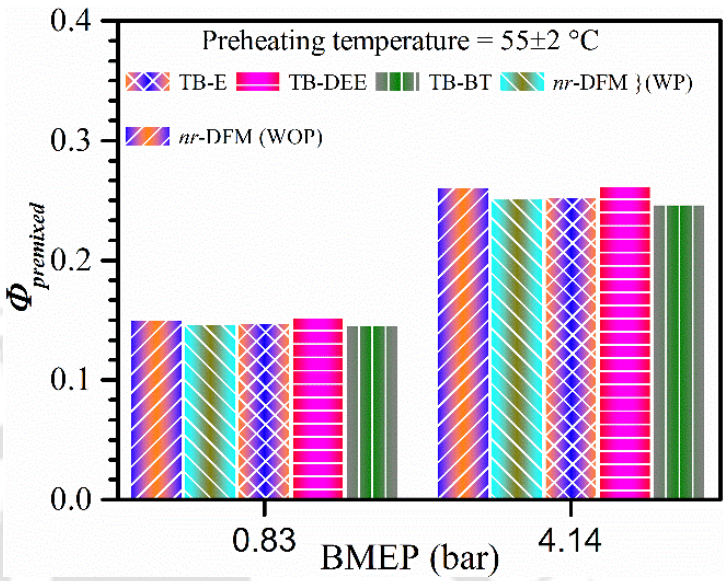

Fig. 7.8 Variations of Φ_{global} with load

The variations of Φ_{global} and $\Phi_{premixed}$ with loads are shown in Figs. 7.7 and 7.8. The optimum but average Φ_{global}/load (bar) are noticed as 0.31/0.83, 0.36/1.65, 0.44/2.48, 0.51/3.31 and 0.57/4.14, respectively. The average $\Phi_{premixed}$ at the load of 0.83 bar and 4.14 bar are calculated as 0.15 and 0.26, respectively. The values of $\Phi_{premixed}$ are varied in between of these two 'part and higher' loads.

7.4 Combustion Analysis

Here, the combustion behaviors of the engine are characterized by considering the parameters such as ID, in-cylinder pressure and NHRR history, CD, CMGT, exhaust gas temperature (EGT) and cycle-by-cycle variations of CPP.

The variations of ID with loads are presented in Fig. 7.9. The ID is the crank angle measurement between the point of static injection of liquid fuel and the point at which the NHRR = 0, J/CAD (SOC) and from which it steeply rises as seen in Figs 7.12 and 7.13. In all states, the lower ID is noticed with preheating of the intake charge. Minimum ID is found with TB-DEE and maximum in *nr*-DFM (WOP). However, the blend TB-BT exhibits a higher ID than the other blends. It may be due to the higher viscosity of the blend TB-BT (Table 7.3). Therefore, the higher surface tension of this blended fuel enhances the size of the fuel droplets that takes a long time to evaporate. The higher ID is observed in DFM as compared to PDM. It may be due to the higher self-ignition temperature of biogas. Another interesting observation at the time of experiments is that the reduction of peak pressure of fuel inside the injector due to the decrease in peak pressure of the combustion chamber in DFM than PDM. This is attributed to the higher

spray droplet size, and the consequence is the higher ID (Heywood 1988). At 0.83 bar, the reductions of IDs in *nr*-DFM (WP), in PDM, with TB-BT, TB-E, and TB-DEE as compared to the one in *nr*-DFM (WOP) are noticed as 10.4%, 12%, 7.2%, 8.8% and 13.6%, respectively. The higher reduction of ID is noticed at higher loads. However, the IDs, in *nr*-DFM (WP), with TB-BT and TB-E are increased with the increase of loads relative to the ID with TB-DEE and in PDM. It may be owing to very high cetane number of DEE that causes an early SOC of the fuel mixture.

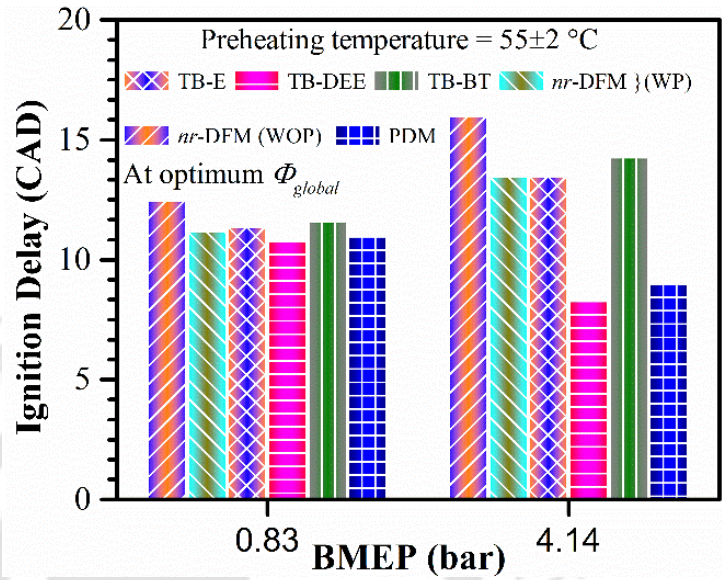

Fig. 7.9 Variations of ID with load

On the other hand, very high CPP and CMGT developed inside the combustion chamber in PDM reduce the ID. At the higher load of 4.14 bar, the IDs in *nr*-DFM (WP) and PDM, with TB-BT, TB-E, and TB-DEE are found to reduce by 15.63%, 43.75%, 10.63%, 15.63% and 48.13%, respectively, in comparison to *nr*-DFM (WOP). The ID in the present study is found to be substantially lower than the one estimated by Bora and Saha (2014), Bora and Saha (2015a), Bora (2015). It may be due to the consumption of a very high amount of biogas. They have (Bora and Saha, 2014; Bora and Saha, 2015a; Bora 2015) considered the static injection timing of 23 CAD bTDC (337 CAD) to estimate the ID and have found the IDs within the range of ~23-30 CAD, however, the NHRR, or in other words, the SOC has been noticed before to the TDC (360 CAD). The variations of ID can also be expressed with the Arrhenius equation (Aklouche et al., 2018) as below:

$$ID = z1 \times \Phi_{global}^{z2} \times p^{z3} \times exp\left(-{}^{E_A}/_{RT_{CMGT}}\right) \quad (7.1)$$

where, z1, z2, and z3 are the constants, and E_A, R, T_{CMGT} are the activation energy of the fuel (kJ/kg), universal gas constant (J/kg K) and the cylinder mean gas temperature (K). This equation indicates that higher the Φ_{global}, higher will be the ID. Whereas, lower the E_A and higher the T_{CMGT}, lower will be the ID. The term E_A is inversely proportional to the cetane number. Consequently, at the optimum Φ_{global}, the lower ID with TB-DEE is obtained due to

the higher cetane number of DEE. Hence, optimization of Φ_{global} in DFM is crucial to get the efficient results in DFM. In the present investigation, similar results of ID are obtained as that of Barik and Murugan (2014).

The characteristics of the in-cylinder pressure histories in different modes of engine operation and with various oxygenated fuels blended with diesel are shown in Figs 7.10 and 7.11. Cylinder pressure history is the key parameter to characterize and to generate the parameters that are essential to understanding the engine combustion behavior. In this investigation, the higher CPP is observed in PDM. However, with preheating and with the blended fuels, the CPPs are noticed to be significantly higher than the one estimated without preheating. The magnitude of CPPs and the corresponding crank angle positions with preheating, and with various blended fuels relative to *nr*-DFM (WOP) at the loads of 1.65 bar and 4.14 bar are presented in Table 7.4. At the part load of 1.65 bar and higher loads of 4.14 bar, the CPPs (bar)/CAD in *nr*-DFM (WOP) are found as 54.49/369 and 65.06/371, respectively. In DFM, at all loads, the maximum CPPs are observed with the TB-DEE blend. It may be due to very high cetane number (>125) of DEE and, hence, pretends as an ignition improver. This is attributed to the early starts of SOC in presence of DEE and, diminishes the effects of the

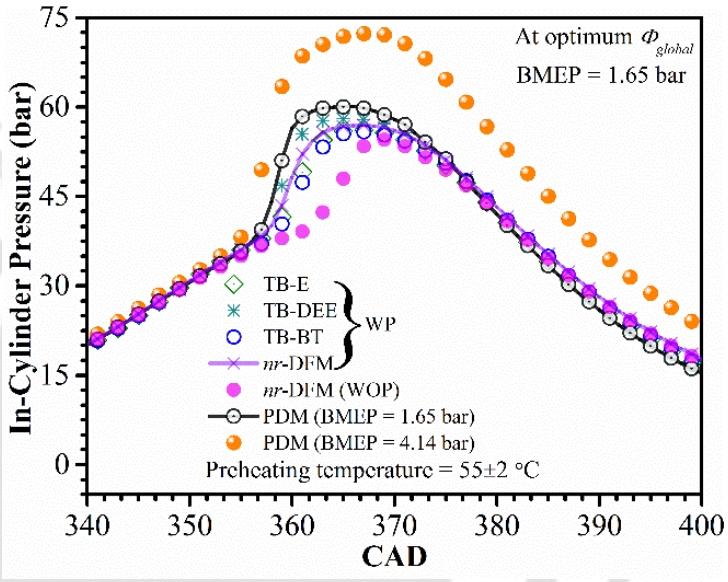

Fig. 7.10 Variations of in-cylinder pressure (AL: 1.65 bar) with CAD

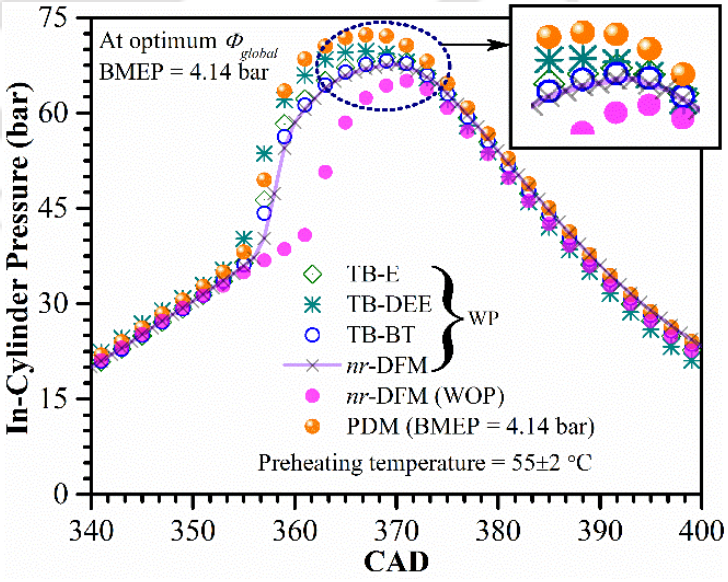

Fig. 7.11 Variations of in-cylinder pressure (AL: 4.14 bar) with CAD

ignition inhibitor agent CO_2 that is present in biogas (Pizzuti et al., 2016). Consequently, the higher shifting of crank angle position towards TDC is observed with TB-DEE relative to *nr*-DFM (WOP). Hence, the CPP with TB-DEE is noticed to be higher and even found nearest to the TDC than PDM, and the trend of CPP is found similar to that of PDM. These are accredited to the efficient utilization of the expansion stroke and the corresponding higher power output. The other reasons for the augmentation of the combustion in DFM with TB-DEE include the higher cumulative LHV, diesel likes viscosity and density and the DEE has the extra inbuilt oxygen molecules with higher cetane number. It is to be noted that the blends TB-BT, TB-E, and TB-DEE are prepared based on the same oxygen quantity. The higher CPP with the best quality concerning nearest position to TDC, is noticed with TB-DEE and worst with TB-BT. The blend TB-BT has the higher density and viscosity relative to diesel and other blended fuels. It causes the higher surface tension during the entrainment of air into the spray jets. Another fact is that due to the reduction (in terms of replacements of the pilot fuel) of the pilot (liquid) fuel quantity that sprayed over the gas mixture in DFM, the peak fuel pressure in the high pressure fuel line reduces, and this is noticed during experiments. Therefore, the corresponding jet velocity is reduced. These are attributed to the higher droplets size and the corresponding inefficient combustion with TB-BT (Heywood 1988). However, in this present research work, substantially higher peak pressures are obtained in DFM than that have been noticed at advanced IT = 29 CAD bTDC and CR = 18 by Bora and Saha (2015a), Bora (2015). On the other hand, Verma et al. (2017a) and Barik and Murugan (2014) found higher CPP than the PDM. It can only be possible with the richer mixture of fuel and air.

Table 7.4 The CPPs and corresponding crank angle positions at different states

Engine Operation	Relative to *nr*-DFM (WOP) (360 CAD = 0 CAD)			
	AL: 1.65 bar		**AL:** 4.14 bar	
	Increment of **CPP** (%)	**Position** (CAD) (aTDC)	Increment of **CPP** (%)	**Position** (CAD) (aTDC)
nr-DFM (WP)	4.39	6	3.92	10
TB-BT	2.44	7	4.84	10
TB-E	3.17	6	5.67	9
TB-DEE	6.46	5	7.27	6
PDM	10.26	6	11.16	8

In *nr*-DFM (WOP), CPP (bar)/position (CAD) (aTDC) at (a) **AL:** 1.65 bar is 54.9/9 and (b) **AL:** 4.14 bar is 65.06/11

The engine in-cylinder NHRR histories at the loads of 1.65 bar and 4.14 bar, with crank angles, are shown in Figs 7.12 and 7.13 without and with preheating and with various blended fuels. The higher peak of NHRR and the corresponding optimum crank-angle position (left side,

relative to TDC) of NHRR (Figs 7.12 and 7.13) are always desirable to achieve an efficient utilization of expansion energy. The above discussion on the in-cylinder pressure history reveals that the preheating and the fuel characteristics have great influences on the SOC and behaviors on the CPP. The physical reasons on the development of cylinder pressure and NHRR are similar as these two parameters are internally related to each other.

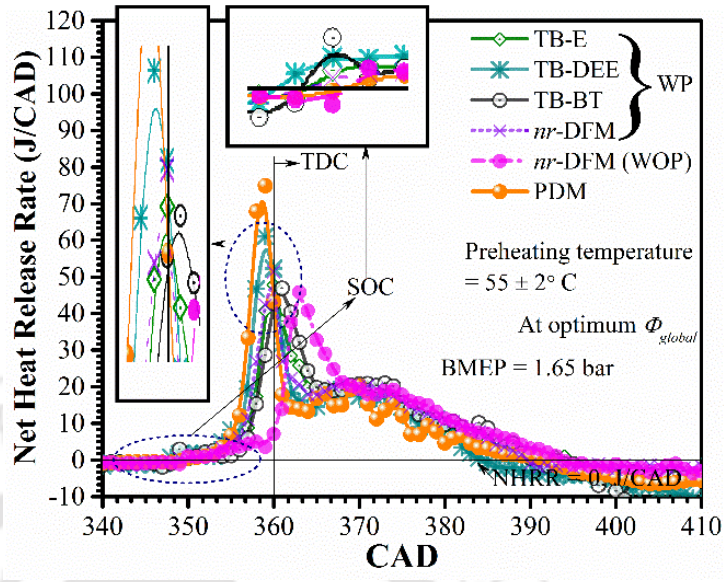

Fig. 7.12 Variations of NHRR (AL: 1.65 bar) with CAD

The generation of NHRR, however, can also be expressed in terms of the following Arrhenius equation (Chintala and Subramanian, 2017).

$$ROR = l_1 \times exp\left(-\frac{E_A}{RT_{CMGT}}\right) \times [Fuel]^{l_2} \times [Oxidizer]^{l_3} \quad (7.2)$$

where, ROR is the rate of reaction and, l_1, $l_2$and l_3 are the constants. The equation 7.2 reveals that the fuel with an oxidizer and higher in-cylinder temperature will have the crucial impact to accelerate the rate of reaction of fuel to release the more quantity of heat. Consequently, the oxygen present in fuels behaves like an oxidizer, and the preheating augmented the parameter T_{CMGT}, hence, there definitely will be the acceleration of ROR. Thus, the higher NHHRs are observed with the oxygenated fuels as compared to the one without

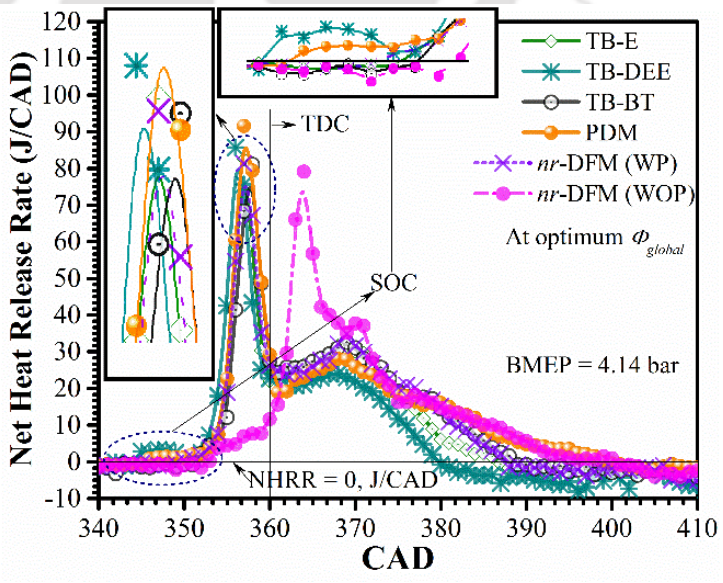

Fig. 7.13 Variations of NHRR (AL: 4.14 bar) with CAD

preheating and investigation without the oxygenated fuels. The enhancement of CMGT and the detailed discussion has been made later in this section. The NHHR estimated at each of the loads are observed to be significantly higher with preheating and with the oxygenated blended fuels than the cases without preheating (Table 7.5). Besides, the NHRRs are noticed to be substantially higher than those reported work (Bora and Saha, 2015a; Bora, 2015).

Table 7.5 The peaks of NHRR and the corresponding crank angle positions

Engine Operation	Relative to *nr*-DFM (WOP)			
	AL: 1.65 bar		**AL:** 4.14 bar	
	Increment of **the peak of NHRR** (%)	**Position** (CAD) (aTDC)	Increment of **the peak of NHRR** (%)	**Position** (CAD) (bTDC)
nr-DFM (WP)	12.07	0	2.69	3
TB-BT	2.30	1	2.45	2
TB-E	4.32	0	4.25	3
TB-DEE	33.26	1	8.24	4
PDM	63.53	1	15.77	3

In *nr*-DFM (WOP), the peaks of NHRR (J/CAD)/ CAD (aTDC) at (a) AL= 1.65 bar is 45.82/3 and (b) AL = 4.14 bar is 79.12/4

The variations of CDs with loads at optimized Φ_{global} and with various blended fuels are shown in Fig 7.14. The CD depends on the premixed combustion and diffusion combustion phases. The shorter CD is the consequences of the rapid premixed combustion and the corresponding shorter diffusion combustion phases. The higher CD is noticed with diesel fuel in PDM. In PDM with diesel fuel, there is no propagation of flame. Therefore, in PDM the diffusion combustion predominates over premixed combustion.

The shorter CD is desirable in order to have the efficient utilization of the expansion power. The shorter CD is noticed in DFM as compared to PDM as there is the propagation of the flame front. However, the maximum CD in DFM is observed in *nr*-DFM (WOP). The reasons for a higher CD in *nr*-DFM (WOP) are already discussed previously. In DFM with blended fuels, the lowest CD is observed with TB-DEE and higher with TB-BT. Nevertheless, the lower CD with TB-DEE would be due to the higher cetane number of DEE and enrichment of oxygen at the time of combustion. Being the higher cetane fuel (>125), DEE helps an early starts of SOC, and the release of extra oxygen helps to promote a faster flame propagation. The blend of DEE also has the higher LHV (Table 7.3) in comparison to other blends. On the other hand, in TB-E, the volume quantity of ethanol is lower in comparison to the volume quantity of BT and DEE in TB-BT and TB-DEE, respectively. It is to be noted that the oxygen amount in ethanol

molecule is higher than BT and DEE. Therefore, the lower volume percentage of ethanol in the blend (as compared to the volume percentage of BT and DEE in TB-BT and TB-DEE, respectively) and the effects of preheating of the intake charge diminish the effects of a higher heat of vaporization of ethanol on combustion. Consequently, the improvement in combustion is noted with TB-E than TB-BT. However, at part load, the CD is found to be marginally higher with TB-BT and TB-E. It may be due to the higher heat of vaporization of ethanol and higher viscosity of butanol (BT).

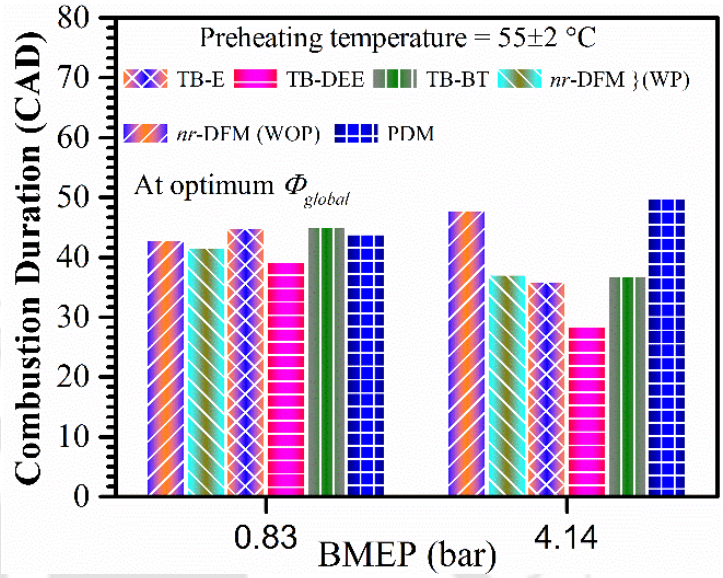

Fig. 7.14 Variations of CD with load

At the part load of 0.83 bar, the CD in *nr*-DFM (WOP) is found as 43 CAD. At this load, the CDs in *nr*-DFM (WP) and with TB-DEE are noticed to be reduced by 3.02% and 8.60%, respectively, as compared to *nr*-DFM (WOP). While, at this part load, there are increments of CD by 5.12%, 4.65% and 2.33% with the blends of TB-BT, TB-E and in *nr*-DFM (WP) with respect to *nr*-DFM (WOP), respectively. At the higher load of 4.14 bar, the CDs are estimated to be reduced by 22.50%, 22.92%, 25.00%, and 40.42% in *nr*-DFM (WP), with the blends of TB-BT, TB-E, and TB-DEE, respectively, relative to *nr*-DFM (WOP). Whereas, in PDM, the CD in comparison to *nr*-DFM (WOP) is found to enhance by 4.17%. In DFM, Barik and Murugan (2014) also found the similar trend of the CD.

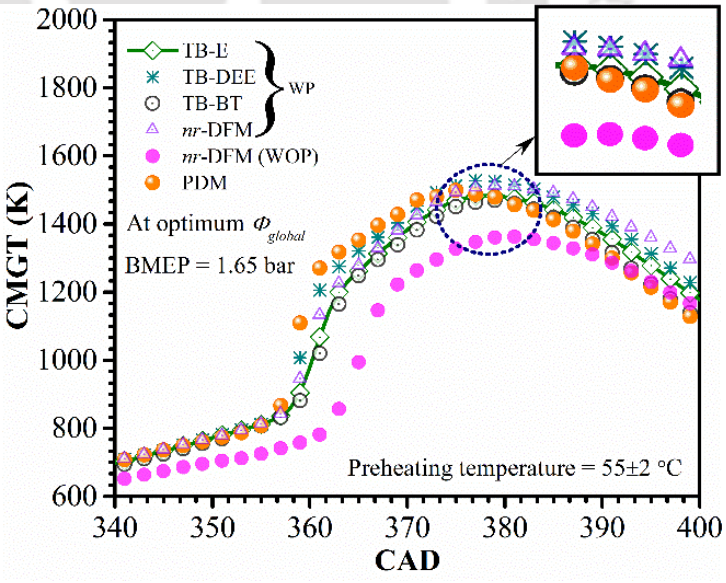

Fig. 7.15 Variations of CMGT with CAD (AL: 1.65 bar)

At the part load of 1.65 bar and the higher load of 4.14 bar and various states, the variations of cylinder mean gas temperature (CMGT) are portrayed in Figs 7.15 and 7.16, respectively. The parameter CMGT is the footprint of the indication of the progress of engine combustion. The higher CMGT and CPP imply the shorter physical period and earlier starting of chemical reaction (Heywood, 1988; Aklouche et al., 2018). These, attribute to the higher NHRR and shorter CD and a clear indication of the improvement in the combustion process. However, the position of the CMGT during combustion is important to utilize the power. The parameter, CMGT is directly proportional to the in-cylinder pressure. Therefore, the physical reasons of the variations of CMGT are similar to that with in-cylinder pressure and NHRR variations as discussed above. At the load of 1.65 bar and 4.14 bar, the peaks of CMGT in *nr*-DFM (WOP) are estimated to be 1362.20 K and 1657.38 K at the corresponding crank angle positions of 380 CAD and 381 CAD, respectively. The peaks of the CMGT and corresponding positions in *nr*-DFM (WP), TB-BT, TB-E, TB-DEE and in PDM relative to *nr*-DFM (WOP) are represented in Table 7.6.

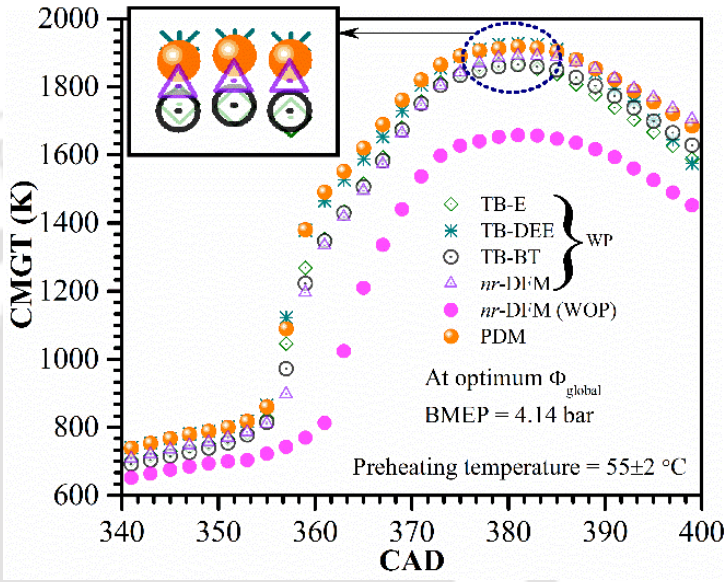

Fig. 7.16 Variations of CMGT with CAD (AL: 4.14 bar)

Table 7.6 The peaks of CMGT and the corresponding crank angle positions

Engine Operation	Relative to *nr*-DFM (WOP)			
	AL: 1.65 bar		**AL:** 4.14 bar	
	Increment of **the peak of CMGT** (%)	**Position** (CAD) (aTDC)	Increment of **the peak of CMGT** (%)	**Position** (CAD) (aTDC)
nr-DFM (WP)	11.07	19	14.13	22
TB-BT	7.88	19	12.51	21
TB-E	8.87	18	12.75	20
TB-DEE	12.08	17	16.35	20
PDM	9.99	15	15.68	21

In *nr*-DFM (WOP), the peaks of CMGT (K)/CAD (aTDC) at (a) AL= 1.65 bar is 1362.20/20 and (b) AL = 4.14 bar is 1657.38/21

At all loads, the maximum peak of the CMGT is noticed with TB-DEE. On the whole, the substantial improvement in CMGT is found with the preheating and with the blended fuels (TB-BT, TB-E, and TB-DEE). The CMGT is directly proportional to the reference temperature as indicated in the equation (Appendix-A). Therefore, the small variations of reference temperature will have the great influence on the variations in CMGT. Besides, the release of extra oxygen after immediate SOC helps to enhance the CMGT.

The variations of exhaust gas temperature (EGT) (with loads and under various conditions) are shown in Fig. 7.17. The higher EGT means, the higher loss of energy into the dead state. Therefore, the lower EGT is always desirable. Throughout the load spectrum, higher EGT is noticed in *nr*-DFM (WOP) and lower with TB-DEE. The lower EGT is noticed at part loads and higher at higher loads. With the increasing of loads, there is an increment of fuel consumption with the simultaneous higher rate of releasing of heat due to higher CPP and CMGT. The EGT is noticed to be lower with the case of preheating and with blended fuels. It may be due to the higher shifting of CPP towards TDC and the corresponding efficient utilization of the expansion power. At 0.83 and 4.14 bar, the EGTs in *nr*-DFM (WOP) are observed as 462.16 K and 606.16 K. At 0.83 bar, the reduction of EGTs in *nr*-DFM (WP), with the blends of TB-BT, TB-E, and TB-DEE and in PDM relative to *nr*-DFM (WOP) are estimated as 1.30%, 3.89%, 4.54%, 7.79% and 7.14%, respectively. At 4.14 bar, the EGTs in *nr*-DFM (WP), with the blends of TB-BT, TB-E, and TB-DEE and in PDM as compared to *nr*-DFM (WOP), are found to decline by 2.47%, 4.95%, 5.44%, 7.92%, and 5.94%, respectively.

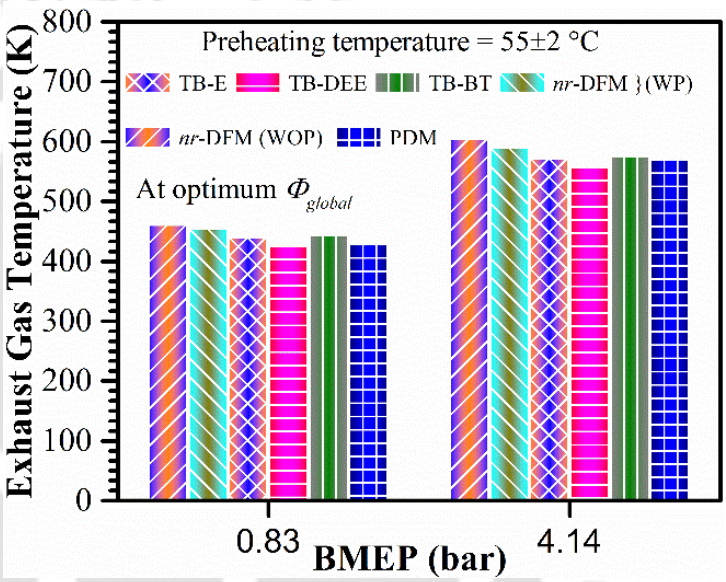

Fig. 7.17 Variations of EGT with load

The variations of COV of IMEP in PDM and in DFM are shown in Fig. 7.18. The maximum COV is noticed at part loads as compared to higher loads in all the cases. Nevertheless, there are the significant reductions in COV with preheating (at all loads) and with ternary blends of oxygenated fuels. The lowest COV is noticed with TB-DEE. It may be due to the early SOC and presence of oxgen in the biodiesel and DEE besides the propagation of flame through

biogas (with CO_2 as major constituent). It is to be noted that the IT and CR have been kept constatnt at 23 CAD bTDC and at CR = 17.5. Therefore, the IT can be advanced for the engine operation at lower load (as compared to higher loads) to ensure the proper dispersion of ignition kernels in combustion chamber to facilitate the flame propagation and hence an efficient engine performance.

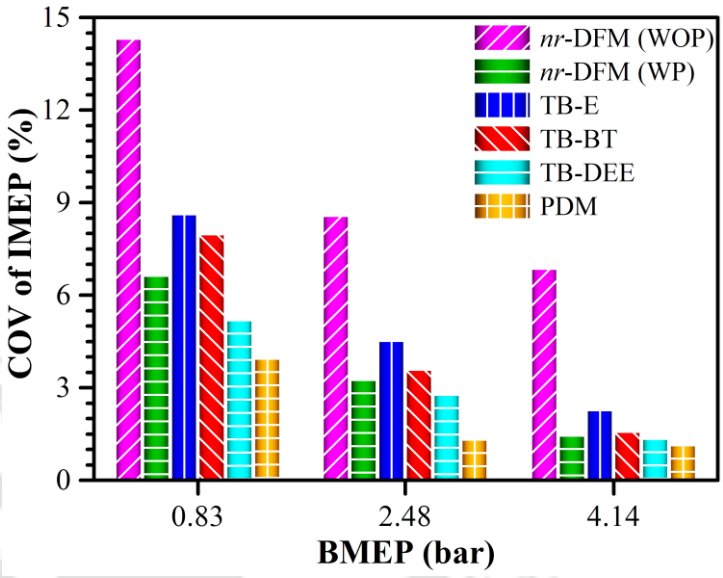

Fig. 7.18 Variations of COV of IMEP with load

The cyclic variations of CPP with the engine operating cycles at 0.83 bar and 4.14 bar are shown in Fig. 7.19 and 7.20, respectively. In the previous chapter, the physical effects of preheating and the enrichment of oxygen at the time of combustion on engine cyclic variations have been elaborated (Figs. 6.18 and 6.19). It has been noticed that with preheating, with the increasing of loads and with the use of oxygenated fuels, the cyclic variations have been reduced significantly. However, the lowest cyclic variations are noticed in PDM at all loads. In DFM, the lower cycle-by-cycle variations with TB-DEE may be due to the diesel-like fuel characteristics of this blended

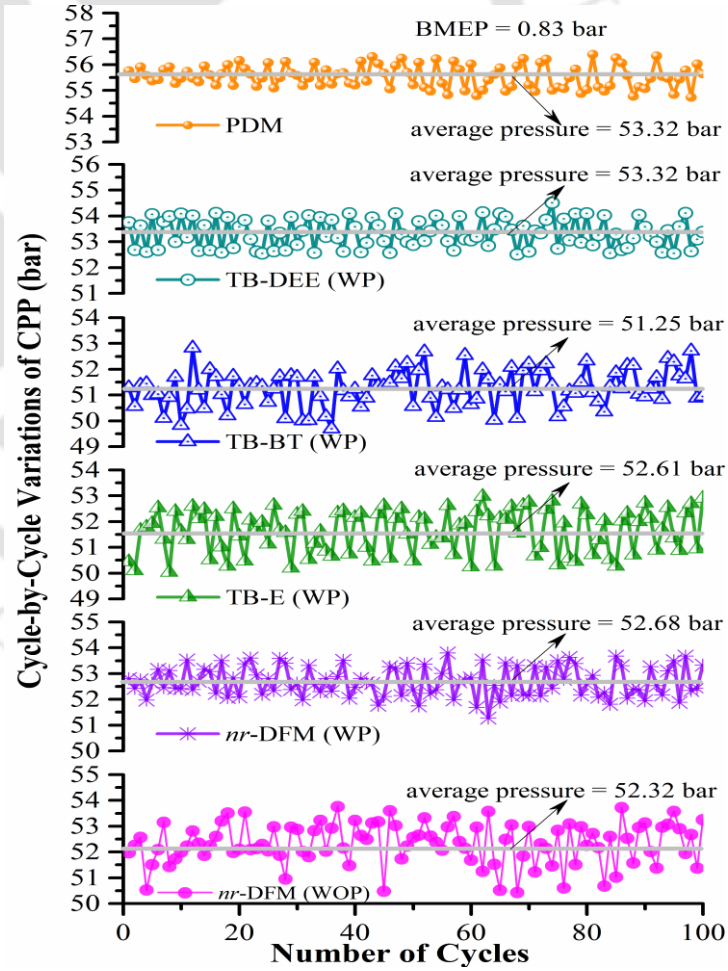

Fig. 7.19 Variations of cyclic variations of CPP (AL: 0.83 bar)

fuel (Table 7.3). Another reason for lower cycle-by-cycle variations with TB-DEE may be due to the formation of a homogeneous fuel-air mixture in the presence of a lower quantity of DEE in TB-DEE. Conversely, the higher viscosity and density of TB-BT promote to form a mixture that is more heterogeneous with the consequence of higher cyclic variations.

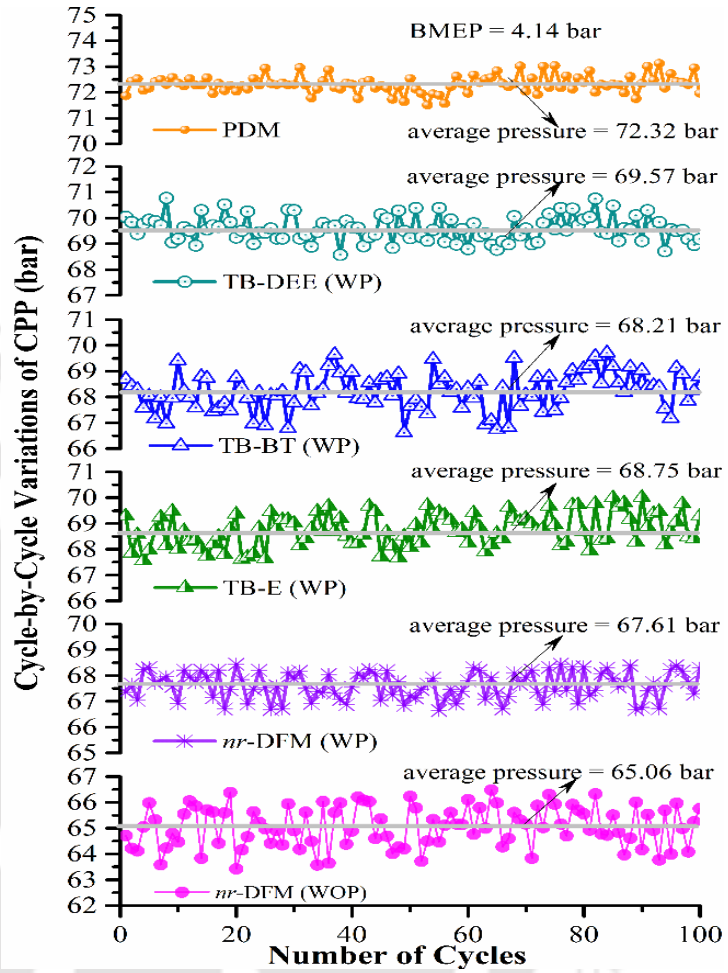

Fig. 7.20 Variations of cyclic variations of CPP (AL: 4.14 bar)

7.5 Emission Analysis

In the analysis of emission characteristics in different modes of engine operation, the parameters CO, HC, and NO_x are considered. In general, the higher CO and HC emission in biogas DFM are noticed. However, the drastic curtailment of the emission of NO_x is revealed in DFM as compared to PDM. The reasons for higher CO and HC emissions in biogas DFM engine are mainly due to the lowering of CMGT, deficiency of oxygen, and the act of CO_2 as the flame extinction agent present in biogas.

The characteristics of CO emission with loads, without and with preheating and with various blended fuels are depicted in Fig 7.21. Throughout the load spectrum, the lowest CO is identified with TB-DEE blend. Higher CO is noticed in *nr*-DFM (WOP). With preheating and with blended fuels, the reducing trends of CO emission with the increasing of loads are demonstrated. The CO is found to be marginally higher with TB-E than that in PDM. On the other hand, significantly higher CO emission is noticed with TB-BT and in *nr*-DFM (WP) in comparison to PDM but substantially lower than that in *nr*-DFM (WOP). At 0.83 and 4.14 bar, the emissions of CO (vol.%) in PDM are measured as 0.064% and 0.029%, respectively. At 0.83 bar, the increments of CO, with TB-E, TB-BT, in *nr*-DFM (WP) and *nr*-DFM (WOP) in

comparision to PDM are estimated as 7.81%, 32.81%, 39.06% and 87.50%, respectively. However, at this load with respect to PDM, the reduction of CO of 10.94% is found with TB-DEE blend. At 4.14 bar (load =100%), the reductions of CO relative to PDM are calculated as 6.90%, 34.48% and 51.72% with TB-BT, TB-E, and TB-DEE, respectively. While at this higher load, in comparison to PDM, the increment of CO emissions in *nr*-DFM (WP) and in *nr*-DFM (WOP) are noticed as 68.97% and 375.86%, respectively. The factors that influence the reduction of CO with TB-DEE (from part to higher loads) are higher cetane number that helps an early SOC, higher CMGT, faster flame propagation, and release of extra oxygen at the time of combustion.

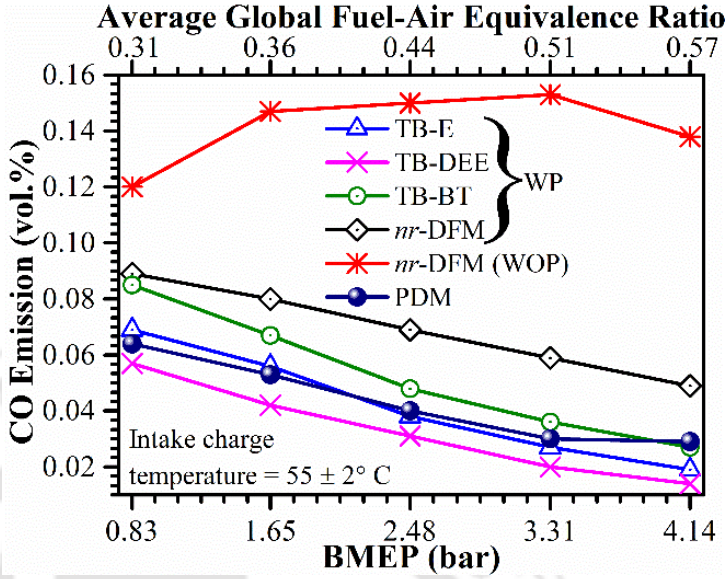

Fig. 7.21 Variations of CO emission with load

The variations of HC with loads and at various states are shown in Fig. 7.22. The HC is noticed to be reduced with the increase of loads and is found lower with the blended fuels. However, at higher loads (3.31 and 4.14 bar), the reductions of HC are found to be more with TB-E and TB-DEE blends. At 0.83 bar, the HC in *nr*-DFM (WOP) is measured to be 211 ppm. At this load, the reductions of HC in *nr*-DFM (WP), with TB-BT, TB-E, TB-DEE and in PDM with reference to *nr*-DFM (WOP) are estimated as 4.74%, 22.75%, 32.23%, 36.02%, and 73.46%, respectively. At the higher load of 4.14 bar, the HC in *nr*-DFM (WOP) is measured as 131 ppm. With this same higher load, the reduction of HC in *nr*-DFM (WP), with TB-BT, TB-E, TB-DEE and in PDM as compared to *nr*-DFM (WOP) are observed

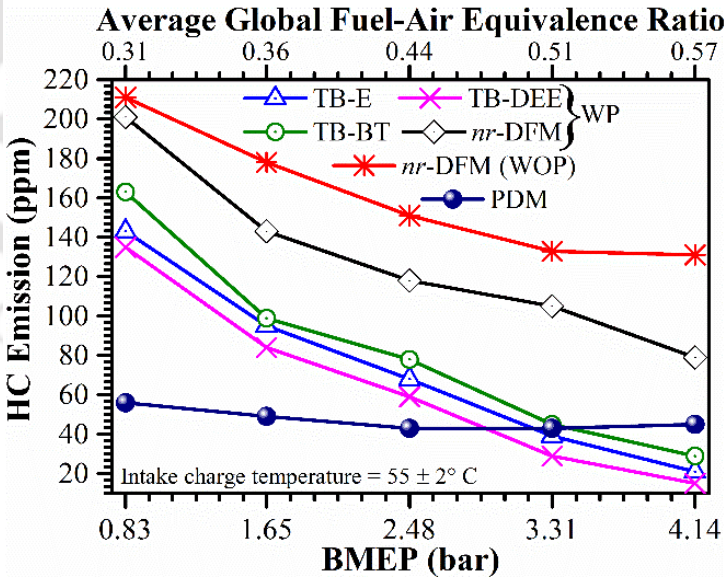

Fig. 7.22 Variations of HC emission with load

as 39.69%, 77.86%, 83.97%, 88.55% and 65.65%, respectively. The characteristics of the emission of NO_x in various states are portrayed in Fig. 7.23. In DFM, the lowest NO_x is noted in *nr*-DFM (WOP) and maximum in PDM. In order to compare the emission of NO_x, the emission in PDM is considered as the reference frame. At the load of 0.83 bar, the NO_x in PDM is found to be 179 ppm. With this load, the reductions of NO_x in *nr*-DFM (WOP), *nr*-DFM (WP), with the blends of TB-BT, TB-E, and TB-DEE in comparison to PDM are estimated as 83.80%, 82.31%, 74.30%, 70.39%, and 65.36%, respectively. At 4.14 bar (=100%) the NO_x in PDM is found as 1196 ppm. With reference to PDM, the reduction of NO_x at 4.14 bar, in *nr*-DFM (WOP), *nr*-DFM (WP), with the blends of TB-BT, TB-E, and TB-DEE are noticed as 63.04%, 34.70%, 34.45%, 25.84% and 5.43%, respectively. The higher emission of NO_x with TB-DEE in DFM may be due to the higher cumulative LHV of this blend and release of extra oxygen during combustion that helps to prevail an atmosphere to generate more emission of NO_x. In this section, the emission data that are measured in ppm and in vol.% are converted into gm/kWh, presented in Appendix-D.

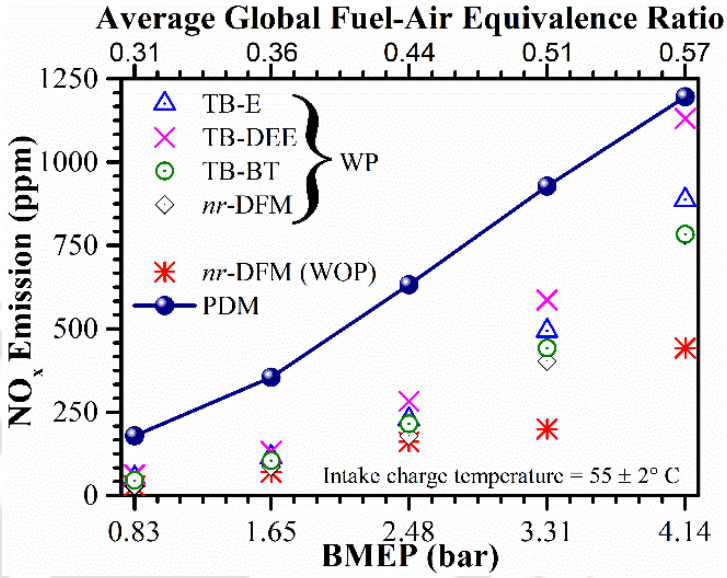

Fig. 7.23 Variations of NO_x emission with load

7.6 Summary

In this chapter, three ternary blends (TB-E, TB-BT, and TB-DEE) in DFM are considered as the pilot fuels. The study demonstrates that the use of renewable fuels with preheating can be a viable method to improve the overall performance of the biogas run DFM engines. The results achieved in this section are stated below:

Performance:

- The higher BFR is noticed with the TB-DEE blend, which is considerably lower than that of *nr*-DFM (WOP). There is a marginal variation of BFR at part load. At 4.14 bar, the minimum reduction of BFR with TB-DEE with respect to *nr*-DFM (WOP) is assessed to be lower by 5.16%.

- In ascending order, the BSECs are noticed as $BSEC_{PDM}$< $BSEC_{TB\text{-}DEE}$< $BSEC_{TB\text{-}E}$< $BSEC_{nr\text{-}DFM\ (WP)}$< $BSEC_{TB\text{-}BT}$< $BSEC_{nr\text{-}DFM\ (WOP)}$. At part loads, there is a marginal reduction of BSECs in comparison to *nr*-DFM (WOP). However, at 4.14 bar, there is a considerable reduction of BSECs with the blends of TB-E and TB-DEE as compared to the one in *nr*-DFM (WOP) and they are estimated to be 5.66% and 6.27%, respectively.
- Overall, the BTE is found to be higher with preheating and with the blended fuels. At 4.14 bar, the maximum increment of BTE with the blend of TB-DEE and in PDM in comparison to the one in *nr*-DFM (WOP) are calculated to be 6.69% and 21.46%, respectively. Throughout the load spectrum, higher BES is noticed with TB-DEE. The BES/BFES from part to higher loads are found to vary approximately as 50%/50%.
- In all cases, the LFRs with preheating and with the blended fuels are noticed to be higher. At the loads of 0.83 bar/4.14 bar, the maximum increment of LFRs with TB-DEE relative to the one in *nr*-DFM (WOP) is found as 7.74%/6.50%. At the loads of 0.83 bar/4.14 bar, the maximum ADR is also estimated as 55.04%/59.84% with TB-DEE.

Combustion:

- The similar trends of IDs are noticed with TB-DEE and in PDM. At all loads, the maximum and minimum IDs are noticed in *nr*-DFM (WOP) and with the TB-DEE blend, respectively. At 0.83 bar/4.14 bar, the maximum reduction of ID with TB-DEE relative to the one without preheating is calculated as 13.6%/48.13%.
- In all cases, the higher increment and higher shifting (towards TDC) of CPPs are found with preheating, with the blended fuels and at higher loads. At 4.14 bar, the maximum increment of CPP (7.27%) and shifting (6 CAD aTDC) are noted with the blend of TB-DEE as compared to the case without preheating.
- Overall, the higher NHRRs are found with preheating, with the use of blended fuels and at higher loads. At 4.14 bar, the maximum rise of NHRRs (%)/CAD (bTDC) with TB-DEE blend as compared to the one in *nr*-DFM (WP) is evaluated as 8.24%/4 in in *nr*-DFM (WP).
- As there is flame propagation, the shorter CD is noticed in DFM than PDM. At all loads, the maximum CD is noticed in *nr*-DFM (WOP). At 4.14 bar, the maximum reductions of CD with TB-DEE blend in comparison to *nr*-DFM (WOP) is estimated to be 40.42%.
- At all loads, the maximum CMGT is assessed with the TB-DEE blend. At the loads of 1.65 bar and 4.14 bar, the maximum increment of the peak of CMGT (%)/CAD (aTDC)

with TB-DEE as compared to the one in *nr*-DFM (WOP) are calculated as 12.08/17 and 16.35/20, respectively.

- Throughout the load spectrum, higher EGT is noticed in *nr*-DFM (WOP) and lower with TB-DEE. At 0.83 bar/4.14 bar, the highest reduction of EGTs with TB-DEE blend relative to the one in *nr*-DFM (WOP), are evaluated as 7.79%/7.92%. The cyclic variations are found to reduce with the increase of loads. It is found to be lower with the TB-DEE blend.

Emission:

- From part to higher loads, the CO emissions are found to be lower with TB-DEE blend. At 0.83 bar, there is a 10.94% reduction of CO emission with the TB-DEE blend. At 4.14 bar, the reductions of CO with TB-BT, TB-E and TB-DEE with respect to the one in PDM are observed as 6.90%, 34.48% and 51.72%, respectively.
- In DFM with blended fuels, the HC is observed to be lower than that in PDM within the range of higher loads of 3.31 to 4.14 bar. At the loads of 0.83 bar/4.14 bar, the maximum reductions of HC with TB-DEE as compared to the one in *nr*-DFM (WOP), are evaluated as 36.02%/88.55%.
- The NO_x in DFM is found to be substantially lower than the PDM. With reference to PDM, the maximum reduction of NO_x of 63.04% at 4.14 bar is found in *nr*-DFM (WOP).

Chapter-8

Results of Energy and Exergy Analysis

Chapter

Highlights:

- *Comparative energetic and exergetic analysis have been conducted.*
- *The higher energy recovery is noticed in PDM and with the blends of TB-DEE*
- *There is a considerable recovery of energy is noticed with the use of the heat exchanger.*
- *Higher energy in cooling water is observed with preheating and with blended fuels*
- *The maximum recoverable exergy is noticed in PDM and with the blends of TB-DEE.*

Overview: *It is known that the analysis of energy in a system associated with the "first law of thermodynamics" has no quality in terms of energy utilization. It is the "second law of thermodynamics" that helps to identify the probability of using of maximum available energy in the system. Nowadays, the researchers are using the "second law" as the optimization tool to maximize the performance of the engineering devices that are associated with energy interactions among system, boundaries, and surroundings. Therefore, the exergy or second law analysis has been gaining popularity to extract more amount of energy available in the input energy with a lesser loss. Recently, the trends of energy analysis associated with exergy analysis in the evolution of engine performance become widely popular. However, the exergy analyses with biogas DFM with the intake charge preheating and with the use of various oxygenated fuels blended with diesel are very limited. Hence, the investigation reported in this chapter elaborates the exergy behaviour of the biogas run DFM engine with intake charge preheating using various oxygenated liquid fuels (butanol, biodiesel, ethanol and diethyl ether) blended with diesel as the pilot fuel.*

***Chapter Layout*:**

8.1 Thermodynamic Study

Concerning an efficient energy utilization and balance of energy to optimize the necessary parameters, the thermodynamic study is essential. It is the backbone of study to know "how the energy is lost" to the dead state and to reduce the same to improve the engine performance in terms of power output and efficiency (Sahoo, 2011). The analysis of energy based on the "first law of thermodynamics" has no quality due to the missing of the adequate information like reasons of the destruction of energy, production of maximum useful energy and corresponding maximum efficiency (Heywood, 1988). The "first law of thermodynamics" states the balance of energy at the time of thermodynamic process involving interactions of energy between system and surroundings (Nag 2009). Whereas the "second law" addresses the balance of available energy or exergy (Rakopoulos et *al*., 2008). The exergy is extremely important for the energy conversion devices in order have the maximum energy efficiency. It is the "second law" that informs about the occurrence of irreversibility and the corresponding destruction of energy and the destruction of energy into the dead state (Rakopoulos and Kyritsis, 2006). The exergy or availability of a thermodynamic system involving an exchange of energy is defined as the maximum useful energy that can be produced when the system is brought to the thermodynamic equilibrium state with its surroundings (Moran and Shapiro, 1995). The production of energy from an internal combustion engine is associated with the destruction of exergy in various parts of the engine. Therefore, the exergy analysis is vital to achieve the maximum possible engine performance (Caton, 2000). Most of the researchers noticed that the exergy destroyed due to internal irreversibility at the time of combustion (Rakopoulos and Giakoumis, 1997a; Rakopoulos and Giakoumis, 1997b; Som and Datta, 2008).

The exergy analysis of biogas run DFM engines is very limited and the analysis is only limited to the atmospheric temperature of the intake charge and at various ITs and CRs (Bora 2015). None has carried out the exergy analysis considering (a) lower to very high global fuel-air equivalence ratios (Φ_{global}), (b) part to higher loads, (c) preheating of intake charge and (d) various ternary blends of oxygenated fuels as pilot fuels. The renewable oxygenated liquid fuels include biodiesel, butanol, ethanol, and diethyl ether. Three ternary blends of diesel-biodiesel-butanol (TB-BT), diesel-biodiesel-ethanol (TB-E), and diesel-biodiesel-diethyl ether (TB-DEE) are prepared. The details of the compositions of each blend are articulated in the previous chapter (Chapter 7). In the energy analysis, the parameters that embrace are rate of energy input (Q_{in}) in the form of the energy available in the total fuels that consumed per unit

time, shaft power (Q_s), rate of energy transferred to the cooling water (Q_{cw}), rate of energy transport with the exhaust gas (Q_{eg}), loss of uncounted energy per unit time (Q_{un}), energy efficiency (η_I) and exhaust gas temperature (EGT). Whereas, in the exergy analysis the parameters exergy input per unit time (E_{in}), exergy in cooling water per unit time (E_{cw}), exergy in exhaust gas per unit time (E_{eg}), rate of exergy destruction (E_{des}), exergy efficiency (η_{II}) and rate of entropy generation (S_{gen}) are considered.

8.2 Energy and Exergy Distribution

The evaluations of energy and exergy distributions throughout the applied load on the engine have been carried out by considering the design of experiments as discussed from Chapter 3 to 7. In the analysis, one part load (in torque unit) of 0.83 bar and one higher load of 4.14 bar are considered. At these part and higher loads, the higher values of Φ_{global} are considered as 0.87 and 0.89, respectively. In all other cases, the results are acquired at the optimum Φ_{global}, and at the various applied loads and with the various blends and states. The temperature ~30 °C and the atmospheric pressures are are considered as dead state. Experiments, as stated are carried out at the standard CR = 17.5 and IT = 23 CAD bTDC. The relations of the parameters in energy and exergy are addressed in Appendix-C.

Table 8.1 Energy data per unit time at the load of 0.83 bar and at various states

Engine Operation		**Load** = 0.83 bar (= 20%) (At standard **CR** = 17.5, **IT** = 23 CAD bTDC)				
		Q_{in} (kW)	Q_s (kW)	Q_{cw} (kW)	Q_{eg} (kW)	Q_{un} (kW)
nr-DFM (WOP) at Φ_{global} = 0.87		21.72	0.69	1.50	2.23	17.29
At optimum Φ_{global}	*nr*-DFM (WOP)	7.62	0.70	1.76	1.63	3.53
	nr-DFM (WP)	7.69	0.70	2.11	1.29	3.59
	TB-BT	7.47	0.70	2.26	1.04	3.48
	TB-E	7.46	0.71	2.33	0.96	1.98
	TB-DEE	7.43	0.70	2.41	0.80	1.88
PDM		5.55	0.71	2.56	0.57	1.72

8.2.1 Energy Analysis

The input energy and the distribution of the input energy are presented in Table 8.1 and Table 8.2 for part (0.83 bar) and higher (4.14 bar) loads. The graphical representation on the variation of input energy (Q_{in}) at optimum and at higher Φ_{global}, without and with preheating and with ternary blends (TBs) of TB-BT, TB-E, and TB-DEE are shown in Fig. 8.1. At very high Φ_{global} (from part to higher loads), the maximum input energy is noticed in *nr*-DFM (WOP). At 0.83 bar and at 4.14 bar in *nr*-DFM (WOP) the input energies at the optimum Φ_{global}, are estimated

to be 7.62 kW and 13.58 kW, respectively. At 0.83 bar, energy input in *nr*-DFM (WOP) at higher Φ_{global} of 0.87 as compared to the optimum Φ_{global} of 0.30 is found to be higher by 185.04%. While, at a maximum load of 4.14 bar, energy input at higher Φ_{global} of 0.89 in comparison to the optimum Φ_{global} of 0.53 is observed to be increased by 55.67%. At 100% load (= 4.14 bar), similar energy input in a biogas run DFM engine is also noticed by Bora (2015). At 100% load, he found 40.94% higher energy input relative to *nr*-DFM (WOP) at the optimum Φ_{global}. It means that the investigator carried out the investigation at higher Φ_{global} to consume more biogas as the primary fuel. The higher energy input at higher Φ_{global} may be due to the higher biogas consumption than that at the optimum Φ_{global}. At all loads and at optimum Φ_{global}, the energy input is noticed to be substantially lower than that at higher Φ_{global}. In addition, the energy inputs at optimum Φ_{global} with preheating and with the blended fuels are noticed to be lower as compared to the case without preheating and at optimum Φ_{global} with diesel as the pilot fuel. At the load of 0.83 bar, the reductions of energy input with the blends of TB-BT, TB-E, and TB-DEE in comparison to the one in *nr*-DFM (WOP) are calculated as 1.97%, 2.10%, and 2.49%, respectively. At 4.14 bar, the reduction of energy input with respect to *nr*-DFM (WOP) in *nr*-DFM (WP), with the blends of TB-BT, TB-E, and TB-DEE are found as 1.55%, 4.42%, 5.89%, and 6.70%, respectively. It is to be noted that all the experiments with blended fuels are conducted with preheating and at the optimum Φ_{global}. In this investigation on an average, the actual diesel fuel replacements of 53%-59% are noticed through the load spectrum of 0.83 to 4.14 bar. In these loads, the BFR is varied on an average from 0.72 to 1.25 kg/h, which is substantially lower than that constrained by Bora (2015). It is because, the investigator (Bora, 2015) regulate the BFR at the point where the signs of misfire are noticed. Overall, the reduction of Q_{in} at optimum Φ_{global} (with preheating and with the oxygenated fuels) may be due to the higher input fuel energy conversion together with a comparatively advanced CA50 and a shorter CD. These have made a proper conversion of heat energy to shaft energy.

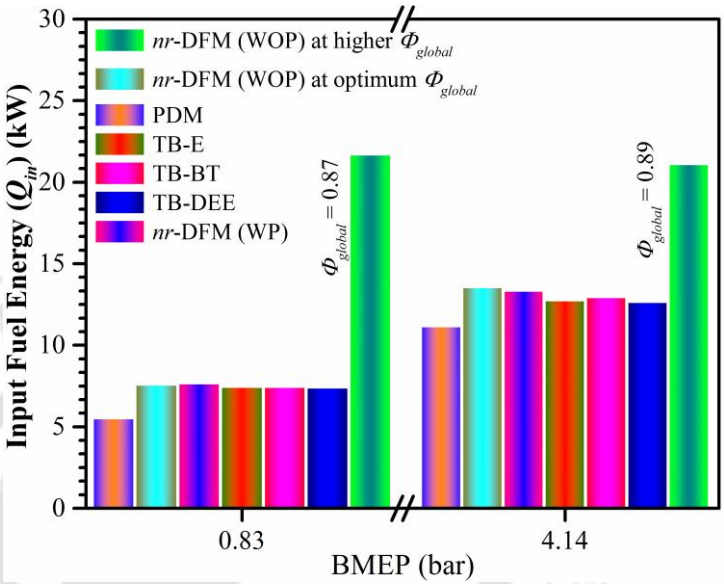

Fig. 8.1 Characteristics of Q_{in} with load

The variations of shaft energy with loads are shown in Fig. 8.2. It is to be noted that the shaft power is the function of applied load and engine speed. Hence, at a particular load and the corresponding engine speed, the variations are observed to be minor. These negligible variations are noticed due to the uncertainties of in engine speed and the applied load on the engine. However, at higher Φ_{global}, a slight increment of shaft power is noticed. It may be due to the higher fuel accumulation in the combustion chamber that enhances the engine speed. The diesel engine used in the present investigation has the rated power of 3.5 kW. In PDM, Bora (2015) estimated the shaft power that is more than the rated power. However, the shaft powers achieved in this study are approximately similar to that have found by Debnath (2013). Moreover, the energy input in this study is noticed to be 9.55% lower than the energy input as compared to that by Debnath (2013) in PDM. Hence, the enhancement of the shaft power would be due to the higher fuel consumption that enhances the engine speed, and thus, a higher shaft energy is achieved by Bora (2015).

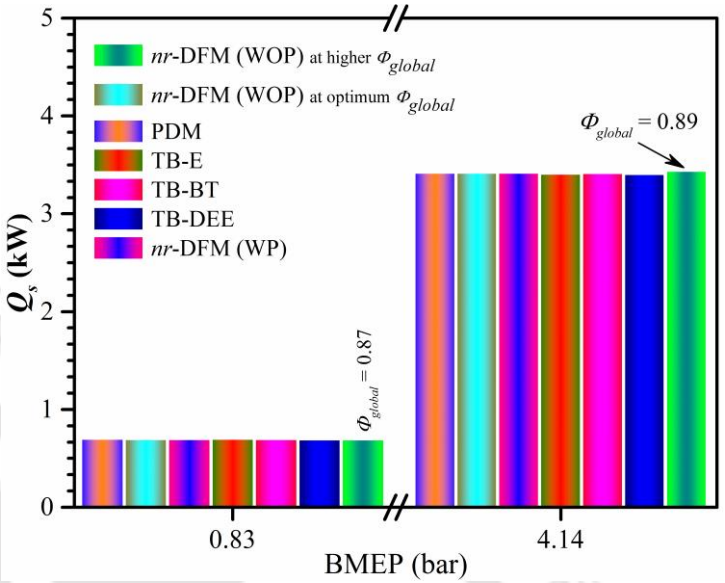

Fig. 8.2 Characteristics of Q_s with load

Table 8.2 Energy data per unit time at the load of 4.14 bar and at various states

Engine Operation		**Load** = 4.14 bar (=**100%**) (At **CR** = 17.5, **IT** = 23 CAD bTDC)					
		Q_{in} (kW)	Q_s (kW)	Q_{cw} (kW)	Q_{eg} (kW)	Q_{un} (kW)	η_I (%)
nr-DFM (WOP) at Φ_{global} = 0.89		21.14	3.44	2.86	6.06	8.77	16.30
At optimum Φ_{global}	*nr*-DFM (WOP)	13.58	3.42	3.15	4.82	2.19	25.22
	nr-DFM (WP)	13.37	3.42	3.32	4.19	2.43	25.60
	TB-BT	12.98	3.42	3.58	3.80	2.17	26.35
	TB-E	12.78	3.42	3.66	3.72	1.98	26.73
	TB-DEE	12.67	3.42	3.87	3.51	1.88	26.90
PDM		11.18	3.43	4.05	2.80	0.90	30.63
PDM (Debnath 2013)		12.36	3.43	4.08	2.24	2.61	28.90
PDM (Bora 2015)		12.64	3.51	5.02	3.04	1.05	27.76
DFM (Bora 2015)		19.14	3.49	5.67	7.98	1.99	18.25

The variations of energy loss to the cooling water per unit time (Q_{cw}) are portrayed in Fig. 8.3 with various blended fuels and states. The Q_{cw} is noticed to increase with the increase of loads. It may be due to the enhancement of cylinder peak pressures (CPPs) and the corresponding peaks of the CMGT with the increase of loads as presented in Table 8.3 and 8.4. Nevertheless, the higher transfer of heat energy to the cooling water means the higher loss of energy. Therefore, the loss of energy should be as minimum as possible. In PDM, the loss of heat to the cooling water at 100% load (= 4.14 bar) is found to be approximately equal to one estimated by Debnath (2013). However, at this same load, the transferred of heat to the cooling water is found to be 19.32% lower relative to the heat loss that is reported by Bora (2015). Another noticeable issue is that in this study, the heat loss in cooling water is found to be lower in DFM than PDM. Earlier Bora (2015) noticed a higher loss of heat to the cooling water in DFM than PDM. In the present study, on an average drop in the loss of heat energy by 37.99% is recorded in comparison to the loss of heat as reported by Bora (2015). Moreover, the Q_{cw} is observed to have been reduced with the increase of Φ_{global} and is found marginally higher with preheating and with the oxygenated blended fuels. The enhancement of Φ_{global} means the corresponding increment of biogas consumption that reduces the CMGT. On the other hand, preheating and the use of oxygenated blended fuels enhance the CMGT. Hence, Q_{cw} is the in-cylinder temperature (CMGT) dependent parameter. Higher the in-cylinder temperature, higher will be the Q_{cw}. At the load of 0.83 bar, the Q_{cw} in *nr*-DFM (WOP) are found as 1.76 kW. At this load, with reference to the *nr*-DFM (WOP), the Q_{cw} in *nr*-DFM (WP), with the blends of TB-BT, TB-E, and TB-DEE and in PDM are found to increase by 19.89%, 28.41%, 32.39%, 36.93, and 45.45%, respectively. However, at this part load, without preheating and at the higher Φ_{global} of 0.87, the marginal reduction of Q_{cw} with respect to *nr*-DFM (WOP) at the optimum Φ_{global} (~ 0.31) is noted. At 100% load (= 4.14 bar), the Q_{cw}, in *nr*-DFM (WOP) is noticed as 3.15

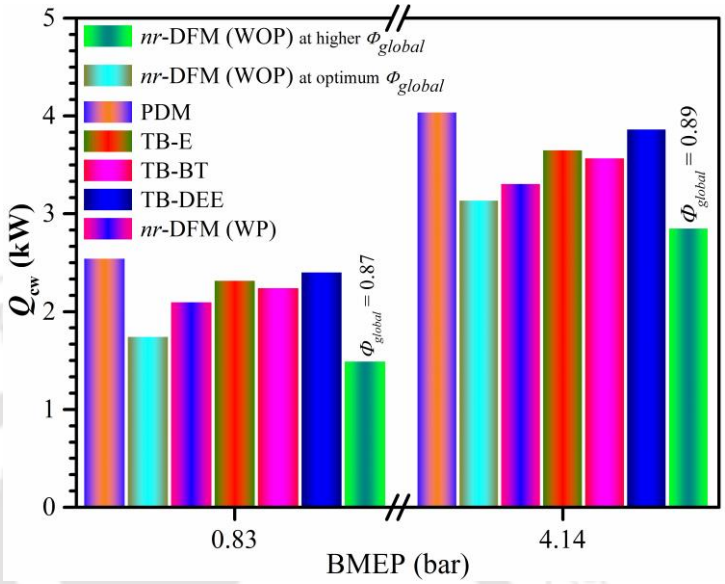

Fig. 8.3 Characteristics of Q_{cw} with load

kW. At this load, relative to *nr*-DFM (WOP), the increments of Q_{cw} in *nr*-DFM (WP), with the blends of TB-BT, TB-E, and TB-DEE and in PDM are computed as 5.40%, 13.65%, 16.19%, 22.86%, and 28.57%, respectively. The adequate reduction of Q_{cw} of 9.21% with the higher Φ_{global} = 0.89 with respect to *nr*-DFM (WOP) at optimum Φ_{global} (~0.57) is acquired.

The variations of heat energy loss with exhaust gas (Q_{eg}) with loads and at various conditions are shown in Fig. 8.4. The heat loss with exhaust gas (Q_{eg}) is found to be lower at lower loads and higher at higher loads. It may be due to the improvement of combustion with the consequence of higher CMGT. However, at all loads, with preheating and with blended fuels, Q_{eg} is noticed to be lower as compared to the case without preheating. On the other hand, the lowest Q_{eg} in all cases is observed in PDM. The physical reason for this behavior of Q_{eg} might be due to the nearest position of CA50, CPPs towards TDC, shorter CD and efficient utilization of the expansion energy (Table 8.3). Therefore, the lower Q_{eg} is noticed in DFM with TB-DEE and very high Q_{eg} is found with higher Φ_{global} and without preheating. The loss of heat energy into the dead state with the exhaust gas is undesirable.

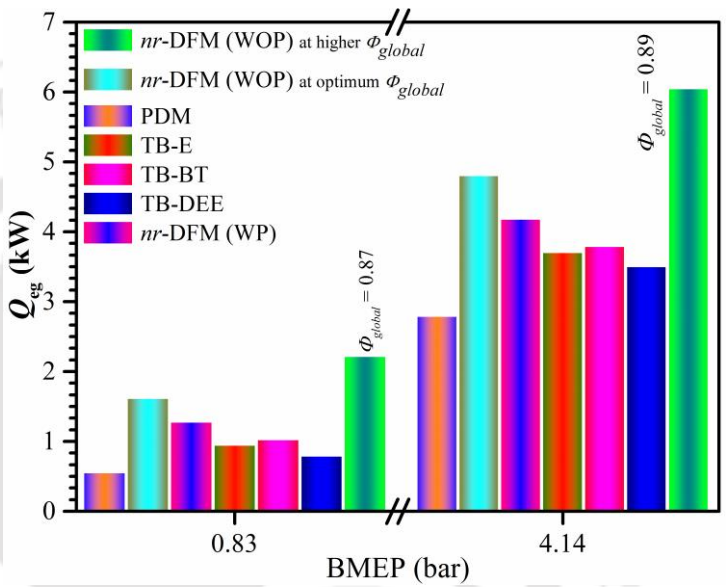

Fig. 8.4 Characteristics of Q_{eg} with load

At 100% load (= 4.14 bar), Bora (2015) found substantially higher Q_{eg} of 39.60% as compared to that in *nr*-DFM (WOP) at the optimum Φ_{global} (~0.57). At 0.83 bar, the Q_{eg} in *nr*-DFM (WOP) at optimum Φ_{global} (~0.30) is noticed as 1.63 kW. At this load and relative to this *nr*-DFM (WOP), the reduction of Q_{eg} in *nr*-DFM (WP), with the blends of TB-BT, TB-E, and TB-DEE and in PDM are computed as 20.86%, 36.20%, 41.10%, 50.92%, and 65.03%, respectively. While, at this part load, the significant increment of Q_{eg} at higher Φ_{global} (~0.87) with respect to *nr*-DFM (WOP) at optimum Φ_{global} (~0.31) is calculated as 36.81%. At the higher load of 4.14 bar and at optimum Φ_{global} (~0.57), the Q_{eg} in *nr*-DFM (WOP) is noted as 4.82 kW. At this load, with respect to *nr*-DFM (WOP), the reduction of the Q_{eg} in *nr*-DFM (WP), with the blends of TB-BT, TB-E, and TB-DEE and in PDM are reckoned as 13.07%,

21.16%, 22.82%, 27.18%, and 41.91%, respectively. While without preheating an increment of 25.73% of Q_{eg} is estimated with higher Φ_{global} (~0.89) in DFM in comparison to *nr*-DFM (WOP).

The variations of loss of uncounted energy per unit time (Q_{un}) with loads at various conditions are shown in Fig. 8.5. The Q_{un} is noticed to be lower with the increase of loads. It may be due to the higher energy utilization at higher loads. A very high Q_{un} at higher Φ_{global} is noticed at all loads. It may be due to the accumulation of very high amount total fuels inside the combustion chamber, retardation of CA50 and increment of CD. It is to be noted that the higher Φ_{global} means a higher amount of methane as well as CO_2 in biogas. The Q_{un} in PDM and most of the cases in DFM at higher Φ_{global} are found to be approximately equal to one achieved by Bora (2015). The Q_{un} is found to be higher in the case of without preheating, while, it reduces with preheating and with the use of blended fuels at the preheated environment of the inducted charge. At the load of 0.83 bar, the Q_{un} in *nr*-DFM (WOP) is found as 3.53 kW. In *nr*-DFM (WP), slightly higher Q_{un} than *nr*-DFM (WOP) is noticed. However, at this load, with the blends of TB-BT, TB-E, and TB-DEE and in PDM, the Q_{un} are found as 3.48 kW, 1.98 kW, 1.88 kW, and 1.72 kW, respectively. At the load of 4.14 bar, the Q_{un} in *nr*-DFM (WOP) is calculated as 2.19 kW. At this load, it is also noticed that there is a marginal increment of Q_{un} in *nr*-DFM (WP). At 4.14 bar, the reduction of Q_{un} in comparison to *nr*-DFM (WOP) with the blends of TB-BT, TB-E, and TB-DEE and in PDM are estimated as 0.91%, 9.59%, 14.16%, and 58.90%, respectively.

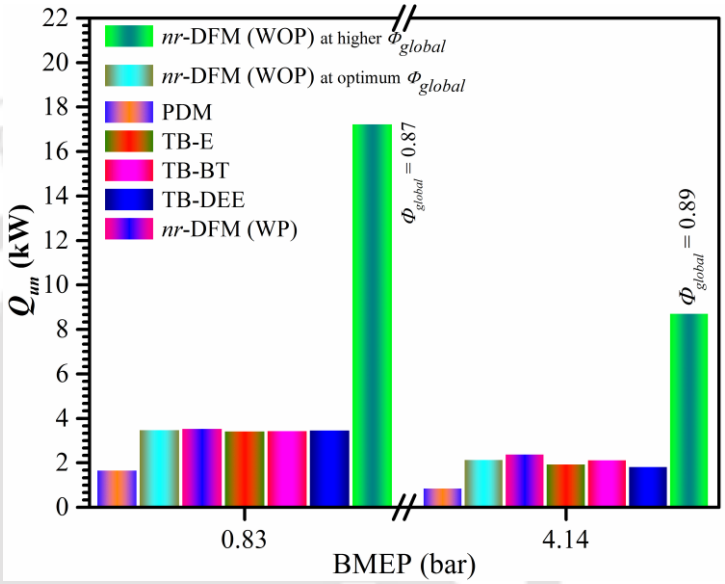

Fig. 8.5 Characteristics of Q_{un} with load

The variations of energy efficiency (η_I) with loads, without and with preheating and with various blended fuels are shown in Fig. 8.6. Higher energy efficiency is noticed in PDM at all loads than DFM. However, the η_I with the blended fuels in DFM are found to be competitive

to PDM. It may be due to the improvement of combustion because of the releasing of extra oxygen from the blended fuels at the time of combustion. This is reflected to the advanced CA50 and relatively shorter CD. Higher η_I in DFM is noticed with TB-DEE. While, at the higher Φ_{global}, lower η_I is noticed throughout the load spectrum. It may be due to the higher accumulation of biogas and the corresponding displacement of the fresh air. The efficiency in DFM is found to be substantially higher than that obtained by Bora (2015). At 100% load (= 4.14 bar), the η_I in DFM at the standard CR = 17.5 and IT = 23 CAD bTDC, is found to be 43.34% higher than that obtained by Bora (2015). In this study, at this higher load, in *nr*-DFM (WOP), the η_I is estimated as 25.22%. Therefore, the increment of η_I as compared to *nr*-DFM (WOP) are computed in *nr*-DFM (WP), with the blends of TB-BT, TB-E, and TB-DEE and in PDM as 1.51%, 4.48%, 5.99%, 6.66% and 21.45%, respectively. However, at this load and with higher Φ_{global} of 0.89, the reduction of η_I with respect to *nr*-DFM (WOP) is observed as 35.37%. It this Φ_{global} (= 0.89), the misfire along with a substantial retardation of CA50 and a higher CD is observed.

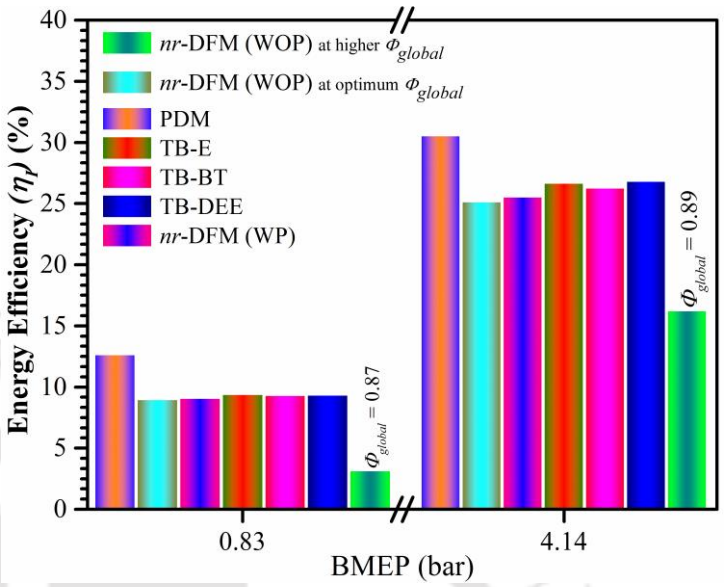

Fig. 8.6 Characteristics of energy efficiency with load

The variations of exhaust gas temperature (EGT) with loads and at different states are depicted in Fig. 8.7. In the experiments, a lower EGT is noticed in PDM for all loads. The EGT depends on the fuels characteristics, positions of the CPPs and the peaks of the CMGTs. Besides, the diesel-like fuel in PDM and highly flammable gaseous fuels (Karim, 1980) in DFM are favorable to achieve an efficient engine performance. The highly flammable gaseous fuel generates higher flame speed at the time of combustion. In biogas DFM engine, CO_2 present in biogas behaves like an ignition inhibitor and slow down the flame speed. In addition, biogas also has a very high self-ignition temperature, and higher heat capacity that causes the higher ID, retardation of CA50 relative to TDC and enhancement of CD. Hence, in biogas DFM engine, a higher EGT is noticed. However, the combined effects of the use of liquid (pilot)

oxygenated fuels blended with diesel, preheating the intake charge and the optimization of Φ_{global} can enhance the flame speed of the DFM engine run on biogas. The optimum Φ_{global} will modulate the correct amount biogas that inducted through intake port, while the intake charge preheating will increase the temperature in the combustion chamber. Consequently, due to the release of extra oxygen on combustion of oxygenated pilot fuel, the flame speed will increase. Hence, the entire combustion process can be expected to be improved. Thus, at optimum Φ_{global}, with preheating and with use of the oxygenated blended fuel, there are the relative advancement of CA50 and CPPs (Table 8.3) towards TDC and the shorter CD have resulted the lower EGT. In DFM, the lower EGT is noticed with TB-DEE and higher in *nr*-DFM (WOP) and at higher Φ_{global}. At the load of 0.83 bar, the EGT in *nr*-DFM (WOP) is found as 462.16 K. At this load, with reference to the *nr*-DFM (WOP), the reduction of EGT in *nr*-DFM (WP), with the blends of TB-BT, TB-E, and TB-DEE and in PDM are evaluated as 1.30%, 3.89%, 4.54%, 7.14%, and 7.34%, respectively. Whereas, at 0.83 bar, the enhancement of EGT as compared to *nr*-DFM (WOP) is acquired as 16.88%. At 4.14 bar, the EGT in *nr*-DFM (WOP) is calculated as 599.16 K. At this load, the reduction of EGT in *nr*-DFM (WP), with the blends of TB-BT, TB-E, and TB-DEE and in PDM with respect to *nr*-DFM (WOP) are observed as 1.34%,

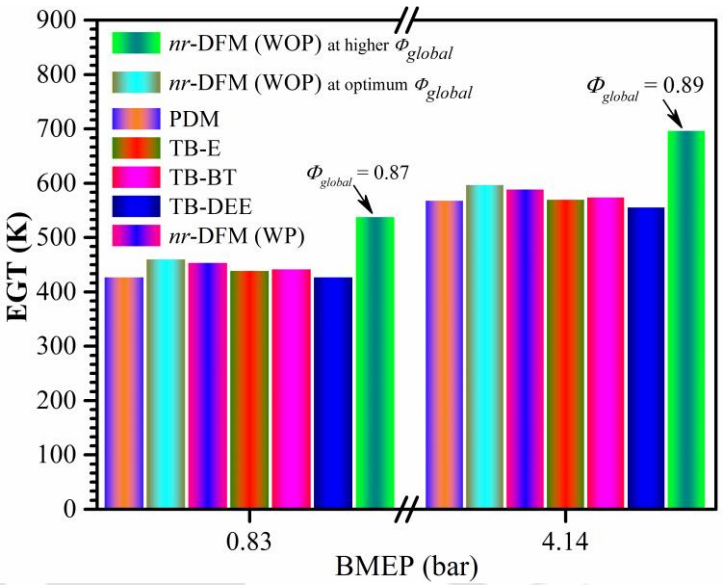

Fig. 8.7 Characteristics of EGT with load

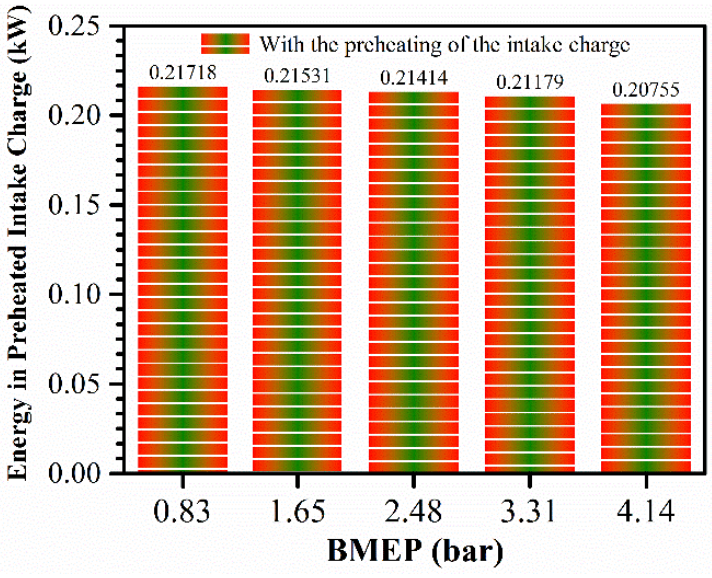

Fig. 8.8 Characteristics of energy addition to the preheated intake charge

3.84%, 4.51%, 6.84, and 4.84%, respectively. At 4.14 bar, the increment of EGT with higher Φ_{global} (~0.89) in comparison to *nr*-DFM (WOP) is computed as 16.69%.

Table 8.3 The CPPs and corresponding crank angle positions at different states

Engine Operation		Results at CR = 17.5, IT = 23 CAD bTDC			
		AL: 1.65 bar		**AL:** 4.14 bar	
		CPP (bar)	**Position** (CAD) (aTDC)	**CPP (bar)**	**Position** (CAD) (aTDC)
At optimum Φ_{global}	*nr*-DFM (WOP)	54.49	9	65.06	11
	nr-DFM (WP)	56.88	6	67.61	10
	TB-BT	55.82	7	68.21	10
	TB-E	56.22	6	68.75	9
	TB-DEE	58.01	5	69.79	6
PDM		60.08	6	72.32	8
Bora and Saha (2014) (WOP) (biogas + diesel)		38.01	-	43.53	-
Bora and Saha (2017) (WOP) (at optimum states: CR=18, IT=29 CAD bTDC, biogas + RBB)		46.23	-	58.00	-

RBB = Rice bran biodiesel

Table 8.4 The peaks of CMGT at different states and the corresponding crank angle positions

Engine Operation		**Results:** at CR = 17.5, IT = 23 CAD bTDC			
		AL: 1.65 bar		**AL:** 4.14 bar	
		Peak CMGT (K)	**Position** (CAD) (aTDC)	**Peak CMGT (K)**	**Position** (CAD) (aTDC)
At optimum Φ_{global}	*nr*-DFM (WOP)	1362.20	20	1657.38	21
	nr-DFM (WP)	1513.03	19	1891.60	22
	TB-BT	1469.48	19	1864.75	21
	TB-E	1483.05	18	1868.64	20
	TB-DEE	1526.72	17	1928.39	20
PDM		1498.28	15	1917.27	21

At different loads with preheating, variations of additions of heat energy per unit time to the inducted intake charge by the use of engine exhaust gas with the cross-flow heat exchanger (CFHE), are shown in Fig. 8.8. It can be seen in Fig. 8.8 that the addition of heat energy with preheating reduces upon increasing of loads. It may be due to the reduction of total inducted mass (biogas + air) that reduces the addition of enthalpy into the inducted stream of air and biogas mixture. However, these reductions with the increasing of loads are noticed to be marginal because of the marginal reduction of the mass consumption of the intake charge. The additions of heat energy, or in others words, the recovered heat energy is also found to considerable as depicted in Fig. 8.8.

Table 8.5 Exergy data at the load of 0.83 bar and at various states

Engine Operation		Load = 0.83 bar (= 20%) (At CR = 17.5, IT = 23 CAD bTDC)					
		E_{in} (kW)	E_s (kW)	E_{cw} (kW)	E_{eg} (kW)	E_{des} (kW)	η_{II} (%)
nr-DFM (WOP) at Φ_{global} = 0.87		21.65	0.69	0.0012	0.77	20.18	6.80
At optimum Φ_{global}	*nr*-DFM (WOP)	8.19	0.70	0.0033	0.38	7.11	13.20
	nr-DFM (WP)	7.76	0.70	0.0061	0.36	6.70	13.70
	TB-BT	7.74	0.70	0.0074	0.34	6.69	13.50
	TB-E	7.73	0.71	0.0091	0.33	6.68	13.51
	TB-DEE	7.50	0.70	0.0107	0.30	6.49	13.48
PDM		5.94	0.71	0.0144	0.27	4.96	16.61

8.2.2 Exergy Analysis

The exergy distributions per unit time, at the loads of 0.83 bar and 4.14 bar are presented in Tables 8.5 and 8.6, respectively. The variation of exergy input per unit time (E_{in}) is shown in Fig. 8.9. The maximum E_{in} in all loads are noticed at higher Φ_{global} as depicted in Tables 8.5 and 8.6 and in Fig. 8.9. At the loads of 0.83 bar and 4.14 bar, the exergy input at the higher Φ_{global} of 0.87 and 0.89 are noticed as 21.65 kW and 21.10 kW, respectively. However, the substantial lower E_{in} is noticed at the optimized Φ_{global} that controls the proportion of total fuel and air consumptions which improves the engine combustion in DFM. Moreover, it is also noticed that at optimum Φ_{global} (at each of the applied loads), the E_{in} reduces with preheating and with the use of oxygenated injected pilot fuels. The lower E_{in} and corresponding higher exergy efficiency mean the higher utilization of input energy. Consequently, lower E_{in} at all loads is achieved with TB-DEE. At the load of 0.83 bar and 4.14 bar, the E_{in} in *nr*-DFM (WOP) are estimated at 8.19 kW and 14.03 kW, respectively. At 0.83 bar, the reduction of E_{in}, with respect to in *nr*-DFM (WOP) are found as 5.25%, 5.49%, 5.62%, 8.42%, 27.47% in *nr*-DFM (WP), with the blends of TB-BT, TB-E,

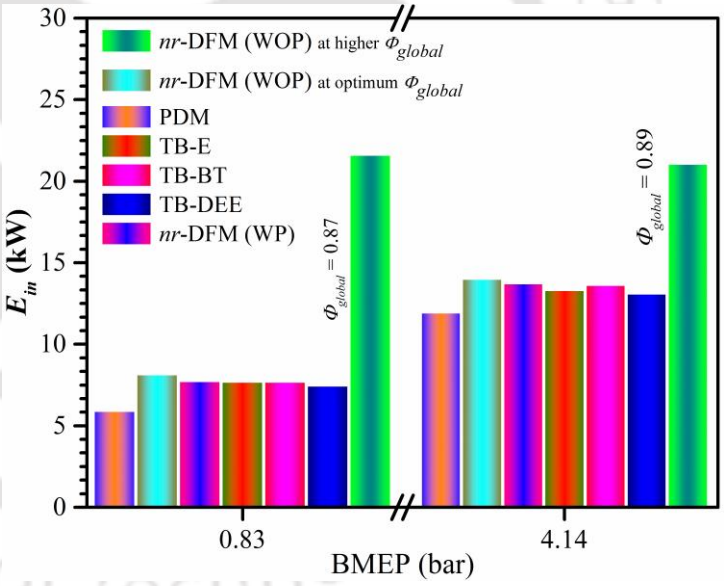

Fig. 8.9 Characteristics of E_{in} with load

and TB-DEE, and in PDM, respectively. While there is a drastic increment of E_{in} of 164.35% with higher Φ_{global} of 0.87 as compared to that in *nr*-DFM (WOP). Similarly, at 4.14 bar, the reductions of E_{in} in *nr*-DFM (WP), with the blends of TB-BT, TB-E and TB-DEE, and in PDM relative to *nr*-DFM (WOP) are calculated as 1.92%, 2.57%, 4.92%, 6.41%, 14.61%, respectively. Whereas, at this load, the increment of 50.39% of E_{in} with higher Φ_{global} of 0.89 in comparison to *nr*-DFM (WOP) at optimum Φ_{global} is evaluated. In this study, at 100% load (= 4.14 bar), the substantial reduction of E_{in} in DFM relative to one obtained by Bora (2015) are assessed as 27.34%, 28.74%, 29.21%, 30.92%, and 32.00% at optimum Φ_{global} in *nr*-DFM (WOP), *nr*-DFM (WP), with the blends of TB-BT, TB-E and TB-DEE, respectively. These attribute to the higher exergy utilization and substantial improvement in engine performance as compared to the past study (Bora, 2015).

The exergy recovery per unit time from the exhaust gas (using the CFHE) and that transferred to the intake charge with loads are portrayed in Fig. 8.10. The exergy input due to preheating is noticed to be lower than the rate of heat addition to the intake charge (biogas + air). It may be due to the suction in the intake pipeline in which the negative pressure gradient is the driving force to draw the biogas-air stream into the engine. As a result, the heat energy is absorbed in the suction pipeline with the consequence of lower exergy input per unit time due to the preheating. The lower exergy addition per unit time is noticed at higher loads due to the reduction of total mass input (intake charge) in the suction line owing to the enhancement of in-cylinder temperature.

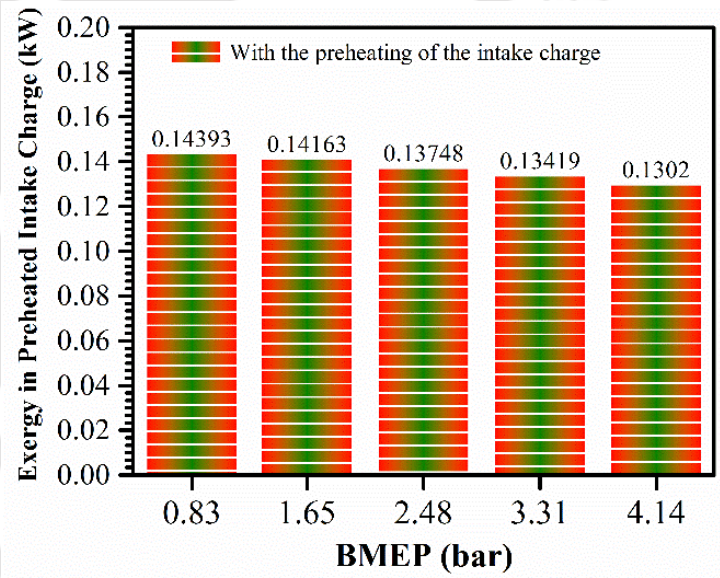

Fig. 8.10 Characteristics of exergy in preheated intake charge (kW) with load

The exergy in cooling water per unit time (E_{cw}) is shown in Fig. 8.11. The higher E_{cw} is the effects of higher in-cylinder temperature (CMGT) that developed due to the improvement in

combustion. Therefore, higher E_{cw} is noticed in PDM and with the blended fuels as compared to the case without preheating and at higher Φ_{global}.

Table 8.6 Exergy data at the load of 4.14 bar and at various states

Engine Operation		**Load** = 4.14 bar (= **100%**) (At **CR** = 17.5, **IT** = 23 CAD bTDC)						
		E_{in} (kW)	E_s (kW)	E_{cw} (kW)	E_{eg} (kW)	E_{des} (kW)	η_{II} (%)	S_{gen} (kW/K)
nr-DFM (WOP) at Φ_{global} = 0.89		21.10	3.44	0.020	2.51	15.12	28.32	0.093
At optimum Φ_{global}	*nr*-DFM (WOP)	14.03	3.42	0.029	1.47	9.11	35.10	0.030
	nr-DFM (WP)	13.76	3.42	0.042	1.42	8.87	35.52	0.029
	TB-BT	13.67	3.42	0.057	1.36	8.83	35.41	0.029
	TB-E	13.34	3.42	0.067	1.32	8.54	35.97	0.028
	TB-DEE	13.13	3.41	0.088	1.23	8.40	36.03	0.027
PDM		11.98	3.43	0.085	1.17	7.31	39.03	0.024
PDM (Sahoo 2010)		18.23	3.69	0.642	2.59	11.30	38.21	-
DFM (Sahoo 2010)		18.61	3.69	0.177	3.21	11.57	38.03	-
PDM (Debnath 2013)		13.64	3.43	0.03	0.73	9.45	30.74	-
PDM (Bora 2015)		13.07	3.51	0.110	1.04	8.39	35.75	-
DFM (Bora 2015)		19.31	3.49	0.180	2.25	13.36	30.83	~0.043

In PDM, diesel is the single injected pilot as well as primary fuel having very high cetane number, LHV, and lower viscosity in comparison to other fuels used in the present study. On the other hand, the advancement of CA50 and reduction of CD with the oxygenated fuels at the preheated atmoshophere augmented the heat release rate thereby increasing the in-cylinder pressure and temperature, with the result of a higher E_{cw}. The E_{cw} is found to increase with the increase of loads due to higher accumulation of fuels to overcome the higher imposed loads and the corresponding improvement in engine combustion process in all modes of engine operation. The lower E_{cw} without preheating in DFM is due to the cooling effects of biogas that has very high self-ignition temperature as it contains CO_2 as the major component.

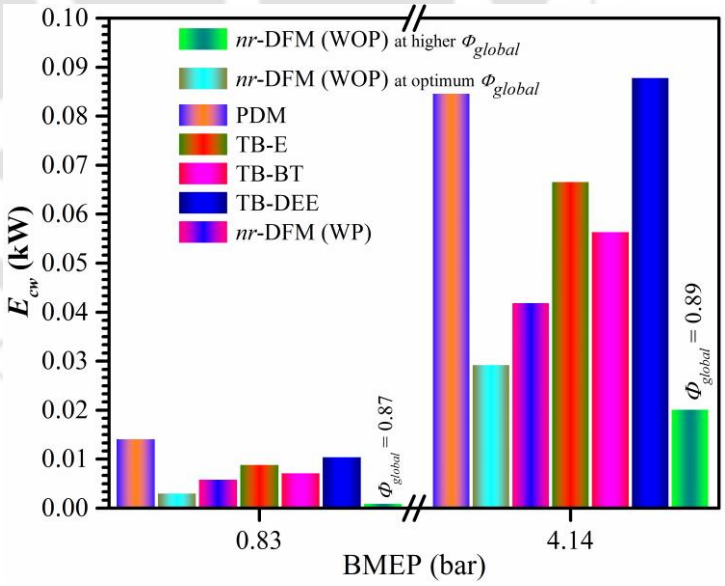

Fig. 8.11 Characteristics of E_{cw} with load

At the loads of 0.83 bar/4.14 bar, the E_{cw}, at optimum Φ_{global} in *nr*-DFM (WOP) are estimated at 0.0033 kW and 0.029 kW respectively. At the part load of 0.83 bar, the E_{cw} in *nr*-DFM (WP), with the blends of TB-BT, TB-E, and TB-DEE and in PDM are found to increase by 84.85%, 124.24%, 175.76%, 224.24% and 336.36% as compared to *nr*-DFM (WOP). At the higher loads of 4.14 bar, the increment of E_{cw}, in *nr*-DFM (WP), with the blends of TB-BT, TB-E, and TB-DEE and in PDM with respect to *nr*-DFM (WOP) are observed as 44.83%, 96.55%, 131.03%, 203.45%, and 193.10%, respectively. Sahoo (2010) noticed the increment of exergy of 262.72% in cooling water in PDM in comparison to DFM.

The variation in exergy in exhaust gas per unit time (E_{eg}) is shown in Fig. 8.12. The higher exergy in the exhaust gas is not desirable. The E_{eg} fully depends on positions of CA50, CPPs, peak positions of CMGTs, the efficiency of thermal energy conversion into mechanical energy and shorter CD. The positions of CA50, CPPs, and CMGTs nearer to TDC and the shorter CD mean better thermal energy conversion and utilization and the corresponding lower E_{eg}. Consequently, the lowest E_{eg} is noticed in PDM, with preheating and with various blended fuels in DFM in comparison to the one without preheating. At 0.83 bar/4.14 bar, the E_{eg} in *nr*-DFM (WOP) are noticed as 0.38 kW/1.47 kW, respectively. At 0.83 bar, the reductions of E_{eg} in *nr*-DFM (WP), with the blends of TB-BT, TB-E, and TB-DEE and in PDM relative to *nr*-DFM (WOP) at optimum Φ_{global} are estimated as 5.26%, 10.53%, 13.16%, 21.05% and 28.95%, respectively. While, at the part load of 0.83 bar and at higher Φ_{global} = 0.87, the drastic increment of 102.63% of E_{eg} with respect to the optimum Φ_{global} is calculated. Likewise, at the load of 4.14 bar, the reductions of E_{eg} as compared to *nr*-DFM (WOP) at optimum Φ_{global} in *nr*-DFM (WP), with the blends of TB-BT, TB-E and TB-DEE and in PDM are found as 3.40%, 7.48%, 10.20%, 16.33% and 20.41%, respectively. However, at this load, the increment of 70.75% of E_{eg} at the

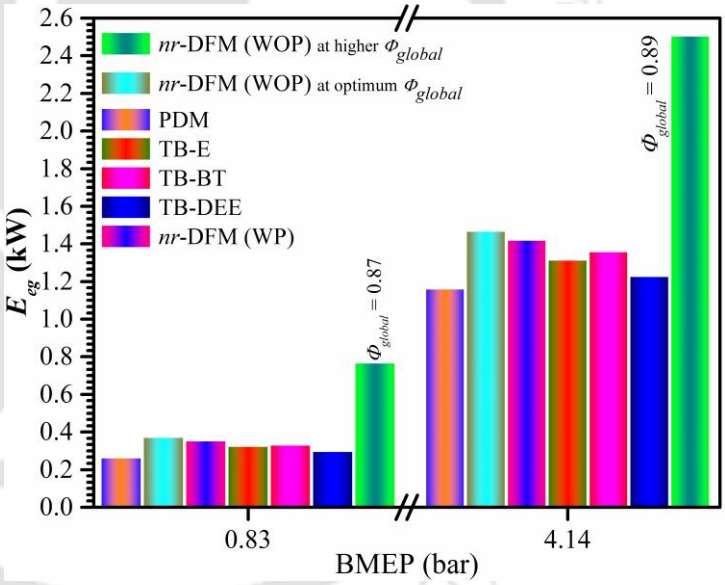

Fig. 8.12 Characteristics of E_{eg} with load

higher Φ_{global} of 0.89 as compared to optimum Φ_{global} in *nr*-DFM (WOP) is noticed. Similar results are also achieved by Sahoo (2010) and Bora (2015).

The lower rate of destruction of exergy (E_{des}) is always desirable to achieve the best utilization of the input energy. The variations of E_{des} are shown in Fig. 8.13. The exergy destructions at all loads are found to be lower in PDM. Whereas, in DFM with preheating and with the use of blended oxygenated fuels, the E_{des} are noticed to be lower than that one without preheating. At loads of 0.83/4.14 bar, the E_{des} in *nr*-DFM (WOP) are estimated as 7.11 kW/9.11 kW, respectively. At all loads and at optimum Φ_{global}, the variations of E_{des} are found to be nearer to each other. However, there are the decreasing trends of E_{des} with preheating and with the use of blended oxygenated fuels in DFM. At 0.83 bar, the reductions of E_{des} in *nr*-DFM (WP), with the blends of TB-BT, TB-E, and TB-DEE and in PDM in comparison to *nr*-DFM (WOP) are noticed as 5.76%, 5.91%, 6.05%, 8.72%, and 30.24%, respectively. Whereas, at this load, approximately three times higher E_{des} is observed at higher Φ_{global} of 0.87 as compared to that obtained at optimum Φ_{global} in *nr*-DFM (WOP). At 4.14 bar, the maximum reduction of E_{des} with TB-DEE and in PDM as compared to *nr*-DFM (WOP) are found to be 7.79% and 19.76%, respectively. The physical reasons of exergy destruction are similar to those of entropy generation (S_{gen}) (Knizley et al., 2012).

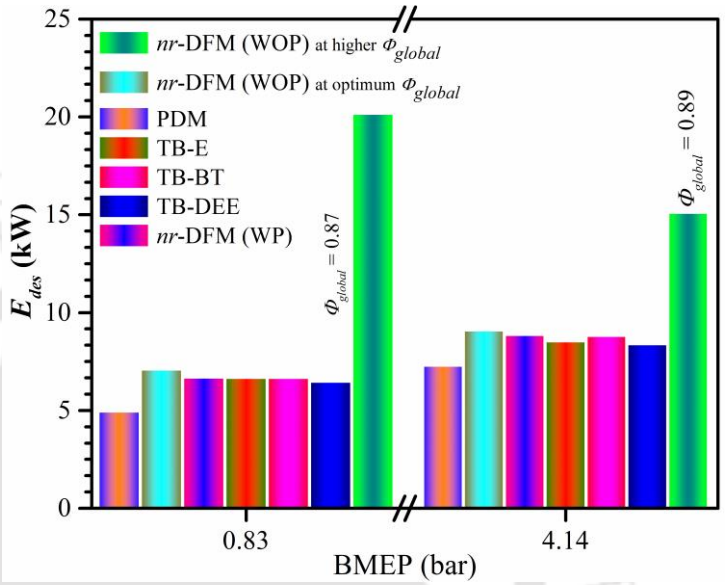

Fig. 8.13 Characteristics of E_{des} with load

The variations of exergy efficiency (η_{II}) are shown in Fig. 8.14. The higher η_{II} means the higher utilization of input energy or exergy. The higher η_{II} is noticed with preheating and with various oxygenated fuels at preheated atmosphere of the intake charge. It may be due to the progress of combustion upon preheating and with the use of oxygenated blends that release extra oxygen and helps to accelerate the flame front to propagate through the gas mixture inside the combustion chamber. At the loads of 0.83 bar/4.14 bar, the η_{II} in *nr*-DFM (WOP), are assessed as 13.20%/35.10%, respectively. At 0.83 bar the increments of η_{II} in *nr*-DFM (WP), with the blends of TB-BT, TB-E and TB-DEE, and in PDM with respect to *nr*-DFM (WOP) are

evaluated as 3.79%, 2.27%, 2.35%, 2.12%, and 25.83%, respectively. While, at the higher load of 4.14 bar, the maximum enhancements of η_{II} are calculated with TB-DEE and in PDM relative to *nr*-DFM (WOP) as 2.65% and 11.20%, respectively. In this present research work, at 100% load (= 4.14 bar), a similar η_{II} as reported by Sahoo (2010) is achieved. Moreover, the η_{II} in this investigation is found to be higher by 15.49% relative to one obtained by Bora (2015).

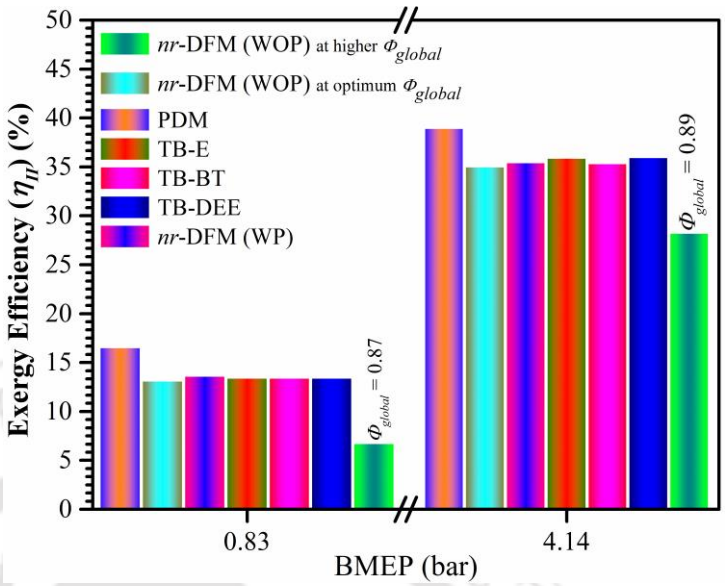

Fig. 8.14 Characteristics of exergy efficiency *(η_{II})* with load

The rate of generation of entropy (S_{gen}) is shown in Fig. 8.15. The higher the entropy generation means there will be the more loss of energy due to friction. Hence, the S_{gen} should be as minimum as possible. Comparatively lower S_{gen} at lower loads relative to higher loads is noticed. It may be due to the higher interactions of the gas mixtures and various moving parts in the combustion chamber. The maximum entropy generation is found at higher Φ_{global} at all loads. It may be due to the higher COV of IMEP, retarted CA50 and longer CD with increasing Φ_{global} due to higher induction of biogas. It is to be noted that higher induction of biogas necessarily would have higher amount of CO_2, which in turn, enhances the irreversibility by means of S_{gen} (Knizley et al., 2012). The S_{gen} is calculated based on the exergy destruction. Hence, the physical reasons of exergy destruction and entropy generation are similar. The lower S_{gen} with blended fuels (mainly with TB-DEE) may be due to the generation of higher

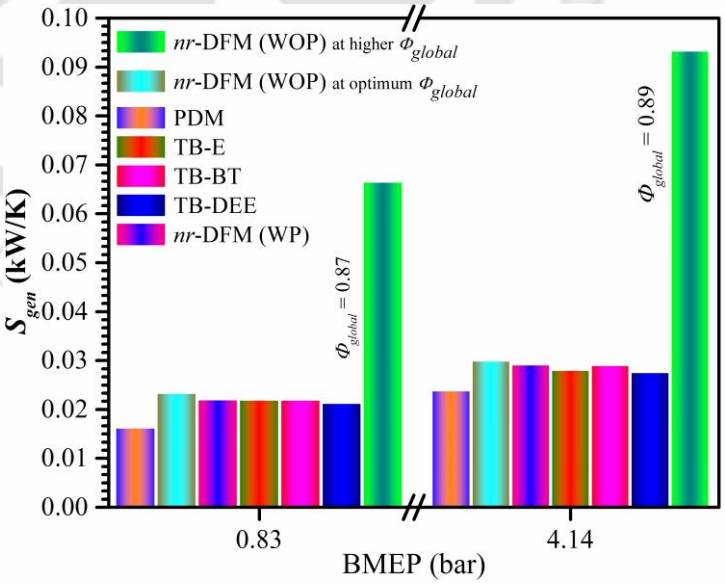

Fig. 8.15 Characteristics of S_{gen} with load

in-cylinder temperature that helps to burn almost all the fuel elements, besides causing an advancement of CA50 and a reduction of COV of IMEP. At the loads of 0.83 bar/4.14 bar, the S_{gen} in *nr*-DFM (WOP) are calculated as 0.023 (kW/K)/0.030 kW/K, respectively. At 0.83 bar, the reductions of S_{gen} in *nr*-DFM (WP), with the blends of TB-BT, TB-E, and TB-DEE as compared to *nr*-DFM (WOP) are estimated as 5.70%, 5.83%, 5.93%, and, 8.72%, respectively. While, at 4.14 bar, the reduction of S_{gen} with this same comparisons are noticed as 3.33%, 3.33%, 6.67%, and 10.00%, respectively.

8.3 Summary

The results of energy and exergy distribution over the applied load spectrum, from lower to higher Φ_{global}, without/with preheating and with the use of various blended liquid oxygenated pilot fuels are summarized below:

- At 4.14 bar, the highest reduction of energy input with TB-DEE with respect to the one in *nr*-DFM (WOP) with TB-DEE is found as 6.70%. The energy input is found to increase drastically with the increase of Φ_{global}.
- At the loads of 0.83 bar/4.14 bar, on an average 9.32%/26.17% of the input energy can be recovered in DFM. While rests of the energies are transported to the cooling water, exhaust gas and as uncounted losses. The maximum energy recovery of 26.99% is noticed with the TB-DEE blend.
- The energy in cooling water is found to be higher in *nr*-DFM (WP) and with the blended oxygenated fuels (TB-E, TB-BT, and TB-DEE). At 4.14 bar, the maximum increments of Q_{cw} with the TB-DEE blend and in PDM relative to the one in *nr*-DFM (WOP), are computed as 22.86%, and 28.57%, respectively.
- In DFM, the lower energy in exhaust gas is noticed with the blended fuels due to better utilization of the expansion energy. At 4.14 bar, concerning *nr*-DFM (WOP), the maximum reductions of Q_{eg} with the blend TB-DEE and in PDM are reckoned as 27.18%, and 41.91%, respectively. There is an adequate energy recovery with the use of the cross-flow heat exchanger.
- At 4.14 bar, the maximum recoverable exergy with respect to the input exergy, in PDM and with the blends of TB-DEE are found as 39.03% and 36.03%, respectively.

Chapter-9

Conclusions and Future Scopes

Chapter

Highlights:	**Overview:** *Researchers all over the world have noticed difficulties to achieve an efficient overall performance in DFM engine in comparison to PDM. All most all the investigators have found the performance penalty in DFM at standard setting (mainly CR and IT) of the engine operating parameters as compared to PDM. Another noticeable point is that biogas has lower LHV, very high self-ignition temperature and very high amount of CO_2 that worsen the combustion quality. Besides, very few experimental studies have been carried out in DFM with the aim of higher consumption of biogas (at misfire limit of gas mixture). The researchers have noticed the performance penalty of the biogas run DFM engine even at the advanced IT and at higher CR. Thus, in the present study, the parameters optimum global fuel-air equivalence ratio, preheating of intake charge and use of various renewable oxygenated fuel are observed to be crucial to make the biogas DFM engine performance (at standard IT = 23 CAD bTDC and CR = 17.5) competitive to PDM. The aim of this chapter is to summarize all the key findings of the present investigation.*
• *Presents the contribution of the present research work* • *Summarize the key findings achieved in various parametric states* • *Briefly discusses on application potential of the present study* • *Recommends the future scopes of the present study*	

***Chapter Layout*:**

9.1 Contribution of the Present Research Work

It is an extremely challenging task to achieve a competitive engine performance by DFM as compared to PDM at the standard CR and IT. In this benchmark research work, the methodology adapted to the biogas run DFM engine comprises the following:

- the optimization of Φ_{global} at each of the applied load on the engine
- the preheating of the intake charge (biogas-air mixture)
- the implementation of binary and ternary blends of oxygenated renewable fuels, and
- the thermodynamic potential study to understand the physical relations among different parameters involves in the estimation of engine performance, combustion and emissions.

9.1.1 Results of Biogas Run DFM Engine Using Diesel and the Optimization of Φ_{global}

The investigations have been carried out with numerous Φ_{global} to optimize the working range of Φ_{global} from part to higher loads and with intake charge preheating. The key findings obtained in this part of the study are summarized below:

Role of Φ_{global} on Engine Performance

- The results obtained in *nr*-DFM (WOP/WP) mode reveal the decisive influence of Φ_{global} on engine performance and pollutant emission. The ranges of optimum Φ_{global}/load (bar.) are found as 0.29–0.31/0.83, 0.35–0.36/1.65, 0.40–0.43/2.48, 0.47–0.5/3.31, and 0.53–0.60/4.14.
- At 0.83 bar, there is an increment of BTE by 5.72% with preheating. At the higher load of 4.14 bar., a reduction of BTE by 55.21% is noticed (without preheating) on increasing the Φ_{global} from 0.53 to 0.89; while with preheating (at Φ_{global} = 0.58), there is an increment of BTE by 2.60% in comparison to the one without preheating.
- The BFR (kg/h)/Φ_{global} are varied within the range of 0.67/0.30 to 3.99/0.89. Within this range of BFR (kg/h)/Φ_{global}, the DR (%)/BES (%) are found in the range of 30.69%/46.69% to 92.49%/97.55%, respectively.
- The analysis reveals that a lower Φ_{global} at part load and higher Φ_{global} at higher load is suitable for improving the biogas DFM engine performance. With preheating, the optimum Φ_{global}/load (bar.) are observed as 0.31/0.83, 0.35/1.65, 0.42/2.48, 0.48/3.31, and 0.58/4.14.

Role of Φ_{global} on Engine Combustion

- In the tested range of loads, the IDs are found to increase drastically with the increase of Φ_{global}. At 4.14 bar, the increment of ID with the increase of Φ_{global} from 0.53 to 0.89 is is found to be 37.14%. However, with preheating, the ID is found to decrease.
- A drastic reduction of NHRR is noticed at higher Φ_{global}. At 0.83 bar, the peaks of NHRR (J/CAD)/Φ_{global} are observed to be 47.72/0.30, 11.12/0.87. At 4.14 bar, the maximum (with preheating) and minimum peaks of NHRRs (J/CAD)/Φ_{global} are noticed as 88.17/0.58, and 21.71/0.89, respectively.
- The CPPs are observed to be reduced drastically with the increase of Φ_{global}. Upon increase of Φ_{global}, the crank angle positions of the CPPs are shifted toward right sides of the TDC. However, with preheating, it shifts towards TDC.
- The cycle-by-cycle variations of CPP are found to be higher at the higher Φ_{global}. However, it reduces with the increase of loads and preheating.
- The CD is found to increase with the increase of Φ_{global}. There is a drastic reduction of CMGT at higher Φ_{global}. At 4.14 bar, the reduction of CMGT is estimated as 20.99% on increase of Φ_{global} from 0.53 to 0.89 relative to the Φ_{global} of 0.53.

Role of Φ_{global} on Engine Emission

- At 0.83 bar (with preheating and at Φ_{global} = 0.31), the reduction of CO by 29.41% is noticed in comparison to the one without preheating. While, at 4.14 bar, there is a reduction of CO (with preheating and Φ_{global} = 0.58) by 65.49% as compared to the one without preheating. The emission of CO_2 is observed to increase with an increase of Φ_{global} and with intake charge preheating.
- The HC is found to very high at higher Φ_{global}. However, at optimum Φ_{global}, with preheating, the HC is found to reduce. At higher load (4.14 bar) and with preheating, a reduction of HC by 53.33% is recorded. A drastic reduction of NO_x is observed with the increment of Φ_{global}. While, with preheating, the NO_x is found to increase.

9.1.2 Results of Biogas Run DFM Engine Using Binary Blend (Diesel and Ethanol)

In this subsection, results of *nr*-DFM (WOP/WP), with E-5 blend at the optimized Φ_{global} are summarized. The results of PDM, in some cases, are also presented in order to have a direct comparison.

Performance Analysis

- At the loads of 1.65/4.14 bar, the BFRs with E-5 blend are noticed to be 0.66 kg/h/1.18 kg/h. At 4.14 bar, the BES in all states (except for the case of without preheating) are found to lesser than 50%.
- The BSEC in *nr*-DFM (WP) and with E-5 blend are found nearer to each other, while it is noticed to be lower than that in *nr*-DFM (WOP). At 4.14 bar, in *nr*-DFM (WP) and with E-5 blend, the BTEs are observed as 1.75% and 2.98% higher in comparison to *nr*-DFM (WOP).
- A higher reduction of VE is noticed in DFM. With preheating, this drop is found to be more. At 4.14 bar, in *nr*-DFM (WP) and with E-5 blend, the VEs are found to reduce by 6.19% and 5.98%, respectively.

Combustion Analysis

- The ID in PDM reduces with increasing of loads, while the reverse trends is noticed in DFM. The IDs with *nr*-DFM (WP) and E-5 blend are noticed to be closer to each other. However, on an average, it is found to lesser by 7.46% than that in *nr*-DFM (WOP).
- At 1.65 bar, there is an increment of NHRR of 0.74% and 12% attained with the E-5 blend and in *nr*-DFM (WP), respectively, in comparison to *nr*-DFM (WOP). At higher loads, more shifting of peaks of NHRR towards left from the TDC is noticed.
- In general, there is an increment of CPP with the preheating and shifting of the crank angle position of CPP towards TDC. At 4.14 bar, the CPP (bar)/CAD in *nr*-DFM (WOP), *nr*-DFM (WP) and with E-5 blend are found as 65.1/371, 68.1/370 and 66.2/369, respectively.

Emission Analysis

- There is a significant reduction of CO emission with preheating and with E-5 blend. At 4.14 bar, the reduction of 17.2% of CO emission with E-5 blend relative to PDM, is assessed.
- The lower emission of HC at the higher load is achieved with the E-5 blend. However, at part loads, the emissions of HC are found to be higher in comparison to PDM. At 4.14 bar, the reduction of 31.11% of HC with E-5 in contrast to PDM blend is evaluated.
- The NO_x emission is found to increase with increase of loads, preheating and with E-5 blend. Substantial reduction in NO_x emission in DFM relative to PDM is attained. At

4.14 bar, the reduction of NO_x in *nr*-DFM (WOP), *nr*-DFM (WP) and with E-5 blend in comparison to PDM are found to be 62.87%, 34.70% and 28.51%, respectively.

9.1.3 Results of Biogas Run DFM Engine Using Ternary Blends (Diesel, Biodiesel, and Ethanol)

In this subsection, the results of DFM (at the optimum Φ_{global} and with preheating) with ternary blends of diesel-biodiesel-ethanol (viz. TB-E1, TB-E2, TB-E3, TB-E4 and TB-E5) are summarized below:

Performance:

- The BFRs are observed to be confined within the ranges of 0.722-0.731 to 1.173-1.180 from the part (0.83 bar) to higher (4.14 bar) loads. Due to lower cumulative LHV than the pure diesel fuel, the higher BFRs are observed with the TB-Es fuel.
- The lower BSEC is observed with the TB-E3 blend in comparison to other blends. At 4.14 bar (=100% load), with TB-E3, the BTE is evaluated as 26.73% which is 1.29% and 5.04% higher than that in *nr*-DFM (WP) and with TB-E1 blends, respectively. A lower VE is found in DFM. The higher reduction of VE is observed with preheating. At the loads of 1.65 bar/4.14 bar, the higher LFRs are observed with TB-E3 blend and they are estimated as 31.16%/39.64%.
- The maximum ADR is also noticed with TB-E3 blend. At the loads of 1.65/4.14 bar, the ADRs are found as 51.81%/57.75%. At 4.14 bar, the maximum BES is noticed to be 48.68% with TB-E3 blend and the corresponding BFES is found as 51.32%.

Combustion:

- The ID in PDM is found lower and reduces with the increase of loads, whereas in DFM the reverse trends are noticed. In DFM, the ID reduces with the intake chare preheating. The lower IDs in DFM are achieved in *nr*-DFM (WP) and with TB-E3 blend. At 4.14 bar, in *nr*-DFM (WP), and with TB-E3 blend, the IDs are found to be lower for each of the cases by 15.63% than that in *nr*-DFM (WP).
- In DFM, there is a shifting of CPP (CAD) as compared to the case of without preheating. The higher gain of energy with preheating is noticed with TB-E3 blend and in *nr*-DFM (WP) relative to that in *nr*-DFM (WOP).
- The peak of the NHRR in *nr*-DFM (WOP) is found to be lower and gets shifted towards the right of TDC. While, with preheating, the peak of NHRR is noticed to be closer to

TDC (3 CAD bTDC). In DFM, at 4.14 bar, the maximum peak of NHRR of 82.5 J/CAD is observed in DFM with TB-E3 blend.

- The CMGTs are observed to be higher for preheating as well as with the blended fuels. At 4.14 bar, the higher CMGT of 1868.64 K is observed with TB-E3 blend. The cyclic variations with preheating, with the increasing of loads and with TB-E3 blend, are noticed to be lower. The higher cyclic variations are attained in *nr*-DFM (WOP).

Emission:

- Overall, there is a substantial reduction of CO emission in DFM at the preheated state of the intake charge and with the use of oxygenated liquid fuels. At the loads of 1.65/4.14 bar, the maximum reduction of CO of 61.90/86.23% are noticed with TB-E3 blend as compared to *nr*-DFM (WOP).
- Similar results for HC emission are also noticed with preheating and with the blended fuels. At 4.14 bar, a substantial reduction of 83.97% of HC with the TB-E3 blend relative to *nr*-DFM (WOP) is achieved. The lower NO_x is attained in DFM, however, found higher with preheating and with the blended fuels. At 4.14 bar, the maximum reduction of NO_x in *nr*-DFM (WOP) as compared to PDM is estimated to be 63.04%.

Among all the blends, TB-E3 is noticed to be optimum and with this blend, a diesel-like overall performance is achieved.

9.1.4 Results of Biogas Run DFM Engine Using Ternary Blends (Diesel-Biodiesel-Butanol/Diesel-Biodiesel-Diethyl Ether)

In this subsection, the results of DFM with three ternary blends (TB-E, TB-BT, and TB-DEE) as the pilot fuels have been summarized below:

Performance:

- The higher BFR is noticed with the TB-DEE blend, which is considerably lower than that of *nr*-DFM (WOP). There is a marginal variation of BFR at part load. At 4.14 bar, the minimum reduction of BFR with TB-DEE with respect to *nr*-DFM (WOP) is assessed to be lower by 5.16%.
- At part loads, there is a marginal reduction of BSECs in comparison to *nr*-DFM (WOP). However, at 4.14 bar, there is a considerable reduction of BSECs with the blends of TB-E and TB-DEE as compared to the one in *nr*-DFM (WOP) and they are estimated as 5.66% and 6.27%, respectively.

- Overall, the BTE is found to be higher with preheating and with the blended fuels. At 4.14 bar, the maximum increment of BTE with the blend of TB-DEE in comparison to that in *nr*-DFM (WOP) is calculated to be 6.69%.
- Throughout the load spectrum, higher BES is noticed with TB-DEE. The BES/BFES from part to higher loads are found to vary approximately as 50%/50%.
- In all cases, the LFRs with preheating and with the blended fuels are noticed to be higher. At the loads of 0.83 bar/4.14 bar, the maximum increment of LFRs with TB-DEE relative to *nr*-DFM (WOP) is found as 7.74%/6.50%. At the loads of 0.83 bar/4.14 bar, the maximum ADR of 55.04%/59.84% is also found with TB-DEE.

Combustion:

- The similar trends of IDs are noticed with TB-DEE and in PDM. At all loads, the maximum and minimum IDs are noticed in *nr*-DFM (WOP) and with TB-DEE blend, respectively. At 0.83 bar/4.14 bar, the maximum reduction of ID with TB-DEE relative to the one without preheating is calculated as 13.6%/48.13%.
- In all cases, the higher increment and higher shifting (towards TDC) of CPPs are found with preheating, with the blended fuels and at higher loads. At 4.14 bar, the maximum increment of CPP (7.27%) and shifting (6 CAD aTDC) are noted with the blend of TB-DEE as compared to the case without preheating.
- Overall, the higher NHRRs are found with preheating, with the use of blended fuels and at higher loads. At 4.14 bar, the maximum rise of NHRRs (%)/CAD (bTDC) with TB-DEE blend as compared to that in *nr*-DFM (WP) is evaluated as 8.24%/4 in in *nr*-DFM (WP).
- As there is flame propagation, the shorter CD is noticed in DFM than PDM. At all loads, the maximum CD is noticed in *nr*-DFM (WOP). At 4.14 bar, the maximum reductions of CD with TB-DEE blend in comparison to that in *nr*-DFM (WOP) is estimated to be 40.42%.
- At all loads, the maximum CMGT is assessed with the TB-DEE blend. At the loads of 1.65 bar and 4.14 bar, the maximum increment of the peak of CMGT (%)/CAD (aTDC) with TB-DEE as compared to the one in *nr*-DFM (WOP) are calculated as 12.08/17 and 16.35/20, respectively.
- Throughout the load spectrum, higher EGT is noticed in *nr*-DFM (WOP) and lower with TB-DEE. At 0.83 bar/4.14 bar, the highest reduction of EGTs with TB-DEE blend

relative to that in *nr*-DFM (WOP), are evaluated as 7.79%/7.92%. The cyclic variations are found to reduce with the increase of loads. It is found to be lower with the TB-DEE blend.

Emission:

- From part to higher loads, with TB-DEE blend, the CO emissions are found to be lower. At 0.83 bar, there is a 10.94% reduction of CO emission with the TB-DEE blend. At 4.14 bar, the reductions of CO with TB-BT, TB-E and TB-DEE with respect to the one in PDM are observed as 6.90%, 34.48% and 51.72%, respectively.
- In DFM with blended fuels, the HC is observed to be lower than that in PDM within the range of higher loads of 3.31 to 4.14 bar. At the loads of 0.83 bar/4.14 bar, the maximum reductions of HC with TB-DEE as compared to that in *nr*-DFM (WOP) are found as 36.02%/88.55%.
- The NO_x in DFM is found to be substantially lower than in PDM. With reference to PDM, the maximum reduction of NO_x of 63.04% at 4.14 bar is found in *nr*-DFM (WOP).

9.1.5 Results of Energy and Exergy Analysis

The results of energy and exergy distribution over the applied load spectrum, without/with preheating and with the use of various blended liquid oxygenated pilot fuels are summarized below:

- At 4.14 bar, the highest reduction of energy input with TB-DEEwith respect to that in *nr*-DFM (WOP) is found as 6.70%. The energy input is found to increase drastically with the increase of Φ_{global}.
- At the loads of 0.83 bar/4.14 bar, on an average 9.32%/26.17% of the input energy can be recovered in DFM. While rests of the energies are transported to the cooling water, exhaust gas and as uncounted losses. The maximum energy recovery of 26.99% is noticed with the TB-DEE blend.
- In DFM, the lower energy in exhaust gas is noticed with the blended fuels due to better utilization of the expansion energy. At 4.14 bar, concerning *nr*-DFM (WOP), the maximum reductions of Q_{eg} with the blend TB-DEE and in PDM are reckoned as

27.18%, and 41.91%, respectively. There is an adequate energy recovery with the use of the cross-flow heat exchanger.

- The energy in cooling water is found to be higher in *nr*-DFM (WP) and with the blended oxygenated fuels (TB-E, TB-BT, and TB-DEE). At 4.14 bar, the maximum increments of Q_{cw} with the TB-DEE blend and in PDM relative to the one in *nr*-DFM (WOP), are computed as 22.86%, and 28.57%, respectively.
- At 4.14 bar, the maximum recoverable exergy with respect to the input exergy, in PDM and with the blends of TB-DEE are found as 39.03% and 36.03%, respectively.

9.2 Application Potential

The nobility of a new technology is to keep enduring of the existing technologies upon which the development and progress of the society are significantly dependent. The billions and billions existing diesel engines have been working in transport as well as in stationary power productions sectors to serve the nations throughout the world. However, the fossil diesel has been depleting with acceleration and emitting carcinogen pollutant into green environment. Besides, most of the engines working commercially have the standard CR and IT. Thus, there is a huge possibility to implement the present methodology in existing diesel engines to reduce the emissions as well as to achieve a performance competitive to PDM.

Some of the key data (at standard CR and IT) obtained from the biogas run DFM engine are shown in Table 9.1. Form the entire investigation, the emission levels of the DFM engine, in general, are found to be lower at higher loads as compared to the values at lower loads. In any case, these are observed to be within the limits of the specified norms (Table 1.3) as discussed earlier. For clarity, these emission data in gm/kW-h are presented in Appendix-D. Thus, it is evident from the tabulated data (Table 9.1) that the biogas run DFM engine can efficiently be used to generate the power in rural areas particularly in the developing countries like India.

Table 9.1 Key data of the present research work

Engine Mode	Pilot Fuels	BTE (%)	BFR	ADR (%)	NHRR (J/)	CPP (bar)	CMGT (K)	Emissions		
								CO (vol.%)	HC (ppm)	NOx (ppm)
PDM	Pure Diesel	30.6	-	-	91.6	72.3	1917.2	0.029	45	1196
DFM	TB-BT	26.3	1.15	55.49	81.0	68.2	1864.7	0.027	29	784
	TB-E	26.7	1.17	57.75	82.4	68.7	1868.6	0.019	21	887
	TB-DEE	26.9	1.21	59.84	85.6	69.7	1928.3	0.014	15	1131

At applied load = 4.14 bar, engine standadrd CR = 17.5 and IT = 23 CAD bTDC

9.3 Future Scopes

In this research work, an attempt has been made to improve the biogas run DFM engine overall performance at the standard CR and IT and competive to PDM. This is to convert the existing diesel engines (existing technology) into DFM without altering the engine operating parameters. Besides, it is will be easier to fall back to the PDM when there is a shortage of gaseous fuels. Hence, the present study definitely will have the great impact on the society of engine research. Though the attempt has been made to cover all the aspects to improve the performance of the biogas run DFM engine (at the standard CR and IT) in the present study, however, there is enough scope to carry out further investigations to make the biogas biogas DFM engine more efficient. In this context, some scopes and suggestions for future studies are underlined here.

- Upgraded biogas as the inducted gaseous fuel can be efficiently implemented in DFM. Simultaneously, various liquid oxygenated fuels as the pilot fuel can be used to improve the engine performance.
- The blends of upgraded biogas and hydrogen as the inducted (primary or secondary) fuel and various oxygenated fuels blended with diesel (as the pilot) can be used simultaneously in DFM engine.
- Owing to the introduction of biogas in engine cylinder, the speed increases due to enhancement of cumulative LHV of the total fuel used. The existing governor is incompetent to control the engine rpm. Hence, there is a scope to design a suitable governor for the DFM engine for smooth operation.
- The raw biogas blended with CH_4/LPG can be used to do the further investigation using the same experimental methodology.
- Raw biogas is the less reactive gaseous fuel. Therefore, the engine can be run in reactivity controlled compression ignition (RCCI) mode to achieve ultra-low emissions as well as higher engine efficiency.
- There is scope to study on the effects of injection pressure for further improvement of the of the biogas DFM engine performance, combustion and emission characteritics.
- There is also a scope to run the engine on long-term basis to inspect the various parts such as nozzle tip, engine valves, piston, cylinder walls etc.
- A computer code can be developed to validate the present study, using single or multi zone models. Consequently, numerous study can be done using various parameters.

REFERENCES

Abassi A, **Khalilarya Sh**, and **Jafarmadar S**, (2010), The influence of the inlet charge temperature on the second law balance under the various operating engine speeds in di diesel engine, *Fuel*, **89**, 2425–2432.

Abd Alla GH, **Soliman HA**, **Badr OA**, and **Abd Rabbo MF**, (2000), Effect of pilot fuel quantity on the performance of a dual fuel engine, *Energy Conversion and Management*, **41**, pp. 559–572.

Abd-Alla GH, **Soliman HA**, **Badr OA**, and **Abd-Rabbo MF**, (2001), Effect of diluent admissions and intake air temperature in EGR on the emissions of an IDI dual fuel engine, *Energy Conversion and Management*, **42**, pp. 1033–1045.

Ahuja D, and **Tatsutani M**, (2009), Sustainable energy for developing countries, SAPIENS, 2, pp. 1–16.

Aklouche FZ, **Loubar K**, **Bentebbiche A**, **Awad S**, and **Tazerout M**, (2018), Predictive model of the diesel engine operating in dual-fuel mode fueled with different gaseous fuels, *Fuel*, **220**, pp. 599-606.

Aleiferis PG, and **Behringer MK**, (2015), Flame front analysis of ethanol, butanol, iso-octane and gasoline in a spark-ignition engine using laser tomography and integral length scale measurements, *Combustion and Flame*, **162**, pp. 4533–4552.

Alkidas AC, (1999), Combustion-chamber crevices: the major source of engine-out hydrocarbon emissions under fully warmed conditions, Progress in Energy and Combustion Science, 25, pp. 253–273.

Al-Najem NM, and **Diab JM**, (1992), Energy – exergy analysis of a diesel engine, *Heat Recovery Systems and CHP*, 81, pp. 2097-2102.

Alptekin E, (2017), Evaluation of ethanol and isopropanol as additives with diesel fuel in a CRDI diesel engine, *Fuel*, 205, pp. 161-172.

Ayres RU, **Ayres LW**, and **Warr B**, (2003), Exergy, power and work in the US economy, 1900–1998, *Energy*, 28, pp. 219–273.

Badr O, **Karim GA**, and **Liu B**, (1999), An examination of the flame spread limits in a dual fuel engine, *Applied Thermal Engineering*, 19, pp. 1071-1080.

Bailey B, **Eberhardt J**, **Goguen S**, and **Erwin J**, (1997), Diethyl ether (DEE) as a renewable diesel fuel, SAE Paper no. 972978.

Bahman N, **Vahab P**, **Gholamhassan N**, **Talal Y**, and **Barat G**, (2007), Experimental investigation of performance and emission parameters of a small diesel engine using CNG and biodiesel, *SAE*, paper no. 2007-32-0075.

Balat M, and **Balat H**, (2009), Biogas as a renewable energy source- a review, *Energy Sources, Part A* 31, pp. 1280-93.

Balmer RT, (1999), Thermodynamics, Jaico Publication, ISBN: 81-7224-783-4.

Barik D, and **Murugan S**, (2014), Investigation on combustion performance and emission characteristics of a DI (direct injection) diesel engine fueled with biogas-diesel in dual fuel mode, *Energy*, 72, pp. 760–771.

Barik D, and **Murugan S**, (2016), Experimental investigation on the behavior of a DI diesel engine fueled with raw biogas–diesel dual fuel at different injection timing, *Journal of the Energy Institute*, 89(3), pp. 373–388.

Barik D, and **Murugan S**, (2016a), Effects of diethyl ether (DEE) injection on combustion performance and emission characteristics of karanja methyl ester (KME)-biogas fueled dual fuel diesel engine, *Fuel*, 164, pp. 286–296.

Barik D, and **Sivalingam M**, (2014), Investigation on performance and exhaust emissions characteristics of a DI diesel engine fueled with karanja methyl ester and biogas in dual fuel mode, *SAE Technical Paper*, SAE International.

Bedoya ID, **Arrieta AA**, and **Cadavid FJ**, (2009), Effects of mixing system and pilot fuel quality on diesel–biogas dual fuel engine performance, *Bioresource Technology*, 100, pp. 6624–6629.

Bedoya ID, **Saxena S**, **Cadavid FJ**, **States U**, and **Dibble RW**, (2011), Numerical analysis of biogas composition effects on combustion parameters and emissions in biogas fueled HCCI engines for power generation, *Proceedings of the ASME 2011 Internal Combustion Engine Division Fall Technical Conference ICEF2011 Morgantown, West Virginia*, West Virginia, pp. 1–18.

Bhale PV, **Deshpande NV**, and **Thombre SB**, (2009), Improving the low temperature properties of biodiesel fuel, *Renewable Energy*, 34, pp. 794–800.

Bora BJ, **Saha UK**, **Chatterjee S**, and **Veer V**, (2014), Effect of compression ratio on performance, combustion and emission characteristics of a dual fuel diesel engine run on raw biogas, *Energy Conversion and Management*, 87, pp. 1000–1009.

Bora BJ, (2015), Standardizing the specifications of a biogas run dual fuel diesel engine for stationary applications, Ph.D. thesis, Department of Mechanical Engineering, Indian Institute of Technology Guwahati, India.

Bora BJ, and **Saha UK**, (2015a), Improving the performance of a biogas powered dual fuel diesel engine using emulsified rice bran biodiesel as pilot fuel through adjustment of compression ratio and injection timing, *ASME Journal Engineering for for Gas Turbines and Power*, 137(9), p. 91505.

Bora, BJ, and **Saha UK**, (2015b), Comparative assessment of a biogas run dual fuel diesel engine with rice bran oil methyl ester, pongamia oil methyl ester and palm oil methyl ester as pilot fuels, *Renewable Energy*, 81, pp. 490–498.

Bora BJ, and **Saha UK**, (2016a), Optimisation of injection timing and compression ratio of a raw biogas powered dual fuel diesel engine, *Applied Thermal Engineering*, 92, pp. 111–121.

Bora BJ, and **Saha UK**, (2016b), Experimental evaluation of a rice bran biodiesel - biogas run dual fuel diesel engine at varying compression ratios, *Renewabe Energy*, 87, pp. 782–790.

Bora BJ, and **Saha UK**, (2016c), Estimating the theoretical performance limits of a biogas powered dual fuel diesel engine using emulsified rice bran biodiesel as pilot fuel, *ASME Journal of Energy Resources Technology*, **138**(2), p. 21801.

Bora BJ, and **Saha UK**, (2016d), Theoretical performance limits of a biogas – diesel powered dual fuel diesel engine for different combinations of compression ratio and injection timing, *ASCE Journal of Energy Engineering*, 142(2), p. E4015001-9.

Bora BJ, and **Saha UK**, (2017), Emission reduction operating parameters for a dual-fuel diesel engine run on biogas and rice-bran biodiesel, *ASCE Jouranl Energy Engineering*, 143(4), p. 4016064.

Borgnakke C, and **Sonntag RE**, (2013), Fundamentals of thermodynamics, 8th Edition, John Wiley & Sons, Inc., ISBN 978-1-118-13199-2.

Borjesson P, and **Berglund M**, (2006), Environmental systems analysis of biogas systems—Part 1: Fuel-cycle emissions, *Biomass and Bioenergy*, 2006, 30(5) pp. 469–85.

BP (British Petroleum) statistical review of world energy, June 2013.

BP Energy Outlook (2017). (https://www.bp.com/content/dam/bp/pdf/energy-economics/energyoutlook-2017/bp-energy-outlook-2017.pdf.)

BP Energy Outlook (2018). **(**https://www.bp.com/content/dam/bp/en/corporate/ pdf/energy-economics/energy-outlook/bp-energy-outlook-2018.pdf.)

Busby JW, and **Shidore S**, (2017), When decarbonization meets development: the sectoral feasibility of greenhouse gas mitigation in India, *Energy Research & Social Science*, 23, pp. 60–73.

Cacua K, **Amell A**, and **Cadavid F**, (2012), Effects of oxygen enriched air on the operation and performance of a diesel-biogas dual fuel engine, *Biomass and Bioenergy*, **45**, pp. 159–167.

Caton JA, (2000), On the destruction of availability (exergy) due to combustion processes - with specific application to internal-combustion engines, *Energy*, 25, pp. 1097–1117.

Caton PA, **Hamilton LJ**, and **Cowart JS**, (2011), Understanding ignition delay effects with pure component fuels in a single-cylinder diesel engine, *ASME Journal of Engineering for Gas Turbines and Power*, 133(3), p. 32803.

Caton JA, (2012), The thermodynamic characteristics of high efficiency, internal-combustion engines, *Energy Conversion and Management*, 58, pp. 84–93.

Carlucci AP, **Ficarella A**, **Laforgia D**, and **Strafella L**, (2017), Improvement of dual-fuel biodiesel-producer gas engine performance acting on biodiesel injection parameters and strategy, *Fuel* 209, 754-768.

Central Pollution Control Board, Ministry of environment, forecast and climate change, Parivesh Bhawan, East Arjun Nagar, Delhi-110032.

Cetinkaya M, **Ulusoy Y**, **Tekin Y**, and **Karaosmanoglu F**, (2005), Engine and winter road test performances of used cooking oil originated biodiesel, *Energy Conversion and Management*, 46 pp. 1279–91.

Chintala V, and **Subramanian KA**, (2014), Assessment of maximum available work of a hydrogen fueled compression ignition engine using exergy analysis, *Energy*, 67, pp. 162-175.

Chintala V, and **Subramanian KA**, (2017), A comprehensive review on utilization of hydrogen in a compression ignition engine under dual fuel mode, *Renewable and Sustainable Energy Reviews*, 70, pp. 472–491.

Cheng J, (2010), Biomass to renewable energy process, CRC Press, Taylor and Francis Group, North Carolina, ISBN-978-1-4200-9517-3.

Chen Z, **Liu J**, **Han Z**, **Du B**, **Liu Y**, and **Lee C**, (2013), Study on performance and emissions of a passenger-car diesel engine fueled with butanol-diesel blends, *Energy*, 55, pp. 638–646.

Corrêa SM, and **Arbilla G**, (2005), Formaldehyde and acetaldehyde associated with the use of natural gas as a fuel for light vehicles, *Atmospheric Environment*, 39, 4513-4518.

Debnath BK, (2013), Experimental and theoretical routes towards assessing the potential of emulsified palm biodiesel as an alternative to diesel fuel, Ph.D. thesis, Department of Mechanical Engineering, Indian Institute of Technology Guwahati, India.

Debnath BK, **Sahoo N**, and **Saha UK**, (2013a), Adjusting the operating characteristics to improve the performance of an emulsified palm oil methyl ester run diesel engine, *Energy Conversion and Management*, 69, pp. 191–198.

Debnath BK, **Sahoo N**, and **Saha UK**, (2013b), Thermodynamic analysis of a variable compression ratio diesel engine running with palm oil methyl ester, *Energy Conversion and Management*, 65, pp. 147–154.

Debnath BK, **Bora BJ**, **Sahoo N**, and **Saha UK**, (2014a), Influence of emulsified palm biodiesel as pilot fuel in a biogas run dual fuel diesel engine, *ASCE Journal of Energy Engineering*, 140(3), p. A4014005.

Debnath BK, **Sahoo N**, and **Saha UK**, (2014b), Theoretical route toward the estimation of second law potential of an emulsified palm biodiesel run diesel engine, *ASCE Journal of Energy Engineering*, 140(3), A4014007-1-10.

De Oliveira A, **De Morais AM**, **Valente OS**, and **Sodré JR**, (2015), Combustion characteristics, performance and emissions from a diesel power generator fuelled by B7-ethanol blends, *Fuel Processing Technology*, 139, pp. 67–72.

Dentice d'Accadiaa M, and **Vanoli L**, (2004), Thermoeconomic optimisation of the condenser in a vapour compression heat pump, *International Journal of Refrigeration*, 27, pp. 433–441.

Dhole AE, **Yarasu RB**, **Lata DB**, **Priyam A**, (2014), Effect on performance and emissions of a dual fuel diesel engine using hydrogen and producer gas as secondary fuels, *International Journal of Hydrogen Energy*, 39, pp. 8087-8097.

Ding X, and **Hill PG**, (1986), Emissions and fuel economy of a prechamber diesel engine with natural gas dual fueling, SAE Paper no. 860069.

Doğan O, (2011), The influence of n-butanol/diesel fuel blends utilization on a small diesel engine performance and emissions, *Fuel*, 90, pp. 2467-2472.

Duc MP, and **Wattanavichien K**, (2007), Study on biogas premixed charge diesel dual fuelled engine, *Energy Conversion and Management*, 48, pp. 2286–2308.

Elliot MA, and **Davis RE**, (1951), Dual fuel combustion in diesel engines, *Industrial Engineering Chemistry*, 43, pp. 2854-2863.

Emiroğlua AO, and **Şen M,** (2018), Combustion, performance and exhaust emission characterizations of a diesel engine operating with a ternary blend (alcohol-biodiesel-diesel fuel), *Applied Thermal Engineering*, 133, pp. 371-380.

Fang Q, **Fang J**, **Zhuang J**, and **Huang Z**, (2013), Effects of ethanol-diesel-biodiesel blends on combustion and emissions in premixed low temperature combustion, *Applied Thermal Engineering*, **54**(2), pp. 541–548.

Feroskhan M, **Ismail S**, **Reddy MG**, and **Teja AS**, (2018), Effects of charge preheating on the performance of a biogas-diesel dual fuel CI engine, *Engineering Science and Technology, an International Journal*, 21, pp. 330-337.

Flynn PF, **Hoag KL**, **Kamel MM**, and **Primus RJ**, (1984), A new perspective on diesel engine evaluation based on second law analysis, SAE, Paper No. 840032.

Fu Y, **Xiao B**, **Zhang C**, **Liu J**, **Fang J**, (2018), A new method for online estimation of the piston maximum temperature in diesel-natural gas dual fuel engine, *ASME Journal of Engineering for Gas Turbines and Power*, 140, p. 061507-1-8.

Geo VE, **Sonthalia A**, **Nagarajan G**, and **Nagalingam B**, (2017), Studies on performance, combustion and emission of a single cylinder diesel engine fuelled with rubber seed oil and its biodiesel along with ethanol as injected fuel, *Fuel*, 209, pp. 733–741.

Giakoumis EG, (2007), Cylinder wall insulation effects on the first- and second-law balances of a turbocharged diesel engine operating under transient load conditions, *Energy Conversion and Management*, 48, pp. 2925–2933.

Glassman I, and **Yetter RA,** (2008), Combustion, Fourth Edition, Academic Press (an imprint of Elsevier), California, USA.

Guan C, **Cheung CS**, **Ning Z**, **Wong PK**, and **Huang Z**, (2017), Comparison on the effect of using diesel fuel and waste cooking oil biodiesel as pilot fuels on the combustion, performance and emissions of a LPG-fumigated compression-ignition engine, *Applied Thermal Engineering*, 125, pp. 1260-1271.

Hagen M, **Polman E**, **Jensen J**, **Myken A**, **Jonsson O**, and **Dahl A**, (2001), Adding gas from biomass to the gas grid, 144. Malmo, Sweden: Swedish Gas Center; 2001 July, Report SCG 118.

Hagen LM, **Olesky LM**, **Bohac SV**, **Lavoie G**, and **Assanis D**, (2013), Effects of a low octane gasoline blended fuel on negative valve overlap enabled HCCI load limit, combustion phasing and burn duration, *ASME Journal of Engineering for Gas Turbines and Power*, 135(7), p. 72001.

Heywood JB, (1988), Internal Combustion Engine Fundamentals, McGraw-Hill, New York.

Hinton N, and **Stone R**, (2014), Laminar burning velocity measurements of methane and carbon dioxide mixtures (biogas) over wide ranging temperatures and pressures, Fuel, **116**, pp. 743–750.

Huang J, and **Crookes RJ**, (1998), Assessment of simulated biogas as a fuel for the spark ignition engine, *Fuel*, 77, pp. 1793–801.

Hulwan DB, and **Joshi SV**, (2011), Performance, emission and combustion characteristic of a multicylinder DI diesel engine running on diesel-ethanol-biodiesel blends of high ethanol content, *Applied Energy*, 88(12), pp. 5042–5055.

Hwang JT, **Nord AJ**, and **Northrop WF**, (2017), Efficacy of add-on hydrous ethanol dual fuel systems to reduce NO_x emissions from diesel engines, *ASME Journal of Energy Resources Technology*, 139(4), p. 042206.

Ibrahim A, (2016), Performance and combustion characteristics of a diesel engine fuelled by butanol–biodiesel–diesel blends, *Applied Thermal Engineering*, 103, pp. 651-659.

IEA, World Energy Outlook (2013), OECD-IEA, Paris.

India: Greenhouse Gas Emissions, (2007), Ministry of environment and forests, Government of ndia 2010. http://www.moef.nic.in/downloads/public-information/Report_INCCA.pdf.

India Energy Outlook: IEA Special Report (2015). (https://www.iea.org/publications/freepublications/publication/IndiaEnergyOutlook_WEO2015.pdf)

International Energy Agency, World Energy Outlook (2007) China and India insights. (https://www.iea.org/publications/freepublications/publication/WEO_2007.pdf.)

Jena J, and **Misra RD**, (2014), Effect of fuel oxygen on the energetic and exergetic efficiency of a compression ignition engine fuelled separately with palm and karanja biodiesels, *Energy*, 68, pp. 411-419.

Kalsi SS, and **Subramanian KA**, (2017), Effect of simulated biogas on performance, combustion and emissions characteristics of a bio-diesel fueled diesel engine, *Renewable Energy*, 106, pp. 78–90.

Kanga R, Zhou, L Hua J, Feng, D, Wei, H, and **Chen R,** (2019), Experimental investigation on combustion characteristics in dual-fuel dual - injection engine, *Energy Conversion and Management*, 181, pp. 15-25.

Kárászová M, **Sedláková Z**, and **Izák P**, (2015), Gas permeation processes in biogas upgrading: a short review, Chem Papers, 69(10), pp. 1277–83.

Karagöz Y, **Sandalc T**, **Koylu UO**, **Dalkılıç AS**, and **Wongwises S**, (2016), Effect of the use of natural gas–diesel fuel mixture on performance, emissions, and combustion characteristics of a compression ignition engine, *Advances in Mechanical Engineering*, 8(4), pp. 1–13.

Karim GA, (1980), A review of combustion processes in the dual fuel engine- the gas diesel engine, *Progress in Energy and Combustion Science*, 6, pp. 277-285.

Karim GA, (1987), The dual fuel engine" in: R.L. Evans (Eds.), Automotive Engine Alternatives, Plenum Press, New York.

Karim GA, (1991), An examination of some measures for improving the performance of gas fuelled diesel engines at light load, SAE Paper no. 912366.

Karim GA, and **Wierzba I**, (1992), Methane-carbon dioxide mixtures as a fuel, *SAE Technical Paper*, SAE International.

Khoobbakht G, **Najafi G**, **Karimi M**, and **Akram A**, (2016), Optimization of operating factors and blended levels of diesel, biodiesel and ethanol fuels to minimize exhaust emissions of diesel engine using response surface methodology, *Applied Thermal Engineering*, 99, pp. 1006–1017.

Khoobbakht G, **Akram A**, **Karimi M**, and **Najafi G**, (2016), Exergy and energy analysis of combustion of blended levels of biodiesel, ethanol and diesel fuel in a DI diesel engine, *Applied Thermal Engineering*, 99, pp. 720–729.

Knizley AA, Srinivasan KK, Krishnan SR, and **Ciatti SA**, (2012), Fuel and diluent effects on entropy generation in a constant internal energy-volume (UV) combustion process, *Energy*, 43, pp. 315-328.

Korakianitis T, **Namasivayam AM**, and **Crookes RJ**, (2010), Hydrogen dual-fuelling of compression ignition engines with emulsified biodiesel as pilot fuel, *International Journal of Hydrogen Energy*, 35, pp. 13329-13344.

Korakianitis T, **Namasivayam AM**, and **Crookes RJ**, (2011), Diesel and rapeseed methyl ester (RME) pilot fuels for hydrogen and natural gas dual-fuel combustion in compression–ignition engines, *Fuel* 90, pp. 2384-2395.

Kotas TJ, (1985), The exergy method of thermal plant analysis, London, UK Butterworths.

Krich K, **Augenstein A**, **Batmale J**, **Benemann J**, **Rutledge B**, and **Salour D**, (2005), Upgrading dairy biogas to biomethane and other fuels. In: Andrews K., Editor. Biomethane from dairy waste - A sourcebook for the production and use of renewable natural gas in california. california: Clear concepts, pp. 47-69.

Krishnan SR, (2001), Heat release analysis of dual fuel combustion in a direct injection compression ignition engine, MS thesis, Department of Mechanical Engineering, University of Alabama, USA.

Krishnan SR, (2005), Experimental investigations and phenomenological simulation of combustion in a low pilot-ignited natural gas engine with a focus on advanced injection timings, PhD thesis, Department of Mechanical Engineering, University of Alabama, USA.

Krishnan SR, **Biruduganti M**, **Mo Y**, **Bell SR**, and **Midkiff KC**, (2002), Performance and heat release analysis of a pilot-ignited natural gas engine, *International Journal of Engine Research*, 3(3), pp. 171-184.

Kumar KS, and **Raj RTK**, (2013), Effect of fuel injection timing and elevated intake air temperature on the combustion and emission characteristics of dual fuel operated diesel engine, *Procedia Engineering*, 64, pp. 1191–1198.

Kumar M, **Tsujimura T**, and **Suzuki Y**, (2018), NO_x model development and validation with diesel and hydrogen/diesel dual-fuel system on diesel engine, *Energy*, 145, pp. 496-506.

Lau SC, **Annamalai K**, and **Shelton SV**, (1987), Optimization of air-cooled condenser, *ASME Journal of Energy Resources Technology*, 109, pp. 90-95.

Lee D, **Roh HG**, **Park S**, and **Lee CS**, (2012), A study of the effects of diesel-biodiesel-bioethanol fuels on emission reduction in a compression ignition engine, *Proceedings of the Institution of Mechanical Engineers, Part D: Journal of Automobile Engineering*, **226**(3), pp. 410–418.

Li H, Liu S, Liew C, Gatts T, Wayne S, Clark N, and **Nuszkowski J,** (2018), An Investigation of the combustion process of a heavy-duty natural gas-diesel dual fuel engine, *ASME Journal of Engineering for Gas Turbines and Power*, 140, p. 091502-1-10.

Li Q, **Xu J**, **Du W**, **Li Y**, and **Liu D**, (2013), Ethanol as the acyl acceptor for biodiesel production, *Renewable and Sustatinable Energy Reviews*, 25, pp. 742-748.

Li Y, **Jia M**, **Kokjohn SL**, **Chang Y**, and **Reitz R**, (2018), Comprehensive analysis of exergy destruction sources in different engine combustion regimes, *Energy*, 149, pp. 697-708.

Lior N, and **Zhang N**, (2007), Energy, exergy, and Second Law performance criteria, *Energy*, 32, pp. 281–296.

Liu Z, (1995), An examination of the combustion characteristics of compression ignition engines fuelled with gaseous fuels, Ph.D. thesis, Department of Mechanical Engineering, University of Calgary, Canada.

Liu Z, and **Karim G**, (1997), Simulation of combustion processes in gas-fuelled diesel engines, *Proceedings of the Institution of Mechanical Engineers, Part A: Journal of Power and Energy*, 211(2), pp. 159–169.

Liu J, **Yang F**, **Wang H**, **Ouyang M**, and **Hao S**, (2013), Effects of pilot fuel quantity on the emissions characteristics of a CNG/diesel dual fuel engine with optimized pilot injection timing, *Applied Energy*, 110, pp. 201–206.

Lounici M, **Loubar K**, **Tazerout M**, and **Balistrou M**, (2014), Experimental investigation on the performance and exhaust emission of biogas-diesel dual-fuel combustion in a ci engine, SAE Technical Paper 2014-01-2689.

Ma F, and **Hanna MA**, (1999), Biodiesel production: a review, *Bioresource technology*, 70, pp. 1–15.

Mahabadipour H, Srinivasan KK, and **Krishnan SR,** (2016), **"**Lost Available IMEP": A second-law-based performance parameter for IC engines, *ASME 2016 Internal Combustion Engine Division Fall Technical Conference*, Greenville, South Carolina, USA, October 9 –12, 2016.

Mahabadipour H, Srinivasan KK, and **Krishnan SR,** (2017), A second law-based framework to identify high efficiency pathways in dual fuel low temperature combustion, *Applied Energy*, 202, pp. 199 –212.

Maji S, **Pal A**, and **Arora BB**, (2008), Use of CNG and diesel in CI engines in dual fuel mode, *SAE*, paper no. 2008-28-0072.

Maroneze MM, **Zepka LQ**, **Vieira JG**, **Queiroz MI**, and **Jacob-Lopes E**, (2014), Production and use of biogas in Europe: a survey of current status and perspectives, *Revista Ambiente & Água*, 9(3), pp. 445–58.

Masahiro I, **Tetsuya T**, and **Hironobu U**, (2003), Effect of egr and preheating on natural gas combustion assisted with gas-oil in a diesel engine, *JSME International Journal Series B Fluids and Thermal Engineering*, 46(1), pp. 124–130.

Makareviciene V, **Sendzikiene E**, **Pukalskas S**, **Rimkus A**, and **Vegneris R**, (2013), Performance and emission characteristics of biogas used in diesel engine operation, *Energy Conversion and Managment*, **75**, pp. 224–233.

Mattson J, **Reznicek E**, and **Depcik C**, (2016), Second-Law heat release modeling of a compression ignition engine fueled with blends of palm biodiesel, *ASME Journal of Engineering for Gas Turbines and Power*, 138, p. 091502-1-10.

Masimalai S, and **Nandagopal S,** (2016), Combined effect of oxygen enrichment and dual fueling on the performance behavior of a CI engine fueled with pyro oil–diesel blend as Fuel, *ASME Journal of Energy Resources Technology*, 138, p. 032206-1-8.

Mustafi NN, and **Raine RR**, (2008), A study of the emissions of a dual fuel engine operating with alternative gaseous fuels, SAE Paper no. 1394.

Mustafi NN, **Raine RR**, and **Verhelst S**, (2013), Combustion and emissions characteristics of a dual fuel engine operated on alternative gaseous fuels, *Fuel*, 109, pp. 669–678.

Nagarajan G, **Rao AN**, and **Renganarayanan S**, (2002), Emission and performance characteristics of neat ethanol fuelled di diesel engine, *International Journal of Ambient Energy*, 23(3), pp. 149–158.

Nathan SS, **Mallikarjuna JM**, and **Ramesh A**, (2010), An experimental study of the biogas-diesel HCCI mode of engine operation, *Energy Conversion and Management*, 51(7), pp. 1347–1353.

National Energy Map for India: Technology Vision (2030). (http://www.teriin.org/div/psa-fullreport.pdf.)

National Policy on Biofuels, (2009), Ministry of New and Renewable Energy, Government of India.

Nonaka HOB, and **Pereira FM**, (2016), Experimental and numerical study of CO_2 content effects on the laminar burning velocity of biogas, *Fuel*, **182**, pp. 382–390.

Nwafor OMI, (2003), Combustion characteristics of dual-fuel diesel engine using pilot injection ignition, *Journal of Institution of Engineers (India)*, 84, pp. 22-5.

Olivier JGJ, **Muntean M**, and **Peters JAHW**, (2015), Trends in global CO_2 emissions: 2015 report, PBL Netherlands Environ Assess Agency Eur Comm Jt Res Cent 2015, pp. 1–78.

Pan W, **Yao C**, **Han G**, **Wei H**, and **Wang Q**, (2015), The impact of intake air temperature on performance and exhaust emissions of a diesel methanol dual fuel engine, *Fuel*, **162**, pp. 101–110.

Papadias DD, and **Ahmed S**, (2012), Database of trace contaminants in LFG and ADG. Argonne National Laboratory. (Excel files available for download at: http://www.cse.anl.gov/FCs_on_biogas; 2012.)

Papagiannakis RG, and **Hountalas DT**, (2003), Experimental investigation concerning the effect of natural gas percentage on performance and emissions of a DI dual fuel diesel engine, *Applied Thermal Engineering*, 23, pp. 353–365.

Papagiannakis RG, **Hountalas DT**, **Zannis TC**, and **Yfantis EA**, (2009), Comparative evaluation of the effect of intake charge temperature, pilot fuel quality and injection advance on dual fuel compression ignition engine performance characteristics and emitted pollutants, Paper No. *IMECE2009-10435*, ASME International Mechanical Engineering Congress and Exposition, November 13–19, Florida, USA.

Papagiannakis RG, (2013), Study of air inlet preheating and EGR impacts for improving the operation of compression ignition engine running under dual fuel mode, *Energy Conversion and Management*, 68, pp. 40–53.

PARIS SUMMIT (2015) Analysis: India's climate pledge suggests significant emissions growth up to 2013. http://www.carbonbrief.org/indias-indc.

Park SH, **Yoon SH**, and **Lee CS**, (2011), Effects of multiple-injection strategies on overall spray behavior, combustion, and emissions reduction characteristics of biodiesel fuel, *Applied Energy*, **88**(1), pp. 88–98.

Park SH, **Cha J**, and **Lee CS**, (2012), Impact of biodiesel in bioethanol blended diesel on the engine performance and emissions characteristics in compression ignition engine, *Applied Energy*, 99, pp. 334–343.

Park SH, **Yoon SH**, **Cha J**, and **Lee CS**, (2014), Mixing effects of biogas and dimethyl ether (DME) on combustion and emission characteristics of DME fueled high-speed diesel engine, *Energy*, 66, pp. 413–422.

Parlak A, (2005), The effect of heat transfer on performance of the Diesel cycle and exergy of the exhaust gas stream in a LHR Diesel engine at the optimum injection timing, *Energy Conversion and Management*, 46, pp. 167–179.

Patro TN, (1994), Burning rate assessment of hydrogen-enriched fuel combustion in diesel engines, *International Journal of Hydrogen Energy*, 19 (3), pp. 275-284.

Paul A, **Panua R**, and **Debroy D**, (2017), An experimental study of combustion, performance, exergy and emission characteristics of a CI engine fueled by Diesel-ethanol-biodiesel blends, *Energy*, 141, pp. 839-852.

Paykani A, **Saray RK**, **Shervani-Tabar MT**, and **Mohammadi-Kousha A**, (2012), Effect of exhaust gas recirculation and intake pre-heating on performance and emission characteristics of dual fuel engines at part loads, *Journal of Central South University*, **19**(5), pp. 1346–1352.

Persson M, and **Wellinger A**, (2006), Biogas upgrading to vehicle fuel standards and grid injection, *IEA Bioenergy* (Report).

Pidol L, **Lecointe B**, **Starck L**, and **Jeuland N**, (2012), Ethanol-biodiesel-diesel fuel blends: performances and emissions in conventional diesel and advanced low temperature combustions, *Fuel*, 93, pp. 329–338.

Pizzuti L, **Martins CA**, and **Lacava PT**, (2016), Laminar burning velocity and flammability limits in biogas: a literature review, *Renewable and Sustainable Energy Reviews*, 62, pp. 856–865.

Poonia MP, **Ramesh A**, and **Gaur RR**, (1999), Experimental Investigation of the factors affecting the performance of a LPG - diesel dual fuel engine, *SAE Technical Paper*, SAE International.

Porpatham E, **Ramesh A**, and **Nagalingam B**, (2007), Effect of hydrogen addition on the performance of a biogas fuelled spark ignition engine, *International Journal of Hydrogen Energy*, 32(12), pp. 2057–2065.

Pulkrabek WW, (2003), Engineering fundamentals of the internal combustion engine, Pearson Education (Singapore) Pte. Ltd., Indian Branch, Delhi, India.

Pundir BP, (2010), I. C. engines combustion and emissions, Narosa Publishing House Pvt. Ltd., New Delhi, India.

Rahmouni C, **Tazerout M**, and **Corre LO**, (2002), A method to determine biogas composition for combustion control, *SAE*, paper no. 2002-01-1708.

Rakopoulos CD, and **Giakoumis EG**, (1997a), Development of cumulative and availability rate balances in a multi-cylinder turbocharged indirect injection diesel engine, *Energy Conversion and Management*, 38(4), pp. 347-369.

Rakopoulos CD, and **Giakoumis EG**, (1997b), Speed and load effects on the availability balances and irreversibilities production in a multi-cylinder turbocharged diesel engine, *Applied Thermal Engineering*, 17(3), 299-313.

Rakopoulos CD, and **Giakoumis EG**, (2006), Second-law analyses applied to internal combustion engine operation, *Progress in Energy and Combustion Science*, 32(1), pp. 2-47.

Rakopoulosa CD, and **Kyritsis DC**, (2006), Hydrogen enrichment effects on the second law analysis of natural and landfill gas combustion in engine cylinders, *International Journal of Hydrogen Energy*, 31, pp. 1384–1393.

Rakopoulos CD, **Scott MA**, **Kyritsisa DC**, and **Giakoumis EG**, (2008), Availability analysis of hydrogen/natural gas blends combustion in internal combustion engines, *Energy*, 33, 248–255.

Rakopoulos DC, **Rakopoulos CD**, **Giakoumis EG**, and **Dimaratos AM**, (2012), Characteristics of performance and emissions in high-speed direct injection diesel engine fueled with diethyl ether/diesel fuel blends, *Energy*, 43, pp. 214-224.

Rakopoulos DC, (2013), Combustion and emissions of cottonseed oil and its bio-diesel in blends with either n-butanol or diethyl ether in HSDI diesel engine, *Fuel*, 105, 603–613.

Rakopoulos DC, **Rakopoulos CD**, **Giakoumis EG**, **Papagiannakis RG**, and **Kyritsis DC**, (2014), Influence of properties of various common bio-fuels on the combustion and emission characteristics of high-speed DI (direct injection) diesel engine: vegetable oil, bio-diesel, ethanol, n-butanol, diethyl ether, *Energy*, 73, pp. 354–366.

Rakopoulos DC, **Rakopoulos CD**, and **Kyritsis DC**, (2016), Butanol or DEE blends with either straight vegetable oil or biodiesel excluding fossil fuel: Comparative effects on diesel engine combustion attributes, cyclic variability and regulated emissions trade-off, *Energy*, 115, pp. 314–325.

Ramadhas AS, **Jayaraj S**, and **Muraleedharan C**, (2008), Dual fuel mode operation in diesel engines using renewable fuels: Rubber seed oil and coir-pith producer gas, *Renewable Energy*, 33, pp. 2077-2083.

Ramôs da Costa YJ, **Barbosa de Lima AG**, **Filho CRB**, **Lima LdeA**, (2012), Energetic and exergetic analyses of a dual-fuel diesel engine, *Renewable and Sustainable Energy Reviews*, 16, pp. 4651–4660.

Rasi S, **Veijanen A**, and **Rintala J**, (2007), Trace compounds of biogas from different biogas production plants, *Energy*, 32, pp. 1375-1380.

Roy MM, **Calder J**, **Wang W**, **Mangad A**, and **Diniz FCM**, (2016), Cold start idle emissions from a modern Tier-4 turbo-charged diesel engine fueled with diesel-biodiesel, diesel-biodiesel-ethanol, and diesel-biodiesel-diethyl ether blends, *Applied Energy*, 180, pp. 52–65.

Ryan WN, **Wissink ML**, **DelVescovo DA**, and **Reitz RD**, (2015), Natural gas for high load dual-fuel reactivity controlled compression ignition in heavy-duty engines, *ASME Journal of Energy Resources Technology*, 137(4), p. 42202.

Ryckebosch E, **Drouillon M**, and **Vervaeren H**, (2011), Techniques for transformation of biogas to biomethane, *Biomass and Bioenergy*, 35, pp. 1633-1645.

SAE, 2002, "Diesel Engine Emission Measurement Procedure," SAE J1003. (DOI: https://doi.org/10.4271/J1003_200210.)

Sakthivel P, **Subramanian KA**, and **Mathai R**, (2018), Indian scenario of ethanol fuel and its utilization in automotive transportation sector, *Resources, Conversion & Recycling*, 132, pp. 102-120.

Sahoo BB, (2010), Clean development mechanism potential of compression ignition diesel engines using gaseous fuels in dual fuel mode, Ph.D. thesis, Department of Mechanical Engineering, Indian Institute of Technology Guwahati, India.

Sahoo BB, **Saha UK**, and **Sahoo N**, (2011a), Theoretical performance limits of a syngas-diesel fueled compression ignition engine from second law analysis, *Energy*, 36, pp. 760-769.

Sahoo BB, **Saha UK**, and **Sahoo N**, (2011b), Effect of load level on the performance of a dual fuel compression ignition engine operating on syngas fuels with varying H_2/CO content, *ASME Journal of Engineering for Gas Turbines and Power*, 133 (12), pp. 122802.

Sahoo BB, **Sahoo N**, and **Saha UK**, (2012a), Dual fuel performance studies of a small diesel engine using green fuels, *Applied Mechanics and Materials*, 110–116, pp. 2101–2108.

Sahoo BB, **Saha UK**, and **Sahoo N**, (2012b), Diagnosing the effects of pilot fuel quality on exergy terms in a biogas run dual fuel diesel engine, *International Journal of exergy*, 10(1), pp. 77-93.

Satyanarayana M, and **Muraleedharan C**, (2011), A comparative study of vegetable oil methyl esters (biodiesels), *Energy*, 36(4), pp. 2129–2137.

Selim MYE, (2005), Effect of engine parameters and gaseous fuel type on the cyclic variability of dual fuel engines, *Fuel*, 84, 961-971.

Senthilraja R, **Sivakumar V**, **Thirugnanasambandham K**, and **Nedunchezhian N**, (2016), Performance, emission and combustion characteristics of a dual fuel engine with diesel-ethanol-cotton seed oil methyl ester blends and compressed natural gas (CNG) as fuel, *Energy*, 112, pp. 899-907.

Sezer I, (2011), Thermodynamic, performance and emission investigation of a diesel engine running on dimethyl ether and diethyl ether, *International Journal of Thermal Sciences*, 50, pp. 1594-1603.

Singh S, Krishnan SR, Srinivasan KK, and Midkiff KC, (2004), Effect of pilot injection timing, pilot quantity, and intake charge conditions on performance and emissions for an advanced low-pilot-ignited natural gas engine, International Journal of Engine Research, 5(4), pp. 329-348.

Sjöberg M, **Dec JE**, (2005), An investigation into lowest acceptable combustion temperatures for hydrocarbon fuels in HCCI engines, *Proceedings of the Combustion Institute*, 30, pp. 2719–2726.

Som SK, and **Datta A**, (2008), Thermodynamic irreversibilities and exergy balance in combustion processes, *Progress in Energy and Combustion Science*, 34, pp. 351–376.

Sonntag RE, and **Wylen GJV**, (1991), Introduction to Thermodynamics," Third edition, John Wiley & Sons.

Srihari S, **Thirumalini S**, and **Prashanth K**, (2017), An experimental study on the performance and emission characteristics of PCCI-DI engine fuelled with diethyl ether-biodiesel-diesel blends, *Renewable Energy*, 107, pp. 440 – 447.

Srinivasan KK, Krishnan SR, and Midkiff KC, (2006), Improving low load combustion, stability, and emissions in pilot-ignited natural gas engines, Proceedings of the Institution of Mechanical Engineers, Part D: *Journal of Automobile Engineering*, 220, pp. 229-239.

Stepanov VS, (1995), Chemical energies and exergies of fuels, *Energy*, 2(3), pp. 235-242.

Stone R, (1999), Introduction to Internal Combustion Engines, Palgrave New York.

Nathan SS, **Mallikarjuna JM**, and **Ramesh A**, (2010), An experimental study of the biogas-diesel HCCI mode of engine operation, *Energy Conversion and Management*, 51(7), pp. 1347–1353.

Tarabet L, **Lounici MS**, **Loubar K**, **Khiari K**, **Bouguessa R**, and **Tazerout M**, (2018), Hydrogen supplemented natural gas effect on a DI diesel engine operating under dual fuel mode with a biodiesel pilot fuel, *International Journal of Hydrogen Energy*, 43, pp. 5961-5971.

Tat ME, (2011), Cetane number effect on the energetic and exergetic efficiency of a diesel engine fuelled with biodiesel, *Fuel Processing Technology*, 92, pp. 1311–1321.

Technology roadmap: biofuels for transport sectors, OECD/IEA-2011. https://www.iea.org/publications/freepublications/publication/Biofuels_Roadmap_WEB.pdf.

Tüccar G, **Özgür T**, and **Aydın K**, (2014), Effect of diesel–microalgae biodiesel–butanol blends on performance and emissions of diesel engine," *Fuel*, 132, pp. 47-52.

Turner SH, and **Weaver CS**, (1994), Dual fuel natural gas/diesel engines: technology, performance and emissions, Gas Research Institute Technical Report no. 94/0094.

Tutak W, (2014), Bioethanol E85 as a fuel for dual fuel diesel engine, *Energy Conversion and Management*, 86, pp. 39–48.

Venu H, and **Madhavan V**, (2017), Influence of diethyl ether (DEE) addition in ethanol-biodiesel-diesel (EBD) and methanol-biodiesel-diesel (MBD) blends in a diesel engine," *Fuel*, 189, 377–390.

Verma S, **Das LM**, and **Kaushik SC**, (2017a), Effects of varying composition of biogas on performance and emission characteristics of compression ignition engine using exergy analysis, *Energy Conversion and Management*, **138**, pp. 346–359.

Verma S, **Das LM**, **Bhatti SS**, and **Kaushik SC**, (2017b), A comparative exergetic performance and emission analysis of pilot diesel dual-fuel engine with biogas, CNG and hydrogen as main fuels, *Energy Conversion and Management*, 151, pp. 764-777.

Verma S, **Das LM**, **Kaushik SC**, **Tyagi SK**, (2018), An experimental investigation of exergetic performance and emission characteristics of hydrogen supplemented biogas-diesel dual fuel engine, *International Journal of Hydrogen Energy*, 43, pp. 2452-2468.

Verma SV, **Bora BJ**, **Sarkar A**, and **Saha UK**, (2014), Experimental investigation of a dual fuel diesel engine run on scrubbed biogas using the method of adsorption, Paper No. ESDA2014-20164, ASME 12th Biennial Conference on Engineering Systems Design and Analysis, June 25–27, Copenhagen, Denmark**.**

Virginio e Silva JO, **Almeida MF**, **Alvim-Ferraz Maria da C**, and **Dias JM**, (2018), Integrated production of biodiesel and bioethanol from sweet potato, *Renewable Energy*, 124, pp. 114-120.

Wannatong K, **Akarapanyavit N**, **Siengsanorh S**, and **Chanchaona S**, (2007), Combustion and knock characteristics of natural gas diesel dual fuel engine, SAE Technical Paper no. 2007-01-2047.

Wang Y, **Liu H**, **Huang Z**, and **Liu Z**, (2016), Study on combustion and emission of a dimethyl ether-diesel dual-fuel premixed charge compression ignition combustion engine with LPG (liquefied petroleum gas) as ignition inhibitor, *Energy*, **96**, pp. 278–285.

Wellinger A, and **Lindberg A**, (2005), Biogas upgrading and utilization. (http://www.biogasmax.eu/media/biogas_upgradingand_utilisation_018031200_1011_24042007.pdf.)

World Energy Outlook (2009) Executive summary. International Energy Agency (IEA), France. http://www.worldenergyoutlook.org/docs/weo2009/WEO2009_es_english.pdf.

Yoon SH, **Hwang JW**, and **Lee CS**, (2009), Effect of injection strategy on the combustion and exhaust emissions characteristics of biodiesel-ethanol blend in a DI diesel engine, *ASME Journal of Engineering for Gas Turbines and Power*, 132, pp. 77–83.

Yoon SH, Park SH, Suh HK, and Lee CS, (2010), Effect of biodiesel-ethanol blended fuel spray characteristics on the reduction of exhaust emissions in a common-rail diesel engine, *ASME Journal of Energy Resources Technology*, 132, pp. 1–7.

Yoon SH, and **Lee CS**, (2011), Experimental investigation on the combustion and exhaust emission characteristics of biogas– biodiesel dual-fuel combustion in a CI engine, *Fuel Processing Technology*, 92, pp. 992-1000.

Zaharin MSM, **Abdullah NR**, **Najafi G**, **Sharudin H**, and **Yusaf T**, (2017), Effects of physicochemical properties of biodiesel fuel blends with alcohol on diesel engine performance and exhaust emissions: a review, *Renewable and Sustainable Energy Reviews*, 79, pp. 475–493.

Zhang ZH, **Chua SM**, and **Balasubramanian R**, (2016), Comparative evaluation of the effect of butanol-diesel and pentanol-diesel blends on carbonaceous particulate composition and particle number emissions from a diesel engine, *Fuel*, 176, pp. 40–47.

Zhu H, **Bohac SV**, **Huang Z**, and **Assanis DN**, (2013), Defeat of the Soot/NO_x trade-off using biodiesel-ethanol in a moderate exhaust gas recirculation premixed low-temperature combustion mode, *ASME Journal of Engineering for Gas Turbines and Power*, **135**(9), p. 91502.

Appendix-A

Equations for Performance and Combustion

I. Performance Analysis:

(i) Stoichiometric Chemical Reaction:

In the evaluation of equivalence ratio and the lower heating values [LHV=HHV-{heat of vaporization of water× (mass of water formed/mass of fuel used)}] of the fuels used, the following equations (A1-A5) are used. Biogas is considered to be composed of methane and carbon dioxide ($x \times CH_4 + y \times CO_2$).

Diesel: $C_{12}H_{26}$

$$C_{12}H_{26} + 18.5 \times (O_2 + 3.76 \times N_2) = 12 \times CO_2 + 13 \times H_2O + 3.76 \times 18.5 \times N_2 \quad \text{(A1)}$$

Ethanol: C_2H_5OH

$$C_2H_5OH + 3 \times (O_2 + 3.76 \times N_2) = 2 \times CO_2 + 3 \times H_2O + 3 \times 3.76 \times N_2 \quad \text{(A2)}$$

Butanol: C_4H_9OH

$$C_4H_9OH + 6 \times (O_2 + 3.76 \times N_2) = 4 \times CO_2 + 5 \times H_2O + 6 \times 3.76 \times N_2 \quad \text{(A3)}$$

Diethyl ether: $C_2H_5OC_2H_5$

$$C_2H_5OC_2H_5 + 6 \times (O_2 + 3.76 \times N_2) = 4 \times CO_2 + 5 \times H_2O + 6 \times 3.76 \times N_2 \quad \text{(A4)}$$

Biogas: $x \times CH_4 + y \times CO_2$

$$x \times CH_4 + y \times CO_2 + 2x \times (O_2 + 3.76 \times N_2) = (x + y) \times CO_2 + 2x \times H_2O + 2x \times 3.76 \times N_2 \quad \text{(A5)}$$

where, $C_{12}H_{26}$ is the chemical structure of diesel (Sahoo et *al*., 2011b), *x* and *y* are the mole fraction of methane (CH_4) and carbon dioxide (CO_2) in biogas are used to calculate the biogas stoichiometric air-fuel ratio. Equation (A1) through (A5) is used to evaluate the global fuel-air equivalence ratio (Φ_{global}).

(ii) Global Fuel-air Equivalence Ratio (Φ)

The global fuel-air equivalence ratio (Φ_{global}) can be expressed as:

$$\Phi_{global} = \frac{\dot{m}_{pd} \times AFR_{pd} + \dot{m}_{bg} \times AFR_{bg}}{\dot{m}_a} \quad \text{(A6)}$$

where,$\dot{m}$, and *AFR* represent the mass flow rate (kg/s) of fuels and theoretical air-fuel ratio respectively; whereas the subscripts *a*, *pd* and *bg* denote the air, pilot diesel and biogas, respectively.

(iii) Diesel Replacement (DR)

The DR is defined as:

$$DR = \frac{\dot{m}_d - \dot{m}_{pd}}{\dot{m}_d} \tag{A7}$$

where, the subscripts *d* and *pd* stand for diesel are used in PDM and DFM, respectively.

(iv) Biogas Energy Share (BES)

The BES is estimated as:

$$BES = \frac{\dot{m}_{bg} \times LHV_{bg}}{\dot{m}_{bg} \times LHV_{bg} + \dot{m}_{pd} \times LHV_{pd}} (\%) \tag{A8}$$

where, *LHV* is the lower heating value.

(v) Brake Power (BP)

$$BP = \frac{2 \times \pi \times N \times F \times r}{60{,}000}, \text{kW} \tag{A9}$$

where, N, F (kg-m/s^2) and r (m) are the engine rpm, load and dynamometer arm radius, respectively.

(vi) Brake Thermal Efficiency (BTE)

$$\eta_{PDM} = \frac{BP}{\dot{m}_d \times LHV_d} \tag{A10}$$

$$\eta_{DFM} = \frac{BP}{\dot{m}_d \times LHV_d + \dot{m}_{bg} \times LHV_{bg}} \times 100\% = \frac{BP}{\sum(\dot{m} \times LHV)_{fuel}} \times 100\% \tag{A11}$$

where, $\sum(\dot{m} \times LHV)_{fuel}$ (kJ/s) is true for all fuels used in the present analysis.

(vii) Brake Specific Energy Consumption (BSEC)

$$BSEC = \frac{\sum(\dot{m} \times LHV)_{fuel}}{BP}, \frac{(\text{kJ/s})_{\text{fuel}}}{\text{kW}} \tag{A12}$$

(viii) Volumetric Efficiency (VE)

The relation of volumetric efficiency is shown as below:

Mass flow rate of air inhaled ($\dot{m}_a$):

$$\dot{m}_a = C_d \times \frac{\pi}{4} \times d^2 \times \sqrt{\frac{2gh \times \rho_{water}}{\rho_{air}}} \times \rho_{air} \times 3600, \text{kg/h} \quad \text{(A13)}$$

where, C_d, d, g, h, ρ_{water}, and ρ_{air} are coefficient of discharge, diameter of orifice (m), manometer height (m), density (kg/m^3) of water and air, respectively.

Mass flow rate of air equivalent to mass in swept volume per cycle ($\dot{m}_{sv}$):

$$\dot{m}_{sv} = \frac{\pi}{4} \times D^2 \times L \times \frac{N}{n} \times 60 \times K \times \rho_{air} \quad \text{(A14)}$$

where, D, L, N, n, and K are engine cylinder diameter (m), engine stroke length (m), number revolutions per cycle (2 for four stroke engine) and number of cylinders.

$$VE = \frac{\dot{m}_a}{\dot{m}_{sv}} \times 100\% \quad \text{(A14)}$$

II. Combustion Analysis:

(i) Ignition Delay:

$$ID = \theta_{SIT} - \theta_{SOC} \quad \text{(A15)}$$

where, θ_{SOI} and θ_{SOC} are the crank angle positions of static injection timing (CAD) and crank angle position at which the NHRR is zero and after which it increases sharply.

Arrhenius equation of ID:

$$ID = z1 \times \Phi_{global}^{z2} \times p^{z3} \times exp\left(-{}^{E_A}/_{RT_{CMGT}}\right) \quad \text{(A16)}$$

where, z1, z2, and z3 are the constants, and E_A, R, T_{CMGT} are the activation energy of the fuel (kJ/kg), universal gas constant (J/kg K) and the cylinder mean gas temperature (K).

(ii) Pressure Smoothing:

The DAS can record the cylinder pressure history at each of the degree of crank angle at all operating cycles. Differentiating the raw pressure data shows a noisy trend between two successive values. Hence, after treatment of these pressure data in the form of smoothing becomes necessary (Stone 1997) and following algorithm for (2b+1) values is used:

$$P_n = \frac{1}{b^2}\left[P_{n-(b-1)} + 2P_{n-(b-2)} + \cdots + bP_n + \cdots + 3P_{n+(b-2)} + 2P_{n+(b-2)} + P_{n+(b-1)}\right] \quad \text{(A17)}$$

The terms in Eq. (A17) are only evaluated when the part of the subscript in brackets is not negative. This is illustrated by the simplest case when b = 2.

$$P_n = \frac{P_{n-1} + 2P_n + P_{n+1}}{4} \quad \text{(A18)}$$

where, *P* is the instantaneous pressure (bar) data. The Eq. (A18) is used for smoothing the instantaneous pressure data (bar) that develop from start and end of combustion.

(iii) Rate of Pressure Rise:

The rate of pressure rise with crank angle is calculated from the smoothened pressure data by using first order finite difference equation with fourth order accuracy (Stone 1997).

$$\frac{dP}{d\theta} = \frac{P_{n-2} - 8 \times P_{n-1} + 8 \times P_{n+1} - P_{n+2}}{12 \times \Delta\theta} \quad \text{(A19)}$$

where, *P* is the instantaneous pressure data and "$\Delta\theta$" is the consecutive change of crank angle.

(iv) Net Heat Release Rate:

Over a complete engine cycle, instantaneous pressure (P_n) and volume (V_n) are the two important parameters to evaluate the net heat release rate (NHRR). In the estimation of NHRR, the specific heat ratio is chosen as 1.35 (Masood et al. 2006; Pirouzpanah et al. 2007). In the crank angle encoder specification, the pulse per revolution is given as 360. It means that for a complete engine cycle 720 instantaneous pressure and volume data are recorded in the DAS. In the present analysis, 20 cycles are taken for a complete cycle to smooth the pressure and NHRR curves. In the assessment of NHRR, simple mathematical techniques are used to combine the ideal gas law and the first law of thermodynamics (Karim 1980, Papagiannakis and Hountalas 2003, Rakopoulos et al. 2016a).

$$\frac{dQ_n}{d\theta} = \frac{\gamma}{\gamma - 1} \times P_n \times \frac{dV_n}{d\theta} + \frac{1}{\gamma - 1} \times V_n \times \frac{dP_n}{d\theta} \quad \text{(A20)}$$

where, $dQ_n/d\theta$, θ, V, γ, are the net heat release rate (J/CAD) concerning crank angle position, crank angle (CAD), instantaneous cylinder volume (m^3) and specific heat ratio. $dV_n/d\theta$ is the change in instantaneous volume per degree of crank angle.

(v) Evaluation of Cylinder Mean Gas Temperature (CMGT)

The CMGT is calculated by considering air as the ideal gas and by using ideal gas equation (Lata and Misra, 2010).

$$(T_{MGT})_n = P_n \times V_n \times \frac{T_{ref}}{P_{ref} \times V_{ref}} \tag{A21}$$

where,$(T_{CMGT})_n, P_n, V_n, T_{ref}, P_{ref}, V_{ref}$ are the cylinder mean gas temperature (CGMT) (K) after closer of inlet valve to any crank angle, instantaneous cylinder pressure (Pa), instantaneous cylinder volume (m^3), temperature (K) of intake charge at engine intake port, cylinder pressure (Pa) and volume (m^3) at intake port, respectively.

(vi) Arrhenius Equations of Reaction

$$ROR = l_1 \times exp\left(-\frac{E_A}{RT_{CMGT}}\right) \times [Fuel]^{l_2} \times [Oxidizer]^{l_3} \tag{A22}$$

where, ROR is the rate of reaction, l_1, $l_2$and l_3 are the constant.

Appendix-B

Experimental Uncertainties

Every measuring devices and instruments will have some uncertainties due to the error of the device itself and the errors during the system performance. In the present study, the uncertainties are estimated by using the most acceptable known theory proposed by Kline and McClintok (1953) and Moffat (1982). The theoretical analysis to evaluate the uncertainties of the various experimental dependant properties is expressed as follows.

If R is the dependant variable (parameter) in any experimental investigation, which is the function of the independent variables (parameters) such as x_1, x_2, x_3,……., x_n. Consequently, the relation can be represented as,

$$R = R(x_1, x_2, x_3 \dots\dots\dots\dots, x_n) \quad \text{(B1)}$$

If ΔR is total uncertainty of the system and ΔR_1, ΔR_2, ΔR_3,…..... ΔR_n are the uncertainties of the dependant variables x_1, x_2, x_3,……., x_n, respectively, then the relation according to this theory can be written as,

$$\Delta R = \left[\left(\frac{\partial R}{\partial x_1}\Delta R_1\right)^2 + \left(\frac{\partial R}{\partial x_2}\Delta R_2\right)^2 + \cdots\dots\dots\dots + \left(\frac{\partial R}{\partial x_n}\Delta R_n\right)^2\right]^{\frac{1}{2}} \quad \text{(B2)}$$

Table B1 Uncertainties of the various independent parameters

Sl. No.	Independent variable	Relative error (%)
1	Engine speed	1.40
2	Engine load	0.15
3	Liquid fuel flow rate	0.40
4	Gas flow rate	0.50
5	Water flow rate	1.00
6	LHV of liquid fuel	1.00
7	LHV of gaseous fuel	1.10
8	Temperature	0.80
9	Cylinder pressure	1.80
10	Cylinder volume	0.10
11	Specific heat of exhaust gas	0.80
12	CO, CO_2, HC, NO_x	4.00

The estimated uncertainties of each of the independent parameters are presented in Table B1. While the uncertainties of the dependent or performance parameters are referred in Table B2.

Table B3 represents the accuracy of the various devices used in the present experimental research work.

The uncertainty estimation in the evaluation of brake power (BP):

The BP of the engine is defined as

$$BP = \frac{2 \times 3.142 \times N \times W \times r}{60 \times 100} \quad \text{(B3)}$$

where, N, W, and r are the engine speed (rpm), applied load (kg) and dynamometer arm length (m). Hence, the parameters N, and W are the independent variables. The uncertainties of these two independent parameters are estimated as 1.4 and 0.15. Hence, the uncertainty of BP is

$$\Delta BP = (0.014^2 + 0.015^2)^{\frac{1}{2}} = 0.021 \approx 2.1\% \quad \text{(B4)}$$

Table B2 Uncertainties of the dependant (performance) parameters

Sl. No.	Parameters	*nr*-DFM (WOP)	*nr*-DFM (WP)	TB-E	TB-DEE
1	Air flow rate	1.4%	1.35	1.32	1.31
2	BSEC	1.5%	1.4%	1.4%	1.4%
3	BTE	1.8	1.5	1.45	1.45
4	NHRR	2.0	1.8	1.75	1.76
5	ID	0.5	0.3	0.35	0.40
6	CMGT	1.0	0.8	0.75	0.73
7	Pressure	1.9	1.5	1.40	1.39
9	CD	2.2	1.9	1.88	1.87

Table B3 Measuring devices specifications

Device used	Brand name	Device type	Accuracy	Resolution	Range
Biogas flow meter	Siya instruments	Mechanical	2%	0.001 m^3	10,000 m^3/h
Fuel flow transmitter	Yokogawa Electrical Corporation	DP transmitter	-	0.1 cc	0-500 mm of WC
Air flow transmitter	WIKA Instruments Ltd	Pressure transmitter	2%	1mm	(-) 250 mm of WC
Pressure sensors	PCB Piezotronics	Piezo type with low noise cable	2%	0.1 psi	5000 psi
Load and	Sensortronics	Strain gauge	-	-	0-50 kg
RPM sensor	Kubler	-	-	1º	5500 rpm
DAS	National Instruments	NI USB-6210	-	-	16-bit, 250 kS/s

Appendix-C

Equations for Thermodynamic Potential Study

I. Energy Analysis:

In compression ignition (CI) engines, the fuel energy supplied per unit time (Q_{in}) is transferred in various (low and high-grade) form of energy namely, shaft power (Q_s), rate of energy transferred to the cooling water (Q_{cw}), rate of energy transport with exhaust gas (Q_{eg}) and uncounted energy losses per unit time (Q_{un}) in the form of friction, radiation, heat transferred to the surrounding, and operating auxiliary equipment's etc. The parametric relations for these various form energies are annexed from the open literature (Heywood, 1988; Al-Najem and Diab, 1992; Sahoo, 2010; Debnath, 2013; Bora, 2015). The analytical expressions for the energy analysis in PDM and in DFM are different and expressed as below:

Energy Analysis in PDM:

- Fuel energy supplied per unit time (Q_{in}):

$$Q_{in} = \dot{m}_d \times LHV_d, \text{ kW} \tag{C1}$$

- Shaft power (Q_s):

$$Q_s = \frac{2 \times \pi \times N \times F \times r}{60{,}000}, \text{kW} \tag{C2}$$

- Rate of energy transferred to the cooling water (Q_{cw}):

$$Q_{cw} = \dot{m}_{cw} \times C_p^{cw} \times \left(T_{cw}^{e} - T_{cw}^{i}\right), \text{ kW} \tag{C3}$$

where, $\dot{m}_{cw}$, C_p^{cw}, T_{cw}^{e} and T_{cw}^{i} are the mass flow rate (kg/s), specific heat (kJ/kg.K), exit and inlet temperature (K) of cooling water passing through the engine jacket, respectively.

- Rate of energy transport with exhaust gas (Q_{eg}):

$$Q_{eg} = (\dot{m}_a + \dot{m}_d) \times C_p^{eg} \times \left(T_{eg}^{i} - T^0\right), \text{ kW} \tag{C4}$$

where, C_p^{eg}, T_{eg}^{i} and T^0 are specific heat (kJ/kg.K), exhaust temperature at calorimeter inlet and ambient temperature (K), respectively. C_p^{eg} is calculated with the balance of heat energy in calorimeter.

$$C_p^{eg} = \frac{\dot{m}_{cmw} \times C_p^{cw} \times \left(T_{cmw}^{e} - T_{cmw}^{i}\right)}{\left(\dot{m}_a + \dot{m}_d\right) \times \left(T_{eg}^{i} - T_{eg}^{e}\right)} \quad \text{(C5)}$$

where, $\dot{m}_{cmw}$, T_{cmw}^{i}, and T_{cmw}^{e}, are the mass flow rate of water through the calorimeter (kg/s), inlet and outlet temperature of water passing through the calorimeter (K), respectively.

- Uncounted energy losses per unit time (Q_{un}):

$$Q_{un} = Q_{in} - \left(Q_s + Q_{cw} + Q_{eg}\right), \text{kW} \quad \text{(C6)}$$

Energy Analysis in DFM:

- Fuel energy supplied per unit time (Q_{in}):

$$Q_{in} = \sum (\dot{m} \times LHV)_{all\ fuels} \quad \text{(C7)}$$

- Rate of energy transport with exhaust gas (Q_{eg}):

$$Q_{eg} = \left(\dot{m}_a + \sum(\dot{m})_{all\ fuels}\right) \times C_p^{eg} \times \left(T_{eg}^{i} - T^0\right), \text{kW} \quad \text{(C8)}$$

Corresponding specific heat of exhaust gas (C_{peg}):

$$C_{peg} = \frac{\dot{m}_{cmw} \times C_p^{cw} \times \left(T_{cmw}^{e} - T_{cmw}^{i}\right)}{\left(\dot{m}_a + \sum(\dot{m})_{all\ fuels}\right) \times \left(T_{eg}^{i} - T_{eg}^{e}\right)} \quad \text{(C9)}$$

II. Exergy Analysis

The exergy is the maximum useful rate of work that can be produced by a system involving energy transformation and interaction with the surroundings. Similar to energy input, the exergy input (E_{in}) is also fragmented into shaft exergy (E_s), exergy in cooling water (E_{cw}), exergy in exhaust gas (E_{eg}) and destructed exergy (E_{des}). In the exergy analysis, exergy efficiency (η_{II}) and rate of entropy generation (S_{gen}) are also considered as the essential parameters. These parameters are estimated with the analytical formula that are available in the open literature (Flynn et al., 1984; Kotas, 1985; Stepanov, 1995, Sahoo, 2010; Debnath, 2013, Paul et al., 2017; Verma et al., 2018) and presented in this section.

Exergy Analysis in PDM:

- Exergy input (E_{in}):

$$E_{in} = \dot{m}_d \times LHV_d \times \left[1.0401 + 0.1728\frac{H}{C} + 0.0432\frac{O}{C} + 0.2169\frac{S}{C} \times \left(1 - 2.0628\frac{H}{C}\right)\right], \text{ kW} \quad \text{(C10)}$$

where, H, C, O, and S are the mass fraction of hydrogen, carbon, oxygen, and sulfur, respectively, present in the fuel.

- Shaft exergy (E_s):

$$E_s = \text{Brake power of the engine, kW} \quad \text{(C11)}$$

- Exergy in cooling water (E_{cw}):

$$E_{cw} = m_{cw} \times C_p^{cw} \times \left[T_{cw}^e - T_{cw}^i - T^0 \times \ln\left(\frac{T_{cw}^e}{T_{cw}^i}\right)\right], \text{ kW} \quad \text{(C12)}$$

- Exergy in exhaust gas (E_{eg}):

$$E_{eg} = (\dot{m}_a + \dot{m}_d) \times \left[C_p^{eg}\left\{T_{eg}^i - T^0 - T^0 \times \ln\left(\frac{T_{eg}^i}{T^0}\right)\right\} + RT^0 \ln\left(\frac{P_{eg}^i}{P^0}\right)\right], \text{ kW} \quad \text{(C13)}$$

where, R, P_{eg}^i, and P^0 are the specific gas constant (0.287 kJ/kg.K), exhaust gas pressure (bar) and the pressure at the dead state (bar), respectively.

- Destructed exergy (E_{des}):

$$E_{des} = E_{in} - \left(E_s + E_{cw} + E_{eg}\right), \text{ kW} \quad \text{(C14)}$$

- Exergy efficiency (η_{II}):

$$\eta_{II} = 1 - \frac{E_{des}}{E_{in}} \quad \text{(C15)}$$

- Rate of entropy generation (S_{gen}):

S_{gen} (kW/K) is defined as the ratio of rate of exergy destruction to the dead state to the temperature at the dead state. It is a crucial parameter to predict the rate of loss of energy into the environment (dead state) and allows more exact calculation of the losses than the traditional approach that uses several correlations (Paul et al., 2017).

$$S_{gen} = \frac{E_{des}}{T^0} \tag{C16}$$

Exergy Analysis in DFM

In DFM, preheating of the intake charge has been done. Therefore, exergy input is the combinations of the exergy in supplied fuels (E_{fuels}) and exergy in preheated air (E_{pa}).

- Exergy in injected pilot fuels ($E_{pilot\ fuels}$):

$$E_{pilot\ fuels} = \sum(\dot{m} \times LHV)_{pilot\ fuels} \times \left[1.0401 + 0.1728\frac{H}{C} + 0.0432\frac{O}{C} + 0.2169\frac{S}{C} \times \left(1 - 2.0628\frac{H}{C}\right)\right], \text{kW} \tag{C17}$$

- Exergy in inducted biogas (E_{bg}):

$$E_{bg} = 0.95 \times \dot{m}_{bg} \times HHV_{bg}, \text{kW} \tag{C18}$$

where, $\dot{m}_{bg}$ and HHV_{bg} are the mass flow rate (kg/s) of inducted biogas and higher heating value of biogas, respectively.

Exergy in preheated air (E_{pa}):

$$E_{pa} = \left(\dot{m}_a + \dot{m}_{bg}\right)\left[C_p^a\left\{T_p - T^0 - T^0 \times \ln\left(\frac{T_p}{T^0}\right)\right\} + R \times T^0 \ln\left(\frac{P^0}{P_p}\right)\right], \text{kW} \tag{C19}$$

where, C_p^a, T_p, and P_p are the constant pressure specific heat (kJ/kg.K), preheating temperature (K), and the suction line pressure at exit of the heat exchanger (bar), respectively.

- Exergy in (E_{in}):

$$E_{in} = E_{pilot\ fuels} + E_{bg} + E_{pa}, \text{kW} \tag{C20}$$

- Exergy in exhaust gas (E_{eg}):

$$E_{eg} = \left(\dot{m}_a + \sum(\dot{m})_{all\ fuels}\right) \times \left[C_p^{eg}\left\{T_{eg}^i - T^0 - T^0 \times \ln\left(\frac{T_{eg}^i}{T^0}\right)\right\} + RT^0 \ln\left(\frac{P_{eg}^i}{P^0}\right)\right], \text{kW} \tag{C21}$$

Appendix-D

Conversion of Emissions Data

In order to have a better clarity, the emission data measured in ppm and in volume percentage are converted in gm/kWh. These data are presented in Tables D1 and D2 at the loads of 0.83 and 4.14 bar, respectively. The emission data have been converted following the standard measurement procedures (SAE J1003, 2002), and the trends at lower and higher loads are found similar to reported work (Verma *et al*., 2018).

Table D1 Emissions in gm/kWh unit (at 0.83 bar, brake power ≈0.72 kW)

Engine Operation		**Load** = 0.83 bar (at **CR** = 17.5, **IT** = 23 CAD bTDC)					
		HC		CO		NO_x	
		ppm	gm/kWh	Vol.%	gm/kWh	ppm	gm/kWh
nr-DFM (WOP) at Φ_{global} = 0.87		797	14.53	0.117	60.73	6	1.19
At optimum Φ_{global}	*nr*-DFM (WOP)	211	13.15	0.112	50.16	29	3.70
	nr-DFM (WP)	201	9.46	0.089	28.74	28	4.71
	TB-BT	163	10.83	0.085	22.46	46	5.06
	TB-E	143	7.39	0.069	14.04	53	5.78
	TB-DEE	135	5.92	0.057	7.37	62	6.14
PDM		56	3.28	0.064	8.68	179	10.35

Table D2 Emissions in gm/kWh unit (at 4.14 bar, brake power ≈ 3.42 kW)

Engine Operation		**Load** = 4.14 bar (at **CR** = 17.5, **IT** = 23 CAD bTDC)					
		HC		CO		NO_x	
		ppm	gm/kWh	Vol.%	gm/kWh	ppm	gm/kWh
nr-DFM (WOP) at Φ_{global} = 0.89		378	4.22	0.045	8.56	72	2.25
At optimum Φ_{global}	*nr*-DFM (WOP)	131	1.19	0.138	21.50	442	8.14
	nr-DFM (WP)	79	0.41	0.049	5.50	781	9.41
	TB-BT	29	0.23	0.027	2.52	784	10.08
	TB-E	21	0.14	0.019	1.52	887	11.68
	TB-DEE	15	0.09	0.014	1.06	1131	14.10
PDM		45	0.30	0.029	3.66	1196	14.36

List of Publications

Book Chapter

1. **Sarkar A**, **Dabi M**, and **Saha UK**, (2018), Supplementing the energy need of diesel engines in indian transport and power sectors, *Sustainable Energy and Transportation : Technologies and Policy*, A. Gautam, S. De, A. Dhar, J.G. Gupta, and A. Pandey, eds., Springer Singapore, Singapore, pp. 61–86.

Journals

2. **Sarkar A**, **Saha UK**, (2019), A critique on the research activities and potential benefits of dual fuel diesel engines run on biogas and oxygenated liquid fuels, *ASME Journal of Engineering for Gas Turbines and Power*, 141, p. 060801-26.
3. **Sarkar A**, and Saha UK, (2018), Effect of intake charge preheating and equivalence ratio in a dual fuel diesel engine run on biogas and ethanol-blended diesel, *ASME Journal of Energy Resources Technology*, 140, p. 041802-1-13.
4. **Sarkar A**, and **Saha UK**, (2018), Impact of intake charge preheating on a biogas run dual fuel diesel engine using ternary blends of diesel-biodiesel-ethanol, *ASCE Journal of Energy Engineering*, 144(3), p. 04018031-1-13.
5. **Sarkar A**, and **Saha UK**, (2018), Role of global fuel-air equivalence ratio and preheating on the behaviour of a biogas driven dual fuel diesel engine, *Fuel***,** 232, 743-754.

Conference

6. **Sarkar A**, and **Saha UK**, (2017), Effect of biogas flow rate and intake charge preheating in a dual fuel diesel engine, *National Conference on Sustainable Mechanical Engineering: Today and Beyond* (SMETB), March 24−25, Tezpur University, India.

Under Review

7. **Sarkar A**, **Saha UK**, (2019), Energetic and exergetic analyses of a dual fuel diesel engine run on preheated intake biogas-air mixture and oxygenated pilot fuels, *Renewable Energy.*
8. **Sarkar A**, **Saha UK**, (2019), Assessment of a light-duty biogas run dual fuel diesel engine using oxygenated ternary blends at the optimum equivalence ratio and under the effect of intake charge preheating, *ASME Journal of Engineering for Gas Turbines and Power*.